Ionic Liquids as Promoters for CO2 Electroreduction by Molecular Catalysts

Elli Vichou

Sorbonne Université

École Doctorale 388 – Chimie Physique et Chimie Analytique de Paris Centre

Laboratoire Interfaces et Systèmes Électrochimiques, LISE – UMR 8235, Sorbonne Université, Paris

Laboratoire de Chimie des Processus Biologiques, CNRS – UMR 8229, Collège de France, Paris

Ionic Liquids as Promoters for CO_2 Electroreduction by Molecular Catalysts

Par **Elli VICHOU**

Thèse de doctorat

Dirigée par Dr. Carlos M. SANCHEZ -SANCHEZ

et Prof. Marc FONTECAVE

Présentée et soutenue publiquement le 14 Décembre 2021, à Paris

Devant un jury composé de :

Mme. Sylvie CHARDON-NOBLAT	Directrice de Recherche CNRS - Université Grenoble Alpes	Rapporteuse
Mme. Sophie GRIVEAU	Maître de Conférences HDR - Chimie ParisTech PSL	Rapporteuse
Mme. Claude JOLIVALT	Professeur à Sorbonne Université	Examinatrice
M. Thomas DONEUX	Professeur à l'Université Libre de Bruxelles	Examinateur
M. Carlos SANCHEZ-SANCHEZ	Chargé de Recherche - HDR CNRS - SorbonneUniversité	Directeur de thèse
M. Marc FONTECAVE	Professeur au Collège de France	Co-directeur de thèse
Mme. Maria GOMEZ-MINGOT	Ingénieure de recherche au Collège de France	Co-encadrante de thèse

TABLE OF CONTENTS

SUMMARY

Carbon dioxide (CO_2) electroreduction by molecular catalysts constitutes a promising method to generate high-value added products such as CO and HCOOH. Ionic Liquids (ILs) as promoters for CO_2 electroreduction has only been extensively addressed in heterogeneous catalysis and in contrast, little study has been devoted to the elucidation of their interaction with molecular electrocatalysts. This thesis studies the application of electrolyte engineering to CO_2 conversion catalyzed by two model molecular catalysts [Re(bpy)$(CO)_3$Cl] and [Rh(bpy)(Cp*)Cl]Cl. Electrolyte engineering strategy allows to modify the electrostatic field present in the double layer at the electrode/solution interface by adding different ionic liquids in solution, which strongly impacts CO_2RR activity and selectivity.

Complex [Re(bpy)$(CO)_3$Cl] as a model catalyst for CO_2 conversion to CO was studied in acetonitrile. The presence of imidazolium-based ILs in solution under CO_2 catalytic conditions causes a decrease in the CO_2 reduction overpotential of about 330 mV, proving the existence of a co-catalytic role of the IL, though this effect was less pronounced when an external proton source was added. The energy efficiency for CO_2 conversion to CO reached by this catalyst in the presence of ILs was lower than the one reached using the benchmark electrolyte. Complex [Rh(bpy)(Cp*)Cl]Cl as a model catalyst for CO_2 conversion to HCOOH was studied in the presence of ILs in both acetonitrile and acidic aqueous solutions, displaying in both cases a significant decrease in overpotential and tuning of its selectivity towards formate production. Thus, a very selective CO_2 to formate conversion (FE_{HCOO^-} > 90 %) with a maximal energy efficiency of 66 % is reached in acetonitrile solution. CO_2 conversion exhibits less selectivity for formate production in acidic aqueous solution than in acetonitrile, but it allows suppressing the competitive hydrogen evolution reaction (HER) and CO_2 conversion at a very low overpotential (0.28 V). For both catalysts mechanistic explanations of the observed interaction with ILs are proposed and in the case of [Rh(bpy)(Cp*)Cl]Cl they also include density functional theory (DFT) calculations. An original protocol for imidazolium-based ILs immobilization at the electrode surface is presented and the enhanced catalytic effect produced during CO_2 electroreduction is evaluated with the aid of model catalyst [Rh(bpy)(Cp*)Cl]Cl in both acetonitrile and aqueous conditions. This immobilization of ILs at the electrode surface exhibits a superior selectivity towards formate than previously stuided ILs in solution. Further characterization by spectroscopic and electrochemical methods strongly suggests that the nature of this immobilized layer of IL is cationic. Finally, the feasibility of the aforementioned CO_2 catalytic system in larger scale is successfully proven by experiments in a flow electrolyzer of 10 cm^2 of electrode area using a gas diffusion electrode as a cathode.

In conclusion, this thesis provides an original approach to increase activity and selectivity in CO_2RR based on electrolyte engineering instead of the conventional catalyst engineering approach, which could be easily extrapolated to other molecular electrocatalytic systems.

Keywords: electrochemical CO_2 reduction reaction; molecular catalysts; imidazolium and pyrrolidinium based ionic liquids; electrolyte engineering; electrodeposited ionic liquid layer; flow electrolyzer.

RÉSUMÉ

L'électroréduction du dioxyde de carbone (CO_2) par des catalyseurs moléculaires constitue une voie prometteuse pour générer des produits à haute valeur ajoutée tels que le CO et le HCOOH. Les liquides ioniques (ILs) en tant que promoteurs de l'électroréduction du CO_2 n'ont été largement abordés que dans la catalyse hétérogène et, en revanche, peu d'études ont été consacrées à l'élucidation de leur interaction avec les électrocatalyseurs moléculaires. Cette thèse étudie l'application de l'ingénierie électrolytique à la conversion du CO_2 catalysée par deux catalyseurs moléculaires modèles : [Re(bpy)$(CO)_3$Cl] et [Rh(bpy)(Cp*)Cl]Cl. La stratégie de l'ingénierie électrolytique permet de modifier le champ électrostatique présent dans la double couche à l'interface électrode/solution en ajoutant différents liquides ioniques en solution, ce qui impacte fortement l'activité et la sélectivité du CO_2RR.

Le complexe [Re(bpy)$(CO)_3$Cl] comme catalyseur modèle pour la conversion du CO_2 en CO a été étudié dans l'acétonitrile. La présence d'ILs à base d'imidazolium en solution dans des conditions catalytiques de réduction du CO_2 provoque une diminution du surpotentiel de réduction de CO_2 d'environ 330 mV, prouvant l'existence d'un rôle co-catalytique de l'IL, bien que cet effet soit moins prononcé lorsqu'une source externe de protons était ajoutée. Le rendement énergétique de conversion du CO_2 en CO atteint par ce catalyseur en présence d'ILs était inférieur à celui atteint en utilisant l'électrolyte de référence. Le complexe [Rh(bpy)(Cp*)Cl]Cl en tant que catalyseur modèle pour la conversion du CO_2 en HCOOH a été étudié en présence d'ILs dans l'acétonitrile et dans des solutions aqueuses acides, montrant dans les deux cas une diminution significative du surpotentiel et une orientation de la sélectivité vers la production de formiate. Ainsi, une conversion très sélective du CO_2 en formate (FE_{HCOO^-} > 90 %) avec une efficacité énergétique maximale de 66 % est atteinte dans une solution électrolytique d'acétonitrile. La conversion du CO_2 présente moins de sélectivité pour la production de formiate en solution aqueuse acide qu'en acétonitrile, mais elle permet de supprimer la réaction compétitive d'évolution d'hydrogène (HER) et la conversion de CO_2 à un très faible surpotentiel (0,28 V). Pour les deux catalyseurs, des explications mécanistiques de l'interaction observée avec les IL sont proposées et dans le cas de [Rh(bpy)(Cp*)Cl]Cl, elles incluent également des calculs de la théorie de la fonctionnelle de la densité (DFT). Un protocole original pour l'immobilisation des IL à base d'imidazolium à la surface de l'électrode de travail est présenté et l'effet catalytique accru produit pendant l'électroréduction du CO_2 est évalué à l'aide du catalyseur modèle [Rh(bpy)(Cp*)Cl]Cl dans les deux conditions d'acétonitrile et d'eau .

Cette immobilisation des IL à la surface de l'électrode présente une sélectivité supérieure envers le formiate que les IL précédemment étudiées en solution. Une caractérisation plus poussée par des méthodes spectroscopiques et électrochimiques suggère fortement que la nature de cette couche immobilisée d'IL est cationique. Enfin, l'applicabilité de ce système catalytique à plus grande échelle est

prouvée avec succès par des expériences dans un électrolyseur à flux de 10 cm^2 de surface d'électrode en utilisant une électrode à diffusion de gaz comme cathode.
En conclusion, cette thèse propose une approche originale pour augmenter l'activité et la sélectivité en CO_2RR basée sur l'ingénierie électrolytique au lieu de l'approche conventionnelle de l'ingénierie des catalyseurs, qui pourrait être facilement extrapolée à d'autres systèmes électrocatalytiques moléculaires.

Mots-clés : électroréduction de CO_2, catalyseurs moléculaires, liquides ioniques à base d'imidazolium et pyrrolidinium, ingénierie électrolytique, couche de liquide ionique électrodéposée, électrolyseur à flux.

LIST OF ABBREVIATIONS AND CHEMICAL FORMULAS

Acronyms	Meaning
$[BF_4]^-$	Tetrafluoroborate anion
$[BMIM]^+$	1-Butyl-3-methylimidazolium cation
$[BMIM][BF_4]$	1-Butyl-3-methylimidazolium tetrafluoroborate
$[BMIM][PF_6]$	1-Butyl-3-methylimidazolium hexafluorophosphate
$[BMPyrr]^+$	1-Butyl-1-methylpyrrolidinium hexafluorophosphate
$[DiMIM]^+$	1,2 Dimethylimidazolium cation
$[DiMIM][N(SO_2CF_3)_2]$	1,2 Dimethylimidazolium bis(trifluoromethylsulfonyl)imide
$[EMIM]^+$	1-Ethyl-3-methylimidazolium cation
$[EMIM][BF_4]$	1-Ethyl-3-methylimidazolium tetrafluoroborate
$[EtNH_3][NO_3]$	Ethylammonium *nitrate*
$[EMIM][PF_6]$	1-Ethyl-3-methylimidazolium hexafluorophosphate
$[N(SO_2CF_3)_2]^-$	Bis(trifluoromethylsulfonyl)imide anion
$[PF_6]^-$	Hexafluorophosphate anion
$[TBA]^+$	Tetrabutylammonium cation
$[TBA][PF_6]$	Tetrabutylammonium hexafluorophosphate
$[TCB]^-$	Tetracyanoborate anion
ACN	Acetonitrile
AcOH	Acetic acid
BE	Binding Energy
bpy	bipyridine
BzOH	Benzoic acid
CCE	Constant current electrolysis
CCS	Carbon capture and storage
CCU	Carbon capture and utilization
CE	Counter electrode
CoPc	Cobalt pthalocyanine
CO2RR	Carbon dioxide reduction reaction
CNT	Carbon nanotube
Cp*	Pentamethylcyclopentadienyl
CPE	Constant potential electrolysis
CV	Cyclic voltammetry

DFT	Density Functional Theory
DMF	Dimethyl formamide
DMSO	Dimethyl sulfoxide
DSA	Dimensionally Stable Anode
E_a	Activation energy
E_{cat}	Catalytic Potential
$E_{cat\ max}$	Catalytic Potential at maximum value of catalytic current
$E_{cat/2}$	Catalytic Potential at half of the catalytic current
|Ecell|	Absolute cell potential
EC	Energy Consumption
EE	Energy Efficiency
EtOH	Ethanol
$E_{p1/2}$	Potential of reversible or quasi-reversible peak
E_p	Peak potential
eV	Electron volt
Fc	Ferrocene
FE	Faradaic Efficiency
FeTPP	Iron tetraphenylporphyrin
FID	Flame ionization detector
GC	Gas chromatography
GCE	Glassy carbon electrode
GDE	Gas diffusion electrode
HER	Hydrogen Evolution Reaction
HOMO	Highest occupied molecular orbital
HPC	Hierarchical porous carbon
IC	Ionic chromatography
ILs	Ionic liquids
IM^+	Imidazolium cation
IR	Ohmic drop
j	Current density
jcat	Current density under catalytic conditions
jp	Current density under inert conditions
jcat/jp	Catalytic response
LSV	Linear sweep voltammetry
LUMO	Lowest unoccupied molecular orbital
MOFs	Metal-organic frameworks

NHE	Normal hydrogen electrode
NMR	Nuclear magnetic resonance
NPs	Nanoparticles
Ntf_2^-	$N(SO_2CF_3)_2^-$
OER	Oxygen Evolution Reaction
OCV	Open circuit voltage
PCET	Proton Coupled Electron Transfer
Pc	Phthalocyanine
PFSA	Perfluorosulfonic acid
PTFE	Polytetrafluoroethylene
PVDF	Polyvinylidene difluoride
$Pyrr^+$	Pyrrolidinium cation
RE	Reference electrode
RHE	Reversible hydrogen electrode
RTILs	Room temperature ionic liquids
RVC	Reticulated vitreous carbon
SAM	Self-assembled monolayers
TCD	Thermal conductivity detector
TFE	2,2,2-Trifluoroethanol
TOF	Turn-over-frequency
TON	Turnover number
TPP	Tetraphenylporphyrin
TS	Transition state
WE	Working electrode
XPS	X-ray photoelectron spectroscopy
η	Overpotential
$\|\eta cell\|$	Absolute cell overpotential
$\Delta\eta$	Overpotential difference
ΔEp	Peak-to-peak separation
Γ	Surface Coverage

CHAPTER 1: INTRODUCTION

CHAPTER 1: INTRODUCTION

1.1 Carbon Dioxide and the greenhouse effect

Energy demand has been rising over the past decades and meeting this demand has led to a drastic increase in fossil fuel consumption. As a consequence, the produced quantities of global mean monthly carbon dioxide have also been on an upwards trajectory, reaching an average value of 417 ppm in July of 2021[1]. CO_2 is a well-known greenhouse gas for its capacity to firstly absorb and subsequently re-emit thermal radiation. Average increasing concentrations of CO_2 constitute a trend that surpasses seasonality and have been correlated with changes on the planet's climate and especially the temperature on the Earth's surface and in the oceans[2]. In Figure 1.1 (a) we see the deviation of average temperatures of the past 140 years from the average temperature of the 20th century. Blue bars represent years where the average temperature was lower than the overall average of the examined 140-year time period, while on the opposite, red bars represent higher average temperature values. Plotted alongside them, as a grey line, is the average carbon dioxide concentration measured in ppm[3]. While both temperature and CO_2 concentration increase are moderate over the first 7 decades shown, from the 1950s forwards, however, the rate of CO_2 increase is five times higher and it is reflected in the average + 0.14 °C per decade compared to the previously measured + 0.04 °C value. The result of such increase is not only witnessed by an increase in average temperature on Earth, a phenomenon also referred to as climate change, but is also felt particularly in marine ecosystems. In this case, increasing CO_2 causes an acidification of oceanic pH, disrupting the quantities of dissolved calcium carbonate, an essential element for organisms that utilize it to construct their skeletons[4]. Furthermore, some studies suggest that CO_2 uptake by terrestrial and marine ecosystems is affected by their climate and existing atmospheric CO_2 concentration, which means that in the present conditions of positive carbon-feedback, the effects could be accelerated[5].

Given the detrimental effects of overproduction of CO_2, several strategies to contain and reduce carbon dioxide have been in development over the last few years, known as carbon capture and storage (CCS) and carbon capture and utilization (CCU), respectively. CCS is principally exploring ways of injection and sequestration of CO_2 and some industrial plants are already in existence[6]. CCU has the added advantage over CCS of transforming a waste material into useful feedstock chemicals and can be used for storing energy from intermittent renewable energy sources in the form of chemical bonds. Meanwhile, CCS also has the risk of inadvertent CO_2 leaking in the atmosphere from long-term storage. Considering the aforementioned points, CCU appears to be the preferable option[5,7,8]. Currently, CO_2 has some industrial uses, including the food and beverage industries, where it is mainly used as a carbonating agent, as well as a preservative or packaging gas. It also has uses within the pharmaceutical industry, either during the synthetic pathway of drugs, or as a respiratory stimulant. Nevertheless, the aim of these applications is not the decrease of atmospheric CO_2 levels and as a consequence, CO_2 is still liberated at the end of these processes[9].

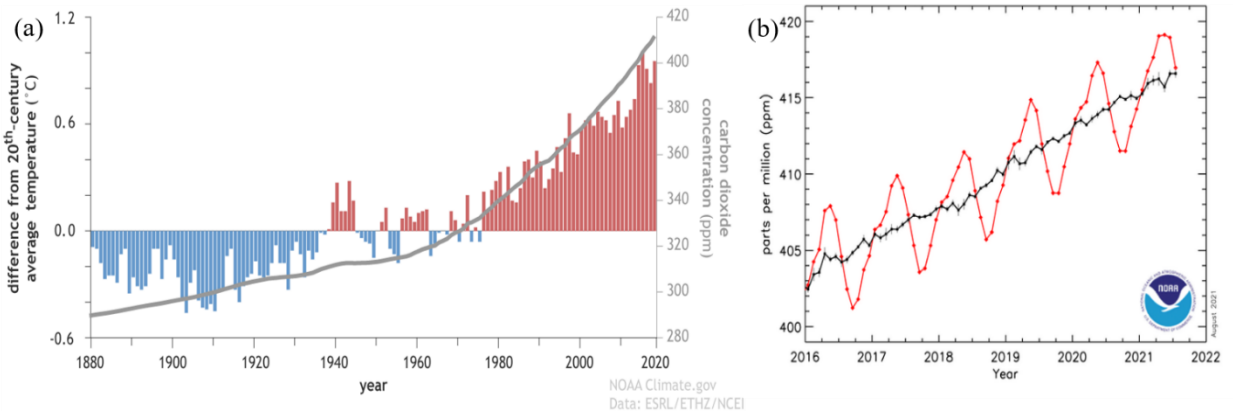

Figure 1.1 (a) The variation of average global temperature throughout the last 140 years as a correlation of CO_2 concentration[3] *and (b) the monthly average CO_2 values of recent years as registered by the Mauna Loa Observatory in Hawaii as averages at the middle of each month (red lines) and after correction according to the seasonal cycle (black lines)*[1].

1.2 Carbon Dioxide Conversion

In order for the excess of CO_2 to be used and the carbon cycle (shown here in Figure 1.2) to be closed, we need to convert CO_2 to other chemicals in a manner that constitutes carbon recycling. More particularly, in order to promote a carbon-neutral outcome, CO_2 that is captured at industrial sources undergoes reductive conversion powered by renewable energy sources to result in added-value products that can be themselves used to satiate the energy demand, as shown in the scheme of Figure 1.2[8,9].

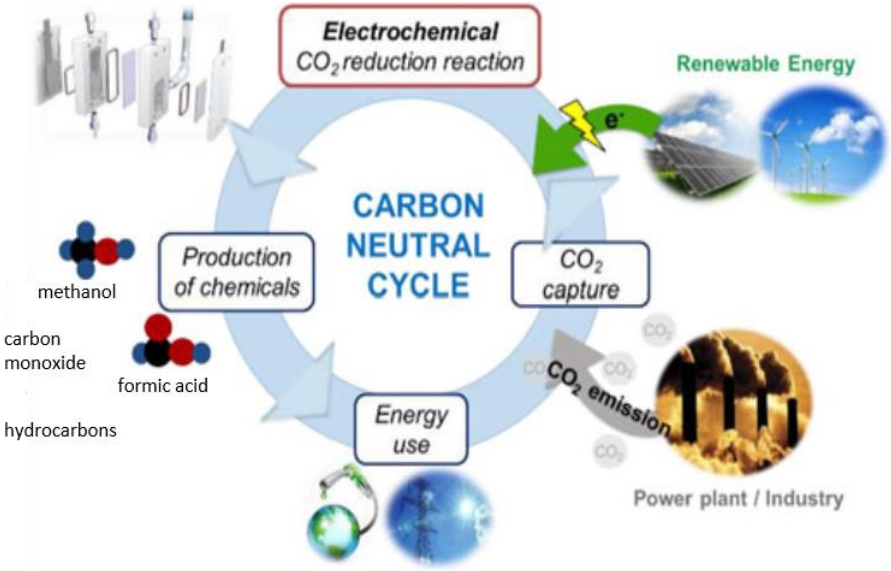

Figure 1.2 A model of a carbon-neutral cycle, where CO_2 is electrochemically transformed to fuels and other chemicals utilizing energy from renewable sources [8].

The principal ways to approach CO_2 conversion are biochemically, thermochemically, photochemically, and electrochemically. Thermochemical CO_2 conversion has long been used for methanol production and during biomass gasification and pyrolysis, where it has a beneficial role in increasing methanol content in the resulting syngas ratio. However, these processes are limited by their intrinsic conditions, such as endothermic nature of the reactions and the necessary high temperature and pressure, which render them overall expensive[10–12]. Meanwhile, biochemical CO_2 conversion by plants, algae and cyanobacteria already occurs naturally as photosynthesis, but by applying genetic engineering we can vastly expand the range of produced molecules to include bio-plastics and bio-fuels[13]. Another approach is taking inspiration from natural systems' capacity of using solar energy to drive CO_2 conversion and applying this concept to molecular systems, known as artificial photosynthesis. The basic principle in photochemical CO_2 conversion, involves light irradiation being absorbed by molecules (photosensitizers) who transfer the absorbed energy to photocatalysts that results in the reduction of tethered CO_2 molecules. While it is a very promising strategy that utilizes a renewable energy source, it still faces challenges in in terms of producing inexpensive and catalytically robust photocatalysts[14–17].

1.3 Electrochemical CO_2 Reduction Reaction (CO_2RR)

Other than the aforementioned conversion approaches, CO_2 can also be electrochemically converted to several different chemical compounds. This method, on which this thesis will focus on, is reliant on an electrical energy input to drive the CO_2 reduction[8,18–25]. However, the CO_2 molecule is intrinsically thermodynamically stable and as a consequence has a significant energetical barrier associated with its initial activation. Furthermore, in order to produce valuable reduction products, it is necessary to go through Proton Coupled Electron Transfer (PCET) reactions, that as their name suggests necessitate the presence of a certain number of protons and electrons. More specifically, the higher the necessary number of protons and electrons are, is also reflected on the kinetic barriers of the reaction. Another challenge related to CO_2 electroreduction is the presence of competing Hydrogen Evolution Reaction (HER), a side-reaction that especially in aqueous media occurs at similar potentials with CO_2RR and at appreciable catalytic rates. The thermodynamic potentials corresponding to CO_2RR to various products in aqueous and in some instances organic solutions are shown in Table 1.1.

Table 1.1 Thermodynamic CO_2 reduction potentials to various products and HER standard potential in aqueous conditions and in a dry acetonitrile solution, adapted from the literature[26]. [a]Potential value reported in reference[27]. [b]Potential value reported in reference[28].

Half reaction of electrochemical CO_2 reduction		Electrode potentials in aqueous solution at pH=7 (V vs SHE)	Electrode potentials in dry acetonitrile (V vs Fc+/Fc)
$CO_2 + 2H^+ + 2e^-$	HCO_2H	-0.61	
$CO_2 + 2H^+ + 2e^-$	$CO + H_2O$	-0.53	-0.12[a]
$CO_2 + 6H^+ + 6e^-$	$CH_3OH + H_2O$	-0.38	
$CO_2 + 8H^+ + 8e^-$	$CH_4 + 2H_2O$	-0.24	0.15[a]
$CO_2 + 12H^+ + 12e^-$	$CH_3CH_2OH + 3H_2O$	0.08	
$2H^+ + 2e^-$	H_2	-0.42	-0.07[b]

Those values are indicative of the minimum potential necessary for each reaction to take place. However, in reality due to kinetic parameters, such as overpotentials, much more negative potentials are required in order to form the reduction intermediates with multiple PCET that lead to these reduction products. In order to overcome these barriers, catalysts are employed in order to change the mechanistic pathway by lowering the activation energy to produce the necessary CO_2 reduction intermediates. A schematic representation of CO_2 electrocatalytic reduction with and without a catalyst is shown in Figure 1.3.

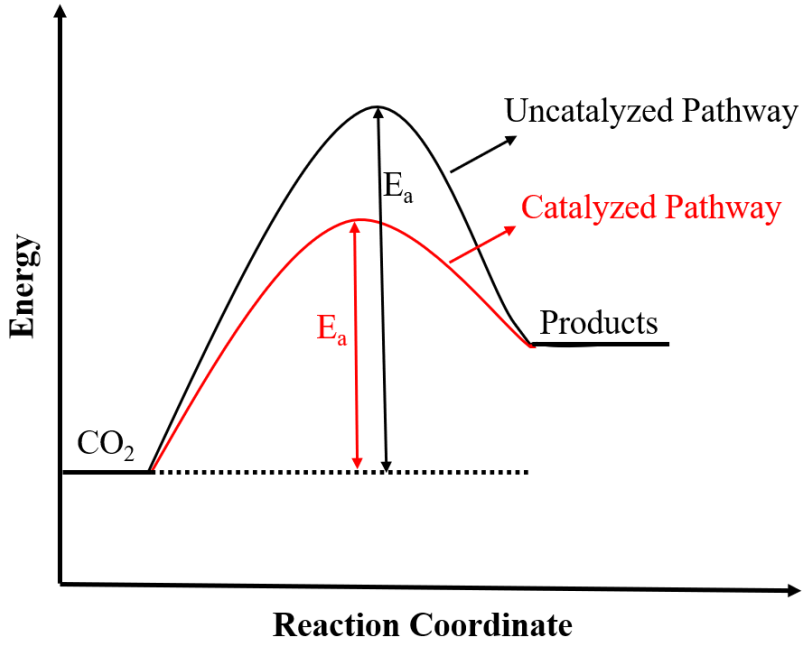

Figure 1.3 Schematic representation of a catalyst's effect on activation energy (E_a) for an endothermic reaction.

1.4 Important Parameters in CO_2 Electroreduction

The catalytic performance of any system is subject to various factors that govern the observed activity of CO_2RR, as well as its selectivity towards added value products. They include first and foremost the choice of catalyst, but equally the electrolyte composition. Other catalysis defining parameters are the electrode shape and configuration within the cell, the presence of co-factors, the CO_2 solubility, the potentials, the electrolyte and local pH, the temperature and pressure under which the electrochemical tests are conducted among others. All the aforementioned parameters have been duly investigated, sometimes even in combination to one another, but there is still room for improvement in our understanding of their effect on CO_2 electroreduction mechanism[18,29,30]. Here below special mention will be made to the factors that were studied during the thesis, as well as the literature necessary to put these studies into context.

1.4.1 Catalytic materials and their catalytic criteria

Electrocatalysts for CO_2RR are the primary defining characteristic of any catalytic system. Their vast majority can be sorted in three categories, either metallic, non-metallic or molecular catalysts[29]. In the first two cases, the electrode itself constitutes the catalytic material and as a consequence the CO_2RR is performed heterogeneously. Many metals have been explored for CO_2RR, often with appreciable catalytic performances and many have been sorted into categories based on the CO_2 reduction product they produce. For example, Ag, Au and Zn are known for CO_2 to CO conversion[31–33], while Sn, Pb, Bi and In selectively result in formate evolution[34–38]. Copper is a unique case, as it is the only element that can produce multi-carbon products, such as hydrocarbons and oxygenates[24,38]. Non-metallic materials have also possessed interesting features for CO_2RR. Under this umbrella fall many porous carbon materials, which through variable porosity and high surface area often exhibit admirable conductivity, good stability all while remaining highly competitive from an economic perspective[39,40]. The final main category of electrocatalysts are molecular catalysts that by either being added in the electrolyte solution or immobilized on the electrode surface can respectively reduce CO_2 homogeneously or heterogeneously[41,42].

1.4.2 Electrolyte composition, CO_2 solubility and pH effect

The catalytic environment is also a crucial parameter when optimizing CO_2RR. On the one hand water is often the solvent of choice because it is the most environmentally friendly and most inexpensive option, both key attributes for industrial applications. It is also in itself a proton source that helps the PCET necessary for decreasing CO_2 reduction barriers to take place. Appropriate conductivity and pH control can be assured by using buffer solutions as supporting electrolytes. Many of the CO_2RR

heterogeneous catalytic systems in aqueous conditions operate at neutral or slightly basic pH values.[29,43] The pH value of an aqueous solution is crucial as it can affect CO_2RR in different ways. Firstly, it regulates CO_2 solubility by determining the carbonic species present in solution according to equation 1, with increasing pH values shifting the balance firstly towards bicarbonate and then carbonate[43]. This is particularly problematic, since crossover of these species to the anode compartment during electrolysis will only regenerate CO_2[44].

$$CO_{2(aq)} + H_2O \leftrightarrow H_2CO_3 \leftrightarrow H^+ + HCO_3^{-2} \leftrightarrow 2H^+ + CO_3^{-2} \quad \text{eq 1}$$

Secondly, pH affects the thermodynamics of CO_2RR, as demonstrated by its Pourbaix diagram[45], with lower pH values reducing the necessary applied potential for CO_2 reduction. However, more acidic conditions equally favor the competing HER. In general, pH values are critical for the product selectivity of CO_2RR. For instance, in the case of copper it has been shown that highly basic conditions aid the C-C coupling of adsorbed *CO species on the electrodes, therefore leading in higher yields of C2 products, such as ethylene and ethanol.[24,38,46,47] Moreover, considering the overall cell potential values resulting from CO_2RR in the cathode coupled with oxygen evolution reaction (OER) in the anode, it was recently shown that a pH gradient between the two was beneficial in minimizing cell overpotential[48]. More specifically, since the most efficient OER catalytic materials are only stable in very alkaline conditions, it would be optimal in terms of energy efficiency to perform CO_2RR in neutral and even acidic conditions[48]. As a consequence, performing CO_2RR under acidic conditions would not only be of particular interest in terms of minimizing carbon loss as carbonate and bicarbonate, but could also help decrease cell potential values, if only under those conditions HER could also be suppressed. Recently, a couple of studies have demonstrated efficient and very selective CO_2RR in very acidic media (pH<1.5), using potassium cations (K^+) from the supporting electrolyte to suppress HER.[44,49] One focuses on copper in 1 M H_3PO_4 and 3 M KCl aqueous solution for multicarbon reduction products[44], while the second studies three carbon deposited catalytic materials SnO_2, Au and Cu in 0.1 M H_2SO_4 + 0.4 M K_2SO_4 aqueous solution resulting in mostly formate, CO and mixed carbon products respectively[49]. Nevertheless, use of water as an electrolyte comes with some drawbacks as well. First amongst them is the limited value of CO_2 solubility, only 33 mM at 25 °C[50]. Another limitation of aqueous conditions is that it often promotes HER at the expense of CO_2RR due to the large accessibility of protons. Finally, when working with molecular electrocatalysts, water as solvent is often not a viable option, because only few of them are soluble in aqueous solutions[42,51]. The aforementioned reasons lead to choosing non-aqueous electrolyte systems, such as various organic solvents (acetonitrile, dimethyl formamide or dimethyl sulfoxide etc.) and Ionic Liquids (ILs). Although organic solvents are inherently toxic and flammable, they also have significantly larger CO_2 solubility values than water, for example in acetonitrile that was used as solvent in this study CO_2 solubility is 280 mM at 25°C[52]. Other advantages

of non-aqueous solvents besides their ability to dissolve most molecular catalysts is that they often increase CO_2 reduction product selectivity by suppressing HER[53].

1.4.3 Other parameters (Cell design, temperature, pressure)

The efficiency of CO_2RR is subject to many more factors, one of which is the nature of the electrodes in terms of geometry, morphology and configuration within the cell where the electrocatalytic measurements take place. The reason for their importance is that they govern the current density, the product selectivity, as well as physical and electrochemical characteristics, such as the mass transfer regime of the system and the system's resistance while current is applied, also known as ohmic drop. The cell configuration most often used for bulk electrochemical CO_2RR as is the case during electrolysis experiments, is an H-type cell[54]. In this configuration there are two distinct compartments, one where reduction reaction takes place and another where species are oxidized, named cathode and anode, respectively. The two compartments have a physical separator between them, which in use with organic solvents is usually a frit and in aqueous conditions a membrane, that also adds resistance to the system. For this reason, the smallest possible distance between the working and counter electrodes, leads to minimized resistance (ohmic drop). The catholyte and anolyte compositions can be the same or not. In our case the same solvent and supporting electrolyte was used, but the molecular catalyst was only added in the cathodic compartment. In some cases, it is also possible to correct up to 85 % of the intrinsic IR drop by using the appropriate module of the potensiostat, making the actual applied potential as close in value to what we define for the electrochemical test[54,55]. Also, stirring both compartments of the H-type cell help minimize mass transport limitations. In the aforementioned conditions we are performing liquid-phase CO_2RR, where the CO_2 gas is either bubbled in the catholyte before electrolysis (static conditions), or the cell is not closed and CO_2 is continuously bubbled. An alternative to addressing the mass transport limitations and ohmic drop is to opt for gas-phase CO_2RR through the use of Gas Diffusion Electrodes (GDEs). In this case CO_2 does not need to be bubbled into the catholyte, but is fed instead through the electrode, ensuring that the reactant (CO_2), catalyst and electrolyte meet only on the electrode interface[56]. Finally, temperature and pressure factor in CO_2RR as well. According to Henry's law, CO_2 solubility increases along with increasing pressure, leading to improved CO_2 electrocatalysis[57]. In a CO_2 to CO reduction study on a silver electrode it was shown that increasing CO_2 pressure also led to higher current density values and favored CO evolution over HER[58]. Meanwhile, in the case of formate evolution from high-pressure CO_2 on tin, lead and indium electrodes, temperature was shown to affect selectivity, though the optimal temperature value that produced maximum formate faradaic efficiency (FE) was not the same for all electrodes tested[59].

1.5 Homogeneous molecular catalysts for CO_2 reduction

Molecular catalysts for CO_2 reduction have been developed over the past decades and are still evolving today thanks to their often-admirable activities, extraordinarily high selectivities towards CO_2RR and to the fact that they provide invaluable mechanistic insight into CO_2RR pathways.

In this thesis, two model molecular catalysts were used, one that selectively reduces CO_2 to CO and another that results in a mixture of formate and H_2. In Figure 1.4 we see some characteristic examples of molecular catalysts containing different metals and ligands that are all highly selective for CO_2 to CO conversion[41,42,60–62]. They all share the similarity that their ligands are bound through the N atom, in most cases the ligands themselves are aromatic in nature and they exhibit their catalytic activity in either organic and/or aqueous electrolyte, based on their respective solubilities. Meanwhile, other studies target electrocatalysts with non-noble metal centers like the Ni cyclam[60] and the substituted iron tetraphenylporphyrin[61] shown in Figure 1.4, we chose to work with the well-established model electrocatalyst [Re(bpy)(CO)$_3$Cl], known also as Lehn's catalyst[62,63]. Not only has its mechanism for CO_2RR been fully elaborated[63,64], but it has also been studied in different electrolytes, with several proton sources and various electron-withdrawing or electron-donating substitutions on its bipyridine ligand[64,65]. Finally and more importantly, the aim of this thesis being mainly to decipher the interactions that occur between molecular catalysts and ILs in order to optimize a CO_2RR catalytic system, this catalyst was particularly interesting because it had already been tested for CO_2RR in a pure IL[66].

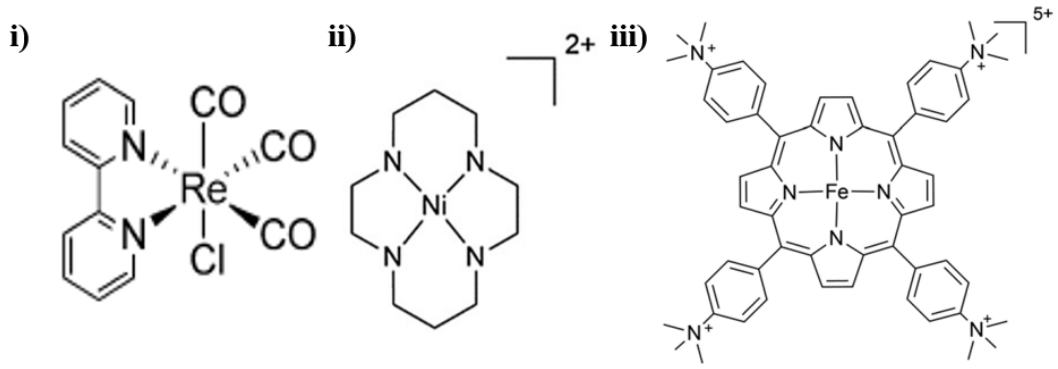

Catalyst	Electrolyte	FE_{CO} (%)	Reference
i)	DMF/H_2O	98	Lehn et. al., 1984[62]
ii)	H_2O, pH 4.1	96	Beley et. al., 1986[60]
iii)	H_2O, pH 6.7	98	Costentin et. al., 2015[61]

Figure 1.4 Structures of molecular catalysts for CO_2 to CO conversion alongside their electrolyte conditions and faradaic efficiency value for CO.

The second model molecular catalyst we have selected reduces CO_2 to formate and it is complex [Rh(bpy)(Cp*)Cl]Cl, represented in Figure 1.5 (b). In Figure 1.5 we see some characteristic examples of molecular catalysts whose principal reduction product is also formate[51,67–73]. The characteristic of these electrocatalysts is their ability to form hydride intermediates that result in C-H bonds, rather than HER which results from either recombination of two hydrides or protonation of one hydride. In the first-generation of electrocatalysts we find noble-metal complexes with bipyridine ligands[67–69] that can produce formate in a non-selective way. A newer generation of catalysts have since emerged that use second or third row metal centers. These metal centers are less nucleophilic, which results in suppressing HER. They also suppress C-O bond cleavage that results in CO production, therefore these complexes favor formate evolution. They include Iridium pincer complexes[71,72] and iron carbonyl clusters[73] that selectively produce formate in some cases even in aqueous media at appreciable rates.

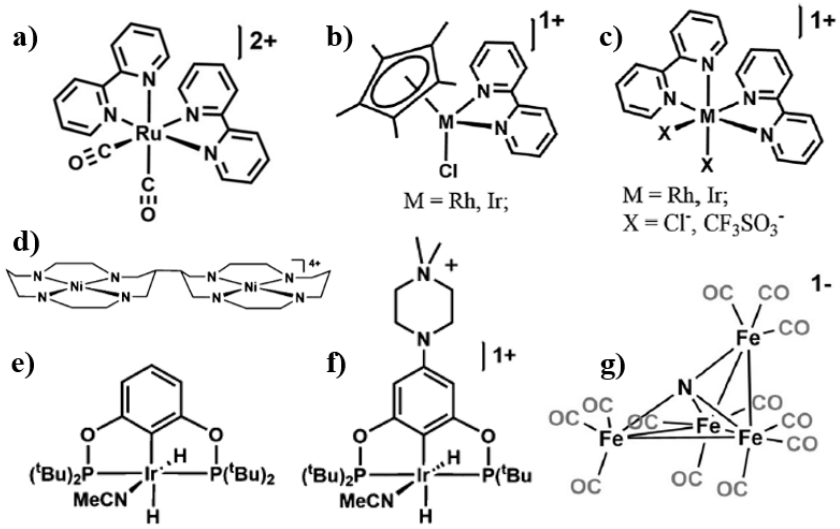

Catalyst	Electrolyte	FE_{HCOO^-} (%)	Reference
a)	CH_3CN/Me_2NH_2Cl	84	Ishida et. al., 1987[67]
b)	CH_3CN/ H_2O	50	Caix et. al., 1997[69]
c)	CH_3CN/TBAH	64	Bolinger et. al., 1985[68]
d)	DMF	75	Collin et. al., 1988[70]
e)	CH_3CN/4 % H_2O	86	Kang et. al., 2013[71]
f)	H_2O pH=7	93	Kang et. al., 2014[72]
g)	H_2O pH=7	96	Taheri et. al., 2015[73]

Figure 1.5 Structures of molecular catalysts for CO_2 to CO conversion alongside their electrolyte conditions and faradaic efficiency value.

The model catalyst we have chosen for our subsequent interaction with ILs study is the Rhodium catalyst depicted in Figure 1.5 b. Since its inception and initial electrochemical test in CH_3CN/H_2O mixtures, it

was for a long time neglected until its use in CO_2 photocatalysis[74] and incorporation in higher-order systems[75] brought it again to the forefront. While other examples of electrocatalysts that yield formate more selectively exist[71,73], it still constitutes an interesting model catalyst in terms of IL interaction, especially because it has a well-known catalytic mechanism and its product selectivity is heavily influenced by the reaction environment.

1.6 Ionic Liquids: From alternative solvents to catalysts for CO_2 reduction

Ionic Liquids (ILs) are salts in liquid state below 100 °C entirely comprised of organic cations and organic or inorganic anions. A subcategory of ILs are Room Temperature Ionic Liquids (RTILs), which are in liquid form below 25 °C. In contrast, normal salts that also consist entirely of anions and cations also possess high melting points due to their strong ionic bond. Therefore, liquidifying them by heating, for example reaching 801 °C for NaCl, renders them molten salts[76,77]. On the contrary, in ILs the cation and anion are typically asymmetric and lead to sterical hinderance that weakens their bonding and as a result lowers their melting point. Although the first IL, $[CH_3CH_2NH_3][NO_3]$, was synthesized in the early 20th century[78], their involvment in many industrial applications and especially the field of electrochemistry was after the dicovery of the air and water stable RTIL 1-ethyl-3-methylimidazolium tetrafluoroborate [EMIM][BF_4], in the early nineties by Wilke's group[79,80]. Their huge number estimated to exceed 10^6,[79] necessitates their classification. This can be based on their ability to be water-miscible or not, or their ability to act as a proton source by possessing an available proton in their cation, in which case they are characterized as protic, while if they do not, they are considered aprotic[81,82]. Another way to sort them into categories is based on the family of the cation, which can be base on an aromatic ring like imidazolium, pyrrolinium, pyridinium etc., a non-aromatic ring such as pyrrolidinium, piperidinium etc. or a heteroatom-cetrered polyaliphatic compound, as is the case with ammonium, sulfonium or phosphonium to name a few. Equally, we can categorize ILs based on their anions, whether they are inorganic, like the following examples: PF_6^-, BF_4^-, BCN_4^-, Br^-, Cl^-, etc. or organic, such as CH_3COO^-, $N(SO_2CF_3)_2^-$, amongst others. In this thesis, we will concentrate our study on imidazolium and pyrrolidinium based ILs seen here in Figure 1.6, which is the reason why we should also define their nomeclature. Especially imidazolium-based ILs have several possible abbreviations, that have been regrouped in three main systems[77]. For example 1-ethyl-3-methylimidazolium can be abbreviated as $[C_2mim]^+$, $[C_2C_1Im]^+$ or as it will be abbreviated in this thesis, $[EMIM]^+$. In such examples "E", "B" and "M" stand for "ethyl" and "butyl" and "methyl" alkyl chain groups respectively, the first letter representing the R_1 and the second the R_2 group on the imidazolium ring. Based on this abbreviation

system, a pyrrolidinium based IL with R_1 = "butyl" and R_2 = "methyl" groups would be abbreviated $[BMPyrr]^+$.

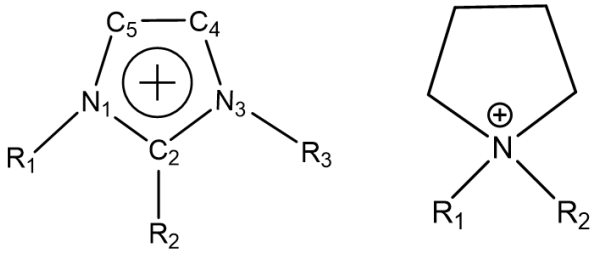

Imidazolium Pyrrolidinium

Figure 1.6 Structure of imidazolium and pyrrolidinium IL cations.

1.6.1 Ionic Liquids as solvents

ILs have been considered as alternative non-aqueous solvents compared to organic solvents that though valuable, also come with a host of inconveniences such as toxicity and flammability. ILs as solvents on the other hand, possess many interesting properties. Especially considering the immense number of possible cation and anion combinations, it is also possible to tune their physicochemical properties to the needs of many electrochemical systems[81,83]. ILs are generally stable over a large thermal window ranging from approximatively -40 °C up to 300 °C[84] and an electrochemical window wide enough to perform many electrochemical processes, such as CO_2RR. Their electrochemical window is confined by the reduction of some IL cations and likewise the oxidation some anions and any present impurities, such as water, can further diminish the IL's range of electrochemical stability[81,85,86]. However, their inherent ionic nature renders them highly conductive, therefore they could act as supporting electrolyte as well as solvent[87]. This fact is furthermore linked to their high dissolving ability, that means ILs have the capacity to dissolve a variety of organic and inorganic compounds including gases like CO_2. More specifically, the CO_2-solubilities of some conventional ILs have been determined and as an example the commonly used imidazolium-based [BMIM][BF_4] can have up to 111 mM of CO_2 dissolved[88], which would place it rather in the middle between the poor CO_2 solubility of water (33 mM)[77] and the superior one of organic solvents, such as acetonitrile (280 mM)[52]. Moreover, ILs by definition have low melting points and are non-volatile compounds, which is useful in terms of preventing loss of solvent and for applications that require high vacuum conditions[89]. However, despite all the aforementioned advantageous features, ILs suffer from high viscosity. High viscosity is problematic in terms of electrochemistry because viscosity is inversely correlated to the conductivity and diffusion of soluble species in the solvent and as a result leads to significant decrease in the maximum current density possible[77]. As a consequence, use of ILs as supporting electrolytes in organic or aqueous conditions is a way to circumvent their high viscosity while maintaining to some degree some of their interesting

properties and it is the strategy chosen in this thesis. Another inconvenience sometimes encountered when using ILs is their hydricity. Water uptake may vary based on the structure of their cations and anions of ILs, but it has been associated with altering their redox behavior[90].

1.6.2 Ionic Liquids as CO_2RR catalysts and co-catalysts

Besides any possible benefits of using ILs as solvent or electrolyte, in the context of CO_2RR one of their main functions is to enhance the catalytic effect. The initial study on the topic was conducted by Rosen et. al.[91] group demonstrating the beneficial role of using an IL on CO_2RR overpotential diminution. More specifically, they reported that the presence of 18 mol % of [EMIM][BF_4] in water significantly reduced the overpotential of a silver electrode for CO_2RR, as represented in Figure 1.7 (a). They proposed that the decrease in the energy of anion radical intermediate $CO_2^{\cdot-}$ in presence of this IL is due to an adduct being formed {EMIM-CO_2}[91]. Since that seminal work, several studies have explored the effect of ILs on promoting heterogeneous CO_2RR[92]. Imidazolium-based ILs were also added in acetonitrile solutions as co-catalysts and/or supporting electrolytes, with additional conventional supporting electrolyte, tetrabutylammonium hexafluorophosphate [TBA][PF_6] in acetonitrile whenever necessary[93–97]. However, other types of ILs, such as guanidinium ILs have also been proven to act as co-catalysts in acetonitrile solutions and having a CO_2RR promoting effect[98]. Furthermore, low concentrations of ILs, as much as 20 mM[96] or 2 mM[97] have been demonstrated to produce a co-catalytic effect on silver electrodes. In those studies, it is also shown that the IL catalytic effect varies based on the nature of the imidazolium cation, but the anion is apparently not significant in tuning their CO_2RR-promoting properties[96,97].

Concerning the mechanism by which ILs promote CO_2RR many studies have been conducted. In the case of imidazolium-based ILs, many endorse Rosen's theory of an {EMIM-CO_2} complex, but different mechanisms have been proposed based on experimental and calculated intermediates and products[99,100]. Important positions of the imidazolium ring are the C2 position, which is the more electron depleted atom and as a consequence considered the reduction site[101] and the C4, C5 atoms that can anchor adsorbed CO_2 by hydrogen bonding[96]. An important distinction has however been made between imidazolium and other families of ILs in a study where 20 different ILs were tested for promoting the CO_2RR catalytic effect on a silver electrode. It concluded that only imidazolium-based ILs are in fact acting as co-catalysts, while other IL cations promote CO_2RR through modification of the double layer (Figure 1.7 b)[97]. An important note should also be made in regards to ILs HER suppression effect. It has been demonstrated on various metallic electrodes, that the addition of 0.1 M [EMIM]Cl in acidic aqueous conditions (pH=1) can lead to significant HER inhibition[102]. On the contrary, under basic conditions (pH=13) this effect is not observed. This effect under acidic conditions was rationalized by the ability of imidazolium cations to interact with the electrodes themselves and therefore displacing hydronium

cations, which leads to fewer active sites for HER. Meanwhile, under basic conditions the positively charged imidazolium cations cannot displace the diffusion of neutral water molecules[102].

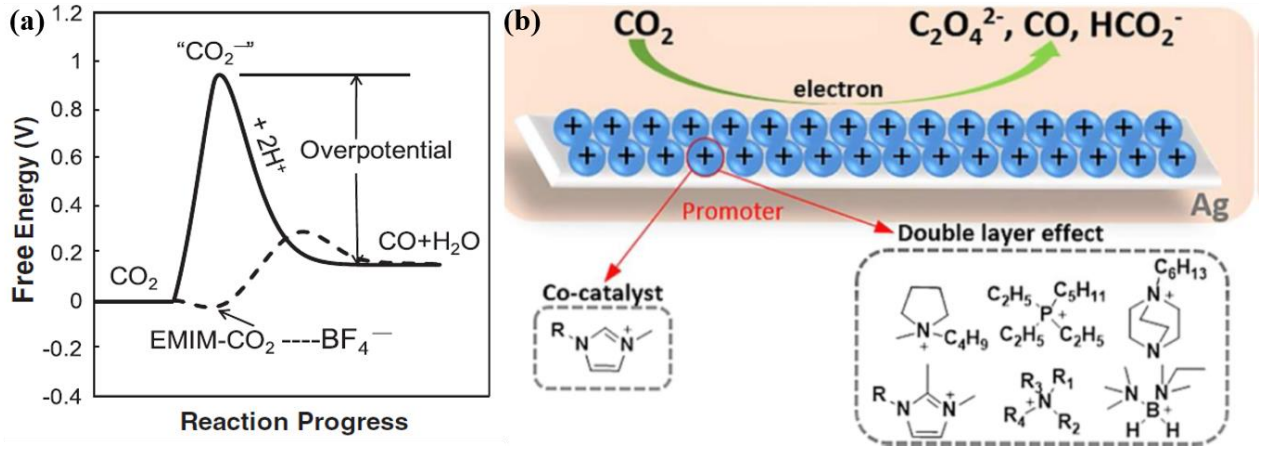

Figure 1.7 Schematic effect of ILs in CO_2 electroreduction. (a) Free energy profile on a silver electrode in either water or acetonitrile (solid plot) or in a water/IL ([EMIM][BF_4]) mixture (dashed plot)[91] *and (b) Diagram of the effect of 2 mM of different ILs as CO_2 reduction promoters on a silver electrode in an acetonitrile solution containing 0.1M [TBA][PF_6]*[97].

1.6.3 Ionic Liquid reduction and immobilization

Another interesting feature of imidazolium-based ILs is their ability to be reduced and result in different catalytic species. This reduction feature is dependent on the electrode material, as we can see in Figure 1.8 a and can occurs at potentials as low as -2.5 V *vs.* Fc^+/Fc in some cases. It is then followed by a oxidation wave around -0.65 V, which has been attributed to the reoxidation of these reduced species[103]. Understanding the nature of these new species derived from the reduced and reoxidized imidazolium can be based on NMR studies of the liquid and gas phase before and after running short electrolysis on Cu, Pt, Au and Hg under an inert atmosphere[86,103]. Possible forms of the produced molecules are shown in Figure 1.8 b[86], though their distribution varies based on the electrode material. This has been correlated to each electrode's ability to adsorb hydrogen, as well as the availability of protons in the solution. In the theoretical scheme presented in Figure 1.8 b, an initial one-electron reduction of an imidazolium leads to an imidazol-2-yl radical (**2**), which can either decompose towards a carbene (**3**) and hydrogen, recombine with another imidazol-2-yl radical to result in a neutral dimer (**4**) or disproportionate that leads to the neutral hydrogenated monomer (**5**). From all these compounds the intermediate and product analysis led to the conclusion that the most present species are the two diastereomers of the neutral dimer (**4**), with a smaller contribution of the hydrogenated monomer (**5**) and the carbene (**3**)[86,103]. This study also mentions that no carbenes were detected, not any of the species named **6**-**9**[86].

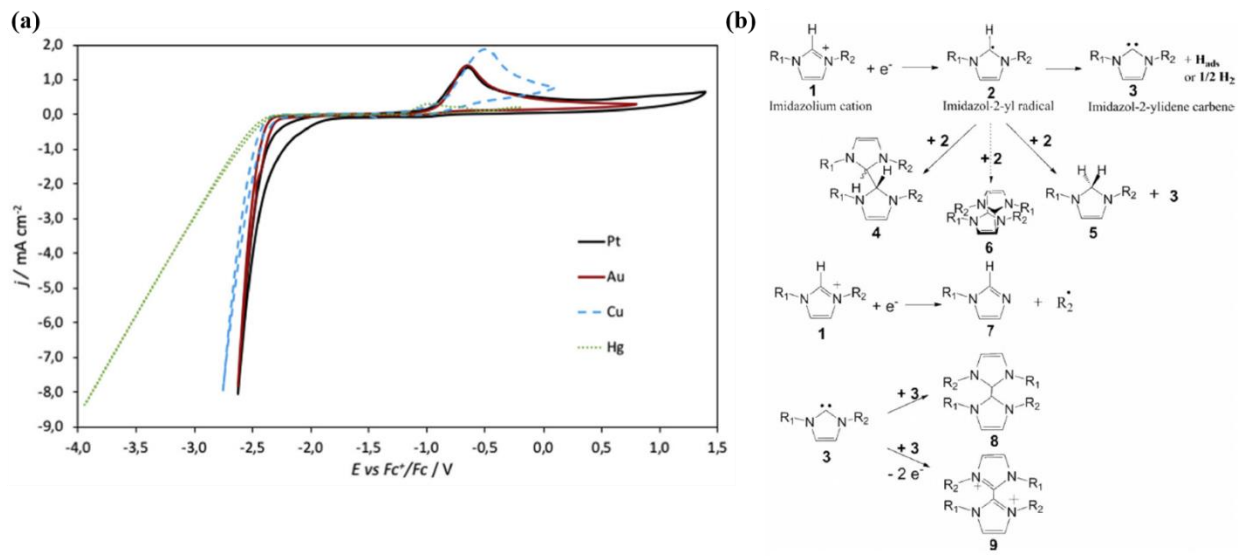

Figure 1.8 (a) Cyclic voltammograms of pure IL [BMIm][NTf2] on Hg, Cu, Au and Pt electrodes under a nitrogen atmosphere. Scan rate = 0.05 V/s, 5th scan shown[86] *and (b) Schematic representation of all suggested cathodic pathways of converting dialkylimidazolium ILs*[103].

Moreover, [EMIM][BF_4] has been reported to form a electrochemical layer on the Cu surface that can suppress HER in favor of CO_2RR[104]. In this study, the HER suppression effect was not solely observed on an initial CV, that is in accordance with $[EMIM]^+$ adsorption on the electrode surface[102], but persisted and even strengthened in consecutive scans, which the authors attribute to a reaction of electrochemical nature between the electrode surface and the IL[104].

1.7 Co-catalytic effect of molecular catalysts and Ionic Liquids

While both molecular catalysts and ILs have been extensively explored independently in catalytic CO_2RR, much less effort has been devoted to studying their combined effect. This is especially evident in homogeneous CO_2RR, where both molecular catalyst and IL coexist in the electrolyte solution. To the best of our knowledge, so far only two types of complexes have been used thus in conjuncture with ILs, Lehn's catalyst ([Re(bpy)$(CO)_3$Cl]) and Iron tetraphenylporphyrin (FeTPP)[66,105,106]. In the case of the former, it was initially demonstrated that when used in pure IL electrolyte, more particularly in [EMIM][TCB], where TCB stands for tetracyanoborate, the onset potential for CO_2RR was shifted anodically by approximatively 450 mV in comparison to when acetonitrile is the solvent and [TBA][PF_6] the supporting electrolyte. Furthermore, while the viscosity of the IL did impair the catalytic current density, the rate constant for CO_2RR was still estimated to have increased by as much as forty times. Both the diminution in overpotential and the increase in the rate constant were attributed to the presence of the IL and the synergistic effect it exerted with Lehn's catalyst[66]. Further study was then conducted

with the same catalyst and varying concentrations of the same IL, but this time in acetonitrile already containing the conventional supporting electrolyte [TBA][PF_6], as well as a benzoic acid (BzOH) used as a proton source. These conditions were investigated by linear sweep voltammetry (LSV) and the observations were that though the gain in overpotential was still apparent as in the purely IL reaction environment, there was no particular effect of the IL on the catalytic current density[105]. Moreover, this study also explored the effect of another IL, [EMIM][PF_6], in order to determine whether the IL anion also affected catalytic performance. This comparison of Lehn's catalyst in acetonitrile with either [EMIM][PF_6] or [EMIM][TCB] *versus* [TBA][PF_6] is shown in the adapted Figure 1.6 (a) and clearly shows that the co-catalytic effect with this molecular catalyst is due to the imidazolium cation and not on the anion present. Further theoretical calculations were conducted to determine the form of the CO_2RR intermediates in presence of IL and benzoic acid and concluded that most likely the imidazolium firstly stabilizes the 2-electron reduced form of the catalyst. This is achieved by the positive charge delocalized on the imidazolium cycle that aids the formation of metallocarboxylate (Re-CO_2) by diminishing the energy of its π orbitals. More particularly, the lowest energy configuration of the catalyst has the imidazolium stacked on top of it, with the imidazolium interacting by π-π stacking with the bipyridine ligand of the molecular complex[105].

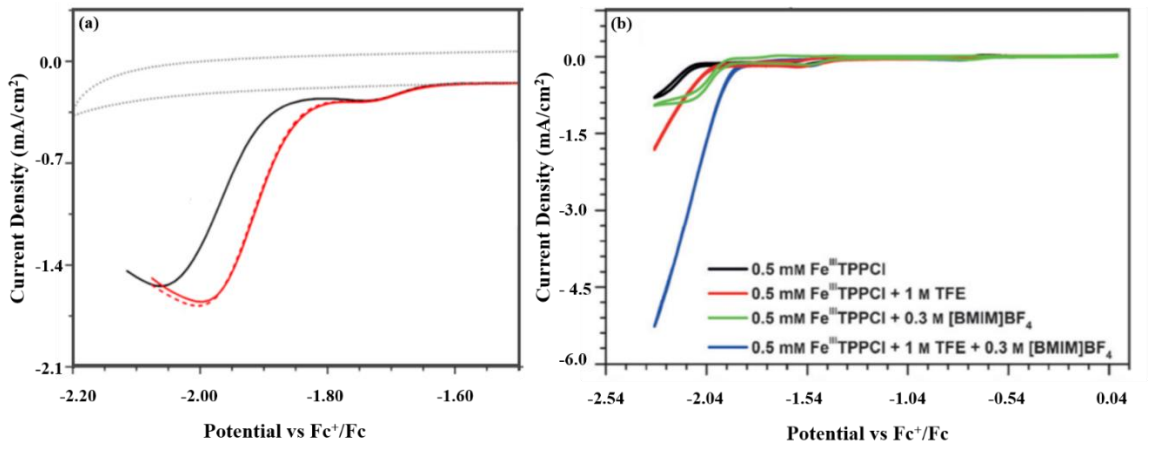

Figure 1.9 Voltammograms of molecular catalysts in organic solvents containing ILs: (a) LSVs (scan rate = 0.35 V/s) of 0.5 mM [Re(bpy)(CO)$_3$Cl] in a CO_2-saturated acetonitrile solution containing 1.08 M [TBA][PF_6], 0.02 M of both BzOH and [TBA][BzO] and 0.1 M of the following supporting electrolytes: [EMIM][TCB] (solid red plot), [EMIM][PF_6] (dashed red plot), [TBA][PF_6] (black plot) and [EMIM][TCB] without the molecular catalyst in solution (dashed grey plot). Adapted from Matsubara et. al.[105] *and (b) CVs (scan rate = 0.05 V/s) of 0.5 mM FeTPP in a CO_2-saturated DMF solution containing: 0.1 M [TBA][PF_6] (black plot), 0.1 M [TBA][PF_6] and 1 M TFE (red plot), 0.1 M [TBA][PF_6] and 0.3 M [BMIM][BF_4] (green plot) and 0.1 M [TBA][PF_6], 0.3 M [BMIM][BF_4], 1 M TFE (blue plot). Adapted from Choi et. al.*[106]

The second example of a molecular catalyst used in solution alongside ILs for CO_2RR is FeTPP tested in N,N-Dimethylformamide (DMF) based electrolyte containing 2,2,2-trifluoroethanol (TFE) as a proton source[106]. The IL used in this study is 1-butyl-3-methylimidazolium tetrafluoroborate, [BMIM][BF_4], at a concentration of 0.3 M and the added proton source is TFE. The cyclic voltammograms under a CO_2 atmosphere with different combinations of all the aforementioned elements are shown in the adapted Figure 1.6 b. In it we can see that the addition of the IL in conjuncture with a proton source leads to an overpotential diminution of approximatively 200 mV and a quadrupling of the observed catalytic current density. Furthermore, the fact that the mere addition of the IL without a proton source present or *vice versa* does not lead to a significant increase in catalytic current suggests that the IL does not act as a proton source, nor is its beneficial effect due to direct interaction between the imidazolium and CO_2. Instead, it is shown that this IL shifts the potentials of FeTPP's reduction waves less negatively and especially the third electron reduction from Fe^I to Fe^0 that is associated with CO_2 reduction. This co-catalytic effect is then attributed to electrostatic stabilization of the negatively-charged reduced catalyst forms $[Fe^ITPP]^-$ and $[Fe^0TPP]^{2-}$ by the imidazolium cation. Finally, another interesting note is the effect of this imidazolium IL on the molecular catalyst selectivity by bulk electrolysis experiments. This demonstrates that when electrolysis was run in presence of the IL, not only could the applied potential be decreased by 190 mV, but it also resulted to more CO produced, the average FE with IL being 93 % *versus* 89 % when there was no addition of IL[106]. Therefore, as we can also see in Figure 1.6, the presence of an imidazolium-based IL led to positive shifts in overpotential in both molecular catalysts and it was attributed to favorable interactions of the imidazolium cation with the catalyst itself. However, the nature of the IL used and its role on the synergistic effect with molecular catalysts for CO_2RR is still to be fully elucidated and will be the subject of study in Chapter 3.

However, other strategies to achieve the combined effect of molecular catalysts and ILs outside having both those components in solution also exist. Though these approaches were not explored in the present thesis, it would be remiss to not mention them. One of them consists in incorporating an IL moiety and more specifically an imidazolium ring, into the structure of the molecular catalyst itself leading to the synthesis of a novel catalyst. Interestingly and also understandably, the two examples of this technique use as scaffold the model catalysts already described with an IL in solution, namely Lehn's catalyst and FeTPP[107,108]. Both structures are represented in Figure 1.7. In the case of the Rhenium catalyst, the functionalization with the imidazolium ring results in anodic shift in the catalysts reduction potentials of approximatively 170 mV compared to the Lehn's catalyst in a CO_2-saturated acetonitrile solution. Moreover, when electrolysis was run for both imidazolium-functionalized and catalyst depicted in Figure 1.10 a at the same potential (-1.77 V *vs.* Fc^+/Fc) for the span of one hour in presence of 9.4 M of H_2O as proton source, the former consumed more charge and resulted in higher CO selectivity, namely 73 % against only 54 % from the catalyst[107].

The other example of imidazolium-functionalized molecular catalyst is a FeTPP containing four methylimidazolium units appended on the porphyrin macrocycle that result in four positively charged 'arms', as depicted in Figure 1.7 b[108]. The presence of these imidazolium units produces significant positive shifts in the catalyst's potential under inert and CO_2 atmospheres in a 9/1 DMF/H_2O with 0.1 M [TBA][PF_6] electrolyte mixture. More specifically, under CO_2 the decrease in overpotential can reach up to 375 mV compared to the non-functionalized FeTPP under the same catalytic conditions. More interesting still, is the fact that the functionalized FeTPP is not only rendered water-soluble by the imidazolium units, but it also displayed higher values of catalytic current density in water than in the DMF/H_2O conditions. This effect, though counter intuitive considering the diminished CO_2 solubility in H_2O compared to DMF, the authors suggest it is explained through the relative permittivity values of both solvents. Since the beneficial effect of imidazolium units has been assigned to electrostatic stabilization of the negatively charged $[FeTPPCO_2]^{2-}$ adduct by the imidazolium cations, their degree of availability is key. If the solvent permittivity is higher, as is the case in water, the dissociation of the IL units comprised of imidazolium cations and chloride anions in solution is higher and therefore the imidazolium groups are more available to participate in Coulombic stabilizing interactions with the catalyst's negative intermediates[108].

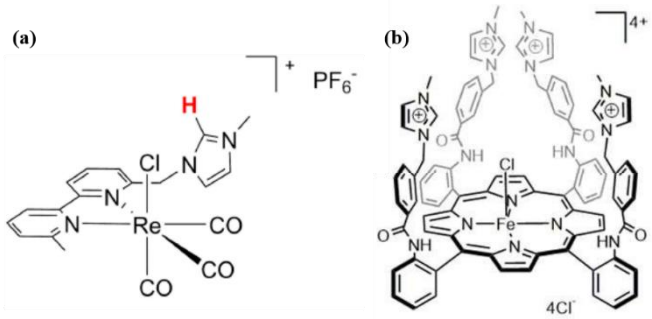

Figure 1.10 Structures of molecular catalysts functionalized with IL moieties: (a) {Re[bpyMe(ImMe)](CO)$_3$Cl}[PF_6] catalyst, where bpyMe(ImMe) is an ortho methyl-bipyridine bearing a methylimidazolium arm on one side[107] *and (b) Iron tetraphenyl porphyrin with four methylimidazolium units attached on the periphery of the porphyrin ligand*[108] .

1.8 Flow electrolyzers: State of the art and incorporation of molecular catalysts

Flow electrolyzers are commonly used to prove the scalability of electrochemical systems from the laboratory environment to the industrial scale. Most studies in flow electrolyzers for CO_2RR use heterogeneous catalysts but the use of those materials leads to questions about the exact nature and density of the active sites that result in CO_2RR products and cannot provide detailed mechanistic insight

into the structure-activity relationship at play that is crucial for optimizing CO_2RR[109]. In contrast, molecular catalysts are by nature well-defined, often extremely selective towards one CO_2RR product, easily tunable through simple synthetic pathways. We can distinguish two different approaches: i) molecular catalysts in solution, in which the CO_2 is bubbled in solution only, and ii) molecular catalysts heterogenized supported on the electrode, in which the CO_2 is bubbled in solution or GDE. So far only a few other examples of molecular CO_2 electrocatalysts in flow electrolyzers exist and most of them involve heterogenized catalysts[109–113]. To the best of our knowledge, the only homogeneous catalyst used in a flow electrolyzer to date for CO_2RR was $[Ni(cyclam)]^{2+}$. This catalyst was used in two organic solutions (ACN and N, N-DMF) in a flow electrolyzer with recirculating flow of the catholyte solution[114].

Most examples of molecular catalysts in flow electrolyzers concern heterogenized catalysts[109–113,115–117]. The process of immobilizing molecular catalysts on solid supports, which are then used in flow electrolyzers. This strategy is advantageous, as it results in higher catalytic efficiency for these molecular systems, that combine elements of molecular and heterogeneous catalysis. Nevertheless, using heterogenized molecular catalysts in flow electrolyzers also presents a disadvantage when considered at an industrial scale. That is the result of increased cost and energy expenditure from having to regularly turn the electrolyzer off-line for catalyst replacement. On the contrary, by using a homogeneous catalyst, the reaction can take place continuously, which is not only economically preferable, but also integral to green chemistry[118].

1.9 Purpose and objectives of the thesis

Performing efficient CO_2RR under environmentally-friendly conditions is a challenge that must be addressed. When approaching this question through electrochemistry, both the choice of catalyst and reaction environment arise as important issues, that should be discussed in relation to one another in order to provide information necessary to develop optimized catalytic systems. The well-defined mechanistic pathways of some molecular catalysts make them ideal models to study this interaction. Meanwhile, the use of ILs as potential alternative electrolytes and CO_2RR co-catalysts is also promising. Nevertheless, rationalization of the interactions of ILs with molecular catalysts was yet to be performed at the beginning of this thesis. The few studies present[66,105,106] demonstrated beneficial catalytic effects from combining molecular catalysts and ILs, but without providing all necessary background on how the nature of the catalyst and the IL impact their interaction.

The objectives of this thesis are thus:

1. To investigate the nature of interaction between ILs and model molecular catalysts.

2. To explore electrolyte engineering and IL immobilization to improve CO_2RR with molecular catalysts.
3. To provide proof of scaling-up the most interesting catalytic system within a flow electrolyzer.

The outline of the thesis is as following:

In Chapter 2, all the reagents and materials involved, as well as instruments used throughout this thesis will be introduced. Besides, electrochemical processes and general operational procedures will be described. Furthermore, the characterization methods and techniques used will be introduced, providing information on the instrument type and configuration. Finally, some inorganic complex synthesis protocols will be included.

In Chapter 3, two model molecular catalysts are used for homogeneous CO_2RR in electrolyte solutions containing 0.5 M of different ILs. Initially, [Re(bpy)$(CO)_3$Cl] is chosen as a model for its high selectivity for CO evolution and its well-established reaction mechanism for CO_2RR. It is subsequently tested in acetonitrile solutions containing a series of ILs in order to determine what features of ILs govern their interaction with the catalyst. Product selectivity is also assessed by electrolysis to determine whether there is an IL effect. Secondly, another model catalyst is chosen, [Rh(bpy)(Cp*)Cl]Cl, this time because its product selectivity is very sensitive to changes in the reaction environment and is active towards both HER and CO_2RR. Cyclic voltammetry studies with ILs in solution are followed by selectivity studies to decipher how ILs impact the activity of this catalyst. The solubility of this catalyst in water, also allows to explore this effect in different electrolyte compositions. Finally, theoretical calculations are provided to corroborate mechanistic explanations of how ILs impact both those catalysts in different ways.

In Chapter 4 an immobilization method for ILs is presented and its CO_2RR effect is assessed with the help of model catalyst [Rh(bpy)(Cp*)Cl]Cl. Optimization studies of this electrodeposited IL layer are presented, while many parameters are investigated. The catalytic effect of said layer on [Rh(bpy)(Cp*)Cl]Cl catalyst is also compared to the effect produced by IL in solution and a covalently attached IL layer. This test is shown in different electrolyte compositions and the comparison is used to draw conclusions on the nature of the electrodeposited IL layer. Its effect on HER is equally investigated, alongside characterization by XPS and CV. Finally, its effect on the product selectivity of the molecular catalyst is assessed by electrolysis.

In Chapter 5 a flow electrolyzer setup is used to scale-up the previously described system of molecular catalyst [Rh(bpy)(Cp*)Cl]Cl in acidic aqueous conditions and in the presence of the electrodeposited IL layer. Through investigation of different electrolyzer configurations, a final setup is presented that allows testing the electrodeposited layer on GDE compared to a bare GDE with the molecular catalyst in solution for charge passed up to 1000 C.

Finally, in Chapter 6 are presented the overall conclusions drawn from the ensemble of the thesis, as well as future directions for this research.

1.10 References

(1) US Department of Commerce, N. Global Monitoring Laboratory - Carbon Cycle Greenhouse Gases https://gml.noaa.gov/ccgg/trends/mlo.html.

(2) *Climate Change 2021: The Physical Science Basis. Contribution of Working Group I to the Sixth Assessment Report of the Intergovernmental Panel on Climate Change*; Masson-Delmotte, V., Zhai, P., Pirani, A., Connors, S. L., Péan, C., Berger, S., Caud, N., Chen, Y., Goldfarb, L., Gomis, M. I., Huang, M., Leitzell, K., Lonnoy, E., Matthews, J. B. R., Maycock, T. K., Waterfield, T., Yelekçi, Ö., Yu, R., Zhou, B., Eds.; Cambridge University Press, 2021.

(3) Global Temperature and Carbon Dioxide https://www.globalchange.gov/browse/multimedia/global-temperature-and-carbon-dioxide.

(4) Orr, J. C.; Fabry, V. J.; Aumont, O.; Bopp, L.; Doney, S. C.; Feely, R. A.; Gnanadesikan, A.; Gruber, N.; Ishida, A.; Joos, F.; Key, R. M.; Lindsay, K.; Maier-Reimer, E.; Matear, R.; Monfray, P.; Mouchet, A.; Najjar, R. G.; Plattner, G.-K.; Rodgers, K. B.; Sabine, C. L.; Sarmiento, J. L.; Schlitzer, R.; Slater, R. D.; Totterdell, I. J.; Weirig, M.-F.; Yamanaka, Y.; Yool, A. Anthropogenic Ocean Acidification over the Twenty-First Century and Its Impact on Calcifying Organisms. *Nature* **2005**, *437* (7059), 681–686. https://doi.org/10.1038/nature04095.

(5) Cox, P. M.; Betts, R. A.; Jones, C. D.; Spall, S. A.; Totterdell, I. J. Acceleration of Global Warming Due to Carbon-Cycle Feedbacks in a Coupled Climate Model. *Nature* **2000**, *408* (6809), 184–187. https://doi.org/10.1038/35041539.

(6) Bui, M.; Adjiman, C. S.; Bardow, A.; Anthony, E. J.; Boston, A.; Brown, S.; Fennell, P. S.; Fuss, S.; Galindo, A.; Hackett, L. A.; Hallett, J. P.; Herzog, H. J.; Jackson, G.; Kemper, J.; Krevor, S.; Maitland, G. C.; Matuszewski, M.; Metcalfe, I. S.; Petit, C.; Puxty, G.; Reimer, J.; Reiner, D. M.; Rubin, E. S.; Scott, S. A.; Shah, N.; Smit, B.; Trusler, J. P. M.; Webley, P.; Wilcox, J.; Dowell, N. M. Carbon Capture and Storage (CCS): The Way Forward. *Energy Environ. Sci.* **2018**, *11* (5), 1062–1176. https://doi.org/10.1039/C7EE02342A.

(7) Spinner, N. S.; Vega, J. A.; Mustain, W. E. Recent Progress in the Electrochemical Conversion and Utilization of CO_2. *Catal. Sci. Technol.* **2011**, *2* (1), 19–28. https://doi.org/10.1039/C1CY00314C.

(8) Lee, M.-Y.; Park, K. T.; Lee, W.; Lim, H.; Kwon, Y.; Kang, S. Current Achievements and the Future Direction of Electrochemical CO_2 Reduction: A Short Review. *Crit. Rev. Environ. Sci. Technol.* **2020**, *50* (8), 769–815. https://doi.org/10.1080/10643389.2019.1631991.

(9) Developments and Innovation in Carbon Dioxide (CO_2) Capture and Storage Technology - 1st Edition, Editor: M. Mercedes Maroto-Valer, https://www.elsevier.com/books/developments-and-innovation-in-carbon-dioxide-co2-capture-and-storage-technology/maroto-valer/978-1-84569-533-0.

(10) Saito, M.; Takeuchi, M.; Watanabe, T.; Toyir, J.; Luo, S.; Wu, J. Methanol Synthesis from CO_2 and H2 over a CuZnO-Based Multicomponent Catalyst. *Energy Convers. Manag.* **1997**, *38*, S403–S408. https://doi.org/10.1016/S0196-8904(96)00302-0.

(11) Parvez, A. M.; Afzal, M. T.; Victor Hebb, T. G.; Schmid, M. Utilization of CO_2 in Thermochemical Conversion of Biomass for Enhanced Product Properties: A Review. *J. CO2 Util.* **2020**, *40*, 101217. https://doi.org/10.1016/j.jcou.2020.101217.

(12) Olah, G. A.; Goeppert, A.; Prakash, G. K. S. Chemical Recycling of Carbon Dioxide to Methanol and Dimethyl Ether: From Greenhouse Gas to Renewable, Environmentally Carbon Neutral Fuels and Synthetic Hydrocarbons. *J. Org. Chem.* **2009**, *74* (2), 487–498. https://doi.org/10.1021/jo801260f.

(13) Jajesniak, P.; Ali, H. E. M. O.; Wong, T. S. Carbon Dioxide Capture and Utilization Using Biological Systems: Opportunities and Challenges. *J. Bioprocess. Biotech.* **2014**, *4* (3), 1–15. https://doi.org/10.4172/2155-9821.1000155.

(14) Kumar, B.; Llorente, M.; Froehlich, J.; Dang, T.; Sathrum, A.; Kubiak, C. P. Photochemical and Photoelectrochemical Reduction of CO_2. *Annu. Rev. Phys. Chem.* **2012**, *63* (1), 541–569. https://doi.org/10.1146/annurev-physchem-032511-143759.

(15) Li, K.; An, X.; Park, K. H.; Khraisheh, M.; Tang, J. A Critical Review of CO_2 Photoconversion: Catalysts and Reactors. *Catal. Today* **2014**, *224*, 3–12. https://doi.org/10.1016/j.cattod.2013.12.006.
(16) Tu, W.; Zhou, Y.; Zou, Z. Photocatalytic Conversion of CO_2 into Renewable Hydrocarbon Fuels: State-of-the-Art Accomplishment, Challenges, and Prospects. *Adv. Mater.* **2014**, *26* (27), 4607–4626. https://doi.org/10.1002/adma.201400087.
(17) Tahir, M.; Amin, N. S. Recycling of Carbon Dioxide to Renewable Fuels by Photocatalysis: Prospects and Challenges. *Renew. Sustain. Energy Rev.* **2013**, *25*, 560–579. https://doi.org/10.1016/j.rser.2013.05.027.
(18) Senocrate, A.; Battaglia, C. Electrochemical CO_2 Reduction at Room Temperature: Status and Perspectives. *J. Energy Storage* **2021**, *36*, 102373. https://doi.org/10.1016/j.est.2021.102373.
(19) Waldie, K. M.; Ostericher, A. L.; Reineke, M. H.; Sasayama, A. F.; Kubiak, C. P. Hydricity of Transition-Metal Hydrides: Thermodynamic Considerations for CO_2 Reduction. *ACS Catal.* **2018**, *8* (2), 1313–1324. https://doi.org/10.1021/acscatal.7b03396.
(20) Todorova, T. K.; Schreiber, M. W.; Fontecave, M. Mechanistic Understanding of CO_2 Reduction Reaction (CO_2RR) Toward Multicarbon Products by Heterogeneous Copper-Based Catalysts. *ACS Catal.* **2020**, *10* (3), 1754–1768. https://doi.org/10.1021/acscatal.9b04746.
(21) Fu, X.; Zhang, J.; Kang, Y. Electrochemical Reduction of CO_2 towards Multi-Carbon Products via a Two-Step Process. *React. Chem. Eng.* **2021**, *6* (4), 612–628. https://doi.org/10.1039/D1RE00001B.
(22) Gao, F.-Y.; Bao, R.-C.; Gao, M.-R.; Yu, S.-H. Electrochemical CO_2-to-CO Conversion: Electrocatalysts, Electrolytes, and Electrolyzers. *J. Mater. Chem. A* **2020**, *8* (31), 15458–15478. https://doi.org/10.1039/D0TA03525D.
(23) Kondratenko, E. V.; Mul, G.; Baltrusaitis, J.; Larrazábal, G. O.; Pérez-Ramírez, J. Status and Perspectives of CO2 Conversion into Fuels and Chemicals by Catalytic, Photocatalytic and Electrocatalytic Processes. *Energy Environ. Sci.* **2013**, *6* (11), 3112–3135. https://doi.org/10.1039/C3EE41272E.
(24) Nitopi, S.; Bertheussen, E.; Scott, S. B.; Liu, X.; Engstfeld, A. K.; Horch, S.; Seger, B.; Stephens, I. E. L.; Chan, K.; Hahn, C.; Nørskov, J. K.; Jaramillo, T. F.; Chorkendorff, I. Progress and Perspectives of Electrochemical CO_2 Reduction on Copper in Aqueous Electrolyte. *Chem. Rev.* **2019**, *119* (12), 7610–7672. https://doi.org/10.1021/acs.chemrev.8b00705.
(25) Sharma, P. P.; Zhou, X.-D. Electrocatalytic Conversion of Carbon Dioxide to Fuels: A Review on the Interaction between CO_2 and the Liquid Electrolyte. *WIREs Energy Environ.* **2017**, *6* (4), e239. https://doi.org/10.1002/wene.239.
(26) Hori, Y. Electrochemical CO_2 Reduction on Metal Electrodes. In *Modern Aspects of Electrochemistry*; Vayenas, C. G., White, R. E., Gamboa-Aldeco, M. E., Eds.; Modern Aspects of Electrochemistry; Springer: New York, NY, 2008; pp 89–189. https://doi.org/10.1007/978-0-387-49489-0_3.
(27) Pegis, M. L.; Roberts, J. A. S.; Wasylenko, D. J.; Mader, E. A.; Appel, A. M.; Mayer, J. M. Standard Reduction Potentials for Oxygen and Carbon Dioxide Couples in Acetonitrile and N,N-Dimethylformamide. *Inorg. Chem.* **2015**, *54* (24), 11883–11888. https://doi.org/10.1021/acs.inorgchem.5b02136.
(28) Ledezma-Yanez, I.; Díaz-Morales, O.; Figueiredo, M. C.; Koper, M. T. M. Hydrogen Oxidation and Hydrogen Evolution on a Platinum Electrode in Acetonitrile. *ChemElectroChem* **2015**, *2* (10), 1612–1622. https://doi.org/10.1002/celc.201500341.
(29) Lu, Q.; Jiao, F. Electrochemical CO_2 Reduction: Electrocatalyst, Reaction Mechanism, and Process Engineering. *Nano Energy* **2016**, *29*, 439–456. https://doi.org/10.1016/j.nanoen.2016.04.009.
(30) Benson, E. E.; Kubiak, C. P.; Sathrum, A. J.; Smieja, J. M. Electrocatalytic and Homogeneous Approaches to Conversion of CO_2 to Liquid Fuels. *Chem. Soc. Rev.* **2008**, *38* (1), 89–99. https://doi.org/10.1039/B804323J.

(31) Zhang, F.; Co, A. C. Direct Evidence of Local PH Change and the Role of Alkali Cation during CO_2 Electroreduction in Aqueous Media. *Angew. Chem. Int. Ed.* **2020**, *59* (4), 1674–1681. https://doi.org/10.1002/anie.201912637.
(32) Chae, S. Y.; Lee, S. Y.; Joo, O.-S. Directly Synthesized Silver Nanoparticles on Gas Diffusion Layers by Electrospray Pyrolysis for Electrochemical CO_2 Reduction. *Electrochimica Acta* **2019**, *303*, 118–124. https://doi.org/10.1016/j.electacta.2019.02.046.
(33) Luo, W.; Zhang, J.; Li, M.; Züttel, A. Boosting CO Production in Electrocatalytic CO_2 Reduction on Highly Porous Zn Catalysts. *ACS Catal.* **2019**, *9* (5), 3783–3791. https://doi.org/10.1021/acscatal.8b05109.
(34) Lai, Q.; Yuan, W.; Huang, W.; Yuan, G. Sn/SnOx Electrode Catalyst with Mesoporous Structure for Efficient Electroreduction of CO_2 to Formate. *Appl. Surf. Sci.* **2020**, *508*, 145221. https://doi.org/10.1016/j.apsusc.2019.145221.
(35) Pander, J. E.; Lum, J. W. J.; Yeo, B. S. The Importance of Morphology on the Activity of Lead Cathodes for the Reduction of Carbon Dioxide to Formate. *J. Mater. Chem. A* **2019**, *7* (8), 4093–4101. https://doi.org/10.1039/C8TA10752A.
(36) Tian, Y.; Li, D.; Wu, J.; Liu, J.; Li, C.; Liu, G.; Chen, D.; Feng, Y. Electroreduction of CO_2 to Formate with Excellent Selectivity and Stability on Nano-Dendrite Bi Film Electrode. *J. CO2 Util.* **2021**, *43*, 101360. https://doi.org/10.1016/j.jcou.2020.101360.
(37) Bohlen, B.; Wastl, D.; Radomski, J.; Sieber, V.; Vieira, L. Electrochemical CO_2 Reduction to Formate on Indium Catalysts Prepared by Electrodeposition in Deep Eutectic Solvents. *Electrochem. Commun.* **2020**, *110*, 106597. https://doi.org/10.1016/j.elecom.2019.106597.
(38) Hori, Y.; Wakebe, H.; Tsukamoto, T.; Koga, O. Electrocatalytic Process of CO Selectivity in Electrochemical Reduction of CO2 at Metal Electrodes in Aqueous Media. *Electrochimica Acta* **1994**, *39* (11), 1833–1839. https://doi.org/10.1016/0013-4686(94)85172-7.
(39) Vasileff, A.; Zheng, Y.; Qiao, S.-Z., Carbon Solving Carbon's Problems: Recent Progress of Nanostructured Carbon-Based Catalysts for the Electrochemical Reduction of CO_2, https://fr.booksc.eu/book/65918241/14a677.
(40) Dai, L. Functionalization of Graphene for Efficient Energy Conversion and Storage. *Acc. Chem. Res.* **2013**, *46* (1), 31–42. https://doi.org/10.1021/ar300122m.
(41) Boutin, E.; Merakeb, L.; Ma, B.; Boudy, B.; Wang, M.; Bonin, J.; Anxolabéhère-Mallart, E.; Robert, M. Molecular Catalysis of CO_2 Reduction: Recent Advances and Perspectives in Electrochemical and Light-Driven Processes with Selected Fe, Ni and Co Aza Macrocyclic and Polypyridine Complexes. *Chem. Soc. Rev.* **2020**, *49* (16), 5772–5809. https://doi.org/10.1039/D0CS00218F.
(42) Qiao, J.; Liu, Y.; Hong, F.; Zhang, J. A Review of Catalysts for the Electroreduction of Carbon Dioxide to Produce Low-Carbon Fuels. *Chem. Soc. Rev.* **2013**, *43* (2), 631–675. https://doi.org/10.1039/C3CS60323G.
(43) König, M.; Vaes, J.; Klemm, E.; Pant, D. Solvents and Supporting Electrolytes in the Electrocatalytic Reduction of CO_2. *iScience* **2019**, *19*, 135–160. https://doi.org/10.1016/j.isci.2019.07.014.
(44) Huang, J. E.; Li, F.; Ozden, A.; Sedighian Rasouli, A.; García de Arquer, F. P.; Liu, S.; Zhang, S.; Luo, M.; Wang, X.; Lum, Y.; Xu, Y.; Bertens, K.; Miao, R. K.; Dinh, C.-T.; Sinton, D.; Sargent, E. H. CO2 Electrolysis to Multicarbon Products in Strong Acid. *Science* **2021**, *372* (6546), 1074–1078. https://doi.org/10.1126/science.abg6582.
(45) Bumroongsakulsawat, P.; Kelsall, G. H. Effect of Solution pH on CO: Formate Formation Rates during Electrochemical Reduction of Aqueous CO_2 at Sn Cathodes. *Electrochimica Acta* **2014**, *141*, 216–225. https://doi.org/10.1016/j.electacta.2014.07.057.
(46) Raciti, D.; Mao, M.; Park, J. H.; Wang, C. Local pH Effect in the CO_2 Reduction Reaction on High-Surface-Area Copper Electrocatalysts. *J. Electrochem. Soc.* **2018**, *165* (10), F799. https://doi.org/10.1149/2.0521810jes.
(47) Liu, X.; Schlexer, P.; Xiao, J.; Ji, Y.; Wang, L.; Sandberg, R. B.; Tang, M.; Brown, K. S.; Peng, H.; Ringe, S.; Hahn, C.; Jaramillo, T. F.; Nørskov, J. K.; Chan, K. pH Effects on the

Electrochemical Reduction of CO_2 towards C2 Products on Stepped Copper. *Nat. Commun.* **2019**, *10* (1), 32. https://doi.org/10.1038/s41467-018-07970-9.
(48) Peugeot, A.; Creissen, C. E.; Schreiber, M. W.; Fontecave, M. Advancing the Anode Compartment for Energy Efficient CO_2 Reduction at Neutral PH. *ChemElectroChem* **2021**, *8* (14), 2726–2736. https://doi.org/10.1002/celc.202100742.
(49) Gu, J.; Liu, S.; Ni, W.; Ren, W.; Haussener, S.; Hu, X. Modulating Electric Field Distribution by Alkali Cations for CO_2 Electroreduction in Strongly Acidic Medium. **2021**. https://doi.org/10.33774/chemrxiv-2021-zgq9k.
(50) Sanchez-Sanchez, C. M. Electrocatalytic Reduction of CO_2 in Imidazolium-Based Ionic Liquids. In *Reference Module in Chemistry, Molecular Sciences and Chemical Engineering. Encyclopedia of Interfacial Chemistry : Surface Science and Electrochemistry*; Wandelt, K., Ed.; Elsevier, 2018; pp 539–551.
(51) Taheri, A.; Berben, L. A. Making C–H Bonds with CO_2: Production of Formate by Molecular Electrocatalysts. *Chem. Commun.* **2016**, *52* (9), 1768–1777.
(52) Tomita, Y.; Teruya, S.; Koga, O.; Hori, Y. Electrochemical Reduction of Carbon Dioxide at a Platinum Electrode in Acetonitrile-Water Mixtures. *J. Electrochem. Soc.* **2000**, *147* (11), 4164.
(53) Sánchez-Sánchez, C. M.; Montiel, V.; Tryk, D. A.; Aldaz, A.; Fujishima, A. Electrochemical approaches to alleviation of the problem of carbon dioxide accumulation. *Pure Appl. Chem.* **2001**, *73* (12), 1917–1927. https://doi.org/10.1351/pac200173121917.
(54) Al-Tamreh, S. A.; Ibrahim, M. H.; El-Naas, M. H.; Vaes, J.; Pant, D.; Benamor, A.; Amhamed, A. Electroreduction of Carbon Dioxide into Formate: A Comprehensive Review. *ChemElectroChem* **2021**, *8* (17), 3207–3220. https://doi.org/10.1002/celc.202100438.
(55) Qiao, J.; Liu, Y.; Zhang, J. *Electrode Kinetics of CO_2 Electroreduction*; Routledge Handbooks Online, 2016. https://doi.org/10.1201/b20177-4.
(56) Higgins, D.; Hahn, C.; Xiang, C.; Jaramillo, T. F.; Weber, A. Z. Gas-Diffusion Electrodes for Carbon Dioxide Reduction: A New Paradigm. *ACS Energy Lett.* **2019**, *4* (1), 317–324. https://doi.org/10.1021/acsenergylett.8b02035.
(57) Supasitmongkol, S.; Styring, P. High CO_2 Solubility in Ionic Liquids and a Tetraalkylammonium-Based Poly(Ionic Liquid). *Energy Environ. Sci.* **2010**, *3* (12), 1961–1972. https://doi.org/10.1039/C0EE00293C.
(58) Corson, E. R.; Creel, E. B.; Kostecki, R.; Urban, J. J.; McCloskey, B. D. Effect of Pressure and Temperature on Carbon Dioxide Reduction at a Plasmonically Active Silver Cathode. *Electrochimica Acta* **2021**, *374*, 137820. https://doi.org/10.1016/j.electacta.2021.137820.
(59) Mizuno, T.; Ohta, K.; Sasaki, A.; Akai, T.; Hirano, M.; Kawabe, A. Effect of Temperature on Electrochemical Reduction of High-Pressure CO_2 with In, Sn, and Pb Electrodes. *Energy Sources* **1995**, *17* (5), 503–508. https://doi.org/10.1080/00908319508946098.
(60) Beley, Marc.; Collin, J. Paul.; Ruppert, Romain.; Sauvage, J. Pierre. Electrocatalytic Reduction of Carbon Dioxide by Nickel Cyclam2+ in Water: Study of the Factors Affecting the Efficiency and the Selectivity of the Process. *J. Am. Chem. Soc.* **1986**, *108* (24), 7461–7467. https://doi.org/10.1021/ja00284a003.
(61) Costentin, C.; Robert, M.; Savéant, J.-M.; Tatin, A. Efficient and Selective Molecular Catalyst for the CO_2-to-CO Electrochemical Conversion in Water. *Proc. Natl. Acad. Sci.* **2015**, *112* (22), 6882–6886. https://doi.org/10.1073/pnas.1507063112.
(62) Hawecker, J.; Lehn, J.-M.; Ziessel, R. Electrocatalytic Reduction of Carbon Dioxide Mediated by $Re(Bipy)(CO)_3Cl$ (Bipy = 2,2′-Bipyridine). *J. Chem. Soc. Chem. Commun.* **1984**, No. 6, 328–330. https://doi.org/10.1039/C39840000328.
(63) Hawecker, J.; Lehn, J.-M.; Ziessel, R. Photochemical and Electrochemical Reduction of Carbon Dioxide to Carbon Monoxide Mediated by (2,2′-Bipyridine)Tricarbonylchlororhenium(I) and Related Complexes as Homogeneous Catalysts. *Helv. Chim. Acta* **1986**, *69* (8), 1990–2012. https://doi.org/10.1002/hlca.19860690824.
(64) Clark, M. L.; Cheung, P. L.; Lessio, M.; Carter, E. A.; Kubiak, C. P. Kinetic and Mechanistic Effects of Bipyridine (Bpy) Substituent, Labile Ligand, and Brønsted Acid on Electrocatalytic

CO_2 Reduction by Re(Bpy) Complexes. *ACS Catal.* **2018**, *8* (3), 2021–2029. https://doi.org/10.1021/acscatal.7b03971.

(65) Smieja, J. M.; Kubiak, C. P. Re(Bipy-TBu)$(CO)_3Cl$−improved Catalytic Activity for Reduction of Carbon Dioxide: IR-Spectroelectrochemical and Mechanistic Studies. *Inorg. Chem.* **2010**, *49* (20), 9283–9289. https://doi.org/10.1021/ic1008363.

(66) Grills, D. C.; Matsubara, Y.; Kuwahara, Y.; Golisz, S. R.; Kurtz, D. A.; Mello, B. A. Electrocatalytic CO_2 Reduction with a Homogeneous Catalyst in Ionic Liquid: High Catalytic Activity at Low Overpotential. *J. Phys. Chem. Lett.* **2014**, *5* (11), 2033–2038. https://doi.org/10.1021/jz500759x.

(67) Ishida, H.; Tanaka, H.; Tanaka, K.; Tanaka, T. Selective Formation of $HCOO^-$ in the Electrochemical CO_2 Reduction Catalysed by $[Ru(Bpy)_2(CO)_2]^{2+}$(Bpy = 2,2′-Bipyridine). *J. Chem. Soc. Chem. Commun.* **1987**, No. 2, 131–132. https://doi.org/10.1039/C39870000131.

(68) Bolinger, C. M.; Sullivan, B. P.; Conrad, D.; Gilbert, J. A.; Story, N.; Meyer, T. J. Electrocatalytic Reduction of CO_2 Based on Polypyridyl Complexes of Rhodium and Ruthenium. *J. Chem. Soc. Chem. Commun.* **1985**, No. 12, 796–797. https://doi.org/10.1039/C39850000796.

(69) Caix, C.; Chardon-Noblat, S.; Deronzier, A. Electrocatalytic Reduction of CO_2 into Formate with $[(\eta^5\text{-}Me_5C_5)M(L)Cl]^+$ Complexes (L = 2,2′-Bipyridine Ligands; M = Rh(III) and Ir(III)). *J. Electroanal. Chem.* **1997**, *434* (1), 163–170.

(70) Collin, J. P.; Jouaiti, A.; Sauvage, J. P. Electrocatalytic Properties of (Tetraazacyclotetradecane)Nickel(2+) and Ni2(Biscyclam)4+ with Respect to Carbon Dioxide and Water Reduction. *Inorg. Chem.* **1988**, *27* (11), 1986–1990. https://doi.org/10.1021/ic00284a030.

(71) Kang, P.; Meyer, T. J.; Brookhart, M. Selective Electrocatalytic Reduction of Carbon Dioxide to Formate by a Water-Soluble Iridium Pincer Catalyst. *Chem. Sci.* **2013**, *4* (9), 3497–3502. https://doi.org/10.1039/C3SC51339D.

(72) Kang, P.; Zhang, S.; Meyer, T. J.; Brookhart, M. Rapid Selective Electrocatalytic Reduction of Carbon Dioxide to Formate by an Iridium Pincer Catalyst Immobilized on Carbon Nanotube Electrodes. *Angew. Chem. Int. Ed.* **2014**, *53* (33), 8709–8713. https://doi.org/10.1002/anie.201310722.

(73) Taheri, A.; Thompson, E. J.; Fettinger, J. C.; Berben, L. A. An Iron Electrocatalyst for Selective Reduction of CO_2 to Formate in Water: Including Thermochemical Insights. *ACS Catal.* **2015**, *5* (12), 7140–7151. https://doi.org/10.1021/acscatal.5b01708.

(74) Todorova, T. K.; Huan, T. N.; Wang, X.; Agarwala, H.; Fontecave, M. Controlling Hydrogen Evolution during Photoreduction of CO_2 to Formic Acid Using $[Rh(R\text{-}Bpy)(Cp^*)Cl]^+$ Catalysts: A Structure-Activity Study. *Inorg. Chem.* **2019**, *58* (10), 6893–6903.

(75) Benseghir, Y.; Lemarchand, A.; Duguet, M.; Mialane, P.; Gomez-Mingot, M.; Roch-Marchal, C.; Pino, T.; Ha-Thi, M.-H.; Haouas, M.; Fontecave, M.; Dolbecq, A.; Sassoye, C.; Mellot-Draznieks, C. Co-Immobilization of a Rh Catalyst and a Keggin Polyoxometalate in the UiO-67 Zr-Based Metal-Organic Framework: In Depth Structural Characterization and Photocatalytic Properties for CO_2 Reduction. *J. Am. Chem. Soc.* **2020**, *142* (20), 9428–9438. https://doi.org/10.1021/jacs.0c02425.

(76) Alvarez-Guerra, M.; Albo, J.; Alvarez-Guerra, E.; Irabien, A. Ionic Liquids in the Electrochemical Valorisation of CO_2. *Energy Environ. Sci.* **2015**, *8* (9), 2574–2599. https://doi.org/10.1039/C5EE01486G.

(77) Sanchez-Sanchez, C. M. Electrocatalytic Reduction of CO_2 in Imidazolium-Based Ionic Liquids. In *Reference Module in Chemistry, Molecular Sciences and Chemical Engineering. Encyclopedia of Interfacial Chemistry : Surface Science and Electrochemistry*; Wandelt, K., Ed.; Elsevier, 2018; pp 539–551.

(78) Walden, P. Molecular Weights and Electrical Conductivity of Several Fused Salts. *Bull Acad Imper Sci St Petersburg* **1914**, *1800*.

(79) Plechkova, N. V.; Seddon, K. R. Applications of Ionic Liquids in the Chemical Industry. *Chem. Soc. Rev.* **2007**, *37* (1), 123–150. https://doi.org/10.1039/B006677J.

(80) Wilkes, J. S.; Zaworotko, M. J. Air and Water Stable 1-Ethyl-3-Methylimidazolium Based Ionic Liquids. *J. Chem. Soc. Chem. Commun.* **1992**, No. 13, 965–967. https://doi.org/10.1039/C39920000965.
(81) Hapiot, P.; Lagrost, C. Electrochemical Reactivity in Room-Temperature Ionic Liquids. *Chem. Rev.* **2008**, *108* (7), 2238–2264. https://doi.org/10.1021/cr0680686.
(82) Greaves, T. L.; Drummond, C. J. Protic Ionic Liquids: Properties and Applications. *Chem. Rev.* **2008**, *108* (1), 206–237. https://doi.org/10.1021/cr068040u.
(83) Farrán, A.; Cai, C.; Sandoval, M.; Xu, Y.; Liu, J.; Hernáiz, M. J.; Linhardt, R. J. Green Solvents in Carbohydrate Chemistry: From Raw Materials to Fine Chemicals. *Chem. Rev.* **2015**, *115* (14), 6811–6853. https://doi.org/10.1021/cr500719h.
(84) Seddon, K. R.; Stark, A.; Torres, M.-J. Influence of chloride, water, and organic solvents on the physical properties of ionic liquids. *Pure Appl. Chem.* **2000**, *72* (12), 2275–2287. https://doi.org/10.1351/pac200072122275.
(85) Schröder, U.; Wadhawan, J. D.; Compton, R. G.; Marken, F.; Suarez, P. A. Z.; Consorti, C. S.; Souza, R. F. de; Dupont, J. Water-Induced Accelerated Ion Diffusion: Voltammetric Studies in 1-Methyl-3-[2,6-(S)-Dimethylocten-2-Yl]Imidazolium Tetrafluoroborate, 1-Butyl-3-Methylimidazolium Tetrafluoroborate and Hexafluorophosphate Ionic Liquids. *New J. Chem.* **2000**, *24* (12), 1009–1015. https://doi.org/10.1039/B007172M.
(86) Michez, R.; Vander Steen, J.; Doneux, T.; Luhmer, M.; Buess-Herman, C. Electroreduction of 1-Butyl-3-Methylimidazolium Bis(Trifluoromethanesulfonyl)Imide Ionic Liquid: Oriented Product Selectivity through the Electrode Material. *Electrochimica Acta* **2018**, *270*, 434–439.
(87) Galiński, M.; Lewandowski, A.; Stępniak, I. Ionic Liquids as Electrolytes. *Electrochimica Acta* **2006**, *51* (26), 5567–5580. https://doi.org/10.1016/j.electacta.2006.03.016.
(88) Kelley, S. P.; Flores, L. A.; Shannon, M. S.; Bara, J. E.; Rogers, R. D. Understanding Carbon Dioxide Solubility in Ionic Liquids by Exploring the Link with Liquid Clathrate Formation. *Chem. – Eur. J.* **2017**, *23* (57), 14332–14337. https://doi.org/10.1002/chem.201703117.
(89) Rogers, R. D.; Seddon, K. R. Ionic Liquids-Solvents of the Future? *Science* **2003**, *302* (5646), 792–793. https://doi.org/10.1126/science.1090313.
(90) Montiel, M. A.; Solla-Gullón, J.; Montiel, V.; Sánchez-Sánchez, C. M. Electrocatalytic Studies on Imidazolium Based Ionic Liquids: Defining Experimental Conditions. *Phys. Chem. Chem. Phys.* **2018**, *20* (28), 19160–19167. https://doi.org/10.1039/C8CP02662A.
(91) Rosen, B. A.; Salehi-Khojin, A.; Thorson, M. R.; Zhu, W.; Whipple, D. T.; Kenis, P. J. A.; Masel, R. I. Ionic Liquid-Mediated Selective Conversion of CO_2 to CO at Low Overpotentials. *Science* **2011**, *334* (6056), 643–644.
(92) Faggion, D.; Gonçalves, W. D. G.; Dupont, J. CO_2 Electroreduction in Ionic Liquids. *Front. Chem.* **2019**, *7*, 102. https://doi.org/10.3389/fchem.2019.00102.
(93) Sun, L.; Ramesha, G. K.; Kamat, P. V.; Brennecke, J. F. Switching the Reaction Course of Electrochemical CO_2 Reduction with Ionic Liquids. *Langmuir* **2014**, *30* (21), 6302–6308. https://doi.org/10.1021/la5009076.
(94) Zhu, Q.; Ma, J.; Kang, X.; Sun, X.; Liu, H.; Hu, J.; Liu, Z.; Han, B. Efficient Reduction of CO_2 into Formic Acid on a Lead or Tin Electrode Using an Ionic Liquid Catholyte Mixture. *Angew. Chem. Int. Ed.* **2016**, *55* (31), 9012–9016. https://doi.org/10.1002/anie.201601974.
(95) Wang, Q.; Chen, C.; Zhong, J.; Zhang, B.; Cheng, Z.; Wang, Q.; Chen, C.; Zhong, J.; Zhang, B.; Cheng, Z. Effect of Alkyl Chain Length of Imidazolium Cation on the Electroreduction of CO_2 to CO on Ag Electrode in Acetonitrile. *Aust. J. Chem.* **2016**, *70* (3), 293–300. https://doi.org/10.1071/CH16138.
(96) Lau, G. P. S.; Schreier, M.; Vasilyev, D.; Scopelliti, R.; Grätzel, M.; Dyson, P. J. New Insights Into the Role of Imidazolium-Based Promoters for the Electroreduction of CO_2 on a Silver Electrode. *J. Am. Chem. Soc.* **2016**, *138* (25), 7820–7823. https://doi.org/10.1021/jacs.6b03366.
(97) Zhao, S.-F.; Horne, M.; Bond, A.; Zhang, J. Is the Imidazolium Cation a Unique Promoter for Electrocatalytic Reduction of Carbon Dioxide? **2016**. https://doi.org/10.1021/acs.jpcc.6b08182.
(98) Vasilyev, D. V.; Dyson, P. J. The Role of Organic Promoters in the Electroreduction of Carbon Dioxide. *ACS Catal.* **2021**, *11* (3), 1392–1405. https://doi.org/10.1021/acscatal.0c04283.

(99) Kumar, B.; Asadi, M.; Pisasale, D.; Sinha-Ray, S.; Rosen, B. A.; Haasch, R.; Abiade, J.; Yarin, A. L.; Salehi-Khojin, A. Renewable and Metal-Free Carbon Nanofibre Catalysts for Carbon Dioxide Reduction. *Nat. Commun.* **2013**, *4* (1), 2819. https://doi.org/10.1038/ncomms3819.

(100) Rosen, B. A.; Haan, J. L.; Mukherjee, P.; Braunschweig, B.; Zhu, W.; Salehi-Khojin, A.; Dlott, D. D.; Masel, R. I. In Situ Spectroscopic Examination of a Low Overpotential Pathway for Carbon Dioxide Conversion to Carbon Monoxide. *J. Phys. Chem. C* **2012**, *116* (29), 15307–15312. https://doi.org/10.1021/jp210542v.

(101) Lane, G. H. Electrochemical Reduction Mechanisms and Stabilities of Some Cation Types Used in Ionic Liquids and Other Organic Salts. *Electrochimica Acta* **2012**, *83*, 513–528. https://doi.org/10.1016/j.electacta.2012.08.046.

(102) Feaster, J. T.; Jongerius, A. L.; Liu, X.; Urushihara, M.; Nitopi, S. A.; Hahn, C.; Chan, K.; Nørskov, J. K.; Jaramillo, T. F. Understanding the Influence of [EMIM]Cl on the Suppression of the Hydrogen Evolution Reaction on Transition Metal Electrodes. *Langmuir* **2017**, *33* (37), 9464–9471. https://doi.org/10.1021/acs.langmuir.7b01170.

(103) Michez, R.; Doneux, T.; Buess-Herman, C.; Luhmer, M. NMR Study of the Reductive Decomposition of [BMIm][NTf_2] at Gold Electrodes and Indirect Electrochemical Conversion of CO_2. *ChemPhysChem* **2017**, *18* (16), 2208–2216. https://doi.org/10.1002/cphc.201700421.

(104) Wang, Y.; Hayashi, T.; He, D.; Li, Y.; Jin, F.; Nakamura, R. A Reduced Imidazolium Cation Layer Serves as the Active Site for Electrochemical Carbon Dioxide Reduction. *Appl. Catal. B Environ.* **2020**, *264*, 118495. https://doi.org/10.1016/j.apcatb.2019.118495.

(105) Matsubara, Y.; Grills, D. C.; Kuwahara, Y. Thermodynamic Aspects of Electrocatalytic CO_2 Reduction in Acetonitrile and with an Ionic Liquid as Solvent or Electrolyte. *ACS Catal.* **2015**, *5* (11), 6440–6452. https://doi.org/10.1021/acscatal.5b00656.

(106) Choi, J.; Benedetti, T. M.; Jalili, R.; Walker, A.; Wallace, G. G.; Officer, D. L. High Performance Fe Porphyrin/Ionic Liquid Co-Catalyst for Electrochemical CO_2 Reduction. *Chem. - Eur. J.* **2016**, *22* (40), 14158–14161.

(107) Sung, S.; Kumar, D.; Gil-Sepulcre, M.; Nippe, M. Electrocatalytic CO_2 Reduction by Imidazolium-Functionalized Molecular Catalysts. *J. Am. Chem. Soc.* **2017**, *139* (40), 13993–13996. https://doi.org/10.1021/jacs.7b07709.

(108) Khadhraoui, A.; Gotico, P.; Boitrel, B.; Leibl, W.; Halime, Z.; Aukauloo, A. Local Ionic Liquid Environment at a Modified Iron Porphyrin Catalyst Enhances the Electrocatalytic Performance of CO_2 to CO Reduction in Water. *Chem. Commun.* **2018**, *54* (82), 11630–11633. https://doi.org/10.1039/C8CC06475J.

(109) Torbensen, K.; Boudy, B.; Joulié, D.; von Wolff, N.; Robert, M. Emergence of CO_2 Electrolyzers Including Supported Molecular Catalysts. *Curr. Opin. Electrochem.* **2020**, *24*, 49–55. https://doi.org/10.1016/j.coelec.2020.07.001.

(110) Torbensen, K.; Han, C.; Boudy, B.; Wolff, N. von; Bertail, C.; Braun, W.; Robert, M. Iron Porphyrin Allows Fast and Selective Electrocatalytic Conversion of CO_2 to CO in a Flow Cell. *Chem. – Eur. J.* **2020**, *26* (14), 3034–3038. https://doi.org/10.1002/chem.202000160.

(111) Abdinejad, M.; Dao, C.; Zhang, X.-A.; Kraatz, H. B. Enhanced Electrocatalytic Activity of Iron Amino Porphyrins Using a Flow Cell for Reduction of CO_2 to CO. *J. Energy Chem.* **2021**, *58*, 162–169. https://doi.org/10.1016/j.jechem.2020.09.039.

(112) Ren, S.; Joulié, D.; Salvatore, D.; Torbensen, K.; Wang, M.; Robert, M.; Berlinguette, C. P. Molecular Electrocatalysts Can Mediate Fast, Selective CO_2 Reduction in a Flow Cell. *Science* **2019**, *365* (6451), 367. https://doi.org/10.1126/science.aax4608.

(113) Wang, M.; Torbensen, K.; Salvatore, D.; Ren, S.; Joulié, D.; Dumoulin, F.; Mendoza, D.; Lassalle-Kaiser, B.; Işci, U.; Berlinguette, C. P.; Robert, M. CO_2 Electrochemical Catalytic Reduction with a Highly Active Cobalt Phthalocyanine. *Nat. Commun.* **2019**, *10* (1), 3602. https://doi.org/10.1038/s41467-019-11542-w.

(114) Jiang, C.; Nichols, A. W.; Walzer, J. F.; Machan, C. W. Electrochemical CO_2 Reduction in a Continuous Non-Aqueous Flow Cell with $[Ni(Cyclam)]^{2+}$. *Inorg. Chem.* **2020**, *59* (3), 1883–1892. https://doi.org/10.1021/acs.inorgchem.9b03171.

(115) Lu, X.; Leung, D. Y. C.; Wang, H.; Xuan, J. A High Performance Dual Electrolyte Microfluidic Reactor for the Utilization of CO_2. *Appl. Energy* **2017**, *194*, 549–559. https://doi.org/10.1016/j.apenergy.2016.05.091.
(116) Jones, J.-P.; Prakash, G. K. S.; Olah, G. A. Electrochemical CO_2 Reduction: Recent Advances and Current Trends. *Isr. J. Chem.* **2014**, *54* (10), 1451–1466. https://doi.org/10.1002/ijch.201400081.
(117) Lu, X.; Wu, Y.; Yuan, X.; Huang, L.; Wu, Z.; Xuan, J.; Wang, Y.; Wang, H. High-Performance Electrochemical CO_2 Reduction Cells Based on Non-Noble Metal Catalysts. *ACS Energy Lett.* **2018**, *3* (10), 2527–2532. https://doi.org/10.1021/acsenergylett.8b01681.
(118) Rogers, L.; Jensen, K. F. Continuous Manufacturing – the Green Chemistry Promise? *Green Chem.* **2019**, *21* (13), 3481–3498. https://doi.org/10.1039/C9GC00773C.

CHAPTER 1: INTRODUCTION

CHAPTER 2: MATERIALS AND METHODS

In the present chapter are detailed all reagents and other materials used throughout this thesis. Moreover, presented here are all experimental procedures, characterization techniques, syntheses and other methods used.

2.1 Reagents, Materials and Instruments

2.1.1 Chemical Reagents

Chemical reagents used in the following chapters are of analytical grade and are listed in Table 2.1. Water used in all experiments is MiliQ grade with a resistivity value of 18.2 MΩ cm.

Table 2.1 Chemical reagents used throughout the PhD thesis.

Reagent name	Reagent formula	Reagent Grade	Brand
Anhydrous acetonitrile	CH_3CN	99.99 %	Sigma-Aldrich
Tetrabutyl ammonium hexafluorophosphate	[TBA][PF_6]	> 99 %	Sigma-Aldrich
Tetrabutyl ammonium tetrafluoroborate	[TBA][BF_4]	> 99 %	Sigma-Aldrich
2,2,2-trifluoroethanol (TFE)	CF_3CH_2OH	> 99 %	Sigma-Aldrich
Acetic acid (AcOH)	CH_3CO_2H	> 99.5 %	TCI chemicals
Sodium acetate	CH_3CO_2Na	> 99 %	Sigma-Aldrich
Sodium formate	HCOONa	> 99 %	Sigma-Aldrich
Ferrocene (Fc)	$(C_5H_5)_2Fe$	98 %	Merck
1-Butyl-3-methylimidazolium hexafluorophosphate	[BMIM][PF_6]	99 %	Io-li-tec
1-Ethyl-3- methylimidazolium hexafluorophosphate	[EMIM][PF_6]	99 %	Io-li-tec
1- Ethyl-3-methylimidazolium tetrafluoroborate	[EMIM][BF_4]	> 98 %	Io-li-tec
1-Butyl-1- methylpyrrolidinium hexafluorophosphate	[BMPyrr][PF_6]	99 %	Io-li-tec
1,2-Dimethylimidazolium bis(trifluoromethylsulfonyl)imide	[DiMIM][$N(SO_2CF_3)_2$]	98 %	Io-li-tec
1-Ethylimidazole	$C_5H_8N_2$	> 98%	Io-li-tec
Chlorotricarbonyl(2,2'-bipyridine)rhenium(I)	[Re(bpy)$(CO)_3$Cl]	99 %	STREM chemicals
Dichloro(pentamethylcyclopentadienyl)rhodium(III) dimer	[Rh(Cp*)Cl]$_2$	99 %	STREM chemicals

2,2'-Bipyridine	$C_{10}H_8N_2$	> 99 %	Merck
4,4'-dimethoxy-2,2'-bipyridine	$C_{12}H_{12}N_2O_2$	98 %	Merck
[2,2'-bipyridine]-4,4'-dicarboxylic acid 4,4'-dimethyl ester	$C_{14}H_{12}N_2O_2$	98 %	Merck
1-bromoethylamine hydrobromide	$BrCH_2CH_2NH_2$ HBr	99 %	Sigma-Aldrich
Potassium chloride	KCl	> 99 %	Sigma-Aldrich
Potassium hydroxide	KOH	> 99.5 %	Sigma-Aldrich
Potassium carbonate	K_2CO_3	> 99 %	Merck
Potassium bicarbonate	$KHCO_3$	> 99.5 %	Merck
Sulfuric acid	H_2SO_4	95%	Merck
Carbon dioxide	CO_2	99.99 %	Air Liquide
Argon gas	Ar	99.99 %	Air Liquide
Hydrogen gas	H_2	99 %	Air Liquide
Carbon monoxide	CO	99 %	Air Liquide
Standard gas mixture for GC calibration	CO_2 containing: H_2, CO, O_2, CH_4, C_2H_4, C_2H_6 (all at 2.0 mol %) and CH_3CHCH_2, $CH_3CH_2CH_3$, $CH(CH_3)_3$, $CH_2C(CH_3)_2$ (all 990 ppm)		Nippon Gases

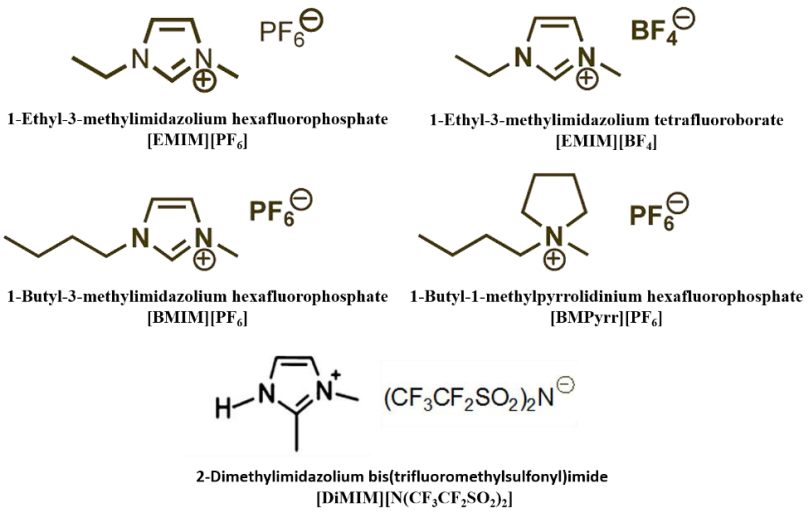

Figure 2.1 Chemical structure, name and the corresponding abbreviation of the ILs used in this work.

2.1.2 Experimental Materials

Electrodes:

- Glassy Carbon Electrode disk (GCE), diameter = 3 mm, purchased from BioLogic. Used as working electrode (WE) for Cyclic voltammetry (CV) experiments.
- GCE plate, geometric area = 2-3 cm^2, 1 mm thick, purchased from Alfa Aesar. Used as WE for Constant Potential Electrolysis (CPE) and Constant Current Electrolysis (CCE) experiments in acetonitrile solutions.
- GCE rod, diameter = 1.2 cm^2, length = 8 cm, purchased from Alfa Aesar. Used as counter electrode (CE) for CPE and CCE experiments with catalyst [Rh(bpy)(Cp*)Cl]Cl.
- Reticulated vitreous carbon (RVC) foam electrode, Duocel® RVC foam, density 45 PPI, geometric area = 3-6 cm^2, purchased from ERG Materials and Aerospace Co. Used as WE for CCE experiments in aqueous solutions with catalyst [Rh(bpy)(Cp*)Cl]Cl.
- Gold Electrode (AuE), diameter = 3 mm, purchased from BioLogic. Used as WE in CV experiments.
- Gold Electrode plate, 0.5 mm thick, 99.95 % purity, purchased from BioLogic. Used for XPS analysis.
- Platinum wire electrode, 0.5 mm diameter, 99.9 % purity, purchased from Alfa Aesar. Used as CE for CV experiments.
- Platinum mesh electrode geometric area = 2-4 cm^2, 0.4 mm nominal space, 0.1 mm diameter, 99.9 % purity, purchased from Goodfellow. Used as CE for CPE experiments with catalyst [Re(bpy)$(CO)_3$Cl].
- Ag/AgCl/$KCl_{saturated}$ reference electrode, purchased from BioLogic. Used as reference electrode (RE) in CV experiments and CPE/CCE experiments with catalyst [Rh(bpy)(Cp*)Cl]Cl.
- Ag wire, 0.5 mm diameter, 99.9 % purity, purchased from Alfa Aesar. Coated with AgCl and used as RE in CV experiments and CPE experiments with catalyst [Re(bpy)$(CO)_3$Cl].

Electrolyzer components:

Flow Electrolyzer parts, all purchased from ElectroCell:

- Cathodes: Graphite electrode, Sigrafine® R8710, geometric area of 10 cm^2, purchased by The Carbon Company or Gas Diffusion Electrode (GDE), Sigracet 28 BC, geometric area of 10 cm^2, purchased from Fuel Cell Store. The GDE must undergo an activation protocol described here in section 2.3.4.

- Anodes: Dimensionally Stable Anode (DSA) electrode, made from a IrO_2–Ta_2O_5 mixed oxide, which also has a 10 cm^2 electrode geometric area or the aforementioned graphite electrode.
- Polytetrafluoroethylene (PTFE) End Frames, each containing 4 inlet/outlet openings of 0.32 cm and another 6 peripheral holes to accommodate the bolts that keep the cell together.
- Stainless Steel Endplates, that provide additional support for the cell.
- Hardware for Cell Assembly, such as nuts, bolts and washers all made from stainless steel and guide pins made from PTFE.
- Flow frames of 2 mm thickness made from PTFE.
- Turbulence Mesh, typically made from PVDF (Polyvinylidene difluoride).
- Gaskets, to separate all cell compartments with 0-4 holes for inlet/outlet based on the position used and/or a center cut-out corresponding to the 10 cm^2 electrode area.
- Nafion 117 membrane of 10 cm^2 geometric area and 183 μm thickness was purchased from ElectroCell. This Nafion perfluorosulfonic (PFSA) acid membrane has improved stability due to lower fluoride ion release and is compatible with water electrolyzers. It was already pre-treated and soaked, so its activation protocol within the electrolyzer involved only an hour-long run with water at 22.1 mL/min prior to use with the electrolyte.
- Tubing used to link the flow electrolyzer with the solution recipients is C-Flex Ultra 14 (Internal Diameter (ID) = 1.6 mm), purchased from Cole-Parmer. It has physical properties similar to silicone with chemical compatibility of Tygon® and suitable for pumping from –40 to 100 °C.
- Catholyte/anolyte recipients are glass bottles of 100 mL, purchased from Dewar.

2.1.3 Instruments

I. A VSP 300 and a SP 300 Potensiostat were used for all cyclic voltammetry and bulk electrolysis experiments and were purchased from BioLogic Instruments.

II. The Gas Chromatography instrument used to detect and quantify all gaseous products during bulk electrolysis was purchased from SRI Instruments, Model 8610 C. H_2 gas was quantified using a thermal conductivity detector (TCD) separated from other gases by a HaySepD precolumn attached to a 3 mm molecular sieve column. Carbon-based products, like CO, are detected by a flame ionization detector (FID) equipped with a methanizer and are separated using a 3 mm molecular sieve column. Calibration of the GC was performed from pure CO and H_2 gases or from a custom standard gas mixture.

III. An ionic exchange chromatograph from Metrohm (883 Basic IC) equipped with a Metrosep. A Supp 5 column and a conductivity detector was used to quantify the Liquid products of bulk electrolysis experiments. Calibration of the IC was performed from formate standards in ultra-pure water.

IV. Nuclear Magnetic Resonance (NMR) was used as a characterization method of synthesized complexes and were performed on a Bruker AVANCE III 300 MHz spectrometer.

V. pH meter used to measure values in aqueous solutions was purchased from Mettler Toledo, Model FiveEasy and was calibrated from standards ranging from pH = 2.00 to pH = 11.00.

VI. Gas triple filter (model CP17976, Agilent) that removes traces of oxygen, moisture and hydrocarbons and results in a concentration of H_2O of the gas outlet lower than 0.1 ppm.

VII. Karl Fischer titration was performed using an instrument from Mettler- Toledo, Model 756/831 KF.

VIII. The glove box used to store the dry ILs was an MBRAUN UNI lab plus workstation kept under an argon atmosphere at H_2O values < 1 ppm and O_2 values < 5 ppm.

IX. The peristatic pump used to feed the flow electrolyzer the electrolyte solution was purchased from Master Flex L/S and the Model was Easy Load II (No 77202-60). It can accommodate pumping speeds from 3 to 300 rpm that using tubing with an interior diameter of 1.6 mm corresponds to 0.66 – 66.4 mL/min. It has two channels that can be simultaneously used at the same speed and is compatible with temperatures ranging from 0 to 40 °C and maximum discharge pressure value of 2.7 bar.

X. The power source (DC) used in experiments with the flow electrolyzer was purchased from MB ELECTRONIQUE, Model IT6874A ITECH and can apply up to 1 A/150 V or 2 A/60 V.

XI. SGE Gas tight Syringe, model 100 R-V-GT (100 µL), purchased from Trajan Scientific Australia Pty Ltd.

2.2 Catalytic parameters for the molecular catalysts

In order to compare catalytic performance of various catalysts we need a set of criteria. Here below are mentioned some catalytic parameters that have been used throughout the thesis:

[1] Faradaic Efficiency (FE): In order to evaluate product selectivity, we use this term to represent the percentage of each reduction product by a set amount of charge passed through the system.

The FE equation is the following: $FE = \frac{n \cdot F \cdot N}{Q}$, where n is the number of electrons involved in the process, F is the Faraday constant (F = 96485 C/mol), N is the number of moles of each product and Q is the amount of charge measured in Coulombs (C).

[2] Overpotential = (applied potential in order for CO_2RR to take place) – (thermodynamic potential of the same reaction).

[3] Catalytic Potential, referred as $E_{cat\ max}$ or $E_{cat/2}$ is the potential that corresponds to the value of maximum or half of the catalytic current respectively. $E_{cat\ max}$ and $E_{cat/2}$ are both used within the thesis.

[4] Current Density (j) is the current divided by the electrode surface and is measured in mA/cm^2.

[5] Catalytic response (j_{cat}/j_p) is the ratio of the current density value under catalytic conditions (for example under CO_2 with/out the presence of an added proton source) divided by the current density value for the same system under inert conditions.

[6] Energy Efficiency (EE): $EE = E_T/E \cdot FE$ (%), where E_T is the theoretical cathodic potential to reduce CO_2 to the product of interest in Volts, E represents the actual cathodic potential applied in Volts and FE is the Faradaic Efficiency for said product, calculated according to equation [1][1,2].

[7] Energy Consumption (EC): $EC = (Q \cdot |Ecell|/ N) \cdot 2.78 \cdot 10^{-4}$ (kWh /kmol), where Q represents the total charge circulated measured in Coulombs, |Ecell| represents the absolute cell potential in volts and N is the number of moles of each product[1].

2.3 Electrochemical characterization

All electrochemical experiments were performed on a VSP-300 or SP-300 potensiostat (BioLogic Science Instruments SAS) and were conducted at room temperature (20 ± 2 °C) in CH_3CN, CH_3CN/H_2O mixtures or aqueous solutions as specified. Either benchmark electrolytes or one of the ILs studied was used as supporting electrolyte in solution. Ar and CO_2 gases used to saturate solutions were purchased from Air Liquide.

2.3.1 Cyclic Voltammetry (CV)

Cyclic voltammetry (CV) experiments were used throughout this thesis in order to obtain quantitative data concerning the electrochemical reactions studied. CV is the most widely used electrochemical

technique and can provide valuable information not solely on reduction and oxidation reactions of molecular species, but equally on transient surface dependent reactions that involve electron transfers. It consists in scanning the potential from an initial value E1 to a final value E2 and then a return sweep back to the initial potential using a triangular potential waveform. All while the potential is swept, the potensiostat registers the current obtained from all electrochemical processes taking place at the electrode interface due to the potential application. The resulting cyclic voltammogram provides on the y axis the response, which is the current recoded, as a function of the parameter imposed, that being the potential represented on the x axis[3].

The cyclic voltammetry (CV) experiments were carried out in a classical three-electrodes electrochemical cell sealed with a Teflon cap (BioLogic), with a 3 mm diameter GCE/AuE as a working electrode, which was polished on a polishing cloth on a 1 µm diamond suspension (Struers), sonicated for 10 seconds, thoroughly rinsed with ethanol and dried under a stream of pressurized air prior to experiments. A platinum wire was used as a counter electrode and was previously flame annealed. The reference electrode was either a silver chloride coated silver wire in saturated KCl solution reference electrode or simply a silver chloride coated silver wire, in which case potentials were calibrated using the Ferrocenium/Ferrocene (Fc^+/Fc) redox couple as internal standard, which was added in solution at the end of each measurement. Only the last cycle of all CVs is shown unless explicitly mentioned otherwise, although in most cases no difference in consecutive scans has been observed.

2.3.2 Constant Potential Electrolysis (CPE) and Constant Current Electrolysis (CCE)

In Constant Potential Electrolysis (CPE), a constant potential is applied for a defined time frame and measure the current response produced on the electrochemical system. The obtained response of current-time association is characteristic of the concentration of electroactive species at the electrode interface. CPE can be used for determining the diffusion coefficient of electroactive species that are adsorbed on the working electrode's surface , as well as a way to investigate the mechanism of different electrode processes. Here this method is used as electrolysis permitting to define the catalytic reduction products within the systems studied, since products accumulate within the electrolysis cell throughout the duration of CPE and therefore reach detectable range concentrations. An alternative technique used for electrolysis is constant current electrolysis (CCE), which consists of keeping a stable current value applied between the working and counter electrodes and registering the potential of the working electrode as a function of time. It is similar in principle to CPE, with the exception that current steps are replacing potential steps, however, it can also provide information concerning the kinetics of the

electrode. Nevertheless, it is often more widely used in industrial settings for CO_2RR catalysis and it was a better way to compare different catalytic conditions when the maximum catalytic potential values were dissimilar.

CPE and CCE experiments were conducted in a gas-tight two-compartment electrochemical cell with a glass frit (porosity level 4) and a PTFE needle valve separating the anodic and cathodic compartments in liquid phase and gas phase, respectively. The volume of anolyte and catholyte were approximatively 5 and 10 mL respectively. The working electrode was either a GCE or RVC plate, the counter electrode was a platinum mesh or GCE rod and the reference electrode was either Ag/AgCl/KClsat reference or a silver chloride coated silver wire, which was calibrated with Fc^+/Fc as an internal redox reference. Anolyte and catholyte contained acetonitrile and 0.5 M of supporting electrolyte (either individual ILs or [TBA][PF_6]), but only in the catholyte 1 mM of complex [Re(bpy)$(CO)_3$Cl] or complex [Rh(bpy)(Cp*)Cl]Cl was added. Ohmic losses in the cell were minimized by placing the electrodes as close as possible to each other and stirring both solution compartments during the experiment. Moreover, 85 % of the electrolyte resistance was compensated by the ohmic drop compensation module of the potentiostat. Both solution compartments were saturated with CO_2 during at least 20 minutes before starting the electrolysis, but no more gas was bubbled during the electrolysis. In both cases, FE is corrected to account for the initial 2 or 3 electron reduction of molecular catalyst [Re(bpy)$(CO)_3$Cl] or [Rh(bpy)(Cp*)Cl]Cl, respectively (1 mM in solution) necessary to generate its active form. Catalyst activation charge = [number of electrons · Faraday constant · mol of catalyst] = [n · 96485 · 6.06 10^{-6}].

2.3.3 Surface Coverage of Chemically Modified Electrodes

The CV measurements used to extrapolate the surface coverage of the working electrodes with a electrodeposited IL layer were measured in an acetonitrile solution containing 0.5 M [EMIM][PF_6] under an inert atmosphere. The electrodeposited IL layer was formed under the same conditions and comparative tests were carried out on both GCE and AuE of the same area. By measuring the reoxidation wave peak area that is linked to the IL quantity reduced, the surface coverage of electrodeposited layer on the electrodes was calculated based on the folowing formula:

$$\Gamma = \frac{Q\ (C)}{n\ F\ (C/mol)\ A\ (cm^2)}$$

where Q is the charge (measured in Coulomb), n is the number of electrons involved in the process (according to the literature[4] n=1), F is the Faraday constant (96500 C/mol) and A is the working electrode geometric area (measured in cm^2)[5,6].

2.3.4 GDE activation protocol

In the flow electrolyzer setup, the GDE cathode had to first undergo an activation protocol in order to produce optimal faradaic efficiency for formate. This consisted of initially running water through it for at least an hour and subsequently running experiments amassing a total charge of approximatively 3000 C. This value was experimentally determined as subsequent experiments before the 3000 C mark led to progressively increasing formate FE values, which stabilized past that point. According to the literature on the topic[7], it is considered that a thin layer of electrolyte forms on top of the GDE as the electrode is progressively wetted. This is likely caused by the creation of oxygen groups on the electrode surface rendering it more hydrophilic and as a consequence more active towards the electrolyte solution. This may also in some cases result in promoting HER, but it was not observed experimentally in this case, since formate efficiency increased instead. It is acknowledged that the nature of the electrolyte as well as the applied potential or current in the case of electro-wetting, to which our system belongs, affect the eventual catalytic activity and selectivity of the electrode[7].

2.4 Physical characterization: X-ray photoelectron spectroscopy on gold plates

X-ray photoelectron spectroscopy (XPS) is a very widely used technique in material science to characterize chemical bonding on solid surfaces by identifying the chemical state of different atoms based on binding energy (BE) values they exhibit. Its principle relies on irradiating a sample kept under ultra-high vacuum with soft X-rays that produce ionizations of electrons from the analyzed atoms or molecules. The binding energy values are obtained from the difference between the energy of the X-ray irradiation and the kinetic energy of excited core level photoelectrons[8,9].XPS spectra in this study were collected on gold plates containing electrodeposited and covalent IL layers using a Omicron Argus X-ray photoelectron spectrometer, equipped with a monochromated Al Kα radiation source (hν = 1486.6 eV) and a 280 W electron beam power. The diameter of analyzed area was 1 mm. The emission of photoelectrons from the sample was analyzed at a takeoff angle of 45° under ultra-high vacuum conditions (≤10−9 mBar). Spectra were carried out with a 100 eV pass energy for the survey scan and 20 eV pass energy for the C 1s and N 1s regions. Binding energies were calibrated against the C 1s (C-C) binding energy at 284.8 eV and element peak intensities were corrected by Scofield factors. The peak areas were determined after subtraction of a linear background. The spectra were fitted using Casa XPS v.2.3.15 software (Casa Software Ltd, U.K.) and applying a GAUSSIAN/LORENTZIAN RATIO G/L

equal to 70/30. XPS analysis was carried out in the available platform of Sorbonne Université by A. Miche (Laboratoire de Réactivité de Surface – UMR 7197).

2.5 Analytical Methods for product quantification

In order to quantify the amount of CO_2 reduction products are being produced during electrolysis we have recourse to analytical techniques, that provide us the values necessary to calculate each product's faradaic efficiency.

2.5.1 Gaseous product detection

Gas products were quantified by gas chromatography from 50 µL aliquots of the headspace of both compartments. Hydrogen (H_2) and carbon monoxide (CO) were detected by a thermal conductivity detector (TCD) and a flame ionization detector (FID) coupled to a methanizer, respectively. The column in both cases was a 3 mm molecular sieve column and in the case of H_2 the sample also passed through a HaySepD precolumn.

2.5.2 Liquid product detection

Liquid products were evaluated using an ionic exchange chromatograph equipped with a Metrosep A Supp 5 column and a conductivity detector. A typical measurement requires the sampling of 50 µL of solution, followed by a 200-400 times dilution based on the observed formate concentration in ultrapure water and injection of 20 µL into the IC chromatograph. For better accuracy it is suggested that recipients for the dilute samples be made from plastic and discarded after one use, that dilution in MiliQ water be done by weighing instead of volumetric measurement and that the sample is filtered or centrifuged prior to analysis.

2.6 ILs drying process and water quantification

Before use in solution with molecular catalyst $[Re(bpy)(CO)_3Cl]$, all ILs were vacuum-dried overnight under stirring using a vacuum pump and then stored in a glove box under argon. The drying procedure followed was reported by Montiel et al.[10] All solutions of ILs in acetonitrile (ILs/CH_3CN) were freshly prepared in the glove box before each experiment. Water content in all the resulting acetonitrile solutions was quantified by Karl Fischer titration, which consists of an electrochemical coulometric method that

consumes water in the oxidation reaction and allows quantifying even traces of humidity in samples. The titration samples mass was of (0.3 – 0.5) g and the measurement range was of 20 – 3000 ppm (detection limit for H_2O quantification 2 ppm). The final concentration of water present in each IL/CH_3CN solution was: 88 ppm for 0.5 M [BMIM][PF_6], 250 ppm for 0.5 M [EMIM][PF_6], 151 ppm for 0.5 M [EMIM][BF_4], 158 ppm for 0.5 M [BMPyrr][PF_6]. No water quantification was performed for [DiMIM][$N(SO_2CF_3)_2$]. Pure acetonitrile water content was 77 ppm.

2.7 Density Functional Theory (DFT) calculations

DFT calculations were carried out at the ωB97X-D level[11] using the Gaussian 16 (rev. C.01) quantum chemistry software[12]. The LANL2DZ[13] basis set and associated pseudopotentials were used to describe Rh ions, which were supplemented by one shell of f-type polarization functions[14]. Remaining atoms were treated with the Pople-type 6-31G(d,p) basis set[15–17]. Solvent effects of acetonitrile were included in the geometry optimizations and energy calculations by means of the IEF-PCM implicit solvent model[18], as implemented in Gaussian 16. The nature of the stationary points on the potential energy surface was confirmed via normal-mode analysis calculations. The standard-state correction to switch from the reference state of 1 atm used in the Gaussian code to 1.0 M in solution at 25 °C (+1.89 kcal/mol) was applied to the free energy of all the species. A dataset collection of the computational results is available in the ioChem-BD repository[19] and can be accessed via: DOI: 10.19061/iochem-bd-6-109.

2.8 Synthesis of complexes [Rh(bpy-X_2)(Cp*)Cl] and [Re(bpy-X_2)$(CO)_3$Cl], where X=H, OCH_3, $COOCH_3$

Syntheses of complexes [Re(bpy-X_2)$(CO)_3$Cl] were performed according to previously described protocols[20–22] and syntheses of complexes [Rh(bpy-X_2)(Cp*)Cl] were adapted from existing protocols in the literature[23–25].

Synthesis of [Rh(2,2'-bipyridine)(Cp*)Cl]Cl :

Protocol adapted from the literature[23–25]. A methanol solution (30 mL) of 1 equivalent $[Rh(Cp^*)Cl]_2$ (200 mg, 0.32 mmol) and 2 equivalents 2 2'-bipyridine (100 mg, 0.64 mmol) was stirred at RT for 2h in the dark. The resulting clear orange-yellow solution was evaporated until dry. The yellow solid was purified by recrystallization. It was dissolved in a minimal quantity of acetonitrile (CH_3CN) and

precipitated upon the addition of ethyl acetate (AcOEt), then collected on a Buchner funnel and dried under vacuo. Yield = 88 %. The purity of the final precipitate was verified by ^{1}H NMR spectroscopy.
^{1}H NMR (300 MHz, DMSO-d6): δ/ppm, 1.01 (s, 15H), 7.89 (t, J = 6.2 Hz, 2H), 8.32-8.34 (m, 2H), 8.72 (d, J = 7.8 Hz, 2H), 8.98 (d, J = 5.4 Hz, 2H).

Synthesis of [Rh(4,4'-dimethoxy-2,2'-bipyridine)(Cp*)Cl] :

Protocol adapted from the literature[24]. A methanol solution (10 mL) of 1 equivalent $[Rh(Cp^*)Cl]_2$ (100 mg, 0.16 mmol) and 2 equivalents 4,4'-dimethoxy-2,2'-bipyridine (82.17 mg, 0.38 mmol) was stirred at RT for 12 h. The solvent was removed in vacuo and the residue was dissolved in a minimum amount of acetonitrile. Addition of ethyl acetate gave a pale-yellow solid which was collected on a Buchner funnel, washed with ether, and dried under vacuo. An analytical sample was obtained by recrystallization from CH_3CN/AcOEt (yield = 90 %) and characterized by ^{1}H NMR spectroscopy.
^{1}H NMR (300 MHz, DMSO-d6): δ/ppm, 1.01 (s, 15H), 4.07 (s, 6H), 7.42 (dd, J = 9.1 Hz, 2H), 8.31 (d, J = 2.4 Hz ,2H), 8.73 (d, J = 6.3 Hz, 2H).

Synthesis of [Rh (2,2'-bipyridine-carboxylic acid methyl ester)(Cp*)Cl] :

Protocol adapted from the literature[24]. A methanol solution (10 mL) of 1 equivalent $[Rh(Cp^*)Cl]_2$ (100 mg, 0.16 mmol) and 2 equivalents 2,2'-bipyridine-carboxylic acid methyl ester (102.55 mg, 0.38 mmol) was stirred at RT for 12 h. The solvent was removed in vacuo and the residue was dissolved in a minimum amount of acetonitrile. Addition of ethyl acetate gave a pale-yellow solid which was collected on a Buchner funnel, washed with ether, and dried in vacuo. An analytical sample was obtained by recrystallization from CH_3CN/AcOEt (yield = 91 %) and characterized by ^{1}H NMR spectroscopy.
^{1}H NMR (300 MHz, DMSO-d6): δ/ppm, 1.01 (s, 15H), 4.03 (s, 6H), 8.26 (m, 2H), 9.21 (t, J = 10.5 Hz ,4H).

Synthesis of *fac*-[Re(4,4'-dimethoxy-2,2'-bipyridine)$(CO)_3$Cl]:

Synthesized according to protocols described in the literature[22]. A toluene solution (25 mL) containing $[Re(CO)_5Cl]$ (100 mg, 0.27 mmol) and 4,4'-dimethoxy-2,2'-bipyridine (60 mg, 0.27 mmol) was refluxed under an Ar atmosphere for 3 h in dim light. After the solution cooled to room temperature, the resulting yellow precipitates were filtered and washed with toluene, hot hexane, and then *n*-pentane. Yield = 95 %. The purity of the final precipitate was verified by ^{1}H NMR spectroscopy.

^{1}H NMR (300 MHz, acetone-*d*6): δ/ppm, 4.13 (s, 6H), 7.29 (dd, J = 5.4 Hz, 2H), 8.17 (d, J = 2.4 Hz, 2H), 8.83 (d, J = 6.6 Hz, 2H).

Synthesis of [Re(2,2'-bipyridine-carboxylic acid methyl ester)$(CO)_3Cl$]:

Synthesized according to protocols described in the literature[22]. $[Re(CO)_5Cl]$ (100 mg, 0.27 mmol) was dissolved in 25 mL of methanol under a nitrogen (inert) atmosphere. 2,2'-bipyridine-carboxylic acid methyl ester (76 mg, 0.28 mmol) was added as a solid, and the obtained colorless solution was heated for 2 h at reflux temperature under inert atmosphere. During this time, the solution became deep yellow. The volume was reduced at 20 mL by rotary evaporation and left to cool at rt, where upon the product precipitated as a pure, yellow solid. Yield = 93 %. The purity of the final precipitate was verified by ^1H NMR spectroscopy.

^1H NMR (300 MHz, CD_3CN): δ/ppm, 4.02 (s, 6H), 8.01 (dd, J = 7.5 Hz, 2H), 8.95 (d, J = 0.9 Hz, 2H), 9.18 (t, J = 6.0 Hz, 2H).

2.9 References

(1) Merino-Garcia, I.; Tinat, L.; Albo, J.; Alvarez-Guerra, M.; Irabien, A.; Durupthy, O.; Vivier, V.; Sánchez-Sánchez, C. M. Continuous Electroconversion of CO_2 into Formate Using 2 Nm Tin Oxide Nanoparticles. *Appl. Catal. B Environ.* **2021**, *297*, 120447. https://doi.org/10.1016/j.apcatb.2021.120447.

(2) Whipple, D. T.; Kenis, P. J. A. Prospects of CO_2 Utilization via Direct Heterogeneous Electrochemical Reduction. *J. Phys. Chem. Lett.* **2010**, *1* (24), 3451–3458. https://doi.org/10.1021/jz1012627.

(3) Elgrishi, N.; Rountree, K. J.; McCarthy, B. D.; Rountree, E. S.; Eisenhart, T. T.; Dempsey, J. L. A Practical Beginner's Guide to Cyclic Voltammetry. *J. Chem. Educ.* **2018**, *95* (2), 197–206. https://doi.org/10.1021/acs.jchemed.7b00361.

(4) Michez, R.; Doneux, T.; Buess-Herman, C.; Luhmer, M. NMR Study of the Reductive Decomposition of [BMIm][NTf_2] at Gold Electrodes and Indirect Electrochemical Conversion of CO_2. *ChemPhysChem* **2017**, *18* (16), 2208–2216. https://doi.org/10.1002/cphc.201700421.

(5) Pugliese, S.; Huan, N. T.; Forte, J.; Grammatico, D.; Zanna, S.; Su, B.-L.; Li, Y.; Fontecave, M. Functionalization of Carbon Nanotubes with Nickel Cyclam for the Electrochemical Reduction of CO_2. *ChemSusChem* **2020**, *13* (23), 6449–6456. https://doi.org/10.1002/cssc.202002092.

(6) Prodromidis, M. I.; Florou, A. B.; Tzouwara-Karayanni, S. M.; Karayannis, M. I. The Importance of Surface Coverage in the Electrochemical Study of Chemically Modified Electrodes. *Electroanalysis* **2000**, *12* (18), 1498–1501. https://doi.org/10.1002/1521-4109(200012).

(7) Senocrate, A.; Battaglia, C. Electrochemical CO_2 Reduction at Room Temperature: Status and Perspectives. *J. Energy Storage* **2021**, *36*, 102373. https://doi.org/10.1016/j.est.2021.102373.

(8) Greczynski, G.; Hultman, L. X-Ray Photoelectron Spectroscopy: Towards Reliable Binding Energy Referencing. *Prog. Mater. Sci.* **2020**, *107*, 100591. https://doi.org/10.1016/j.pmatsci.2019.100591.

(9) Desimoni, E.; Brunetti, B. X-Ray Photoelectron Spectroscopic Characterization of Chemically Modified Electrodes Used as Chemical Sensors and Biosensors: A Review. *Chemosensors* **2015**, *3* (2), 70–117. https://doi.org/10.3390/chemosensors3020070.

(10) Montiel, M. A.; Solla-Gullón, J.; Montiel, V.; Sánchez-Sánchez, C. M. Electrocatalytic Studies on Imidazolium Based Ionic Liquids: Defining Experimental Conditions. *Phys. Chem. Chem. Phys.* **2018**, *20* (28), 19160–19167. https://doi.org/10.1039/C8CP02662A.

(11) Chai, J.-D.; Head-Gordon, M. Long-Range Corrected Hybrid Density Functionals with Damped Atom–Atom Dispersion Corrections. *Phys. Chem. Chem. Phys.* **2008**, *10* (44), 6615–6620. https://doi.org/10.1039/B810189B.

(12) Frisch, J. M.; Trucks, G. W.; Schlegel, H. B.; Scuseria, G. E.; Robb, M. A.; Cheeseman, J. R.; Scalmani, G.; Barone, V.; Petersson, G. A.; Nakatsuji, H.; Li, X.; Caricato, M.; Marenich, A. V.; Bloino, J.; Janesko, B. G.; Gomperts, R.; Mennucci, B.; Hratchian, H. P.; Ortiz, J. V.; Izmaylov, A. F.; Sonnenberg, J. L.; Williams-Young, D.; Ding, F.; Lipparini, F.; Egidi, F.; Goings, J.; Peng, B.; Petrone, A.; Henderson, T.; Ranasinghe, D.; Zakrzewski, V. G.; Gao, J.; Rega, N.; Zheng, G.; Liang, W.; Hada, M.; Ehara, M.; Toyota, K.; Fukuda, R.; Hasegawa, J.; Ishida, M.; Nakajima, T.; Honda, Y.; Kitao, O.; Nakai, H.; Vreven, T.; Throssell, K.; Montgomery, Jr., J. A.; Peralta, J. E.; Ogliaro, F.; Bearpark, J. M.; Heyd, J. J.; Brothers, E. N.; Kudin, K. N.; Staroverov, V. N.; Keith, T. A.; Kobayashi, R.; Normand, J.; Raghavachari, K.; Rendell, A. P.; Burant, J. C.; Iyengar, S. S.; Tomasi, J.; Cossi, M.; Millam, J. M.; Klene, M.; Adamo, C.; Cammi, R.; Ochterski, J. W.; Martin, R. L.; Morokuma, K.; Farkas, O.; Foresman, J. B.; Fox. *Gaussian 16, Revision C.01*; Gaussian, Inc., Wallingford CT; 2016.

(13) Hay, P. J.; Wadt, W. R. Ab Initio Effective Core Potentials for Molecular Calculations. Potentials for the Transition Metal Atoms Sc to Hg. *J. Chem. Phys.* **1985**, *82* (1), 270–283. https://doi.org/10.1063/1.448799.

(14) Ehlers, A. W.; Böhme, M.; Dapprich, S.; Gobbi, A.; Höllwarth, A.; Jonas, V.; Köhler, K. F.; Stegmann, R.; Veldkamp, A.; Frenking, G. A Set of F-Polarization Functions for Pseudo-Potential Basis Sets of the Transition Metals Sc-Cu, Y-Ag and La-Au. *Chem. Phys. Lett.* **1993**, *208* (1), 111–114. https://doi.org/10.1016/0009-2614(93)80086-5.
(15) Francl, M. M.; Pietro, W. J.; Hehre, W. J.; Binkley, J. S.; Gordon, M. S.; DeFrees, D. J.; Pople, J. A. Self-consistent Molecular Orbital Methods. XXIII. A Polarization-type Basis Set for Second-row Elements. *J. Chem. Phys.* **1982**, *77* (7), 3654–3665. https://doi.org/10.1063/1.444267.
(16) Hariharan, P. C.; Pople, J. A. The Influence of Polarization Functions on Molecular Orbital Hydrogenation Energies. *Theor. Chim. Acta* **1973**, *28* (3), 213–222. https://doi.org/10.1007/BF00533485.
(17) Hehre, W. J.; Ditchfield, R.; Pople, J. A. Self—Consistent Molecular Orbital Methods. XII. Further Extensions of Gaussian—Type Basis Sets for Use in Molecular Orbital Studies of Organic Molecules. *J. Chem. Phys.* **1972**, *56* (5), 2257–2261. https://doi.org/10.1063/1.1677527.
(18) Cancès, E.; Mennucci, B.; Tomasi, J. A New Integral Equation Formalism for the Polarizable Continuum Model: Theoretical Background and Applications to Isotropic and Anisotropic Dielectrics. *J. Chem. Phys.* **1997**, *107* (8), 3032–3041. https://doi.org/10.1063/1.474659.
(19) Álvarez-Moreno, M.; de Graaf, C.; López, N.; Maseras, F.; Poblet, J. M.; Bo, C. Managing the Computational Chemistry Big Data Problem: The IoChem-BD Platform. *J. Chem. Inf. Model.* **2015**, *55* (1), 95–103. https://doi.org/10.1021/ci500593j.
(20) Caspar, J. V.; Meyer, T. J. Application of the Energy Gap Law to Nonradiative, Excited-State Decay. *J. Phys. Chem.* **1983**, *87* (6), 952–957. https://doi.org/10.1021/j100229a010.
(21) Ono, Y.; Nakamura, J.; Hayashi, M.; Takahashi, K. I. Effect of Substituent Groups in Rhenium Bipyridine Complexes on Photocatalytic CO_2 Reduction. *Am. J. Appl. Chem.* **2014**, *2* (5), 74. https://doi.org/10.11648/j.ajac.20140205.12.
(22) Takeda, H.; Koike, K.; Inoue, H.; Ishitani, O. Development of an Efficient Photocatalytic System for CO_2 Reduction Using Rhenium(I) Complexes Based on Mechanistic Studies. *J. Am. Chem. Soc.* **2008**, *130* (6), 2023–2031. https://doi.org/10.1021/ja077752e.
(23) Kölle, U.; Grützel, M. Organometallic Rhodium (III) Complexes as Catalysts for the Photoreduction of Protons to Hydrogen on Colloidal TiO_2. *Angew. Chem. Int. Ed. Engl.* **1987**, *26* (6), 567–570. https://doi.org/10.1002/anie.198705671.
(24) Todorova, T. K.; Huan, T. N.; Wang, X.; Agarwala, H.; Fontecave, M. Controlling Hydrogen Evolution during Photoreduction of CO_2 to Formic Acid Using $[Rh(R\text{-}Bpy)(Cp^*)Cl]^+$ Catalysts: A Structure-Activity Study. *Inorg. Chem.* **2019**, *58* (10), 6893–6903. https://doi.org/10.1021/acs.inorgchem.9b00371.
(25) Wang, W.-H.; Suna, Y.; Himeda, Y.; Muckerman, J. T.; Fujita, E. Functionalized Cyclopentadienyl Rhodium(III) Bipyridine Complexes: Synthesis, Characterization, and Catalytic Application in Hydrogenation of Ketones. *Dalton Trans.* **2013**, *42* (26), 9628–9636. https://doi.org/10.1039/C3DT50445J.

CHAPTER 3:

IMIDAZOLIUM- AND PYRROLIDINIUM-BASED IONIC LIQUIDS AS COCATALYSTS FOR CO2 ELECTROREDUCTION IN MODEL MOLECULAR ELECTROCATALYSIS

3.1 Introduction

Carbon dioxide electroreduction reaction (CO_2RR) is considered an environmentally friendly approach that not only allows exploiting a waste material to produce valuable fuels or other chemicals, but also constitutes a promising solution for storing the intermittent energy originating from renewable sources. A first step in that direction would be the electroreduction of CO_2 to CO, which could be used as feedstock in Fischer-Tropsch technologies that result in hydrocarbon products. In addition to this, CO_2 conversion to formate also represents an interesting alternative, since formate is industrially used and considered as a commodity chemical[1]. However, the intrinsic inertness of the CO_2 molecule is an obstacle to its direct reduction, which necessitates the use of a catalyst. Many metal complexes have been identified as efficient homogeneous catalysts for CO_2 reduction, mainly contributing to ameliorating the activity, selectivity and efficiency of this reduction[2–5]. Molecular electrocatalysts have been extensively studied since they offer a high degree of tunability through: i) the metal center, traditionally composed of a noble-metal (Re, Rh, Ru, Pd,…)[6–10], although more recently substituted by earth-abundant transition metals (Ni, Co, Mn, Fe,…)[8,9,11–13] and ii) the choice of ligand, which tunes the electronic (thus the redox potential) and the geometric features[14]. An example of a model molecular catalyst to selectively convert CO_2 to CO is the rhenium (I) complex [Re(bpy)$(CO)_3$Cl], (where bpy is 2,2′-bipyridine), also known as Lehn's catalyst and here seen in Figure 3.1, hitherto referred to as complex [1]. A detailed mechanism for complex [1] has already been well-established[6,7,15]. Furthermore, studies have been carried out incorporating electron donating or electron withdrawing groups on the bpy ligand[16–18], as well as studies where this complex was attached to higher-order systems or immobilized on surfaces[19]. Many of these studies aimed at increasing of efficiency of this catalyst in terms of energy, that is to say maintaining high Faradaic efficiencies for CO_2 to CO conversion at the lowest possible overpotential, while not compromising on current density. Another example of a model molecular catalyst, this time for formate production, is [Rh(bpy)(Cp*)Cl]Cl (where Cp*= pentamethylcyclopentadienyl), also shown in Figure 3.1 and referred to as complex [2]. This catalyst presents three main features of interest in comparison with other molecular catalysts; *i*) it is soluble in aqueous solution, *ii*) it can be used as both CO_2RR and hydrogen evolution reaction (HER) electrocatalyst[10,20]; and *iii*) its reaction mechanism is well-stablished in the literature[10,20]. Moreover, it has been further explored in CO_2 photoreduction[21] and within higher-order systems, such as metal-organic frameworks (MOFs) with appreciable catalytic performance[22].

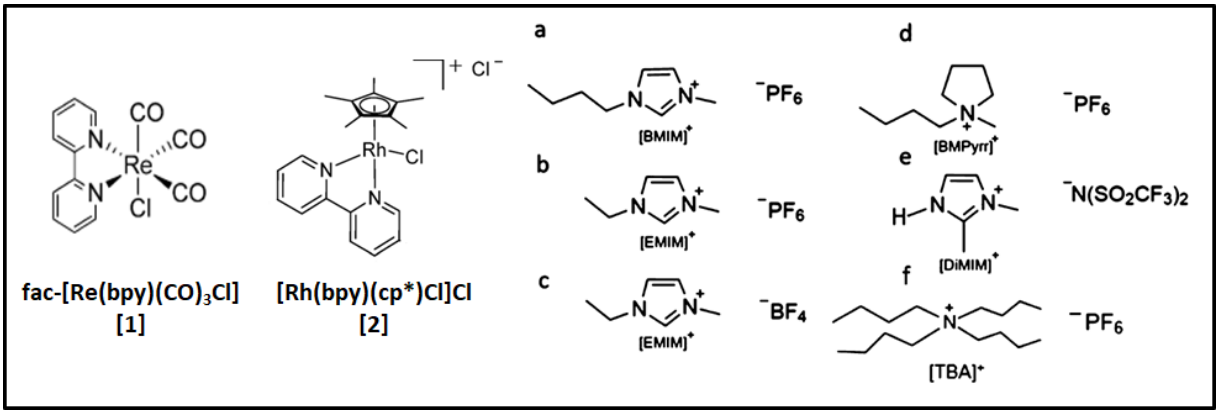

Figure 3.1 Structures of the [Re(bpy)(CO)$_3$Cl] complex [1] and [Rh(bpy)(Cp)Cl]Cl complex [2], where bpy = 2,2'-bipyridine and Cp* = pentamethylcyclopentadienyl, and the supporting electrolytes: (a) 1-Butyl-3-methylimidazolium hexafluorophosphate ([BMIM][PF$_6$]), (b) 1-Ethyl-3-methylimidazolium hexafluorophosphate ([EMIM][PF$_6$]), (c) 1-Ethyl-3-methylimidazolium tetrafluoroborate ([EMIM][BF$_4$]), (d) 1-Butyl-1-methylpyrrolidinium hexafluorophosphate ([BMPyrr][PF$_6$]), (e) 1,2-Dimethylimidazolium bis(trifluoromethylsulfonyl)imide ([DiMIM][N(SO$_2$CF$_3$)$_2$]) and (f) Tetrabutyl ammonium hexafluorophosphate ([TBA][PF$_6$]).*

Both complex [1] and [2] are model CO_2RR catalysts, whose shared similarities include having a p-electron rich bipyridine ligand and sharing HER as the competitive process. Nevertheless, they present different mechanisms for CO_2RR, which are described in scheme 3.1. Complex [1] assumed its active form after having undergone an initial two electron reduction with simultaneous chlorine ligand dissociation and was then capable to coordinate a CO_2 molecule to form a monoanionic intermediate (species B in schema 3.1a)[16]. The CO_2RR mechanism followed beyond that point was however entirely depended on the availability of protons in the reaction medium. In the absence of a specific proton source, an electron-first mechanistic pathway was favored (species C in scheme 3.1 (a)) that led to the formation of dianionic intermediate. On the other hand, in presence of a proton source in solution the mechanism proceeded through a proton-first pathway that led to a neutral catalyst intermediate (species D in scheme 3.1 (a))[16]. HER from complex [1] is also possible and even thermodynamically favored under certain conditions[23], but due to kinetic considerations the formation of species B was favored over the Re-hydride, therefore conferring to complex [1] its high selectivity towards CO production[23,24]. In contrast, complex [2] undergoes an initial two-electron reduction at the Rh center and chloride ligand dissociation followed by the formation of a metal-hydride intermediate and a subsequent ligand-centered reduction step for generating the active form of the catalyst[20]. Then, two competitive reactions could take place, either CO_2 reduction to formate by its insertion in the Rh-H bond (green pathway in Scheme 3.1 (b)) or formation of H_2 by protonation of the hydride (red pathway in Scheme 3.1 (b))[10,20]. Generally, molecular catalysts are seldom soluble in aqueous solution and for this reason most studies were reported in organic

solvents[2,25]. This was the case of complex [1], but complex [2] is a water-soluble catalyst. Altogether, their common points and divergencies make both complex [1] and [2] suitable models for understanding basic aspects of molecular CO_2 electroreduction catalysis.

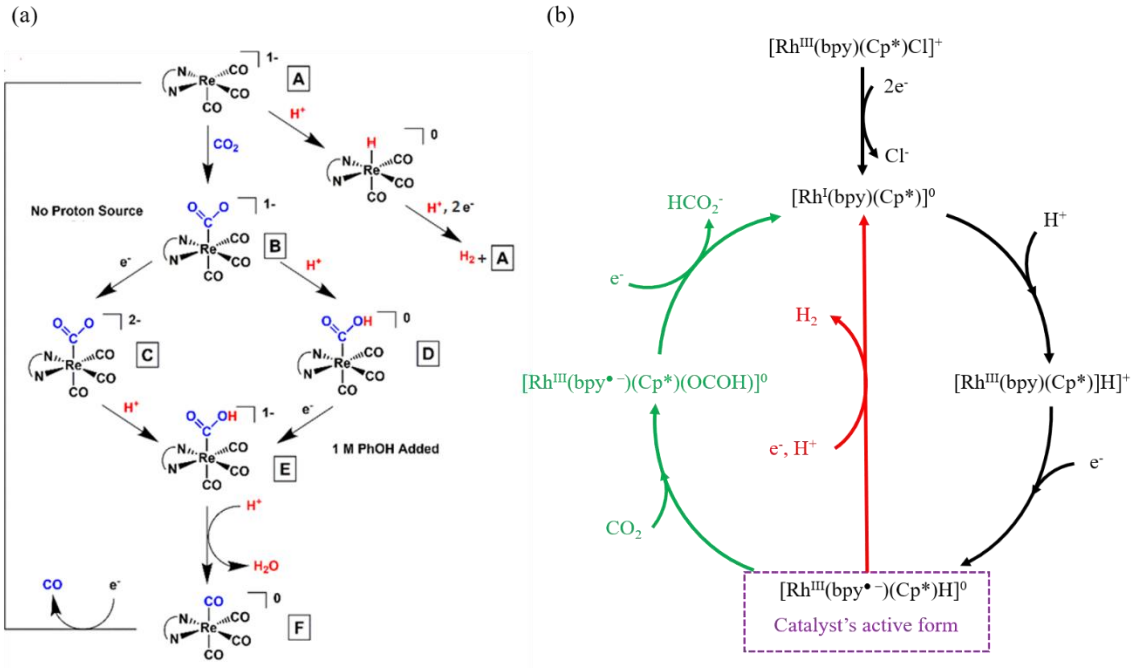

Scheme 3.1 (a) Electrocatalytic cycle of complex [1] for either CO_2 reduction in the absence and presence of an external proton source[16] *or HER*[23,24] *and (b) Electrocatalytic cycle of complex [2] for CO_2 to formate conversion (green pathway) or HER (red pathway)*[10,20].

An alternative strategy to improve catalytic performances, other than the modification of the molecular catalyst itself, would be the modulation of the local electric field in the double layer by electrolyte engineering. The latter corresponds to the control of the ions present at the electrode-electrolyte interface when the electrical double layer is built up. This has been known to impact on the selectivity and the energy efficiency of CO_2RR by stabilizing reaction intermediates and/or blocking competitive mechanistic pathways[26–28].

Pure ionic liquids (ILs) as a solvent or a supporting electrolyte for CO_2RR have attracted a lot of attention in the field of catalysis due to the wide electrochemical potential window provided by ILs[29–32]. However, the high viscosity of most ILs limits their applications as solvents in electrochemistry, since it is inversely proportional to the conductivity of the solvent, it limits diffusion of soluble species and can lead to significant limitations in terms of maximum current density achieved[33]. However, this issue is not as prevalent when they are used as supporting electrolytes mixed with molecular (organic or aqueous) solvents. The positive effect of ILs at the electrode/solution interface either by stabilizing reaction

intermediates and binding the CO_2 molecule or suppressing competitive HER has been already demonstrated on heterogeneous catalysts[34–37]. In contrast, very few studies using ILs in solution have been devoted to molecular catalytic systems and all those studies were conducted in organic solvents[34,38,39]. Notably for the present study, Matsubara et al.[38] combined linear sweep voltammetry (LSV) and density functional theory (DFT) calculations to study the role of a unique imidazolium-based IL $[EMIM]^+$ in acetonitrile for CO_2 electroreduction catalyzed by complex [1]. They reported a significant positive shift of the catalytic onset potential in the presence of ILs[38]. To the best of our knowledge, complex [2] has not yet been used alongside ILs besides the present study.

Taking all this into consideration, we aimed at further studying the effects of different types of ILs in promoting CO_2 electroreduction, however not as solvents but as supporting electrolytes, using the two model molecular catalysts presented. We particularly wanted to address the role of the structure of the IL used and the type of interaction between IL and catalyst, that were at the root of either enhanced catalysis or altered product selectivity. For that purpose, we chose two different molecular catalysts with well-established catalytic mechanisms, complexes [1] and [2], as models and five different ILs (protic and aprotic) as shown in Figure 3.1, allowing to compare four different cations and three different anions, as supporting electrolytes in acetonitrile and one IL in aqueous solution. Figure 3.1 presents three ILs from the imidazolium cation family, namely 1-Ethyl-3-methylimidazolium with either hexafluorophosphate $[PF_6]^-$ ([EMIM][PF_6]) or tetrafluoroborate $[BF_4]^-$ ([EMIM][BF_4]) as the counter-anion, 1-Butyl-3-methylimidazolium hexafluorophosphate ([BMIM][PF_6]), 1,2 Dimethylimidazolium bis(trifluoromethylsulfonyl)imide ([DiMIM][$N(SO_2CF_3)_2$]), a protic IL containing an acidic proton, and one IL from the pyrrolidinium cation family, namely 1-Butyl-1-methylpyrrolidinium hexafluorophosphate ([BMPyrr][PF_6]).

3.2 Results

3.2.1 [Re(bpy)$(CO)_3$Cl] with ILs as electrolyte in acetonitrile under inert conditions

In Figure 3.2 are shown the cyclic voltammograms (CVs) of an acetonitrile solution containing 1 mM complex [1] under inert conditions (Argon saturated) in the presence of different supporting electrolytes including conventional benchmark [TBA][PF_6], one pyrrolidinium based IL [BMPyrr][PF_6] and 3 different imidazolium based ILs ([BMIM][PF_6], [EMIM][PF_6], and [EMIM][BF_4]). A constant electrolyte concentration of 0.5 M was used for studying the electrochemical behavior of complex [1] and to rule out any effect from increasing ionic strength. Moreover, this concentration proved a good compromise by providing a relevant overpotential diminution and enough conductivity when ILs were

in solution, as can be seen in Figure 3.3. Furthermore, all ILs were dried before use as explained in Chapter 2.6, since H_2O content in ILs has been demonstrated to play a relevant role[40,41]. According to previous reports[6,16,42], the first reduction wave shown in Figure 3.2 was attributed to a one-electron reversible reduction centered on the bpy ligand (bpy to bpy^-) and the second more cathodic wave to a one-electron irreversible or quasi-reversible metal centered reduction (Re^I to Re^0). Figure 3.2 (a) presents the behavior of complex [1] in the presence of [TBA][PF_6] and 2 different IL cations (pyrrolidinium and imidazolium), which kept constant the alkyl chain length in the cation. The anion $[PF_6]^-$ was also kept unchanged in all 3 cases to evaluate only the role of the cation. We observed that: (i) both redox processes were significantly shifted anodically in the presence of both ILs as compared to [TBA][PF_6]; (ii) the potential shift of the second reduction wave was much larger than that of the first reduction wave; (iii) these shifts greatly depended on the nature of the IL cation, being much more relevant when the imidazolium cation was present in solution, with the trend in potentials being $[IM]^+ > [Pyrr]^+ > [TBA]^+$. Figure 3.2 (b) shows the complex [1] performance in the presence of 3 different imidazolium based ILs by studying the effect of the alkyl chain length in the cation and the nature of the anion. It shows that those two parameters had only a minor effect on the CVs of complex [1]. Table 3.1 reports the characteristic potentials for all reduction peaks shown in Figure 3.2. Thus, the first reduction potential was shifted positively between 60 and 210 mV by replacing [TBA][PF_6] with an IL. Meanwhile the second reduction peak was also shifted positively between 190 and 370 mV depending on the IL used, with [EMIM][BF_4] being the one that displayed the most important potential shift in Figure 3.2 (b). We equally observed that the current density displayed in Figure 3.2 remained very similar in the presence and absence of ILs and did not vary according to the nature of the IL.

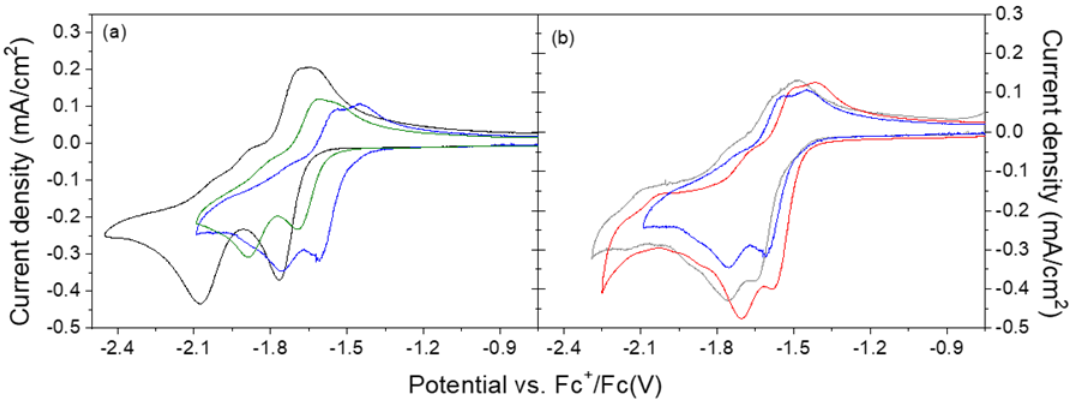

Figure 3.2 Cyclic Voltammograms of 1 mM complex [1] and 0.5 M of different supporting electrolytes in acetonitrile solution under Ar: (a) [TBA][PF_6] (black plot), [BMPyrr][PF_6] (green plot) and [BMIM][PF_6] (blue plot) and (b) [EMIM][BF_4] (red plot), [EMIM][PF_6] (grey plot) and [BMIM][PF_6] (blue plot). Scan rate 0.1 V/s.

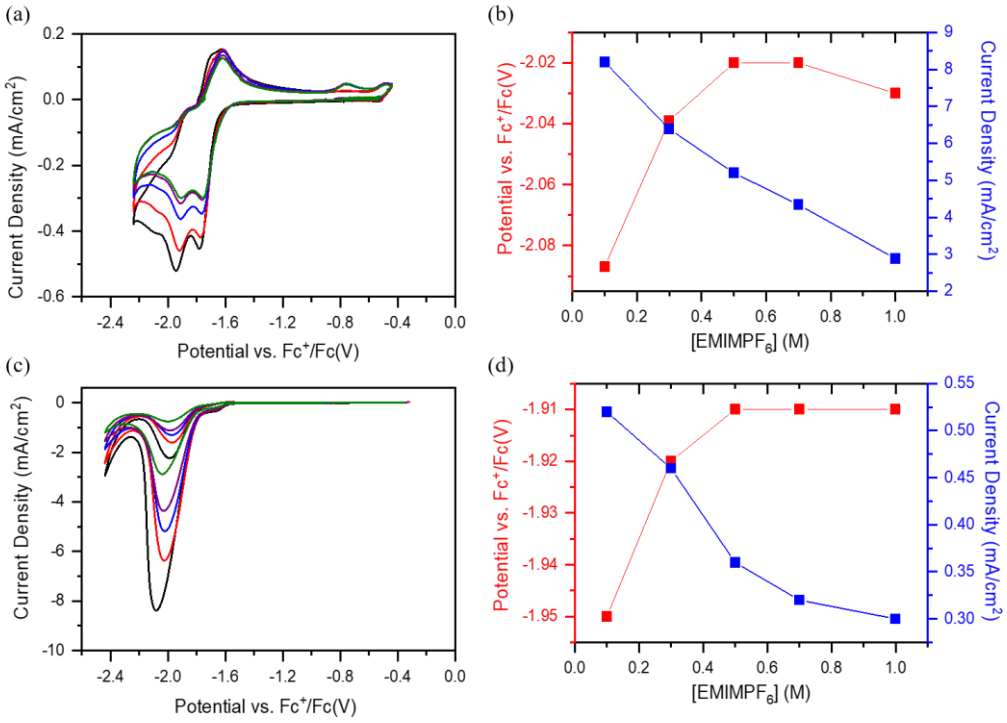

Figure 3.3 CVs of 1 mM complex [1] at increasing concentrations of [EMIM][PF_6] in acetonitrile: 0.1 M (black), 0.3 M (red), 0.5 M (blue), 0.7 M (purple) and 1 M (green): (a) under Ar and (c) under a CO_2 atmosphere in the presence of 1.5 M TFE. Scan rate 0.1 V/s. Also, representation of the variation of the second reduction peak potential of complex [1] and its current density vs. the concentration of [EMIM][PF_6]: (b) under Ar and (d) under a CO_2 atmosphere in the presence of 1.5 M TFE.

Figure 3.4 shows that complex [1] in the presence of [DiMIM][$N(SO_2CF_3)_2$], the only protic IL tested in this work, whose structure is also shown in Figure 3.1 (e), did not show its two characteristic reduction waves in the mixture IL/ CH_3CN. Figure 3.4 seemed to indicate the direct proton reduction present in $[DiMIM]^+$ at the GCE surface.

The reason why we had dried the ILs before use resided in the observation that the H_2O content in the IL/CH_3CN solutions was significant and had a relevant impact on the potentials displayed by the two reduction waves of complex [1]. Table 3.1 shows the H_2O concentration in the IL/CH_3CN solutions quantified by Karl Fischer titration using dried and not dried ILs. In some cases, H_2O concentration greatly decreased after drying, even by an order of magnitude. In Figure 3.5, CVs of complex [1] in CH_3CN solutions using dried ILs and not dried ILs are compared and in all 4 cases the reduction waves of complex [1] were cathodically shifted and the current densities were larger when not dried ILs were used as supporting electrolyte, proving that the drying process of ILs proposed here, in coordination with adopting specific filters that blocked humidity in the gas inlet were important in order to reach reliable results. Furthermore, it indicated that not only the interactions between the complex and the IL that

facilitated the reduction were partly suppressed in the presence of H_2O, but also under these conditions some proton reduction catalysis may occur. As a consequence, all experiments with complex [1], including those reported in Figure 3.2, had thus been carried out with dried ILs exclusively.

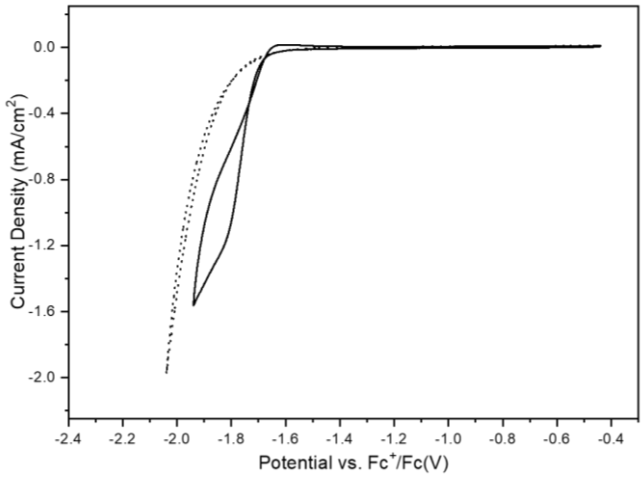

Figure 3.4 CV of 1 mM complex [1] in 0.5 M [DiMIM][N(SO₂CF₃)₂] acetonitrile solution under Ar (black solid line). Blank CV of 0.5 M [DiMIM][N(SO₂CF₃)₂] in acetonitrile under Ar (black dashed line). Scan rate 0.1 V/s.

Table 3.1 H_2O content quantification in 0.5 M IL CH_3CN solutions using Karl-Fischer titration before and after ILs drying treatment.

0.5 M IL in CH_3CN solution	**[H_2O] (ppm) before drying ILs**	**[H_2O] (ppm) after drying ILs**
[BMIM][PF_6]	652	88
[BMPyrr][PF_6]	2557	158
[EMIM][PF_6]	435	250
[EMIM][BF_4]	1821	151

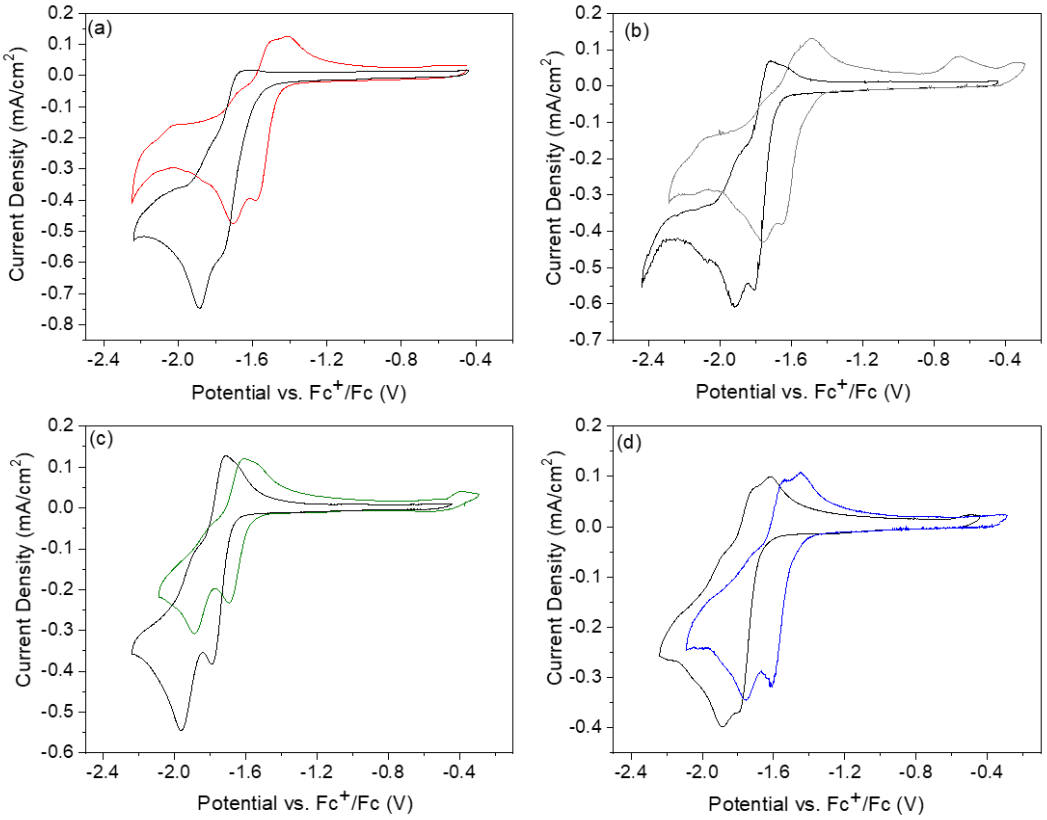

Figure 3.5 CVs of 1 mM complex [1] and 0.5 M of different ILs in acetonitrile solution underAr after following the drying treatment of ILs (colored plots) or without drying (black plots). The drying protocol is described in Chapter 2. IL present: (a) [EMIM][BF_4], (b) [EMIM][PF_6], (c) [BMPyrr][PF_6] and (d) [BMIM][PF_6]. Scan rate 0.1 V/s.

3.2.2 [Re(bpy)$(CO)_3$Cl] with ILs as electrolyte under CO_2 reduction catalytic conditions

We subsequently studied the catalytic properties of complex [1] for CO_2 electroreduction in the presence of all different ILs investigated. Thus, Figure 3.6 shows CVs of complex [1] under catalytic CO_2 conditions without an added proton source. A catalytic wave for CO_2 electroreduction, as expected, was observed at the second complex reduction process, where the catalytically active 2-electron reduced species was generated. Thus, a significant increase in current density (j_{cat}) was observed at the second potential peak in all CVs of Figure 3.6 when CO_2 was present in solution. Figure 3.6 (a) illustrates the catalyst behavior in the presence of conventional benchmark [TBA][PF_6] electrolyte and 2 different IL cations (pyrrolidinium and imidazolium), which kept constant the alkyl chain length in the cation. The anion $[PF_6]^-$ was kept unchanged in all 3 cases. A relevant positive shift due to the presence of ILs in solution was displayed for both reduction waves following the same trend already observed in Figure 3.2 (a) under inert conditions ($[IM]^+ > [Pyrr]^+ > [TBA]^+$). Figure 3.6 (b) shows the catalyst behavior in the presence of 3 different imidazolium based ILs by studying the effect of the alkyl chain length in the

cation and the nature of the anion. Both ILs containing $[EMIM]^+$ cation showed the largest j_{cat} value. Table 3.2 reports an estimation of catalytic current densities obtained in each case by comparison with the corresponding current densities obtained under inert conditions (using the ratio j_{cat}/j_p) and the characteristic potentials for the catalytic peaks shown in Figure 3.6. Thus, the largest j_{cat}/j_p ratios were obtained in 0.5 M [EMIM][PF_6] and 0.5 M [EMIM][BF_4] in CH_3CN. Furthermore, Table 3.2 reports $E_{cat/2}$ values, potentials corresponding to half of the catalytic peak current, as proposed by Kubiak's group when using complex [1][16]. These values showed that catalysis occurred at more positive potentials in the presence of ILs, with positive shifts ranging from 200 to 330 mV depending on the IL used. [EMIM][BF_4] was the IL that displayed the most important potential shift and therefore, the lowest overpotential (1.19 V). Nevertheless, all three imidazolium-based ILs exhibited very close overpotential values. Finally, Figure 3.7 shows that in the case of using [DiMIM][$N(SO_2CF_3)_2$] in solution, the same reduction current was observed when the CV was recorded in the absence or in the presence of CO_2, reflecting that reduction of protons provided by the IL was the predominant reaction.

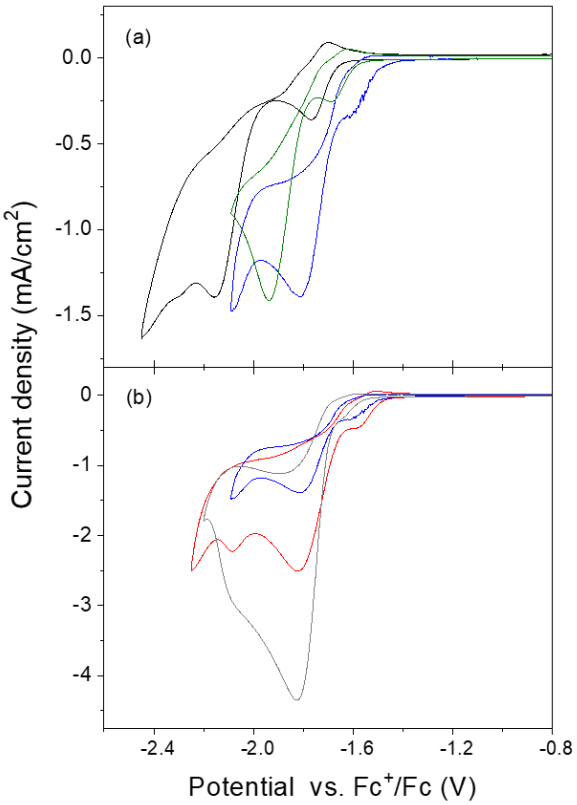

Figure 3.6 Cyclic Voltammograms of 1 mM complex [1] and 0.5 M of different supporting electrolytes in CO_2-saturated acetonitrile solution. (a) [TBA][PF_6] (black plot), [BMPyrr][PF_6] (green plot) and [BMIM][PF_6] (blue plot) and (b) [EMIM][PF_6] (grey plot), [EMIM][BF_4] (red plot) and [BMIM][PF_6] (blue plot). Scan rate 0.1 V/s.

Table 3.2 Descriptors for 1 mM complex [1] under inert conditions (Ar) and CO_2 catalytic conditions in 0.5 M of each supporting electrolyte in CH_3CN. Potential of the Rh-centered reduction peak ($E_{p1/2}$), potential of the bpy-centered reduction peak (E_p), catalytic reduction potential ($E_{cat/2}$), overpotential (η), and ratio of the catalytic peak current density and the peak current density under inert conditions (j_{cat}/j_p).

	Under inert conditions		Under catalytic CO_2 conditions		
Supporting Electrolyte	**$Ep_{1/2}$ (V)[a]**	**E_p (V)[a]**	**$E_{cat/2}$ (V)[a]**	**η (V)[b]**	**j_{cat}/j_p**
[TBA][PF_6]	-1.70	-2.07	-2.06	1.52	3.2
[BMIM][PF_6]	-1.52	-1.76	-1.75	1.21	4.0
[BMPyrr][PF_6]	-1.64	-1.88	-1.86	1.32	4.6
[EMIM][PF_6]	-1.57	-1.75	-1.74	1.20	9.9
[EMIM][BF_4]	-1.49	-1.70	-1.73	1.19	5.3

[a]Potentials are referred vs. Fc^+/Fc (V), [b]Determined based on $E_{cat/2}$ using $E^0_{CO2/CO}$ (CH_3CN) = -0.541 V vs. Fc^+/Fc.[16,43]

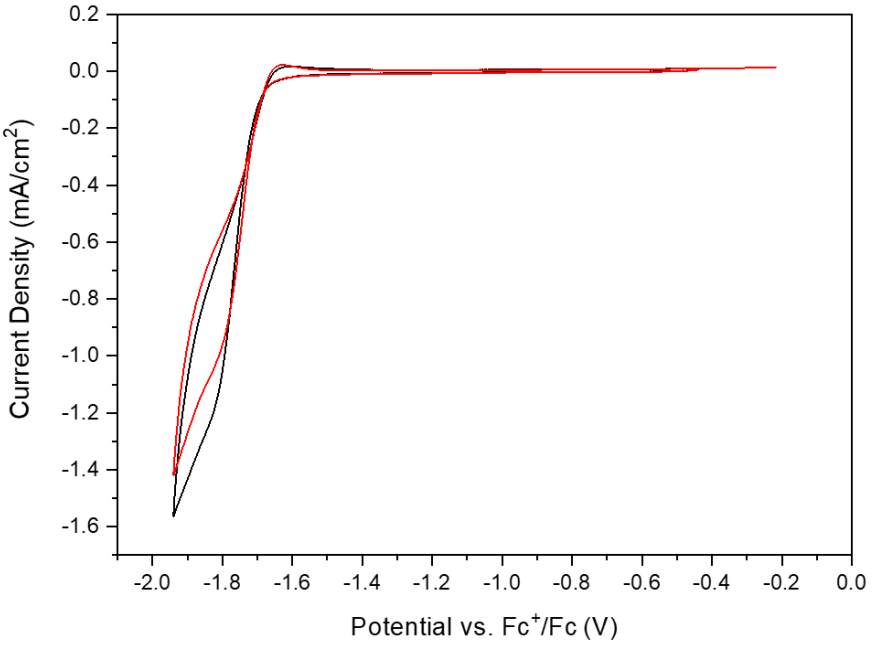

Figure 3.7 CVs of 1 mM complex [1] in 0.5 M [DiMIM][$N(SO_2CF_3)_2$] in acetonitrile underAr (black solid line) and CO_2 (red solid line). Scan rate 0.1 V/s.

It has been previously demonstrated in the literature that CO_2 electroreduction catalyzed by molecular complexes required the presence of a proton source in solution, in order to facilitate the proton-coupled electron transfers (PCET) that are associated with CO_2 reduction. Following previous studies,[16] the weak Brønsted acid 2,2',2''-trifluoroethanol (TFE) was identified as an appropriate proton source and 1.5 M an optimal TFE concentration to give an enhanced activity for CO_2 electroreduction, which was also the case when ILs were in solution, as can be witnessed in Figure 3.8.

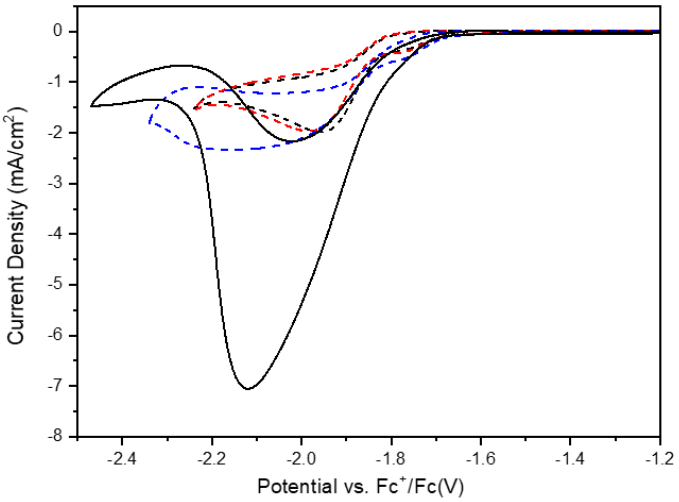

Figure 3.8 CVs of 1 mM complex [1] in 0.5 M [EMIM][PF_6] and different concentrations of TFE in CO_2 saturated acetonitrile solution with no added TFE (black dotted plot), 0.015 M TFE (red dotted plot), 0.15M TFE (blue dotted plot) and 1.5 M TFE (black solid plot). Scan rate 0.1 V/s.

Thus, Figure 3.9 shows CVs of complex [1] under catalytic CO_2 conditions in the presence of 1.5 M TFE as a proton source and 0.5 M of all different supporting electrolytes studied here. Table 3.3 reports an estimation of catalytic current densities obtained in each case by comparison versus inert conditions (j_{cat}/j_p) and the characteristic potentials for the catalytic reduction peaks shown in Figure 3.9. As expected from the literature[16], when using [TBA][PF_6] as supporting electrolyte, a significant shift (130 mV) towards more positive potentials was observed in the catalytic CO_2 reduction wave due to the addition of a weak acid, such as TFE. In contrast, in the case of pyrrolidinium based IL, the $E_{cat/2}$ in CO_2-saturated solution with and without TFE were about the same (see $E_{cat/2}$, Tables 3.2 and 3.3) and in the case of all 3 imidazolium-based ILs, we observed a significant shift (~ 150 mV) towards more negative potentials when TFE was present in solution. Nevertheless, catalysis still occurred at potentials slightly more positive in the presence of ILs as compared to benchmark supporting electrolyte [TBA][PF_6] by 30-70 mV, [BMIM][PF_6] and [BMPyrr][PF_6] being the ones displaying the most positive $E_{cat/2}$ and the lowest overpotential (0.50 V and 0.52 V, respectively). Another effect of the ILs in solution appeared to be a

moderate enhancement of maximum current density as compared to [TBA][PF_6], with [EMIM][BF_4] giving the highest value, in the vicinity of 10 mA/cm^2. However, [BMPyrr][PF_6] exhibited the highest catalytic current ratio due to its lower current under inert conditions.

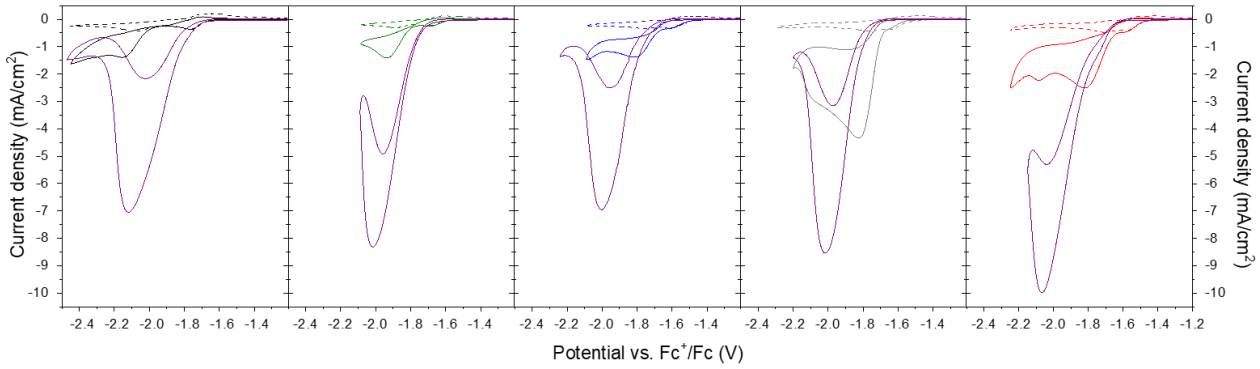

Figure 3.9 Cyclic Voltammograms of 1 mM complex [1] and 0.5 M of different supporting electrolytes in acetonitrile solution under Ar (dashed plots) and CO_2 (solid plots) colored as follows: [TBA][PF_6] (black), [BMPyrr][PF_6] (green), [BMIM][PF_6] (blue), [EMIM][PF_6] (grey), and [EMIM][BF_4] (red), and CO_2 with 1.5 M TFE (solid purple plots in all cases). Scan rate 0.1 V/s.

Table 3.3 Comparison of the catalytic parameters of 1 mM complex [1] under a CO_2 atmosphere in the presence of 1.5 M of TFE in 0.5 M of each supporting electrolyte in CH_3CN: catalytic potential ($E_{cat/2}$), overpotential (η), and ratio of the catalytic peak current density and the peak current density under inert conditions (j_{cat}/j_p).

Supporting Electrolyte	$E_{cat/2}$ (V)[a]	η (V)[b]	j_{cat}/j_p
[TBA][PF_6]	-1.93	0.57	16.0
[BMIM][PF_6]	-1.86	0.50	20.2
[BMPyrr][PF_6]	-1.88	0.52	27.0
[EMIM][PF_6]	-1.90	0.54	19.5
[EMIM][BF_4]	-1.90	0.54	20.9

[a]Potentials are referred vs. Fc^+/Fc (V), [b]Determined based on $E_{cat/2}$ using $E^0_{CO2/CO}$ (CH_3CN, TFE) = -1.36 V vs. Fc^+/Fc.[16,43]

3.2.3 Electrolysis for CO_2 reduction with ILs as electrolyte catalyzed by [Re(bpy)(CO)$_3$Cl]. Impact on reaction selectivity

The catalytic performance of complex [1] with respect to electrochemical CO_2 reduction in the presence of TFE as a proton source and different ILs or conventional benchmark [TBA][PF_6] electrolyte, was also studied by constant potential electrolysis (CPE). Some of the results can be seen in Figure 3.10 and a global overview in Table 3.4. The applied potential was -2.05 V *vs.* Fc^+/Fc for all CPE experiments reported, except for an additional CPE carried out in the absence of TFE at 300 mV more positive potential (-1.75 V *vs.* Fc^+/Fc). The reduction of imidazolium cations on the GC surface under those conditions was completely excluded, since more negative potentials were required for this reduction process (approximatively -2.5 V *vs.* Fc^+/Fc under Ar atmosphere) and they were never reached during experiments with complex [1][44]. Carbon monoxide (CO) and hydrogen (H_2) were the only reduction products detected, with no evidence of any additional product in solution. In all cases, CO remained the major reaction product andthe overall faradaic efficiency was nearly 90 % (Table 3.4). Control CPE experiments containing only [TBA][PF_6] as supporting electrolyte were also conducted at the same potential and the ratio of gas products CO/H_2 in that case was found to be 98/2. Comparing that with the CO/H_2 ratio in the presence of ILs, we observed a slight increase in H_2 production for all ILs. Out of the series, [BMIM][PF_6] and [BMPyrr][PF_6] produced the lowest rate of H_2, while, on the contrary, [EMIM][BF_4] produced the highest. These CPE experiments were also evaluated in terms of energy efficiency (EE). The presence of ILs alongside TFE led to lower FE_{CO} than the one produced by the electrolyte benchmark (61 %, entry 1 in Table 3.3), while [BMPyrr][PF_6] had the greatest EE value amongst all ILs tested, at 53 % (entry 3 in Table 3.4). In all cases the current density during electrolysis was relatively stable within the range (2-6) mA/cm^2, while ILs overall produced higher current density values than the conventional benchmark, as can be observed in Figure 3.10. Meanwhile, CPE for CO_2 reduction in 0.5 M [EMIM][PF_6] solution without TFE reached almost total selectivity for CO production (96 %, entry 6 in Table 3.4), but displayed a poor current density during electrolysis (0.7 mA/cm^2). Finally, CPE with [DiMIM][$N(SO_2CF_3)_2$] as supporting electrolyte resulted in H_2 production only (FY H_2 = 59 %) and an important drop in current density was observed over the first 20 min.

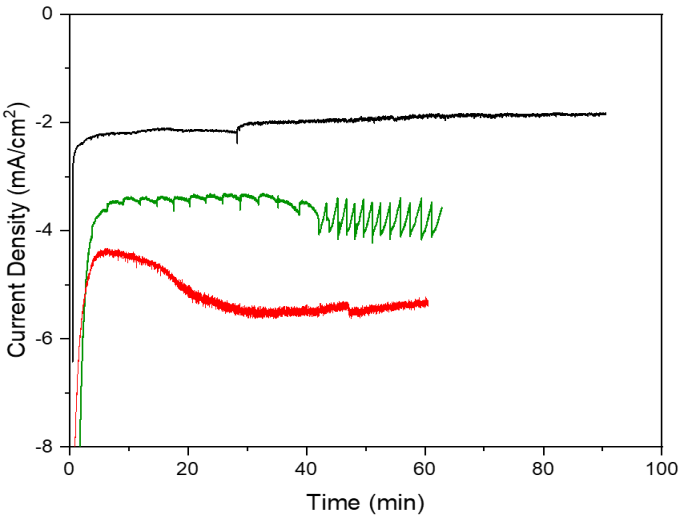

Figure 3.10 Constant potential electrolysis (CPE) at -2.05 V vs. Fc^+/Fc of 1 mM complex [1] in acetonitrile under CO_2 in presence of 1.5 M TFE: in 0.5 M [TBA][PF_6] (black plot), 0.5 M [EMIM][BF_4] (red plot) and [BMPyrr][PF_6] (green plot). Room temperature: 20 ± 2 °C, stirring rate: 400 rpm.

Table 3.4 Electrolysis of 1 mM of complex [1] in 0.5 M supporting electrolyte in CH_3CN in the presence of 1.5 M of TFE under a CO_2 saturated atmosphere. Total electrolysis duration to circulate 14 C.

Entry	Solvent	Supporting Electrolyte	Electrolysis applied potential (V) *vs.* Fc^+/Fc	FE_{CO} (%)[a]	FE_{H2} (%)[a]	Energy Efficiency (%)[c]
1	CH_3CN	0.5 M [TBA][PF_6]	-2.05	92	2	61
2	CH_3CN	0.5 M [BMIM][PF_6]	-2.05	77	8	51
3	CH_3CN	0.5 M [BMPyrr][PF_6]	-2.05	80	10	53
4	CH_3CN	0.5 M [EMIM][BF_4]	-2.05	71	18	47
5	CH_3CN	0.5 M [EMIM][PF_6]	-2.05	77	12	51
6	CH_3CN	0.5 M [EMIM][PF_6][b]	-1.75	96	1	30[d]

[a]Faradaic efficiency for each product (FE_{CO} and FE_{H2}). [b]Electrolysis of 1 mM of complex [1] in 0.5 M [EMIM][PF_6] in CH_3CN under a CO_2 saturated atmosphere to circulate 10 C. [c]Energy Efficiency = $E_T/E \cdot FE$, where $E_T = E°_{CO2/CO}$ (CH_3CN, TFE) = -1.36 V vs. Fc^+/Fc. [d]$E_T = E°_{CO2/CO}$ (CH_3CN) = -0.541 V vs. Fc^+/Fc.

3.2.4 [Rh(bpy)(Cp*)Cl]Cl with ILs as electrolyte in acetonitrile under inert conditions

Figure 3.11 shows the electrochemical response of complex [2] under inert conditions, a similar study to the one initially represented in Figure 3.2 for the case of complex [1]. The molecular catalyst, which in this case corresponds to 1 mM of complex [2], was tested by cyclic voltammetry in an acetonitrile solution under an argon atmosphere in presence of a series of different supporting electrolytes. These were the benchmark electrolyte [TBA][PF_6], the pyrrolidinium-based IL [BMPyrr][PF_6] and the three imidazolium-based ILs, [EMIM][PF_6], [EMIM][BF_4] and [BMIM][PF_6]. The concentration of 0.5 M for all supporting electrolytes was chosen in order to ensure appropriate ionic strength. In the case of complex [2], drying the ILs was abandoned as a practice, since water was eventually used as the optimal proton source reported in the catalytic CO_2 reduction tests[10]. It should also be stressed that, contrarily to the CVs shown previously for complex [1], in the case of complex [2] in order to obtain a better definition of all redox features in the voltammograms a slower scan rate was used, more particularly one at 0.01 V/ s.

According to the literature[10,20,21], the first reduction wave observed in all plots represented in Figure 3.11 and centered at -1.21 V *vs.* Fc^+/Fc has been attributed to a quasi-reversible peak of the metal center reduction from Rh^{III} into Rh^{I}. This wave was characterized by a peak-to-peak separation (ΔE_p) of 150 mV. This step was also coupled with the dissociation of the labile chloride ligand, as was shown in Scheme 3.1 (b). A second reduction wave at more negative potentials, that was centered around -2.7 V *vs.* Fc^+/Fc in the absence of IL in solution, corresponded to a one-electron reversible wave located on the bipyridine ligand[10,20,21]. On the one hand, Figure 3.11 (a) compares the benchmark electrolyte cation $[TBA]^+$ and the non-reducible pyrrolidinium cation $[BMPyrr]^+$ with $[PF_6]^-$ as the counter anion in both cases. The metal-centered reduction peak remained unchanged at -1.21 V *vs.* Fc^+/Fc, but the bipyridine ligand-centered peak was shifted anodically by 80 mV. On the other hand, Figure 3.11 (b) compares the benchmark electrolyte cation $[TBA]^+$ and 3 different imidazolium-based ILs, comprising 2 different cations ($[EMIM]^+$ and $[BMIM]^+$) and two different counter anions ($[PF_6]^-$ and $[BF_4]^-$). In all three cases, the metal-centered reduction peak remained unchanged very close to -1.21 V *vs.* Fc^+/Fc, but the second reduction wave of complex [2] could not be observed because imidazolium cations got reduced at about -2.5 V *vs.* Fc^+/Fc, hindering any process occurring at more negative potentials[30,45,46], as is shown in Figure 3.12. As a consequence, it was not possible to evaluate the impact of imidazolium-based cations in solution on the bipyridine ligand reduction under those inert conditions. The cyclic voltammograms that contained 0.5 M of ILs were also shown to differ from the one with the conventional electrolyte benchmark, since they presented small reduction waves in the interim between the Rh-centered reduction wave and the more cathodic bpy-centered third electron reduction. Those features were only clearly

visible at low scan rate, which is the primary reason this scan rate was selected. Waves in this zone of the voltammogram had already been reported in the initial studies of this catalyst for H_2 evolution and CO_2RR in presence of added acid in solution and they could be attributed to the formation of the hydrido complex and/or the poorly reversible one-electron reduction of said hydrido complex (peaks B and C in Scheme 3.1 (b))[10,20]. Finally, one IL tested with complex [1] was hereby not included and it was the protic IL [DiMIM][$N(SO_2CF_3)_2$]. This IL was abandoned after the poor catalytic results displayed with complex [1]. In Table 3.5 all potentials represented in Figure 3.11 are listed.

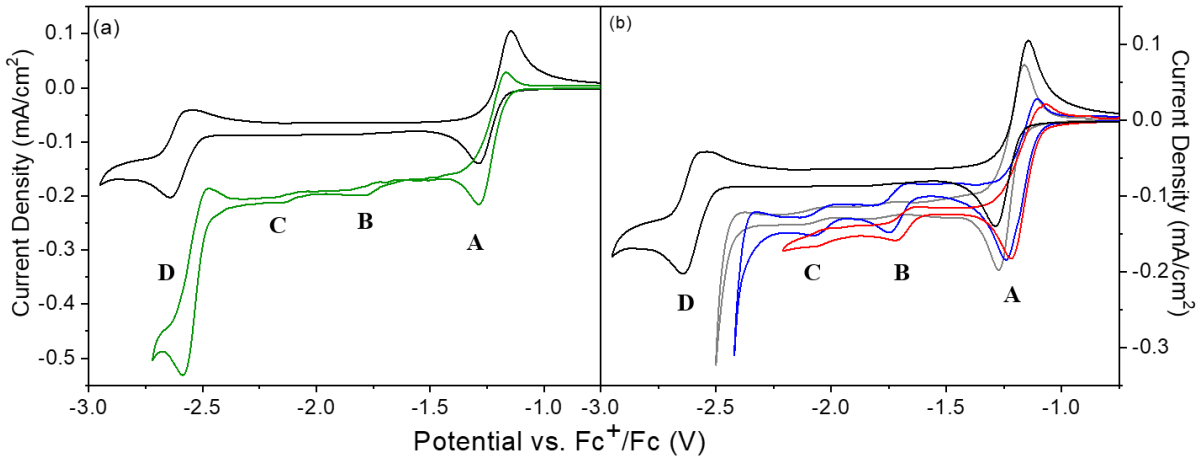

Figure 3.11 Cyclic voltammograms on GCE of 1 mM complex [2] and 0.5 M of different supporting electrolytes in acetonitrile solution under Ar. (a) [TBA][PF_6] (black plot) and [BMPyrr][PF_6] (green plot) and (b) [TBA][PF_6] (black plot), [EMIM][PF_6] (grey plot), [BMIM][PF_6] (blue plot) and [EMIM][BF_4] (red plot). Scan rate 0.01 V/s.

Table 3.5 Descriptors for 1 mM complex [2] under inert conditions (Ar) in 0.5 M of each supporting electrolyte in CH_3CN. Potential of the Rh-centered reduction peak ($E_{p\,A}$), potential of the intermediate peaks ($E_{p\,B}$) and ($E_{p\,C}$) and potential of the bpy-centered reduction peak ($E_{p\,D}$).

	Under inert conditions			
Supporting Electrolyte	**$E_{p\,A}$ (V)[a]**	**$E_{p\,B}$ (V)[a]**	**$E_{p\,C}$ (V)[a]**	**$E_{p\,D}$ (V)[a]**
[TBA][PF_6]	-1.22	-	-	-2.61
[BMIM][PF_6]	-1.17	-1.71	-2.04	-
[BMPyrr][PF_6]	-1.23	-1.75	-2.10	-2.53
[EMIM][PF_6]	-1.22	-1.78	-2.08	-
[EMIM][BF_4]	-1.14	-1.68	-2.04	-

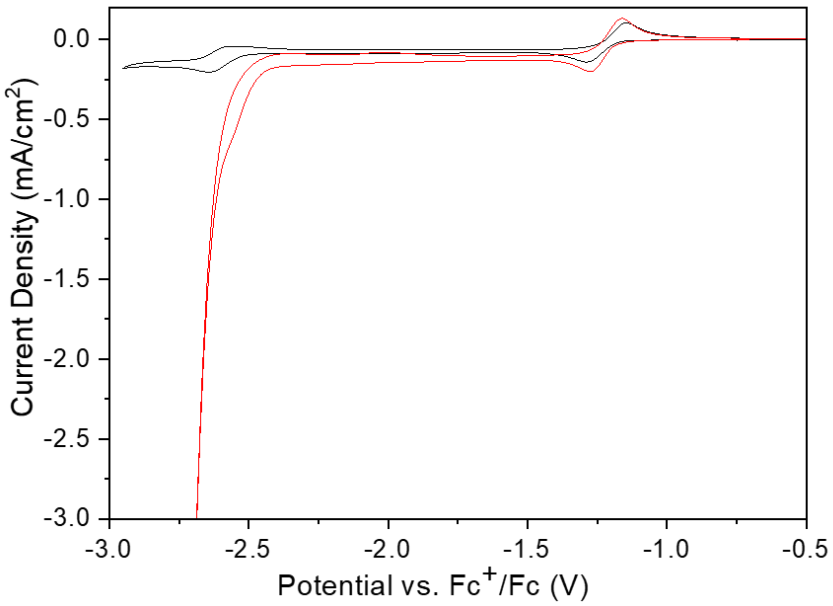

Figure 3.12 Cyclic voltammograms on GCE electrode of 1 mM complex [2] and 0.5 M of different supporting electrolytes in acetonitrile solution under Ar: [TBA][PF_6] (black plot) and [EMIM][PF_6] (red plot). Scan rate 0.01 V/s.

3.2.5 [Rh(bpy)(Cp*)Cl]Cl with ILs as electrolyte in acetonitrile under CO_2 catalytic conditions

Under CO_2 in the presence of H_2O (5 % vol.) as a proton source, an evident catalytic wave was observed in all cases, which was visible within the electrochemical window where the ILs are stable, thus reflecting a large anodic shift of the bpy-centered redox event, as seen in Figure 3.13. In particular, the catalytic wave was shifted from -2.56 V to -2.14 V for [TBA][PF_6] upon addition of H_2O under CO_2 and it also occurred in the presence of ILs. Specifically, they all resulted in lower overpotentials than [TBA][PF_6], the largest decrease (70 mV) being obtained with [EMIM][BF_4] and [EMIM][PF_6] in solution. Table 3.6 reports the values, determined from Figure 3.13, for the following parameters: catalytic potentials (E_{cat} and $E_{cat/2}$), catalytic current densities (j_{cat} and j_{cat}/j_p) and overpotential. The addition of water as proton source also led to a significant increase of current density (for example with the conventional electrolyte: j_{cat}/j_p = 17.5, where j_{cat} corresponds to the maximum catalytic current density) confirming a catalytic process. However, ILs had contrasting effects on the maximal catalytic current density displayed, j_{cat}. While [BMPyrr][PF_6] resulted in decreased current density with respect to [TBA][PF_6], probably due to the limited solubility of this IL in the presence of water, all three imidazolium-based ILs resulted in increased current densities, in the order: [EMIM][PF_6] > [EMIM][BF_4] > [BMIM][PF_6]. For this reason, [EMIM][PF_6] and [EMIM][BF_4] were selected to continue this study in organic-aqueous mixture and aqueous solutions, respectively.

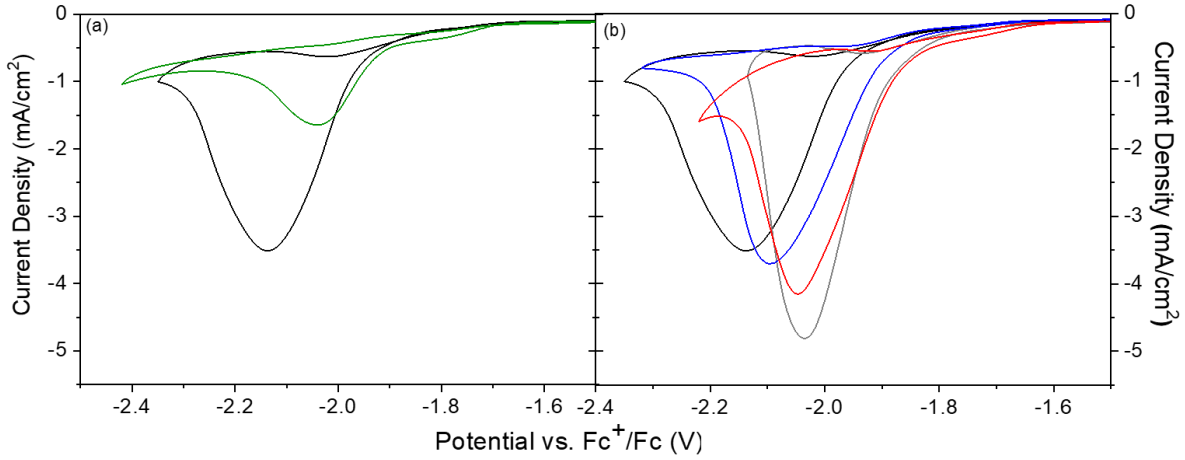

Figure 3.13 Cyclic voltammograms on GCE of 1 mM complex [2] and 0.5 M of different supporting electrolytes in acetonitrile solution containing 5 % (vol.) H_2O under CO_2. (a) [TBA][PF_6] (black plot) and [BMPyrr][PF_6] (green plot) and (b) [TBA][PF_6] (black plot), [EMIM][PF_6] (grey plot), [BMIM][PF_6] (blue plot) [EMIM][BF_4] (red plot). Scan rate 0.01 V/s.

Table 3.6 Comparison of the catalytic parameters of 1 mM complex [2] and 0.5 M of different supporting electrolytes in acetonitrile solution containing 5 % (vol.) H_2O under CO_2. Catalytic potential (E_{cat}), the half wave catalytic potential ($E_{cat/2}$), peak current density exhibited under catalytic conditions (j_{cat}), peak current density exhibited under inert conditions (j_p) and the overpotential (η).

Supporting Electrolyte	**E_{cat} (V)[a]**	**$E_{cat/2}$ (V)[a]**	**j_{cat}**	**j_{cat}/j_p**	**η (V)[b]**
[TBA][PF_6]	-2.14	-2.00	-3.51	17.5	0.68
[BMPyrr][PF_6]	-2.04	-1.95	-1.64	3.1	0.63
[BMIM][PF_6]	-2.09	-1.97	-3.70	-	0.65
[EMIM][PF_6]	-2.03	-1.94	-4.81	-	0.62
[EMIM][BF_4]	-2.04	-1.93	-4.15	-	0.61

[a]Potentials are referred vs. Fc^+/Fc (V). [b]Determined based on $E_{cat/2}$ using $E^0_{CO2/HCOOH}$ (CH_3CN, H_2O) = -1.32 V vs. Fc^+/Fc[47].

3.2.6 [Rh(bpy)(Cp*)Cl]Cl with ILs as electrolyte in organic-aqueous mixture and aqueous solution under CO_2 catalytic conditions

Next, taking advantage of complex [2]'s solubility in both organic and aqueous conditions, we studied the CO_2RR in acetonitrile/aqueous solvent mixtures, as well as different aqueous solutions. Firstly, we tested the catalytic effect of adding an IL in solution in an acetonitrile/H_2O 50/50 (vol.) solvent mixture, as seen in Figure 3.14. However, the supporting electrolytes previously used in the acetonitrile/H_2O 95/5 (vol.) solvent with complex [2] were not adapted to those conditions, as they contained the hydrophobic $[PF_6]^-$ anion. For this reason, we chose to add instead [EMIM][BF_4] and [TBA][BF_4] as electrolytes, since the $[BF_4]^-$ anion is more hydrophilic and as a consequence exhibits higher solubility in aqueous solution. In Figure 3.14, the presence of 0.5 M of the IL led to a modest 40 mV decrease in catalytic half current ($E_{cat/2}$) compared to the benchmark electrolyte. The passage from a acetonitrile/H_2O 95/5 (vol.) to acetonitrile/H_2O 50/50 (vol.) solution was also followed by a decrease in CO_2 solubility from 240 mM to approximatively 116 mM[48]. However, the values of maximum current density were not significantly decreased, as both the benchmark and the IL as electrolytes produce maximum current density values that exceeded 3 mA/cm^2.

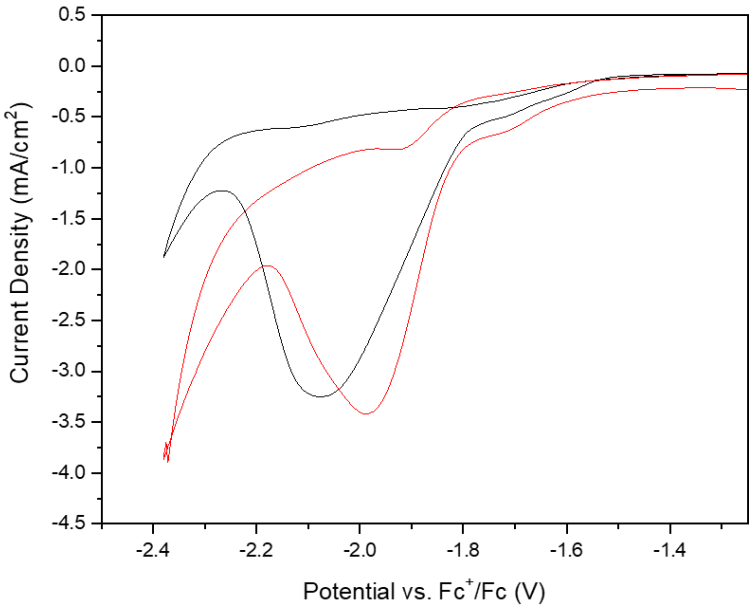

Figure 3.14 Cyclic voltammogram on GCE of 1 mM complex [2] in an acetonitrile/H_2O 50/50 (vol.) solution containing 0.1 M of [TBA][BF_4] (black plot) or 0.5 M [EMIM][BF_4] (red plot) under CO_2. Scan rate 0.01 V/s.

Subsequently, we tested complex [2] in unbuffered aqueous solutions containing only [TBA][BF_4] or [EMIM][BF_4] as supporting electrolytes. The resulting solutions' pH values were measured at 3.8 and 3.1 under CO_2, respectively. The corresponding CVs are shown in Figure 3.15 under Ar (solid black plots) and under CO_2 (solid red plots). This passage from an acetonitrile/H_2O 95/5 (vol.) solution (Figure 3.13 (b)) to purely aqueous conditions led to a large decrease in the catalytic current, by a factor of about 6. This was expected since the CO_2 solubility also decreased from 240 mM to 33 mM (approximatively 7 times lower CO_2 solubility)[30,33,48]. The presence of [EMIM][BF_4] in CO_2-saturated aqueous solution (Figure 3.15 (b), red solid plot) as compared to [TBA][BF_4] (Figure 3.15 (a), red solid plot) also provoked a gain of 80 mV in overpotential for CO_2RR catalysis ($E_{cat/2}$ = -1.37 and -1.45 V *vs*. Ag/AgCl/KCl_{sat}, respectively). Meanwhile, the presence of [EMIM][BF_4] under inert conditions (Figure 3.15 (b), black plot) resulted in a relevant suppression of HER by shifting the cathodic potential limit 200 mV more negatively as compared to [TBA][BF_4] (Figure 3.15 (a), black plot)). Performing CO_2RR in this acidic pH region demonstrated in these aqueous solutions containing [TBA][BF_4] or [EMIM][BF_4] (pH=3.1 – 3.8) also presented an advantage over basic aqueous conditions. That consisted of avoiding CO_2 loss in the form of bicarbonate or carbonate[49], which could be transformed back into CO_2 by the anode[50].

However, the unbuffered aqueous solutions used might not maintain the pH stable during long experiments. This led us to search for a buffer solution that could be stable in this specific acidic region and for that reason an acetate buffer was selected. Also, acetic acid had also previously been reported to have beneficial effect in increasing the current density in catalytic studies with complex [1][16]. In the red dashed plots of Figure 3.15, we therefore see the resulting CVs of complex [2] in a 0.1 M acetate buffer solution at pH=3.8 alongside either [TBA][BF_4] (Figure 3.15 (a)) or [EMIM][BF_4] (Figure 3.15 (b)). In both cases, five times larger j_{cat} was achieved when comparing the j_{cat} in the absence and the presence of acetate buffer, together with a significant decrease in the onset potential of the catalytic reaction.

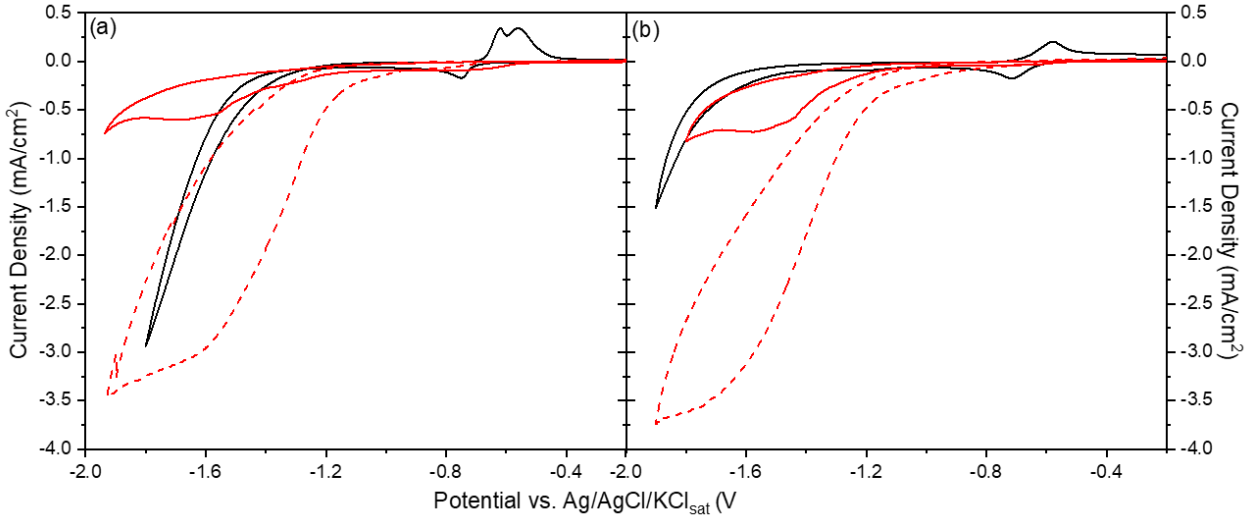

Figure 3.15 Cyclic voltammograms on GCE of 1 mM complex [2] in: (a) 0.1 M [TBA][BF_4] as electrolyte or (b) 0.5 M [EMIM][BF_4] as electrolyte in unbuffered aqueous solution under Ar (black plot), unbuffered aqueous solution under CO_2 (red plot) and 0.1 M acetate buffer solution (pH = 3.8) under CO_2 (red dashed plot). Scan rate = 0.01 V/s.

3.2.7 Electrolysis for CO_2 reduction with ILs as electrolyte catalyzed by [Rh(bpy)(Cp*)Cl]Cl. Impact in reaction selectivity

The effect on products selectivity and energy efficiency of the CO_2RR due to the presence of ILs in the electrical double layer was studied from both potentiostatic and galvanostatic electrolysis, namely constant potential (CPE) and constant current (CCE) electrolysis, respectively. In all experiments, only formate was detected as product in the liquid phase and only H_2 was observed in the gas phase. Table 3.7 shows the overpotential, faradic efficiencies obtained for both products and energy efficiency for CO_2 conversion to formate as a function of the electrolyte, at different values of applied potential during electrolysis (CPE) in acetonitrile/H_2O 95/5 (vol.). As formate can partly migrate from the catholyte to the anolyte[1], a systematic analysis of both catholyte and anolyte solutions was performed in all electrolysis reported here proving that between 15 % and 20 % of the total formate generated during the electrolysis was detected within the anolyte solution. Thus, analyzing the presence of reaction products in both compartments allowed closing efficiently the mass balance of the electrolysis reaching in most cases a total FE (FE_{HCOO^-} + FE_{H2}) between 87 % and 100 %. Table 3.7 shows that H_2 formation was inhibited and the FE_{HCOO^-} increased upon addition of [EMIM][BF_4] or [EMIM][PF_6]. This results in a very selective CO_2 to formate conversion (FE_{HCOO^-} > 90 % and a maximal energy efficiency of 66 %), taking place at much more positive potentials than with [TBA][PF_6] (Table 3.7, entries 1-3). Thus, it was evidenced from the results reported in Table 3.7, the significant role of $[EMIM]^+$ cation at the electrode/solution interface enhancing formate production and suppressing HER.

Table 3.7 Constant potential electrolysis in acetonitrile using 5 % of H_2O (vol.) as proton source in an electrochemical two compartments H-type cell. Total electrolysis duration to circulate 15 C.

Entry	Solvent	Electrolyte	%H_2O (vol.)	Electrolysis applied potential (V) *vs.* Fc^+/Fc	η (V)[a]	FE_{HCOO^-} (%)[b]	FE_{H2} (%)[b]	Energy efficiency (%)[c]
1	CH_3CN	[TBA][PF_6]	5	-2.10	0.78	77	18	48
2	CH_3CN	[EMIM][PF_6][d]	5	-1.89	0.57	90	9	63
3	CH_3CN	[EMIM][BF_4]	5	-1.83	0.51	91	9	66

[a]Determined based on $E_{cat/2}$ using $E^0_{CO2/HCOOH}$ (CH_3CN, H_2O) = -1.32 V vs. Fc^+/Fc. [b]Faradaic efficiency for each product (FE_{HCOOH} and FE_{H2}). [c]Energy Efficiency = $E_T/E \cdot FE$, where E_T = $E^o_{CO2/HCOOH}$ (CH_3CN, H_2O) = -1.32 V vs. Fc^+/Fc. [d]Total charge transferred 10 C.

We subsequently performed CCE experiments in the same H-type cell at -3.33 mA/cm^2 of applied current density in acetonitrile/H_2O 95/5 (vol.) and acetonitrile/H_2O 50/50 (vol.) solutions. The results of these CCEs in terms of overpotential, FE for formate and H_2 and energy efficiency values are shown in Table 3.8. In Figure 3.17 are presented the plots of cathode potential *vs.* electrolysis time (corresponding to Table 3.8, entries 1 and 2), as well as the thermodynamic potential for CO_2 reduction to formate, which for those conditions had been calculated at -1.32 V *vs.* Fc^+/Fc[47]. The presence of the $[EMIM]^+$ cation led to a significant reduction in the observed overpotential of at least 800 mV. In addition to this, the products ratio (FE_{HCOO^-}/FE_{H2}) doubled from (1.5/1) in presence $[TBA]^+$ (Table 3.8, entry 1) to (3/1) when $[EMIM]^+$ is present at the electrode/solution interface (Table 3.8, entry 2). This increase in product selectivity for formate in the presence of the IL cation was also reflected on the energy efficiency values, which pass from 25 to 47 % for entries 1 and 2, respectively. Finally, by increasing the % of H_2O present in solution from 5 % (entry 1 of Table 3.8) to 50 % (entry 3 of Table 3.8), the products ratio (FE_{HCOO^-}/FE_{H2}) remained almost identical (1.5/1).

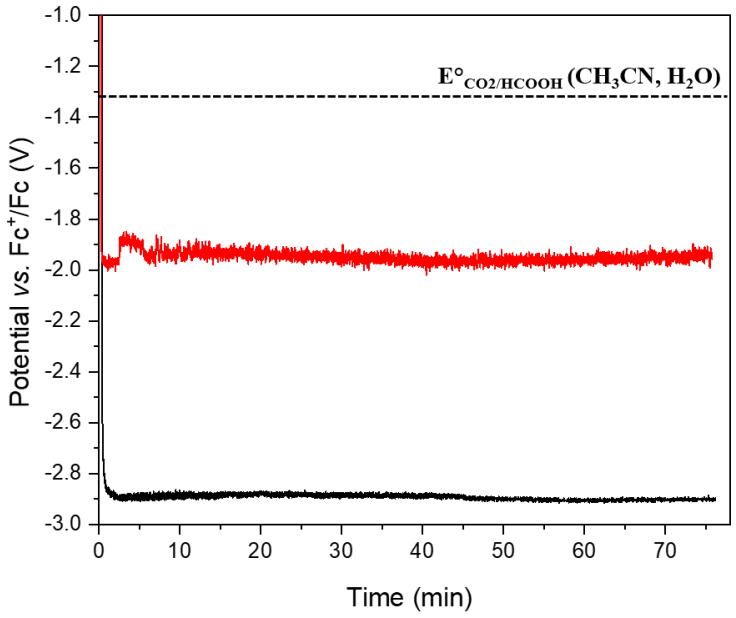

Figure 3.16 Constant current electrolysis (CCE) at -3.33 mA/cm^2 of 1 mM complex [2] in acetonitrile solution under CO_2 in presence of 5 % (vol.) H_2O and: 0.5 M [TBA][PF_6] (black plot) and 0.5 M [EMIM][PF_6] (red plot). Stirring rate: 400 rpm.

Table 3.8 Constant current electrolysis in acetonitrile using different % of H_2O as proton source in an electrochemical two compartments H-type cell. Total electrolysis duration to circulate 15 C.

Entry	Solvent	Electrolyte	%H_2O (vol.)	Electrolysis applied current density (mA/cm^2)	Electrolysis E_{cat} average (V) *vs.* Fc^+/Fc	η (V)[a]	FE_{HCOO^-} (%)[b]	FE_{H2} (%)[b]	Energy efficiency (%)[c]
1	CH_3CN	[TBA][PF_6]	5	-3.33	-2.81	1.49	53	34	25
2	CH_3CN	[EMIM][PF_6]	5	-3.33	-1.95	0.63	69	22	47
3	CH_3CN	[TBA][BF_4]	50	-3.33	-2.60	1.28	47	31	24

[a]Determined based on $E_{cat/2}$ using $E^0_{CO2/HCOOH}$ (CH_3CN, H_2O) = -1.32 V vs. Fc^+/Fc. [b]Faradaic efficiency for each product (FE_{HCOOH} and FE_{H2}). [c]Energy Efficiency = $E_T/E \cdot FE$, where E_T = $E^o_{CO2/HCOOH}$ (CH_3CN, H_2O) = -1.32 V vs. Fc^+/Fc.

We also performed CCE (applied current density -3.33 mA/cm^2) with complex [2] in different aqueous CO_2-saturated solutions. These results are depicted in Figure 3.17 and Table 3.9. The electrolyte system used was either an unbuffered aqueous solution containing 0.1 M of [TBA][BF_4] (entry 1) or 0.5 M of [EMIM][BF_4] (entry 2) as supporting electrolyte or a 0.1 M acetate buffer solution at pH = 3.8 with an additional 0.1 M [TBA][BF_4] (entry 3) or 0.1 M [EMIM][BF_4] (entry 4). Interestingly, this catalyst

exhibited significant FE_{HCOO^-} even in those acidic aqueous solutions, representing one of few examples of a molecular complexes performing CO_2 conversion to formate in both organic and aqueous solutions[51–53]. The blue and red plots of Figure 3.17, which corresponded to entries 1 and 2 of Table 3.9 respectively, showed that a relevant decrease in overpotential (600 mV) together with a slight increase in the selectivity towards formate was achieved when [EMIM][BF_4] was present in the solution instead of [TBA][BF_4]. However, in those unbuffered conditions the initial acidic pH was not stable throughout the electrolysis and as can be seen in Table 3.9, the final pH of entry 1 had increased from 3.8 to 5.5. As a consequence, we then opted for an acetate buffered solution, which successfully maintained pH stable at a value of 3.8. Using the buffered solution in combination with either $[TBA]^+$ or $[EMIM]^+$ led to even lower overpotential values at a constant current density of -3.33 mA/cm^2, as demonstrated in the corresponding green and purple plots of Figure 3.17, as well as entries 3 and 4 of Table 3.9, respectively. Notably, the electrolyte composed by [EMIM][BF_4] and acetate buffer (Table 3.9, entry 4) reached one of the lowest overpotential values reported so far for a homogenous molecular catalyst producing formate in aqueous solution (0.28 V) resulting in a relevant energy efficiency (32 %). In particular, the combination of $[EMIM]^+$ at the electrical double layer together with the acetate buffer solution provoked a significant HER suppression (entry 4 of Table 3.9). Finally, it is also demonstrated that both complex [2] and CO_2 are necessary for CO_2 conversion to formate (entries 5 and 6 of Table 3.9).

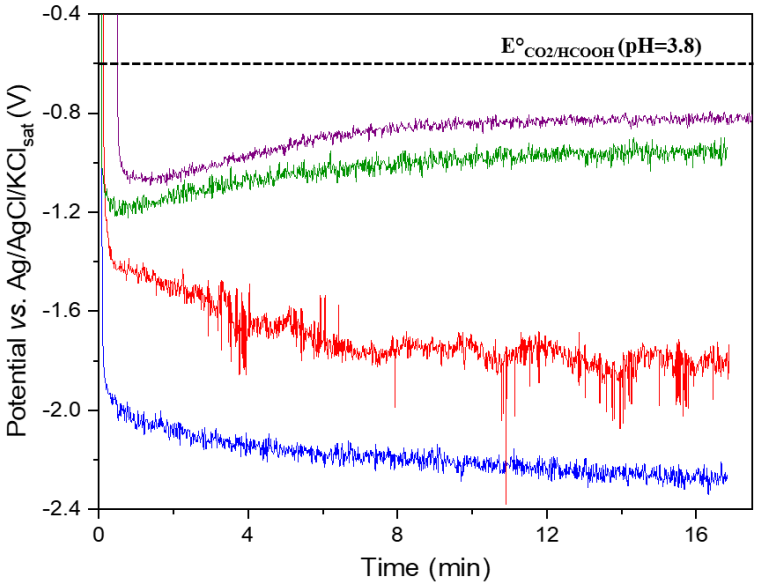

Figure 3.17 Constant current electrolysis (CCE) at -3.33 mA/cm^2 of 1 mM complex [2] under CO_2 with: 0.1 M [TBA][BF_4] as electrolyte in unbuffered aqueous solution (blue plot) or 0.1 M acetate buffer solution (green plot) and 0.5 M [EMIM][BF_4] as electrolyte in unbuffered aqueous solution (red plot) or 0.1 M acetic acetate buffer solution (purple plot). Stirring rate: 400 rpm.

Table 3.9 Constant current electrolysis at -3.33 mA/cm^2 in aqueous solution in an electrochemical two compartments H-type cell. Total electrolysis duration to circulate 10 C.

Entry	Electrolyte	pH_0	pH_f	Electrolysis E_{cat} average (V) *vs.* Ag/AgCl/KClsat	η (V)	FE_{HCOO^-} (%)[a]	FE_{H2} (%)[a]	Energy efficiency (%)
1	0.1 M [TBA][BF_4][b]	3.8	5.5	-2.2	1.58[c]	41	42	12
2	0.5 M [EMIM][BF_4]	3.1	3.4	-1.6	1.02[d]	49	46	18
3	0.1 M [TBA][BF_4][b] + 0.1 M CH_3COONa/CH_3COOH	3.8	3.8	-1.0	0.38[c]	40	55	25
4	0.1 M [EMIM][BF_4] + 0.1 M CH_3COONa/CH_3COOH	3.8	3.9	-0.9	0.28[c]	46	40	32
5[e]	0.1 M [TBA][BF_4][b] + 0.1 M CH_3COONa/CH_3COOH	3.8	3.8	-	-	2	84	
6[f]	0.1 M [TBA][BF_4][b] + 0.1 M CH_3COONa/CH_3COOH	3.8	3.7	-	-	2	87	

[a]Faradaic efficiency for each product (FE_{HCOOH} and FE_{H2}). [b]0.1 M is the maximum solubility of [TBA][BF_4] in aqueous solution. [c]$E^o_{CO2/HCOOH}$ = -0.62 V vs. Ag/AgCl (pH=3.8). [d]$E^o_{CO2/HCOOH}$ = -0.58 V vs. Ag/AgCl (pH=3.1). [e]No complex [2] in solution. [f]No CO_2 in solution (Ar bubbling). pH_0 and pH_f represent initial and final electrolysis solution pH, respectively. Energy Efficiency = $E_T/E \cdot FE_{HCOO^-}$, where $E_T = E^o_{CO2/HCOOH}$ (H_2O).

3.2.8 Density Functional Theory (DFT) calculations on the interaction between [Rh(bpy)(Cp*)Cl]Cl and $[EMIM]^+$ in CO_2RR and HER (Collaborators' contribution)

Finally, we collaborated with Dr. Albert Solé-Daura and Dr. Caroline Mellot-Draznieks who performed DFT calculations to investigate the role of ILs at the electrode/solution interface in both acetonitrile and aqueous solution taking the representative case of the $[EMIM]^+$ cation. Previous computational studies on the reduction of CO_2 catalyzed by complex [2][21] had already shown that the Rh^I species generated after the two-electron reduction of the initial Rh^{III} in complex [2] could reduce a proton to form a Rh^{III}-hydride, which tended to evolve towards the more stable Rh^I species bearing a protonated Cp* ligand[21] . Accordingly, our DFT calculations predicted that the $[Rh^I(bpy)(HCp^*)]^+$ complex was 4.6 kcal/mol more stable than the $[Rh^{III}(bpy)(Cp^*)H]^+$ one in terms of Gibbs free energy. Then, the third reduction of the catalyst that generated its active form is known to be bipyridine-centered. For this reason, we analyzed how the interactions between the $[Rh^I(bpy)(HCp^*)]^+$ species and $[EMIM]^+$ in solution could be related with the experimentally observed shift in the reduction potential that led to the catalyst's active form. Notably, our calculations revealed that the formation of the π *cation*$\cdots\pi$ adduct between the catalyst and $[EMIM]^+$ represented in Figure 3.18 (a) lowers the LUMO energy of the $[Rh^I(bpy)(HCp^*)]^+$ complex by

0.22 eV (Figure 3.18 (b)). Thus, despite that the formation of this *π cation···π* adduct was slightly endergonic (by 2.5 kcal/mol), it facilitated the entrance of an extra electron, resulting in an overall decrease of the calculated reduction potential of 170 mV (Figure 3.18 (b)). This was in fair agreement with the experimental shift (110 mV) observed in the catalytic peak potential (E_{cat}) when comparing [TBA][PF_6] and [EMIM][PF_6] as supporting electrolytes in solution (Table 3.4). After the reduction of the bipyridine ligand, the dissociation of the [Rh^{I}(bpy$^{\bullet-}$)(HCp*)]···[EMIM]+ adduct became thermodynamically unfavorable (by 3.8 kcal/mol) due to the increased charge density supported by the bipyridine ligand, which strengthened its interaction with the electron-deficient $[EMIM]^+$ cation. Likewise, the less stable although catalytically active [Rh^{III}(bpy$^{\bullet-}$)(Cp*)H] species interacted with $[EMIM]^+$ with a binding free energy of –3.5 kcal/mol and therefore, we carried out additional DFT calculations to evaluate whether the favorable formation of such adducts could be responsible for the selectivity variations observed experimentally upon the addition of IL.

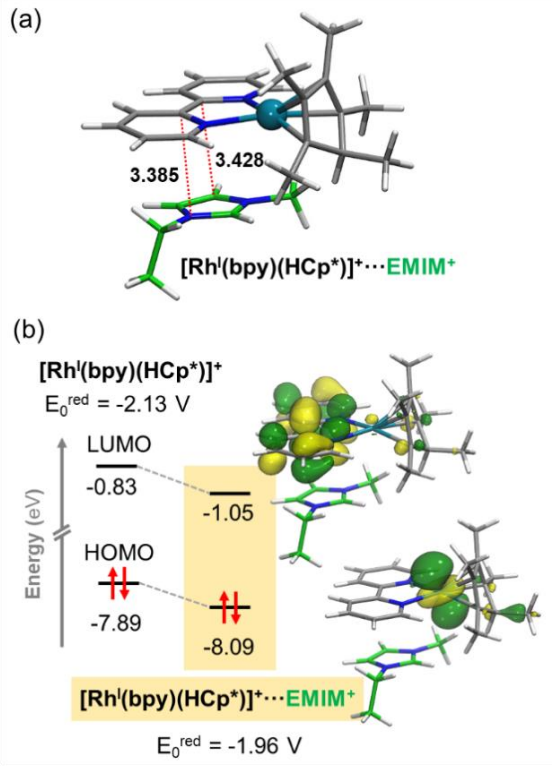

Figure 3.18 (a) Optimized geometry for the non-bonding adduct between the [Rh^{I}(bpy)(HCp)]$^+$ catalyst and $[EMIM]^+$. Key distances are shown in Å and carbon atoms of $[EMIM]^+$ are colored in green for clarity. (b) Schematic frontier MO diagram showing the impact of the interaction with $[EMIM]^+$ on the energy levels and reduction potential of the [Rh^{I}(bpy)(HCp*)]$^+$ species. Orbital energies computed at the ωB97X-D level are given in eV and reduction potentials are referred to the Fc^+/Fc reference electrode.*

Figure 3.19 compares the Gibbs free-energy profiles associated to the mechanistic pathways for formate and H_2 production catalyzed by complex [2] in the presence or absence of an explicit $[EMIM]^+$ interacting at the bipyridine ligand. Starting from the active form of the catalyst A, i.e. the $[Rh^{III}(bpy^{\bullet-})(Cp^*)H]$ species (highlighted with a dashed frame in Scheme 3.1 (b)), the reduction of CO_2 took place through transition state TS1 (represented in Figure 3.19 (b)) overcoming a free-energy barrier of 14.3 kcal mol^{-1} in the absence of IL. This generated a formate ion in addition to the Rh^{II} species B, which tended to undergo disproportionation to generate a Rh^{I} and a Rh^{III} species[54,55].This, together with the protonation of the formate to give formic acid, provided the thermodynamic driving force to the reaction and made it irreversible. On the other hand, the HER in the absence of IL involved the initial formation of a slightly stabilizing adduct followed by the H–H coupling process, which occurred through TS2 (represented in Figure 3.19 (c)) and involved a very smooth barrier of 0.5 kcal mol^{-1}. The formation of the H_2 product releasing a water dimer and species B is highly exergonic (by > 40 kcal mol^{-1}). The first feature that may draw one's attention is that the *standard-state* free-energy barrier for the HER was significantly lower than that associated to the hydrogenation of CO_2, while experimental results using benchmark electrolyte pointed towards formate as a main product (entries 1 and 3 in Table 3.7). However, it is important to note that those experiments were carried out in a CO_2-saturated solution of acetonitrile containing only 5 % (vol.) of H_2O. As such, the concentration of protons is expected to be several orders of magnitude lower than that of CO_2, balancing the preference of the system to proceed through either of these two pathways and explaining the experimentally observed product distribution. Importantly, as shown in red lines in Figure 3.19, the incorporation of $[EMIM]^+$ at the electrode interface was found to increase the free-energy barriers for both CO_2RR and HER pathways. This is due to a reduction of the nucleophilic character of the Rh-hydride intermediate caused by the electron-density polarization from the catalyst to the organic $[EMIM]^+$ cation. However, and most importantly, this effect was much more pronounced in the HER pathway, reducing the free-energy difference between TS1 and TS2 in acetonitrile from 13.8 to 10.3 kcal mol^{-1}, thus shifting the product distribution in favor of formic acid, which qualitatively explained the experimental selectivity trends observed in the presence of $[EMIM]^+$.

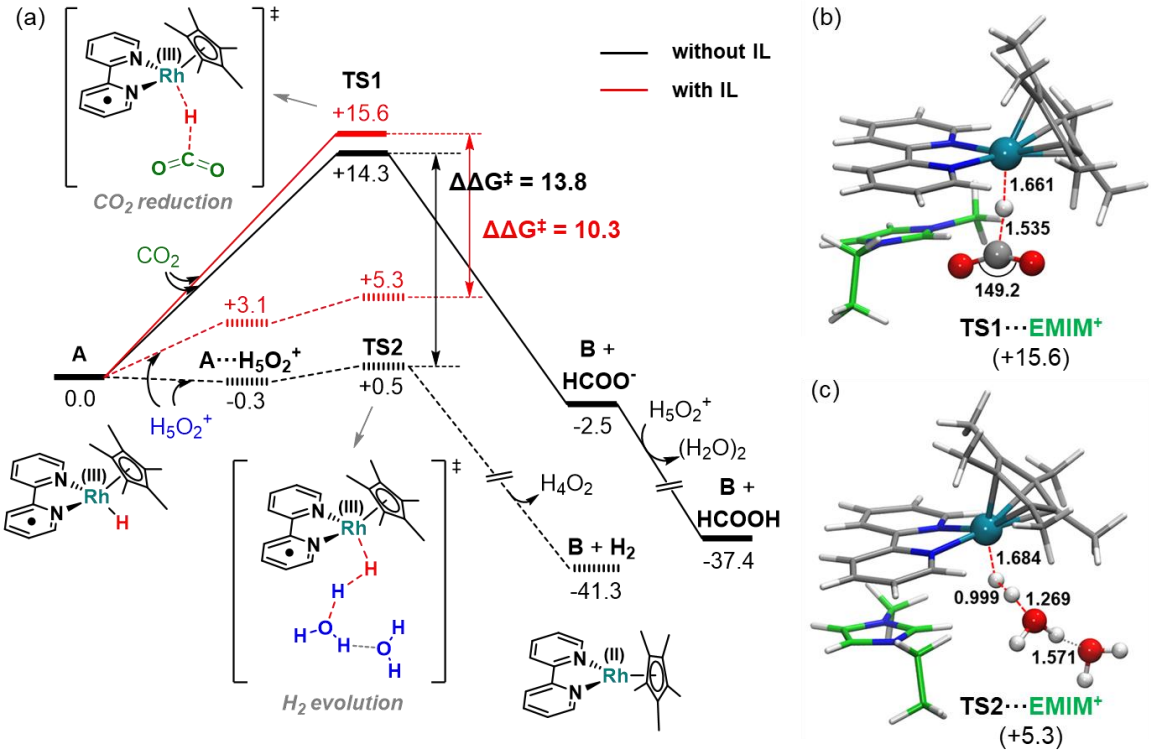

Figure 3.19 (a) Calculated Gibbs free energy profile (kcal·mol^{-1}) for the CO_2RR and the HER (solid and dashed lines, respectively) promoted by the active form of complex [2] (A) in the absence (black lines) or presence (red lines) of an explicit [EMIM]$^+$ cation. (b) and (c) DFT-optimized geometries for the transition states TS1 and TS2 in the presence of [EMIM]$^+$, respectively. Main distances are shown in Å and relative free energies are given in parentheses in kcalmol^{-1}.

With the gained knowledge about the catalyst-IL interactions and the parameters influencing the selectivity of the reaction, we sought to rationalize the experimental outcomes in water solvent. First, the shape of the free-energy profile in water was found not to differ significantly from that calculated in acetonitrile, as shown in Table 3.10. Thus, the decrease of the FE_{HCOO^-} when increasing the water content should be ascribed to concentration effects, as the concentration of protons was directly proportional to that of water, whereas that of CO_2 dropped as the polarity of the solvent increased.

Table 3.10 Key thermodynamic and kinetic parameters of the reaction computed in acetonitrile and water solvent.

process	ΔG or ΔG‡ (kcal·mol^{-1})	
	acetonitrile	water
1 + [EMIM]$^+$ → **1**···[EMIM]$^+$	–3.5	–3.0
1···[EMIM]$^+$ + CO_2 → **TS1**···[EMIM]$^+$	15.6	15.0
1···[EMIM]$^+$ + $H_5O_2^+$ → **TS2**···[EMIM]$^+$	5.3	5.2

3.3 Discussion

The role of ILs in CO_2 electroreduction has been largely investigated in previous studies with heterogeneous catalysts where ILs have demonstrated to promote CO_2 electroreduction by means of inhibiting hydrogen evolution reaction and increasing the concentration of dissolved CO_2 in aqueous based solutions. Overall, by diminishing the energetic barrier of the reaction by formation of adducts[33,56,57] with CO_2 ILs lead to CO_2 activation. Studies with homogeneous catalysts for CO_2 electroreduction in the presence of ILs are much fewer[32,38,39] and the role of the structure of different ILs has never been addressed before in CO_2 conversion by molecular electrocatalysts. Here, we evaluated for the first time the effect of different ILs used as supporting electrolytes in binary mixtures with acetonitrile or totally aqueous solutions on the electroreduction of CO_2 catalyzed by two model molecular complexes, namely complex [1] and complex [2], respectively. In particular, within this structure-activity relationship study, we varied the nature of the cation, anion and cation alkyl chain by a choice of 5 different ILs and in the case of complex [2] varied the solvent/electrolyte system as well.

Firstly, for complex [1] we demonstrated that the presence of IL cations in solution under inert conditions (argon) greatly favored its reduction, as shown by the large impact on its redox potentials, with positive shifts of both one-electron redox events: up to 210 mV for the first reversible reduction wave corresponding to bipyridine reduction and up to 370 mV for the second one, which corresponded to the reduction of Re^{I} to Re^{0}. Furthermore, when CO_2 was present without an added proton source in solution (Figure 3.6), almost the same potential shifts were reported for both reduction waves together with a catalytic wave developed at the second one-electron process (Table 3.2, under CO_2 catalytic conditions). This clearly demonstrated that ILs favor CO_2 electroreduction as compared to [TBA][PF_6]. An in-detail view of all positive shifts on the CO_2 reduction potential led to the following conclusions: (i) those shifts were very sensitive to the nature of the IL cation and all 3 imidazolium-based ILs exhibited a much larger positive potential shift than pyrrolidinium based IL and benchmark electrolyte, following the trend $[IM]^+$ > $[Pyrr]^+$ > $[TBA]^+$; (ii) there was almost no effect on the CO_2 reduction potential with respect to the size of the cation alkyl chain and the nature of the associated anion (Figure 3.6). These observations strongly indicated that the IL cation took part in a direct interaction with the molecular catalyst. Particularly, the aforementioned potential shifts, more relevant on the second electron transfer, could stem from the electrostatic stabilization of the negatively-charged reduced form of complex [1] (equation 1) by the IL cations present in solution (equation 2). This was in agreement with the electrostatic stabilization previously suggested by Choi et al.[39] for the case of FeTPP and Matsubara et al.[38] for the interaction between $[EMIM]^+$ and the negatively charged reduced form of complex [1]. In addition to this, Matsubara et al.[38] proposed several theoretical structures for the interaction between the

imidazolium cation and the reduced form of complex [1] based on DFT calculations. One of those calculated structures suggested that the imidazolium ring lies above the bipyridine ligand due to π+-π interactions. It must be noted that the first one-electron reduction of complex [1] was centered on the bpy ligand, which is an aromatic system containing delocalized π electrons in their π orbitals. Thus, our results showing potential diminution under both Ar and CO_2 in the presence of ILs, which greatly depends on the nature of the IL cation (Figure 3.2 and 3.6), with the trend $[IM]^+ > [Pyrr]^+ > [TBA]^+$, demonstrated the π+-π interaction between the $(bpy)^-$ and the $[IM]^+$ p orbitals initially proposed by Matsubara et al.[38] This interaction was not available neither in the case of $[Pyrr]^+$ nor $[TBA]^+$, which explained higher stabilization effect on delocalized electrons (more relevant overpotential diminution) achieved by $[IM]^+$ in comparison with $[Pyrr]^+$ based ILs.

$$[Re(bpy)(CO)_3Cl] + 2e^- + CO_2 \Leftrightarrow [Re(bpy)(CO)_3CO_2]^- + Cl^- \quad \text{eq. 1}$$

$$[Re(bpy)(CO)_3CO_2]^- + IL^+ \Leftrightarrow [Re(bpy)(CO)_3CO_2]^-[IL]^+ \quad \text{eq. 2}$$

In addition to the potential shift, some difference was observed in Figure 3.6 (b) when comparing catalytic current densities displayed in presence of either $[EMIM]^+$ or $[BMIM]^+$ cations. In particular, $[EMIM][BF_4]$ and $[EMIM][PF_6]$ exhibited the highest (j_{cat}/j_p) ratio. In contrast, the other ILs reported in Table 3.2 gave current enhancement comparable to the benchmark electrolyte. Only the case of $[EMIM][PF_6]$ was studied by CPE at this point exhibiting low current density, but extremely high product selectivity towards CO generation (see Table 3.4).

Finally, electrochemical CO_2 reduction in the presence of TFE as a proton source and ILs was studied by CV (Figure 3.9 and Table 3.3) and CPE experiments (Table 3.4 and Figure 3.10) leading to the following observations from CVs: (i) as expected, addition of TFE resulted in all cases in larger catalytic current densities for CO_2 reduction; (ii) a small but significant and stimulating effect of ILs in decreasing overpotential was observed, reflecting the activating role of ILs also in the presence of TFE; (iii) the catalytic current ratio displayed by imidazolium and pyrrolidinium IL solutions were in all cases at least 25 % higher than $[TBA][PF_6]$ containing solutions, $[BMPyrr][PF_6]$ being the one exhibiting the highest catalytic current ratio. Furthermore, CPE experiments showed that in most cases shorter electrolysis were needed to transfer 14 C when ILs were present in solution, since higher current densities were reached (Figure 3.10) in agreement with previous CVs (Figure 3.9). However, the catalyst was slightly less selective in CO production in the presence of ILs in comparison with benchmark $[TBA][PF_6]$ electrolyte. This was also reflected on the energy efficiency values, which being proportional to the observed FE for CO, decreased in the presence of ILs. $[BMIM][PF_6]$ and $[BMPyrr][PF_6]$ kept a very high FE_{CO}/FE_{H_2} ratio, 91/9 and 89/11 respectively, meanwhile $[EMIM][BF_4]$ led to the lowest selectivity ratio among the

ILs studied (80/20). Finally, with [DiMIM][$N(SO_2CF_3)_2$], the only protic IL tested in this work, reduction of the protons provided by the IL resulted in the production of H_2 as the only product.

Comparing the co-catalyst effect of all ILs studied here under catalytic CO_2 reduction conditions, in the presence and the absence of TFE as a proton source in solution, we demonstrated that the presence of TFE seemed to weaken, at least partially, the electrostatic interaction between the reduced form of complex [1] (equation 1) and IL cations present in solution as described by equation 2, which was responsible for the positive potential shift observed for both electron transfers in Figures 3.2 and 3.6. The overpotential was between 330 and 200 mV lower than in the case of benchmark electrolyte in the absence of TFE (Table 3.2), but only between 70 and 30 mV lower in the presence of TFE (Table 3.3). As reported by Kubiak's group[16], CO_2 reduction catalytic cycle for complex [1] follows two different pathways whether or not a proton source is present in solution, seen in scheme 3.1 (a). Thus, once the reduced form of the catalyst is generated by 2 electron transfers and the CO_2 molecule had been incorporated in complex [1] (equation 1), two possible pathways were described. On the one hand, in the absence of a proton source, a new electron transfer took place forming a di-anion catalytic species: $[Re(bpy)(CO)_3CO_2]^{2-}$ (equation 3), which could be greatly stabilized thanks to the IL cations (equation 4). On the other hand, when an explicit proton donor is added, such as TFE, a "proton first" step controlled the reaction initially forming a non-charged intermediate (equation 5), which then became a mono-anionic catalytic species $[Re(bpy)(CO)_3CO_2H]^-$ after the following electron transfer (equation 6). As a result, these two intermediates on the "proton first" pathway were much less stabilized by the presence of IL cations (equation 7) and for this reason the ILs exhibited a much weaker co-catalytic effect when a proton donor is present in solution.

$$[Re(bpy)(CO)_3CO_2]^- + e^- \Leftrightarrow [Re(bpy)(CO)_3CO_2]^{2-} \quad \text{eq. 3}$$

$$[Re(bpy)(CO)_3CO_2]^{2-} + 2IL^+ \Leftrightarrow [Re(bpy)(CO)_3CO_2]^{2-}[IL]^+[IL]^+ \quad \text{eq. 4}$$

$$[Re(bpy)(CO)_3CO_2]^- + H^+ \Leftrightarrow [Re(bpy)(CO)_3CO_2H] \quad \text{eq. 5}$$

$$[Re(bpy)(CO)_3CO_2H] + e^- \Leftrightarrow [Re(bpy)(CO)_3CO_2H]^- \quad \text{eq. 6}$$

$$[Re(bpy)(CO)_3CO_2H]^- + IL^+ \Leftrightarrow [Re(bpy)(CO)_3CO_2H]^-[IL]^+ \quad \text{eq. 7}$$

When comparing the effect of the presence of ILs and especially imidazolium-based ones on molecular catalysts in acetonitrile a clear distinction between complexes [1] and [2] was observed. By comparing Figures 3.2 and 3.11, we saw that the differing effect of ILs produced on each catalyst under inert conditions. As mentioned before, in the case of complex [1], the potential for both reduction peaks were shifted less negatively, while for complex [2] the Rh-centered peak remained unchanged and the more

negative bpy-centered peak was not even visible with the IL, because it exceeded the point at which imidazolium itself is reduced (see Figure 3.12). Nevertheless, in a CO_2-saturated atmosphere in the presence of a proton source, the catalytic wave of complex [2] was visible in all cases, as it was shifted less negatively than the imidazolium IL reduction. Figure 3.13 demonstrates that all ILs tested here favor CO_2 electroreduction by decreasing the $E_{cat/2}$ between 80 and 30 mV (Table 3.6) as compared to the benchmark electrolyte. This overpotential shift was in the same magnitude as the one observed with catalyst [1] in the presence of TFE, even though these catalysts do not share the same mechanistic pathway for CO_2 reduction. The rationale behind the importance of the cation or anion of an imidazolium IL though was consistent in both cases, displaying that the anion is relatively insignificant in determining catalytic parameters besides hydrophilicity, while that of the cation is comparatively more important, with the $[EMIM]^+$ cation displaying the best catalytic results in both cases.

Complex [2] also presented the opportunity to work in aqueous solution, which had not been possible with complex [1], which was insoluble in purely aqueous unbuffered and subsequently buffered solutions. We were therefore able to explore for the first time the effect of an aqueous soluble IL ([EMIM][BF_4]) as supporting electrolyte in CO_2RR catalyzed by complex [2] in unbuffered aqueous solution. However, a relevant drop in CO_2 solubility was associated with the solvent switch from acetonitrile/H_2O 95/5 (vol.) to aqueous solution, which strongly impacted the catalytic current density achieved (solid red plots in Figure 3.15). Interestingly, we demonstrated the effect of imidazolium-based ILs promoting CO_2 conversion to formate in unbuffered aqueous solution, since a gain of 80 mV in overpotential was achieved in the presence of [EMIM][BF_4] (solid red plot in Figure 3.15 (b)). This tied nicely with the overpotential gain already observed under catalytic conditions with complex [2] and $[EMIM]^+$ based ILs in acetonitrile (Table 3.6). Nevertheless, no proton source optimization was previously performed for catalyzing CO_2RR by complex [2] in aqueous solution, since the catalytic CO_2RR behavior of complex [2] in purely aqueous solution remained unexplored thus far. An additional electrolyte effect in CO_2RR activity was reached by modifying the proton donor source in solution. Thus, acetic acid from an acetate buffer solution (pH = 3.8) acting as a more efficient proton donor source than water has been proved in the present work to enhance up to 5 times the catalytic current density in the presence of either [TBA][BF_4] or [EMIM][BF_4] (dashed red plot in Figure 3.15 (b)). This might result from the acetic acid pKa, concentration and/or its neutral character in comparison with water at pH = 3.8, where it is actually positively charged (H_3O^+), which allows acetic acid to avoid repulsion electrostatic effects from the cations present at the cathodically polarized electrical double layer.

Another point where both complexes' interaction with ILs diverged was in product selectivity. Whereas, we saw that the presence of the IL had only a minor and slightly detrimental role on CO_2 to CO conversion on complex [1], it drastically impacted complex [2]'s product distribution. The CPE and CCE

results of complex [2] in acetonitrile solution reported in Tables 3.7 and 3.8 show that in all cases, H_2 formation was inhibited and the FE_{HCOO^-} increased upon addition of [EMIM][BF_4] or [EMIM][PF_6], reaching as high as $FE_{HCOO^-} \geq 90$ % (entries 2 and 3, Table 3.7), taking place at lower overpotentials and improving the energy efficiency of CO_2 conversion between +15 % and +22 % as compared to [TBA][PF_6]. This selective conversion of CO_2 to formate places complex [2] among the top selective molecular catalysts reported in the literature, which exhibited FE_{HCOO^-} = (80 – 97 %)[25]. Actually, previously reported results using complex [2] and the benchmark electrolyte ([TBA][PF_6]) in electrocatalysis[10] or photocatalysis[58], never reached $FE_{HCOO^-} \geq 50$ %. CCE results in unbuffered aqueous solution reported in Table 3.9 showed a weaker impact enhancing FE_{HCOO^-} in the presence of [EMIM][BF_4] than in acetonitrile solution, reaching as high as FE_{HCOO^-} = 49 % (entry 2), but exhibited a relevant decrease in overpotential (0.6 V) (entries 1 and 2). Comparing CCE results at -3.33 mA/cm^2 in acetonitrile and unbuffered aqueous solutions (Tables 3.8 and 3.9, respectively) reveals that the products ratio (FE_{HCOO^-}/FE_{H2}) decreases, from (3/1) to (1/1) in the specific case of $[EMIM]^+$ as sole supporting electrolyte, in moving from acetonitrile to water because of a dramatic increase in the concentration of protons. Meanwhile the electrolysis measured working electrode potential during galvanostatic electrolysis was significantly diminished in the presence of the IL in both acetonitrile (overpotential difference $\Delta\eta > 800$ mV) and aqueous conditions ($\Delta\eta > 600$ mV), as we can see in Figures 3.17 and 3.18 respectively. Especially in acetonitrile and to a lesser degree in water complex [2] became more selective in formate production in the presence of $[EMIM]^+$ in comparison with the benchmark electrolyte. In addition to this, the combination of a acetate buffer and [EMIM][BF_4] as electrolyte played a dual role on increasing CO_2 conversion activity and selectivity towards formate production (entry 4 of Table 3.9). On the one hand, this buffered solution system reached a significant current density (-3.33 mA/cm^2) and exhibited one of the lowest overpotentials (0.28 V, entry 4 of Table 3.9) reported so far for a homogenous molecular catalyst producing formate in aqueous solution. On the other hand, this buffered solution also inhibited HER compared to [TBA][BF_4] electrolyte in the same acetate buffered solution (entries 3 and 4 of Table 3.9). For the sake of comparison, we have taken the CPE data reported in the literature[53,59] to calculate the overpotential for two of the scarce examples of a molecular catalyst for formate production in neutral aqueous solution. Specifically, these were an Ir pincer complex[59] and an iron carbonyl cluster $[Fe_4N(CO)_{12}]^-$ [53], which displayed overpotentials of 0.8 V at -0.60 mA/cm^2 and 0.35 V at -4 mA/cm^2, respectively. In addition to this, Ir pincer complex required small amounts (ca. 1 %) of acetonitrile in solution, which was not the case for complex [2], working at much higher current density (-3.33 mA/cm^2) in purely acidic aqueous solution. As far as we are aware, not a single example of electrocatalytic formate production using a molecular catalyst in that acidic pH has been reported in the literature. This fact is very relevant in order to avoid significant CO_2 losses due to carbonate and bicarbonate generation in alkaline and neutral aqueous solutions.

In terms of theoretically interpreting the molecular catalyst-IL interaction by DFT, we only had as initial reference the Matsubara et. al.[38] study done on complex [1]. Thus, DFT calculations herein provide consistent theoretical support to understand the impact in formate production catalyzed by complex [2] by adding $[EMIM]^+$ in solution. They illustrate the formation of a π *cation*$\cdots\pi$ adduct between the reduced form of the catalyst and the imidazolium-based cation, which exhibited an overall decrease of the calculated reduction potential matching the experimental results obtained by cyclic voltammetry (Figure 3.13). Moreover, the incorporation of $[EMIM]^+$ at the electrode interface was found to increase the free-energy barriers for both CO_2RR and HER pathways, this effect being much more pronounced in the HER pathway, which proved HER inhibition by the presence of $[EMIM]^+$ at the interface in line with the experimental results in electrolysis (Tables 3.7, 3.8 and 3.9). The stronger impact into the HER pathway demonstrated by DFT calculations can be ascribed to the cationic nature of the $[Rh^{III}(bpy^{\bullet-})(Cp^*)H]\cdots[EMIM]^+$ complex that might have prevented to some extent the approach of other positively charged species such as free protons (H_3O^+), decreasing the local concentration of protons around the catalyst and thus disfavoring the HER process via electrostatic repulsion. Thus, based on these calculations and the aforementioned DFT study on complex [1][38], we observed that the beneficial effect on the catalytic performance for CO_2RR displayed by complexes [1] and [2] in presence of imidazolium based ILs was due in both cases to electrostatic interactions at the electrical double layer between the bipyridine ligand within the molecular catalyst and the imidazolium cation.

3.4 Conclusions

In conclusion, for the first time an electrolyte engineering strategy based on comparing the role as co-catalyst of different ILs, including pyrrolidinium and imidazolium based ILs, for CO_2 electroreduction with two model molecular catalysts is presented here. For the case of CO_2 conversion to CO catalyzed by complex [1], we firstly proved by CV and electrolysis that the use of ILs as a supporting electrolyte in acetonitrile did not only ensure appropriate conductivity, but also displayed co-catalyst features. More particularly, we have demonstrated that under both inert and CO_2 atmosphere, the negatively-charged reduced forms of complex [1] (mono- and di-anion intermediates) were electrostatically stabilized by the IL cations. This stabilization gives as a result an important IL cation-dependent overpotential diminution when compared to a conventional benchmark supporting electrolyte. However, this co-catalyst effect of ILs became less relevant in the presence of a proton source in solution due to the formation of a non-charged intermediate as a result of protonation (equation 5). CPE experiments in the presence of TFE demonstrated a slight decrease of selectivity for CO production when ILs were in solution. Nevertheless, higher current densities during CPEs were reached in the presence of ILs as supporting electrolyte, which

indicated an additional effect of ILs improving the catalytic reaction rate. In the case of complex [1] overall, [BMPyrr][PF_6] and [BMIM][PF_6] exhibited the lowest overpotential and the highest CO selectivity among the ILs studied in the presence of TFE as a proton source. However, the energy efficiency reached by the conventional benchmark electrolyte (61%, Table 3.4) was never overcome by catalytic performance of complex [1] in presence of ILs.

For the case of CO_2 conversion to formate catalyzed by complex [2], ILs were found to interact in a different manner than they previously had with complex [1]. However, studying complex [2] interacting with ILs, we demonstrated a significant impact on the CO_2RR performance and particularly its effect on overpotential, current density and products selectivity. The effect of ILs was not as evident under inert atmosphere as the only observable reduction peak of the catalyst remained at the same potential. Even under CO_2 reduction conditions, the gain in terms of overpotential and current density was modest. The great difference was actually observed by CCE in terms of product selectivity. We proved that aromatic imidazolium-based IL cations, and particularly $[EMIM]^+$, but not pyrrolidinium-based ILs, played a significant role in suppressing HER, enhancing catalytic current (j_{cat}) and decreasing overpotential (η) for the CO_2RR to formate production catalyzed by complex [2] in both acetonitrile and aqueous solutions. To sum up, complex [2] exhibited $FE_{HCOO^-} \geq 90$ % at low overpotentials (0.5 – 0.6 V) and a maximal energy efficiency for CO_2 conversion to formate of 66 % in acetonitrile solution in the presence of [EMIM][BF_4] or [EMIM][PF_6] (Table 3.7). Remarkably, this was the first time that $FE_{HCOO^-} \geq 50$ % is reported for CO_2RR catalyzed by complex [2] in acetonitrile solution. Furthermore, complex [2] represents one of the rare molecular catalysts soluble in aqueous solution. However, its catalytic behavior for CO_2RR in purely aqueous solution was never reported before. Comparing CO_2RR results in acetonitrile and aqueous solutions (Tables 3.8 and 3.9, respectively) revealed that complex [2] became less selective $FE_{HCOO^-} \leq 49$ % and (FE_{HCOO^-}/FE_{H2}) decreased to (1/1) in unbuffered aqueous solution. The use as electrolyte of [EMIM][BF_4] in an acetate buffer solution exhibited the lowest overpotential value (0.28 V, entry 4 of Table 3.9) reported so far for a homogenous molecular catalyst producing formate in aqueous solution. Moreover, this represented the first example of electrocatalytic formate production using a molecular catalyst in acidic aqueous solution (pH = 3.8). The significant role of acetic acid at the electrode/solution interface enhancing catalytic activity for CO_2RR might result from its lower pKa and higher concentration than water protons and/or its neutral character, which avoids electrostatic repulsions at the electrode/solution interface.

Thus, the combination of experimental results and DFT calculations provided here allowed us to reach a deeper mechanistic understanding of the promoter role of $[EMIM]^+$ at the electrode/solution interface enhancing either selective CO_2 conversion to CO or formate and suppressing HER catalyzed by complexes [1] and [2], respectively. This mainly involved the reduction of the potential required to

generate the active form of the catalyst via π^+-π interactions with $[EMIM]^+$ and the electrostatic repulsion of free protons at the electrode/solution interface, despite both complexes following a different reaction mechanism for CO_2RR. In conclusion, the impact of the imidazolium-based IL cation was linked to the interaction between the imidazolium cation and the reduced bipyridine ligand, which was present within the active form of both complexes. Finally, we suggest that other active molecular catalysts for CO_2RR containing bipyridine ligands will probably get a significant promoting effect by incorporating imidazolium-based ILs at the electrode/solution interface.

3.5 References

(1) Merino-Garcia, I.; Tinat, L.; Albo, J.; Alvarez-Guerra, M.; Irabien, A.; Durupthy, O.; Vivier, V.; Sánchez-Sánchez, C. M. Continuous Electroconversion of CO_2 into Formate Using 2 Nm Tin Oxide Nanoparticles. *Appl. Catal. B Environ.* **2021**, *297*, 120447. https://doi.org/10.1016/j.apcatb.2021.120447.

(2) Qiao, J.; Liu, Y.; Hong, F.; Zhang, J. A Review of Catalysts for the Electroreduction of Carbon Dioxide to Produce Low-Carbon Fuels. *Chem. Soc. Rev.* **2013**, *43* (2), 631–675. https://doi.org/10.1039/C3CS60323G.

(3) Francke, R.; Schille, B.; Roemelt, M. Homogeneously Catalyzed Electroreduction of Carbon Dioxide—Methods, Mechanisms, and Catalysts. *Chem. Rev.* **2018**, *118* (9), 4631–4701. https://doi.org/10.1021/acs.chemrev.7b00459.

(4) Benson, E. E.; Kubiak, C. P.; Sathrum, A. J.; Smieja, J. M. Electrocatalytic and Homogeneous Approaches to Conversion of CO_2 to Liquid Fuels. *Chem. Soc. Rev.* **2008**, *38* (1), 89–99. https://doi.org/10.1039/B804323J.

(5) Costentin, C.; Robert, M.; Savéant, J.-M. Catalysis of the Electrochemical Reduction of Carbon Dioxide. *Chem. Soc. Rev.* **2013**, *42* (6), 2423–2436. https://doi.org/10.1039/C2CS35360A.

(6) Hawecker, J.; Lehn, J.-M.; Ziessel, R. Photochemical and Electrochemical Reduction of Carbon Dioxide to Carbon Monoxide Mediated by (2,2′-Bipyridine)Tricarbonylchlororhenium(I) and Related Complexes as Homogeneous Catalysts. *Helv. Chim. Acta* **1986**, *69* (8), 1990–2012. https://doi.org/10.1002/hlca.19860690824.

(7) Hawecker, J.; Lehn, J.-M.; Ziessel, R. Electrocatalytic Reduction of Carbon Dioxide Mediated by $Re(Bipy)(CO)_3Cl$ (Bipy = 2,2′-Bipyridine). *J. Chem. Soc. Chem. Commun.* **1984**, *6*, 328–330. https://doi.org/10.1039/C39840000328.

(8) Nakazawa, M.; Mizobe, Y.; Matsumoto, Y.; Uchida, Y.; Tezuka, M.; Hidai, M. Electrochemical Reduction of Carbon Dioxide Using Iron–Sulfur Clusters as Catalyst Precursors. *Bull. Chem. Soc. Jpn.* **1986**, *59* (3), 809–814. https://doi.org/10.1246/bcsj.59.809.

(9) Ogura, K.; Yoshida, I. Electrocatalytic Reduction of CO_2 to Methanol: Part 9: Mediation with Metal Porphyrins. *J. Mol. Catal.* **1988**, *47* (1), 51–57. https://doi.org/10.1016/0304-5102(88)85072-7.

(10) Caix, C.; Chardon-Noblat, S.; Deronzier, A. Electrocatalytic Reduction of CO_2 into Formate with $[(\eta^5\text{-}Me_5C_5)M(L)Cl]^+$ Complexes (L = 2,2′-Bipyridine Ligands; M = Rh(III) and Ir(III)). *J. Electroanal. Chem.* **1997**, *434* (1), 163–170. https://doi.org/10.1016/S0022-0728(97)00058-2.

(11) Smieja, J. M.; Sampson, M. D.; Grice, K. A.; Benson, E. E.; Froehlich, J. D.; Kubiak, C. P. Manganese as a Substitute for Rhenium in CO_2 Reduction Catalysts: The Importance of Acids. *Inorg. Chem.* **2013**, *52* (5), 2484–2491. https://doi.org/10.1021/ic302391u.

(12) Leung, K.; Nielsen, I. M. B.; Sai, N.; Medforth, C.; Shelnutt, J. A. Cobalt-Porphyrin Catalyzed Electrochemical Reduction of Carbon Dioxide in Water. 2. Mechanism from First Principles. *J. Phys. Chem. A* **2010**, *114* (37), 10174–10184. https://doi.org/10.1021/jp1012335.

(13) Beley, Marc.; Collin, J. Paul.; Ruppert, Romain.; Sauvage, J. Pierre. Electrocatalytic Reduction of Carbon Dioxide by Nickel Cyclam2+ in Water: Study of the Factors Affecting the Efficiency and the Selectivity of the Process. *J. Am. Chem. Soc.* **1986**, *108* (24), 7461–7467. https://doi.org/10.1021/ja00284a003.

(14) Costentin, C.; Drouet, S.; Robert, M.; Savéant, J.-M. A Local Proton Source Enhances CO_2 Electroreduction to CO by a Molecular Fe Catalyst. *Science* **2012**, *338* (6103), 90–94. https://doi.org/10.1126/science.1224581.

(15) Hawecker, J.; Lehn, J.-M.; Ziessel, R. Efficient Photochemical Reduction of CO_2 to CO by Visible Light Irradiation of Systems Containing $Re(Bipy)(CO)_3X$ or $Ru(Bipy)_3^{2+}$–Co^{2+} Combinations as Homogeneous Catalysts. *J Chem Soc Chem Commun* **1983**, *9*, 536–538. https://doi.org/10.1039/C39830000536.

(16) Clark, M. L.; Cheung, P. L.; Lessio, M.; Carter, E. A.; Kubiak, C. P. Kinetic and Mechanistic Effects of Bipyridine (Bpy) Substituent, Labile Ligand, and Brønsted Acid on Electrocatalytic CO_2 Reduction by Re(Bpy) Complexes. *ACS Catal.* **2018**, *8* (3), 2021–2029. https://doi.org/10.1021/acscatal.7b03971.

(17) Manbeck, G. F.; Muckerman, J. T.; Szalda, D. J.; Himeda, Y.; Fujita, E. Push or Pull? Proton Responsive Ligand Effects in Rhenium Tricarbonyl CO_2 Reduction Catalysts. *J. Phys. Chem. B* **2015**, *119* (24), 7457–7466. https://doi.org/10.1021/jp511131x.

(18) Sung, S.; Kumar, D.; Gil-Sepulcre, M.; Nippe, M. Electrocatalytic CO_2 Reduction by Imidazolium-Functionalized Molecular Catalysts. *J. Am. Chem. Soc.* **2017**, *139* (40), 13993–13996. https://doi.org/10.1021/jacs.7b07709.

(19) Blakemore, J. D.; Gupta, A.; Warren, J. J.; Brunschwig, B. S.; Gray, H. B. Noncovalent Immobilization of Electrocatalysts on Carbon Electrodes for Fuel Production. *J. Am. Chem. Soc.* **2013**, *135* (49), 18288–18291. https://doi.org/10.1021/ja4099609.

(20) Caix, C.; Chardon-Noblat, S.; Deronzier, A.; Moutet, J.-C.; Tingry, S. (Pentamethylcyclopentadienyl)(Polypyridyl) Rhodium and Iridium Complexes as Electrocatalysts for the Reduction of Protons to Dihydrogen and the Hydrogenation of Organics. *J. Organomet. Chem.* **1997**, *540* (1), 105–111.https://doi.org/10.1016/S0022-328X(97)00096-X.

(21) Todorova, T. K.; Huan, T. N.; Wang, X.; Agarwala, H.; Fontecave, M. Controlling Hydrogen Evolution during Photoreduction of CO_2 to Formic Acid Using $[Rh(R\text{-}Bpy)(Cp^*)Cl]^+$ Catalysts: A Structure-Activity Study. *Inorg. Chem.* **2019**, *58* (10), 6893–6903.

(22) Benseghir, Y.; Lemarchand, A.; Duguet, M.; Mialane, P.; Gomez-Mingot, M.; Roch-Marchal, C.; Pino, T.; Ha-Thi, M.-H.; Haouas, M.; Fontecave, M.; Dolbecq, A.; Sassoye, C.; Mellot-Draznieks, C. Co-Immobilization of a Rh Catalyst and a Keggin Polyoxometalate in the UiO-67 Zr-Based Metal-Organic Framework: In Depth Structural Characterization and Photocatalytic Properties for CO_2 Reduction. *J. Am. Chem. Soc.* **2020**, *142* (20), 9428–9438. https://doi.org/10.1021/jacs.0c02425.

(23) Keith, J. A.; Grice, K. A.; Kubiak, C. P.; Carter, E. A. Elucidation of the Selectivity of Proton-Dependent Electrocatalytic CO_2 Reduction by *Fac* -$Re(Bpy)(CO)_3Cl$. *J. Am. Chem. Soc.* **2013**, *135* (42), 15823–15829. https://doi.org/10.1021/ja406456g.

(24) Riplinger, C.; Sampson, M. D.; Ritzmann, A. M.; Kubiak, C. P.; Carter, E. A. Mechanistic Contrasts between Manganese and Rhenium Bipyridine Electrocatalysts for the Reduction of Carbon Dioxide. *J. Am. Chem. Soc.* **2014**, *136* (46), 16285–16298. https://doi.org/10.1021/ja508192y.

(25) Taheri, A.; Berben, L. A. Making C–H Bonds with CO_2: Production of Formate by Molecular Electrocatalysts. *Chem. Commun.* **2016**, *52* (9), 1768–1777.

(26) Chen, L. D.; Urushihara, M.; Chan, K.; Nørskov, J. K. Electric Field Effects in Electrochemical CO_2 Reduction. *ACS Catal.* **2016**, *6* (10), 7133–7139. https://doi.org/10.1021/acscatal.6b02299.

(27) Banerjee, S.; Han, X.; Thoi, V. S. Modulating the Electrode–Electrolyte Interface with Cationic Surfactants in Carbon Dioxide Reduction. *ACS Catal.* **2019**, *9* (6), 5631–5637. https://doi.org/10.1021/acscatal.9b00449.

(28) Sa, Y. J.; Lee, C. W.; Lee, S. Y.; Na, J.; Lee, U.; Hwang, Y. J. Catalyst–Electrolyte Interface Chemistry for Electrochemical CO_2 Reduction. *Chem. Soc. Rev.* **2020**, *49* (18), 6632–6665. https://doi.org/10.1039/D0CS00030B.

(29) Hapiot, P.; Lagrost, C. Electrochemical Reactivity in Room-Temperature Ionic Liquids. *Chem. Rev.* **2008**, *108* (7), 2238–2264. https://doi.org/10.1021/cr0680686.

(30) Hanc-Scherer, F. A.; Montiel, M. A.; Montiel, V.; Herrero, E.; Sánchez-Sánchez, C. M. Surface Structured Platinum Electrodes for the Electrochemical Reduction of Carbon Dioxide in Imidazolium Based Ionic Liquids. *Phys. Chem. Chem. Phys.* **2015**, *17* (37), 23909–23916. https://doi.org/10.1039/C5CP02361K.

(31) Montiel, M. A.; Solla-Gullón, J.; Montiel, V.; Sánchez-Sánchez, C. M. Electrocatalytic Studies on Imidazolium Based Ionic Liquids: Defining Experimental Conditions. *Phys. Chem. Chem. Phys.* **2018**, *20* (28), 19160–19167. https://doi.org/10.1039/C8CP02662A.

(32) Grills, D. C.; Matsubara, Y.; Kuwahara, Y.; Golisz, S. R.; Kurtz, D. A.; Mello, B. A. Electrocatalytic CO_2 Reduction with a Homogeneous Catalyst in Ionic Liquid: High Catalytic Activity at Low Overpotential. *J. Phys. Chem. Lett.* **2014**, *5* (11), 2033–2038. https://doi.org/10.1021/jz500759x.

(33) Sánchez-Sánchez, C. M. Electrocatalytic Reduction of CO_2 in Imidazolium-Based Ionic Liquids. In *Reference Module in Chemistry, Molecular Sciences and Chemical Engineering. Encyclopedia of Interfacial Chemistry : Surface Science and Electrochemistry*; Wandelt, K., Ed.; Elsevier, 2018; pp 539–551.

(34) Vichou, E.; Li, Y.; Gomez-Mingot, M.; Fontecave, M.; Sánchez-Sánchez, C. M. Imidazolium- and Pyrrolidinium-Based Ionic Liquids as Cocatalysts for CO_2 Electroreduction in Model Molecular Electrocatalysis. *J. Phys. Chem. C* **2020**, *124* (43), 23764–23772.

(35) Feaster, J. T.; Jongerius, A. L.; Liu, X.; Urushihara, M.; Nitopi, S. A.; Hahn, C.; Chan, K.; Nørskov, J. K.; Jaramillo, T. F. Understanding the Influence of [EMIM]Cl on the Suppression of the Hydrogen Evolution Reaction on Transition Metal Electrodes. *Langmuir* **2017**, *33* (37), 9464–9471. https://doi.org/10.1021/acs.langmuir.7b01170.

(36) Vasilyev, D. V.; Dyson, P. J. The Role of Organic Promoters in the Electroreduction of Carbon Dioxide. *ACS Catal.* **2021**, *11* (3), 1392–1405. https://doi.org/10.1021/acscatal.0c04283.

(37) Rosen, B. A.; Salehi-Khojin, A.; Thorson, M. R.; Zhu, W.; Whipple, D. T.; Kenis, P. J. A.; Masel, R. I. Ionic Liquid-Mediated Selective Conversion of CO_2 to CO at Low Overpotentials. *Science* **2011**, *334* (6056), 643–644.

(38) Matsubara, Y.; Grills, D. C.; Kuwahara, Y. Thermodynamic Aspects of Electrocatalytic CO_2 Reduction in Acetonitrile and with an Ionic Liquid as Solvent or Electrolyte. *ACS Catal.* **2015**, *5* (11), 6440–6452. https://doi.org/10.1021/acscatal.5b00656.

(39) Choi, J.; Benedetti, T. M.; Jalili, R.; Walker, A.; Wallace, G. G.; Officer, D. L. High Performance Fe Porphyrin/Ionic Liquid Co-Catalyst for Electrochemical CO_2 Reduction. *Chem. - Eur. J.* **2016**, *22* (40), 14158–14161.

(40) Kemna, A.; García Rey, N.; Braunschweig, B. Mechanistic Insights on CO_2 Reduction Reactions at Platinum/[BMIM][BF_4] Interfaces from In Operando Spectroscopy. *ACS Catal.* **2019**, *9* (7), 6284–6292. https://doi.org/10.1021/acscatal.9b01033.

(41) Ratschmeier, B.; Kemna, A.; Braunschweig, B. Role of H_2O for CO_2 Reduction Reactions at Platinum/Electrolyte Interfaces in Imidazolium Room-Temperature Ionic Liquids. *ChemElectroChem* **2020**, *7* (7), 1765–1774. https://doi.org/10.1002/celc.202000316.

(42) Sullivan, B. P.; Bolinger, C. M.; Conrad, D.; Vining, W. J.; Meyer, T. J. One- and Two-Electron Pathways in the Electrocatalytic Reduction of CO_2 by Fac-Re(Bpy)(CO)3Cl (Bpy = 2,2′-Bipyridine). *J. Chem. Soc. Chem. Commun.* **1985**, No. 20, 1414–1416. https://doi.org/10.1039/C39850001414.

(43) Azcarate, I.; Costentin, C.; Robert, M.; Savéant, J.-M. Through-Space Charge Interaction Substituent Effects in Molecular Catalysis Leading to the Design of the Most Efficient Catalyst of CO_2-to-CO Electrochemical Conversion. *J. Am. Chem. Soc.* **2016**, *138* (51), 16639–16644.

(44) Zhao, S.-F.; Horne, M.; Bond, A. M.; Zhang, J. Is the Imidazolium Cation a Unique Promoter for Electrocatalytic Reduction of Carbon Dioxide? *J. Phys. Chem. C* **2016**, *120* (42), 23989–24001. https://doi.org/10.1021/acs.jpcc.6b08182.

(45) Michez, R.; Vander Steen, J.; Doneux, T.; Luhmer, M.; Buess-Herman, C. Electroreduction of 1-Butyl-3-Methylimidazolium Bis(Trifluoromethanesulfonyl)Imide Ionic Liquid: Oriented Product Selectivity through the Electrode Material. *Electrochimica Acta* **2018**, *270*, 434–439.

(46) Wang, Y.; Hayashi, T.; He, D.; Li, Y.; Jin, F.; Nakamura, R. A Reduced Imidazolium Cation Layer Serves as the Active Site for Electrochemical Carbon Dioxide Reduction. *Appl. Catal. B Environ.* **2020**, *264*, 118495. https://doi.org/10.1016/j.apcatb.2019.118495.

(47) Huan, T. N.; Simon, P.; Rousse, G.; Génois, I.; Artero, V.; Fontecave, M. Porous Dendritic Copper: An Electrocatalyst for Highly Selective CO_2 Reduction to Formate in Water/Ionic Liquid Electrolyte. *Chem. Sci.* **2016**, *8* (1), 742–747. https://doi.org/10.1039/C6SC03194C.

(48) Tomita, Y.; Teruya, S.; Koga, O.; Hori, Y. Electrochemical Reduction of Carbon Dioxide at a Platinum Electrode in Acetonitrile-Water Mixtures. *J. Electrochem. Soc.* **2000**, *147* (11), 4164. https://doi.org/10.1149/1.1394035.

(49) König, M.; Vaes, J.; Klemm, E.; Pant, D. Solvents and Supporting Electrolytes in the Electrocatalytic Reduction of CO_2. *iScience* **2019**, *19*, 135–160. https://doi.org/10.1016/j.isci.2019.07.014.

(50) Huang, J. E.; Li, F.; Ozden, A.; Sedighian Rasouli, A.; García de Arquer, F. P.; Liu, S.; Zhang, S.; Luo, M.; Wang, X.; Lum, Y.; Xu, Y.; Bertens, K.; Miao, R. K.; Dinh, C.-T.; Sinton, D.; Sargent, E. H. CO_2 Electrolysis to Multicarbon Products in Strong Acid. *Science* **2021**, *372* (6546), 1074–1078. https://doi.org/10.1126/science.abg6582.

(51) Kang, P.; Cheng, C.; Chen, Z.; Schauer, C. K.; Meyer, T. J.; Brookhart, M. Selective Electrocatalytic Reduction of CO_2 to Formate by Water-Stable Iridium Dihydride Pincer Complexes. *J. Am. Chem. Soc.* **2012**, *134* (12), 5500–5503. https://doi.org/10.1021/ja300543s.

(52) Rail, M. D.; Berben, L. A. Directing the Reactivity of $[HFe_4N(CO)_{12}]^-$ toward H^+ or CO_2 Reduction by Understanding the Electrocatalytic Mechanism. *J. Am. Chem. Soc.* **2011**, *133* (46), 18577–18579. https://doi.org/10.1021/ja208312t.

(53) Taheri, A.; Thompson, E. J.; Fettinger, J. C.; Berben, L. A. An Iron Electrocatalyst for Selective Reduction of CO_2 to Formate in Water: Including Thermochemical Insights. *ACS Catal.* **2015**, *5* (12), 7140–7151. https://doi.org/10.1021/acscatal.5b01708.

(54) Kölle, U.; Kang, B.-S.; Infelta, P.; Comte, P.; Grätzel, M. Elektrochemische und pulsradiolytische Reduktion von (Pentamethylcyclopentadienyl)(polypyridyl)rhodium-Komplexen. *Chem. Ber.* **1989**, *122* (10), 1869–1880. https://doi.org/10.1002/cber.19891221008.

(55) Moore, W. N. G.; Henke, W. C.; Lionetti, D.; Day, V. W.; Blakemore, J. D. Single-Electron Redox Chemistry on the [Cp*Rh] Platform Enabled by a Nitrated Bipyridyl Ligand. *Molecules* **2018**, *23* (11), 2857. https://doi.org/10.3390/molecules23112857.

(56) Wang, Y.; Hatakeyama, M.; Ogata, K.; Wakabayashi, M.; Jin, F.; Nakamura, S. Activation of CO_2 by Ionic Liquid EMIM–BF4 in the Electrochemical System: A Theoretical Study. *Phys. Chem. Chem. Phys.* **2015**, *17* (36), 23521–23531. https://doi.org/10.1039/C5CP02008E.

(57) Papasizza, M.; Yang, X.; Cheng, J.; Cuesta, A. Electrocatalytic Reduction of CO_2 in Neat and Water-Containing Imidazolium-Based Ionic Liquids. *Curr. Opin. Electrochem.* **2020**, *23*, 80–88. https://doi.org/10.1016/j.coelec.2020.04.004.

(58) Chambers, M. B.; Wang, X.; Elgrishi, N.; Hendon, C. H.; Walsh, A.; Bonnefoy, J.; Canivet, J.; Quadrelli, E. A.; Farrusseng, D.; Mellot-Draznieks, C.; Fontecave, M. Photocatalytic Carbon Dioxide Reduction with Rhodium-Based Catalysts in Solution and Heterogenized within Metal-Organic Frameworks. *ChemSusChem* **2015**, *8* (4), 603–608.

(59) Kang, P.; Meyer, T. J.; Brookhart, M. Selective Electrocatalytic Reduction of Carbon Dioxide to Formate by a Water-Soluble Iridium Pincer Catalyst. *Chem. Sci.* **2013**, *4* (9), 3497–3502. https://doi.org/10.1039/C3SC51339D.

CHAPTER 4: IMMOBILIZATION OF IONIC LIQUIDS FOR TUNING CO2 ELECTROREDUCTION SELECTIVITY IN MODEL MOLECULAR ELECTROCATALYSIS

CHAPTER 4: IMMOBILIZATION OF IONIC LIQUIDS FOR TUNING CO2 ELECTROREDUCTION SELECTIVITY IN MODEL MOLECULAR ELECTROCATALYSIS

4.1 Introduction

The electrocatalytic carbon dioxide reduction reaction (CO_2RR) on metal-based heterogeneous catalysts is currently exhibiting high activities at low overpotentials, although key parameters such as product selectivity, stability and low current density still need to improve. Nevertheless, there is an increasing interest in merging homogeneous molecular catalysts to tune heterogenous catalysts to address structure-function relationship[1]. Various molecular additives have been explored, immobilized on different electrode materials and enhanced catalytic responses have been registered, even though more structure-activity studies are often necessary to be able to control such effects. These molecular additives are usually small organic molecules, including but not restricted to: amines[2,3], thiols[2–5], amino acids[6], polypyrrole[7], N-heterocyclic carbenes[8], N-substituted bipyridines[9–12]. The effect of the resulting coated electrodes is either an enhancement of CO_2RR by stabilization of reduction intermediates that leads to lowered overpotentials and better selectivities[1], or a suppression of the main parasitic reaction, HER. Notable examples of the former are the electron donating effect of carbenes on a Pd electrode that tunes selectivity towards formate evolution by stabilizing *HCOO intermediates[8] and the stabilization of atop-bound *CO reduction on a copper electrode by arylpyridiniums, that favors further reduction to C2 products and more specifically leads to 72 % ethylene yield at appreciable current densities[11]. On the other hand, molecular additives have been found to dramatically alter selectivity by suppressing HER. A notable case is that of planar silver electrodes, normally very active towards HER, after coated by pyridinium-based molecules exhibit a CO_2-to-CO conversion FE that is over 99 %[12].

Ionic Liquids (ILs) themselves have often been employed in solution in order to promote CO_2RR and tune the reaction selectivity more towards desirable products by the intrinsic ability of their cations, usually belonging to the imidazolium family, to stabilize CO_2 reduction intermediates[13–16]. More recently, a study has also demonstrated their potential in suppressing HER in transition metal electrodes, the chief side-reaction occurring during CO_2RR, in very acidic pH by using 0.1 M of [EMIM]Cl in aqueous solutions.[17] More specifically, it was shown that they have this effect only under acidic conditions, during which the imidazolium cations repel the protons approaching the electrode, while, on the contrary, under alkaline conditions the hydrogen source is water that cannot be electrostatically repelled.[17] As far as the ILs immobilization on electrodes is concerned, there have been examples using either diazonium chemistry[18], thiol groups within self-assembled monolayers (SAM)[19] or covalent grafting.[20] All these methods produce covalently bound IL moieties on the electrode, but to the best of our knowledge they have not been explored in CO_2 electroreduction.

Meanwhile, fundamental studies, where electrochemical IL reduction was studied on different electrode materials and the formed products were analyzed by NMR (liquid phase) or GC (gas phase), resulted in many interesting observations[21,22]. The first information was that IL reduction on different materials

occurs at different potentials and though the primary imidazolium reduction products are the same, their distribution may vary based on the material's ability to absorb hydrogen. In general, the main imidazolium reduction species are a neutral dimer resulting from one-electron transfer between two already reduced imidazol-2-yl radicals and the disproportionation product of the aforementioned radicals to form a neutral monomer. Possible pathways that result in charged monomers and dimers are proposed, but those species were not observed[21,22]. Moreover, some additional studies have demonstrated the electrochemical reduction of [EMIM][BF_4] on a copper electrode to form an electrochemical layer on the Cu surface that can suppress HER in favor of CO_2RR[23]. In particular, the HER suppression effect was not solely observed on an initial CV, that is in accordance with $[EMIM]^+$ adsorption on the electrode surface[17], but persisted and even strengthened in consecutive scans, which the authors attribute to a reaction of electrochemical nature between the electrode surface and the IL[23].

Having observed the ways in which surface engineering may alter the catalytic performance of heterogeneous catalysts, in this chapter we attempted to apply this principle to ILs. In the previous chapter, we reported the reduction of imidazolium-based cations beyond -2.5 V *vs.* Fc^+/Fc in acetonitrile solution and thus here we attempted to electrochemically modify the working electrode with an imidazolium layer. This layer was then assessed using the molecular catalyst [Rh(bpy)(Cp*)Cl]Cl (referred as complex [2]) as a catalytic model under different CO_2 catalytic conditions as they were defined in the previous chapter and characterized by electrochemistry and different surface analysis techniques.

4.2 Results

4.2.1 IL Layer formation and optimization by testing on [Rh(bpy)(Cp*)Cl]Cl model catalyst

The reduction of imidazolium-based cations in acetonitrile solution has been reported in literature[21,22] as well as witnessed in the previous chapter. As can be seen in Figure 4.1, we observed a reduction wave when cycling either a GCE or a AuE in 0.5 M [EMIM][PF_6] solution in acetonitrile under an inert atmosphere beyond their reduction limits (-2.50 V *vs.* Fc^+/Fc in GCE) or (-2.10 V *vs.* Fc^+/Fc in AuE), respectively. A reoxidation peak is observed when the potential reaches -0.7 V, but is only observed as long as the imidazolium is first reduced.

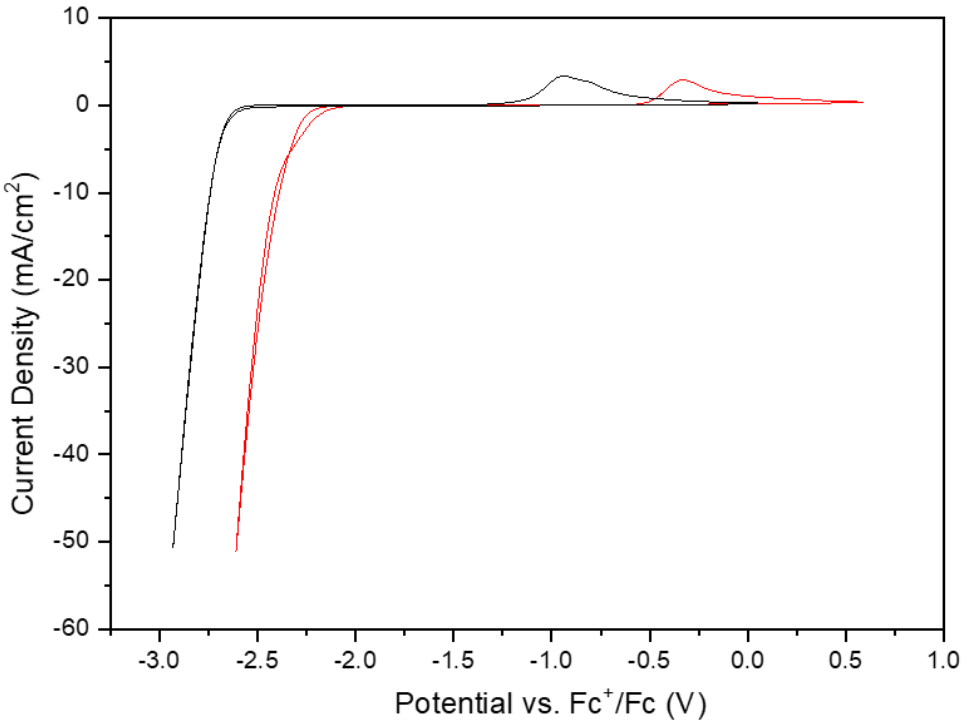

Figure 4.1 Cyclic voltammograms of the electroreduction of 0.5 M [EMIM][PF_6] solution in acetonitrile on a 3 mm GCE (black plot) and AuE (red plot) under Ar. Scan rate of 0.1 V/s.

Subsequently, the modified GCE was removed from the solution, rinsed by acetonitrile and placed in a solution containing the model molecular catalyst [2] in acetonitrile solution containing 0.5 M [TBA][PF_6] as supporting electrolyte under catalytic conditions: saturation of CO_2 and 5 % (vol.) H_2O. The aim was to compare the CO_2 catalytic response of complex [2] by this IL-modified electrode towards a bare electrode with 0.5 M of the same IL in solution. Furthermore, a CV of the bare electrode in standard benchmark conditions, i.e. 0.5 M [TBA][PF_6] was also shown. As seen in Figure 4.2, we immediately remarked that the CVs of the IL-modified electrode and the bare electrode containing IL in the solution had identical shapes with the same onset potentials, which were more anodic than those of the bare electrode in benchmark conditions. Moreover, the presence of the IL provoked an enhancement of almost 1.5 times larger current, independently if the IL is in solution or immobilised on the electrode. This sort of electrode modification by IL reduction will be henceforth referred to as an electrodeposited IL layer.

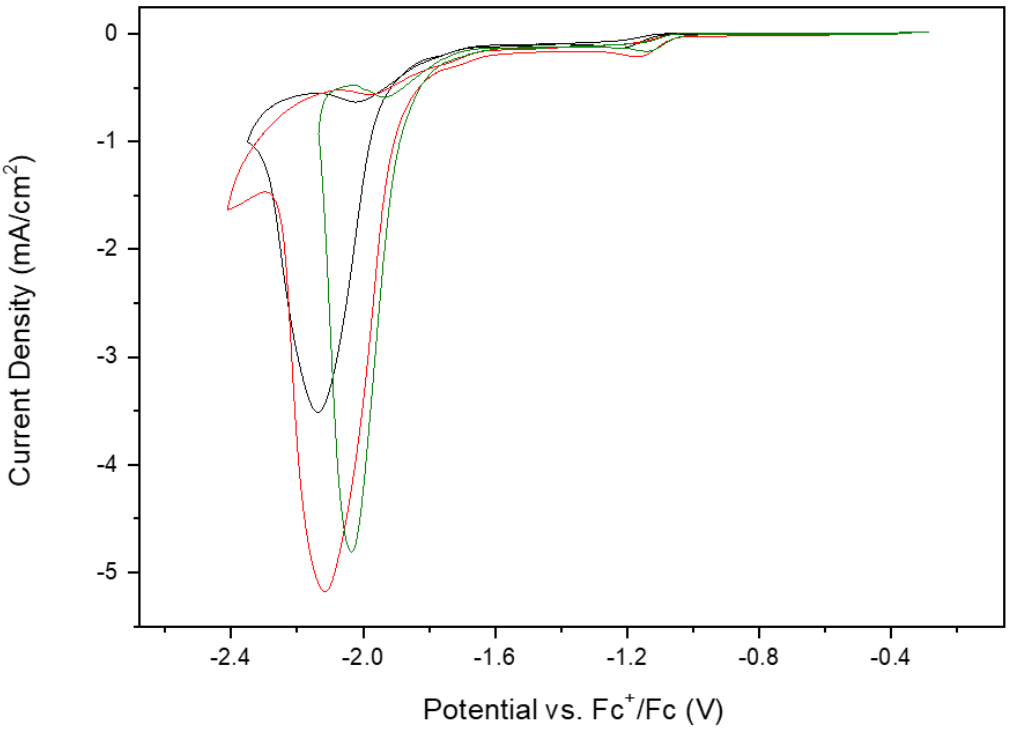

Figure 4.2 Cyclic voltammograms under catalytic conditions of 1 mM [Rh(bpy)(Cp)Cl]Cl in 0.5 M [TBA][PF_6] acetonitrile solution on: a bare GCE (black plot) and an IL-modified CGE by electrodeposited layer (CPE of 10 s at -3.95 V in 0.5 M of [EMIM][PF_6] in acetonitrile) (red plot). Also, CV of bare GCE in a solution containing 0.5 M [EMIM][PF_6] in acetonitrile as supporting electrolyte (green plot). Catalytic conditions: acetonitrile solution under CO_2 with 5 % H_2O (vol.). Scan rate 0.01 V/s. WE=GCE.*

A deeper optimization study of the IL-immobilization was carried out. Different parameters were tested and assessed by the best catalytic response of complex [2] towards CO_2 in terms of simultaneously lowering the overpotential and increasing the current density. First of all, we studied the IL reduction potential window, as presented in Figure 4.3 (a). The electrode was placed in an acetonitrile solution containing 0.5 M [EMIM][PF_6] as supporting electrolyte saturated in argon, and cycled towards subsequently more cathodic potentials up to -3.95 V *vs.* Fc^+/Fc. After each CV for IL layer electrodeposition, the electrode was removed, rinsed with acetonitrile and placed in a solution containing the model molecular catalyst [2] under catalytic CO_2RR conditions (Figure 4.3 (b)). The outcome suggested that the more cathodically we scanned (corresponds to CV in red in Figure 4.3 (a)), which coincided with more imidazolium reduction, the larger the catalytic effect we obtained. Thus, the potential limit to immobilize the IL by CV was selected to be -3.95 V *vs.* Fc^+/Fc. Next, we studied the IL immobilization by constant potential electrolysis (CPE) varying the duration (ranging from 10 s CPE to 15 min CPE) at this selected potential to obtain an optimal electrodeposited IL layer. Based on the

catalytic onset potentials and current density values shown in Figure 4.4, the optimal layer from a catalytic point of view was obtained by 10 sec CPE (red plot in Figure 4.4) and it was almost identical to the effect produced by cycling only once by CV up to -3.95 V (black plot in Figure 4.4). The procedure applied was the same as previously described: first immobilization of the IL using 0.5 M [EMIM][PF_6] as supporting electrolyte in argon saturated acetonitrile solution, rinsing the electrode and then study of the modified electrode in a new solution of complex [2] under CO_2 catalytic conditions. Comparing the catalytic behavior displayed by complex [2] in Figure 4.4, E_{cat} did not vary significantly whereas, on the contrary, the maximal current density appeared to have an inverted relation with the time of CPE; producing the higher current density value the shorter electrolysis. Thus, the selected conditions for the rest of the optimization experiments were 10 s CPE at -3.95 V.

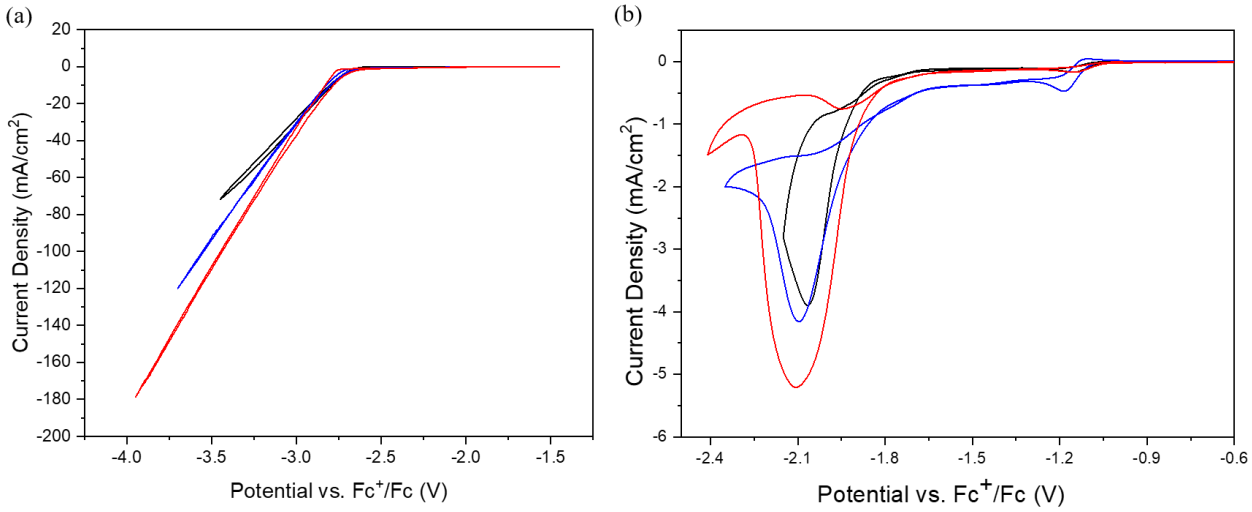

Figure 4.3 (a) Cyclic voltammograms at a scan rate of 0.1 V/s of electrodeposited layer formation on GCE in 0.5 M [EMIM][PF_6] acetonitrile solution with reductive potential limits until: -3.45 V (black plot), -3.75 V (blue plot), -3.95 V (red plot) and (b) the corresponding catalytic condition CVs of 1 mM [Rh(bpy)(Cp)Cl]Cl in 0.5 M [TBA][PF_6] acetonitrile solution on: IL-modified GCE by 1 CV until -3.45 V electrodeposited layer (black plot), IL-modified CGE by 1 CV until -3.75 V electrodeposited layer (blue plot) and IL-modified GCE by 1 CV until -3.95 V electrodeposited layer (red plot). Catalytic conditions: acetonitrile solution under CO_2 with 5 % H_2O (vol.). Scan rate 0.01 V/s. WE=GCE.*

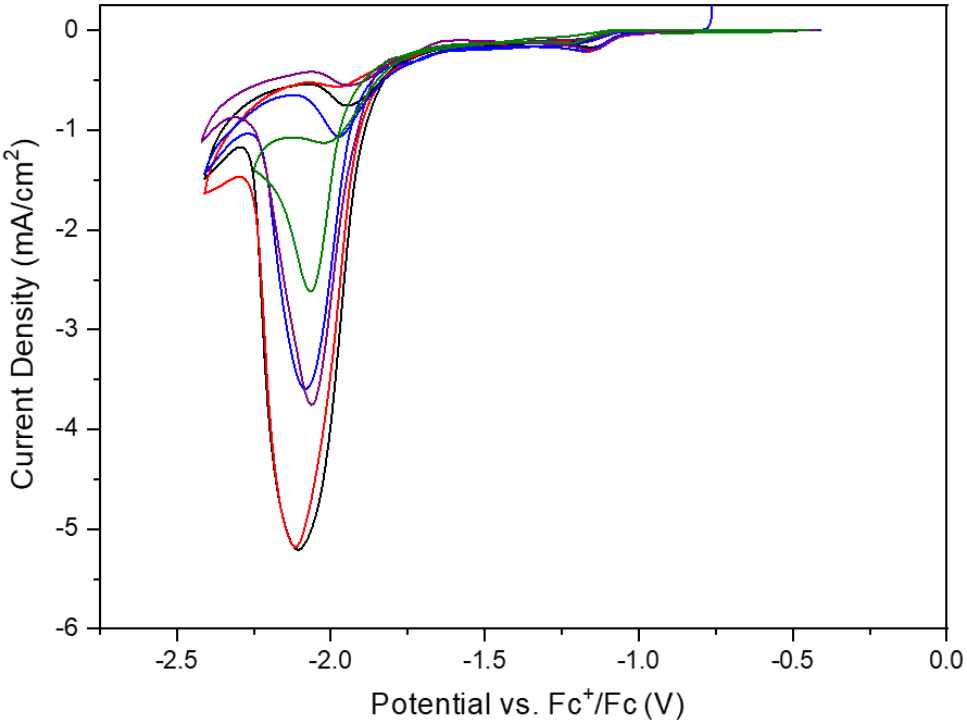

Figure 4.4 Cyclic voltammograms under catalytic conditions of 1 mM [Rh(bpy)(Cp)Cl]Cl in 0.5 M [TBA][PF_6] acetonitrile solution on an IL-modified GCE by electrodeposited layer formed by CPE at -3.95 V in 0.5 M [EMIM][PF_6] acetonitrile solution by: 10 s (red plot), 30 s (blue plot), 60 s (purple plot), 15 min (green plot) and by 1 CV until -3.95 V at a scan rate of 0.1 V/s (black plot). Catalytic conditions: acetonitrile solution under CO_2 with 5 % H_2O (vol.). Scan rate 0.01 V/s. WE=GCE.*

In order to see if the packaging of IL molecules affected the IL layer on the electrode, we also studied the effect of IL concentration used for the electroreduction of [EMIM][PF_6]. Figure 4.5, shows the CVs on complex [2] under CO_2 catalytic conditions with electrodes where different electrodeposited IL layers have been formed using different concentrations of [EMIM][PF_6], from 0.01 M to 1 M by applying a CPE of 10 s at -3.95 V. These results showed that 0.5 M [EMIM][PF_6] was the concentration that resulted in the highest catalytic current density. In the same line, we also decided to test if there was any effect on the anion used to electrodeposit the IL layer (CPE of 10 s at -3.95 V). Figure 4.6 (a) shows that there is no effect on the anion used to generate the layer, showing that both [EMIM][PF_6] and [EMIM][BF_4] gave similar results in terms of electrodeposition of an IL layer. Then, we decided to study the effect of a more bulky imidazolium cation and we tested the electroreduction of [BMIM][PF_6] as shown in 4.6 (b), which exhibited the same decrease in overpotential displayed by [EMIM][PF_6], but was less catalytically efficient. Finally, in order to evaluate the effect of CO_2 during the IL layer formation, we performed the electroreduction of [EMIM][PF_6] in non inert conditions. Figure 4.7 shows the CVs of complex [2] under CO_2 catalytic conditions when comparing the electrodeposition of the [EMIM][PF_6] layer in argon and CO_2 atmospheres in GCE, respectively. It is evident that the electrodeposited layer

grown under CO_2 does not produce any clear impact on the catalytic behaviour of complex [2], since it closely resembles the response of the bare electrode also shown in Figure 4.7 for the shake of comparison.

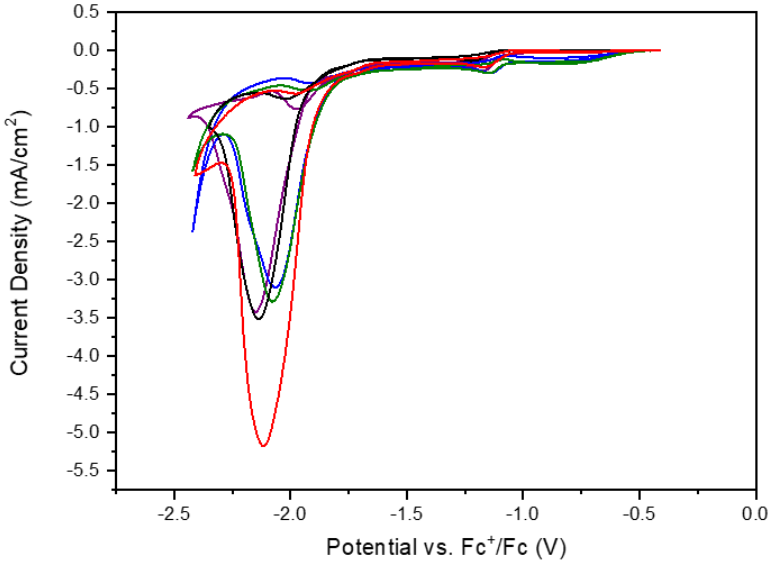

Figure 4.5 Cyclic voltammograms under catalytic conditions of 1mM [Rh(bpy)(Cp)Cl]Cl in 0.5 M [TBA][PF_6] acetonitrile solution on an IL-modified GCE (electrodeposited IL layer by CPE for 10 s at -3.95 V) using different concentrations of [EMIM][PF_6] in acetonitrile: 0.01 M (black plot), 0.1 M (blue plot), 0.5 M (red plot) and 1 M (green plot) and CV on a bare GCE (purple plot). Catalytic conditions: acetonitrile solution under CO_2 with 5 % H_2O (vol.). Scan rate 0.01 V/s. WE=GCE.*

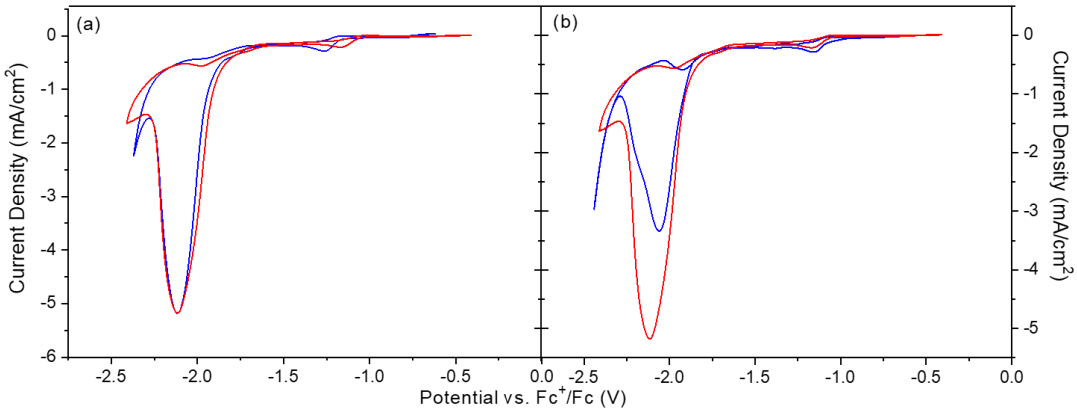

Figure 4.6 Cyclic voltammograms under catalytic conditions of 1mM [Rh(bpy)(Cp)Cl]Cl in 0.5 M [TBA][PF_6] acetonitrile solution on an IL-modified GCE (electrodeposited IL layer by CPE of 10 s at -3.95 V) in: (a) 0.5 M [EMIM][PF_6] acetonitrile solution (red plot) and in 0.5 M of [EMIM][BF_4] acetonitrile solution (blue plot) or (b) 0.5 M [EMIM][PF_6] acetonitrile solution (red plot) and in 0.5 M of [BMIM][PF_6] acetonitrile solution (blue plot). Catalytic conditions: acetonitrile solution under CO_2 with 5 % H_2O (vol.). Scan rate 0.01 V/s. WE=GCE.*

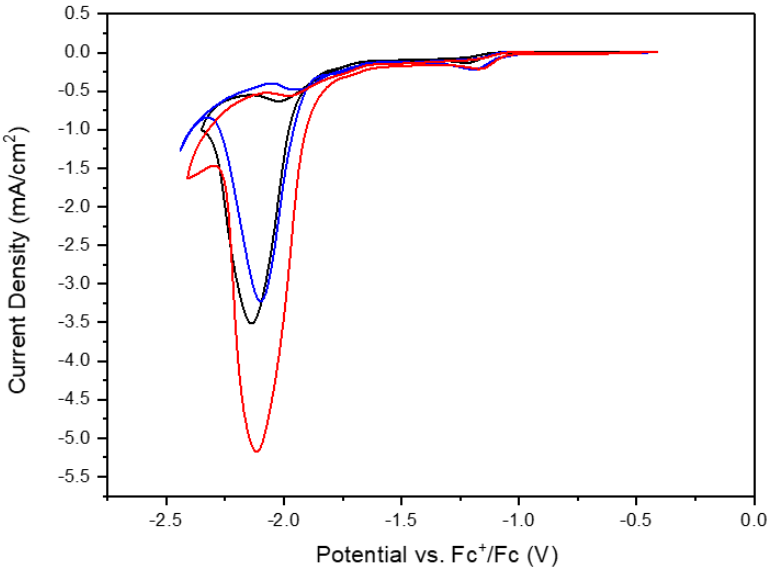

Figure 4.7 Cyclic voltammograms under catalytic conditions of 1mM [Rh(bpy)(Cp)Cl]Cl in 0.5 M [TBA][PF_6] acetonitrile solution on an IL-modified GCE (electrodeposited IL layer by CPE of 10 s at -3.95 V in 0.5 M [EMIM][PF_6] acetonitrile solution) : Under Argon (red plot) and under CO_2 (blue plot). CV of bare GCE (black plot). Catalytic conditions: acetonitrile solution under CO_2 with 5 % H_2O (vol.). Scan rate 0.01 V/s. WE=GCE.*

The reduction and electrodeposition of imidazolium-based ILs is also possible in aqueous solutions, as can be seen in Figure 4.8. In this case, a GCE was modified by CV until -2.5 V *vs.* Ag/AgCl/KClsat in an aqueous solution containing 0.5 M [EMIM][BF_4] as supporting electrolyte under an inert atmosphere, since salts containing $[PF_6]^-$ anion are not soluble in water. The CV limit chosen was less cathodic in these conditions, since beyond that point H_2 bubbles were evident on the electrode surface. Subsequently, this GCE was removed from that solution, rinsed and its catalytic activity for CO_2RR was evaluated in a new acetonitrile solution of complex [2] (black plot in Figure 4.9). In addition to this, we also explored the catalytic effects on CO_2RR of immobilizing ILs following a different synthetic route already described in the literature[20], which gives as a result the formation of a covalently grafted IL layer on the electrode. Basically, this synthetic route follows two steps: firstly, the electrochemical grafting of 2-bromoethylamine to the electrode surface by oxidation, which leads to the attachment of a layer bearing a Br end group and an amine grafted to the electrode. Thus, a second step based on the chemical reaction between the Br terminated layer and the 1-ethylimidazole in acetonitrile solution. The result is a layer bearing imidazolium-based IL moiety attached on the electrode surface. The catalytic effect for CO_2RR of this covalent layer was never explored before with molecular catalysts. Therefore, in Figure 4.9, the effect of both electrodeposited $[EMIM]^+$ layer in aqueous solution and covalent $[EMIM]^+$ layer was evaluated under CO_2 catalytic conditions of complex [2]. We can observe that the onset catalytic

potential is unaltered regardless of the solvent in which the electrodeposition took place, as well as being nearly identical to the one belonging to the covalent IL layer. However, in the case of the covalent layer, the maximum current density observed is larger than the electrodeposited layer.

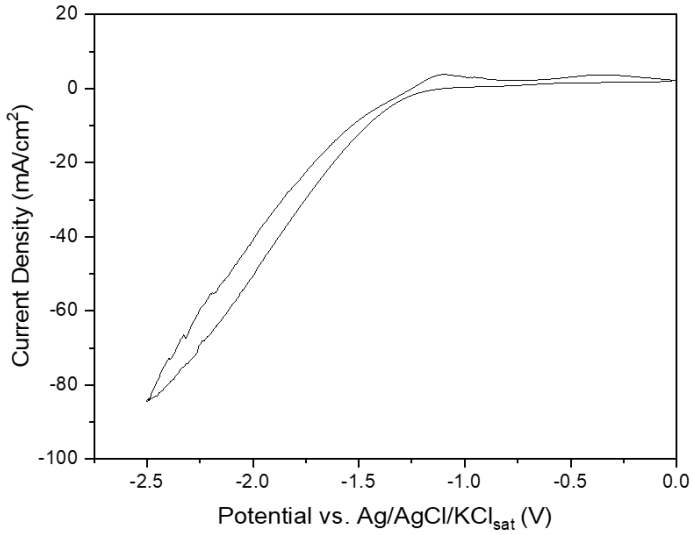

Figure 4.8 Cyclic voltammogram of 0.5 M [EMIM][BF_4] aqueous solution under argon. Scan rate 0.1 V/s. WE= GCE.

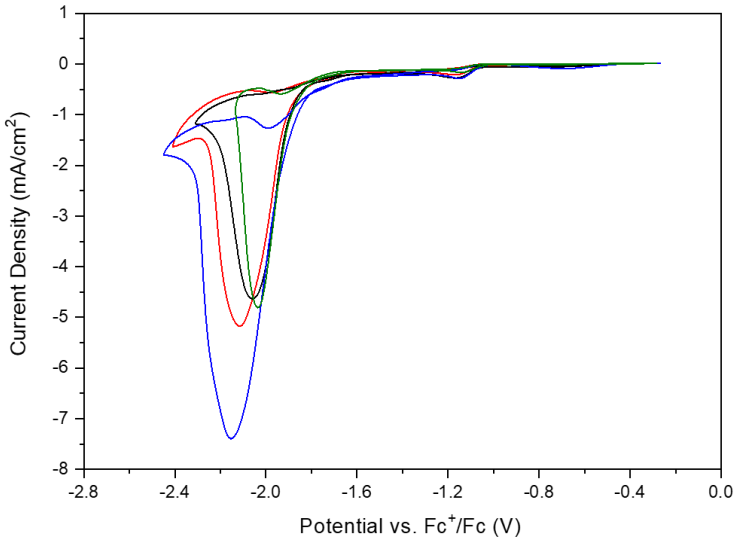

Figure 4.9 Cyclic voltammograms under catalytic conditions of 1 mM [Rh(bpy)(Cp)Cl]Cl in 0.5 M [TBA][PF_6] acetonitrile solution on: an IL-modified CGE (electrodeposited IL layer by CPE of 10 s at -3.95 V in 0.5 M [EMIM][PF_6] acetonitrile solution (red plot), an IL-modified GCE (electrodeposited IL layer grown by CPE of 10 s at -2.50 V vs. Ag/AgCl/KClsat in 0.5 M [EMIM][BF_4] aqueous solution) (black plot) and an IL-modified GCE by a covalent grafting of IL layer as described in the literature[20] (blue plot). Also, CV of bare GCE in a solution containing 0.5 M [EMIM][PF_6] in acetonitrile as supporting electrolyte (green plot). Catalytic conditions: under CO_2 with 5 % H_2O (vol.). Scan rate 0.01 V/s. WE=GCE.*

4.2.2 Electrodeposited IL Layer testing in different solvents

We subsequently explored the effects of the aforementioned optimized electrodeposited IL layer in the CO_2RR catalytic behavior of complex [2] using different solvents, always exploiting complex [2]'s solubility in both organic and aqueous media. In Figure 4.10 we explore a 50/50 % (vol.) acetonitrile/water mixture. We compared the catalytic response on a bare GCE without any IL in solution (black plot), a bare electrode in solution containing IL as supporting electrolyte (green plot), the electrodeposited IL layer (red plot) and the covalent IL layer (blue plot) under the same catalytic conditions. We first remarked that in terms of onset potential both IL layers closely resemble each other, as well as the IL in solution, being all three less cathodic than the control conditions (bare WE without IL). In terms of the current density observed however, both IL-modified electrodes produced a larger catalytic density, which was similar than in acetonitrile/water 95/5 % (vol.), than the bare GCE whether or not IL is present in solution.

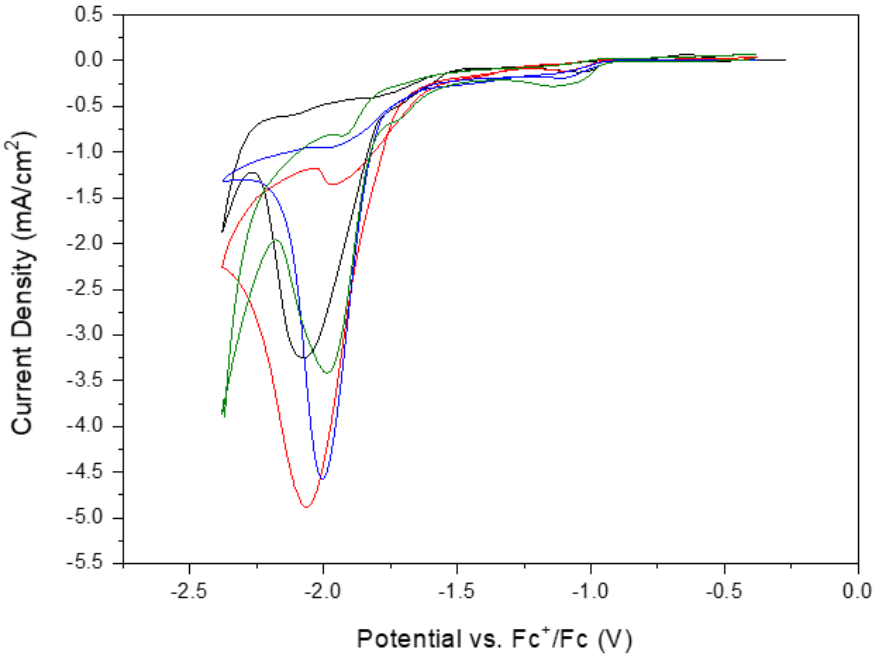

Figure 4.10 Cyclic voltammograms under catalytic conditions of 1mM [Rh(bpy)(Cp)Cl]Cl in acetonitrile/water mixture solution on: a bare GCE in 0.5 M [TBA][BF_4] solution (black plot), a bare GCE in 0.5 M [EMIM][BF_4] solution (green plot), an IL-modified GCE with an electrodeposited layer (CPE of 10 s at -3.95 V in 0.5 M [EMIM][PF_6] in acetonitrile solution) in 0.5 M [TBA][BF_4] solution (red plot) and an IL-modified GCE with a covalent [EMIM]$^+$ layer in 0.5 M [TBA][BF_4] solution (blue plot). Catalytic conditions: acetonitrile/water 50/50 % (vol.) solution under CO_2. Scan rate 0.01 V/s. WE=GCE.*

Next, the catalytic effect of the electrodeposited layer using complex [2] as a model system was explored in purely aqueous conditions, with either [TBA][BF_4] or [EMIM][BF_4] as the supporting electrolyte. In Figure 4.11 (a) are presented the catalytic CVs in a 0.1 M [TBA][BF_4] aqueous solution of 1 mM complex [2] on either a bare GCE (black plot) or an IL-modified GCE by an electrodeposited layer (red plot). Firstly, we observe that the passage from an acetonitrile/H_2O 95/5 % (vol.) to an aqueous solution entails a significant decrease in current density. This is consistent with the decrease in CO_2 solubility from 240 mM to 33 mM[13,15,24]. Aside from this effect however, the addition of an electrodeposited IL layer on the GCE surface leads to both a decrease in the catalytic onset potential and a modest increase in terms of current density in regards to the bare electrode. In Figure 4.11 (b) though, where 0.5 M [EMIM][BF_4] is present as the supporting electrolyte, the effect of an additional electrodeposited IL layer on the catalytic activity seems to be insignificant from a CV point of view.

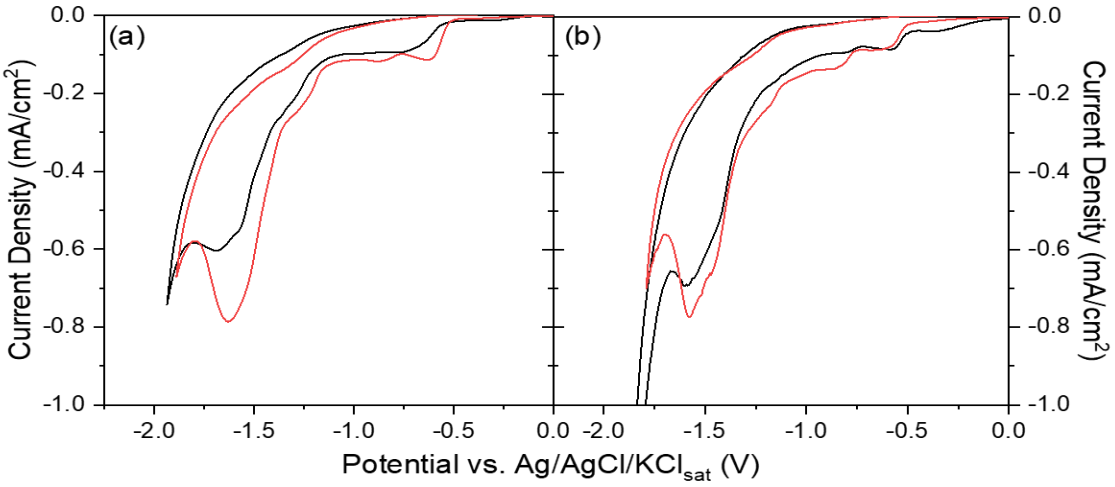

Figure 4.11 Cyclic voltammograms under catalytic conditions of 1mM [Rh(bpy)(Cp)Cl]Cl in unbuffered aqueous solution under CO_2 atmosphere on a bare GCE (black plot) or IL-modified GCE by an electrodeposited IL layer (CPE of 10 s at -3.95 V vs. Fc^+/Fc in 0.5 M [EMIM][PF_6] acetonitrile solution) (red plot) in (a) 0.1 M [TBA][BF_4] and (b) 0.5 M [EMIM][BF_4]. Scan rate 0.01 V/s. WE=GCE.*

4.2.3 Electrodeposited IL layer impact on CO_2RR catalyzed by [$Re(CO)_3$(bpy)Cl] in acetonitrile

Even though the main work on layer optimization was done using complex [2] as shown above, complex [1] was also tested with the electrodeposited layer to demonstrate whether such a surface modification strategy could produce an effect with other molecular catalysts. For this reason, in Figure 4.12 we compare the effect of an IL electrodeposited layer on the CO_2 catalytic activity of 1 mM complex [1] in acetonitrile solution, with 0.5 M of the same IL in solution and the control conditions (bare GCE, no IL either in solution nor immobilized). This figure shows the CVs under argon (Figure 4.12 (a)), under CO_2 (Figure 4.12 (b)) and finally upon explicit addition of 1.5 M TFE as a proton source (Figure 4.12 (c)).

We can observe that the electrodeposited IL layer produced an enhanced catalytic effect by decreasing the overpotential compared to control conditions with this molecular catalyst as well. Under inert conditions the reduction waves of complex [1] shift to less cathodic potentials when an electrodeposited IL layer is present, however the effect is not as prominent as with the same IL in solution on a bare electrode. Under CO_2 the bpy-centered initial wave is superposable for both ILs, in solution and electrodeposited layer, even if the second Re-centered reduction wave is significantly lower in terms of current density for the electrodeposited IL layer than for the IL in solution. Finally, in the presence of the external proton source the onset potential for immobilized IL and IL in solution is essentially identical.

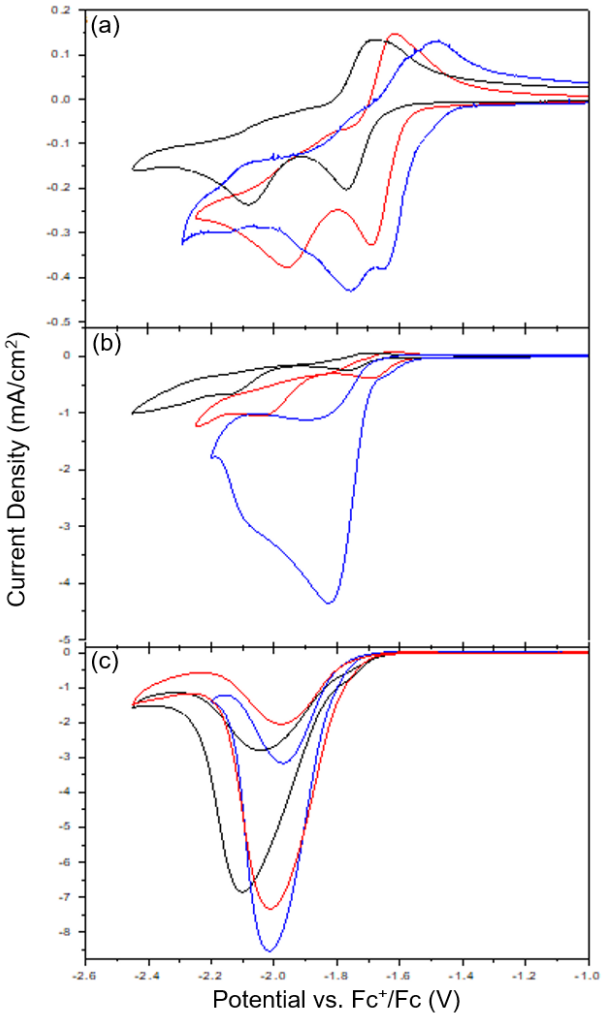

Figure 4.12 Cyclic voltammograms of 1mM [Re(CO)$_3$bpyCl] in a 0.5 M [TBA][PF$_6$] acetonitrile solution on a bare GCE (black plot), in a 0.5 M [EMIM][PF$_6$] acetonitrile solution on a bare GCE (blue plot) and in a 0.5 M [TBA][PF$_6$] acetonitrile solution on an IL-modified GCE with an electrodeposited layer (CPE of 10 s at -3.95 V in 0.5 M [EMIM][PF$_6$] in acetonitrile solution) (red plot): (a) under Argon, (b) under CO_2 and (c) under CO_2 with 1.5 M TFE. . Scan rate 0.1 V/s.

4.2.4 IL layer characterization. Surface coverage evaluation, XPS analysis and CVs with redox probes

In Figure 4.13 (black plot) we see the cyclic voltammogram of the electrodeposited layer once removed from the solution where it was immobilized, rinsed with acetonitrile and placed in a different acetonitrile solution containing only the benchmark electrolyte [TBA][PF_6] under inert atmosphere. This characterization CV starts from open circuit potential towards oxidation and interestingly we remark an oxidation wave around -0.7 V, which resembles the reoxidation wave also observed during the CV for IL layer formation (Figure 4.1). It should also be mentioned that this wave is only present in the first CV cycle after IL layer formation (black plot) and it is not visible in subsequent consecutive cycles (blue plot). In addition to this, Figure 4.13 (black plot) shows an additional oxidation wave at approximatively 1.18 V, which is in agreement with imidazole electrochemical oxidation reported in the literature. Moreover, we compared by CV the electrodeposited IL layer (Figure 4.13), the covalently grafted IL layer (Figure 4.14 (a)) and a bare GCE with ethylimidazole in solution (Figure 4.14 (b)). In all three CVs there is a reduction wave at -2.8 V and an oxidation wave at 1.2 V, which correspond to imidazolium/imidazole redox processes.

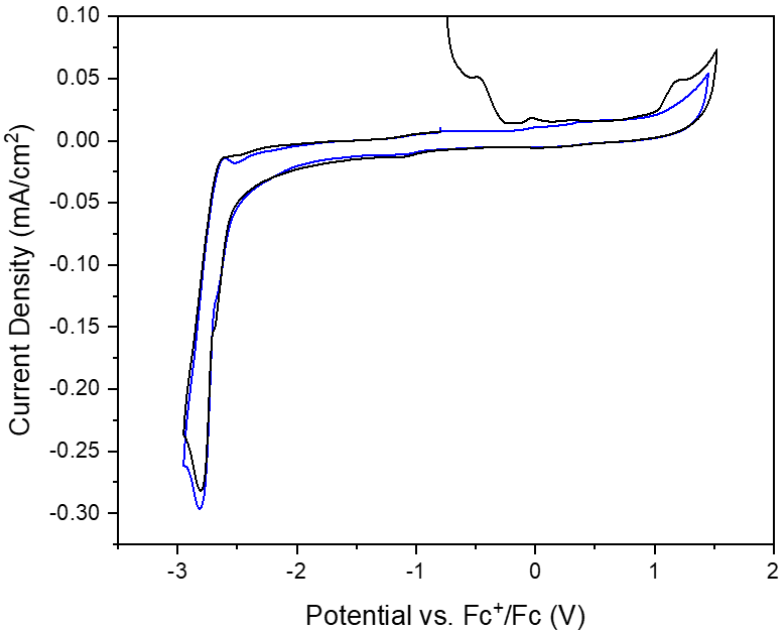

Figure 4.13 Cyclic voltammograms of an IL-modified GCE by an electrodeposited layer (CPE of 10 s at -3.95 V in 0.5 M of [EMIM][PF_6] in acetonitrile under argon) tested in a 0.5 M [TBA][PF_6] acetonitrile solution under Ar. First cycle (black plot) and second cycle (blue plot). Scan rate 0.01 V/s. WE= GCE.

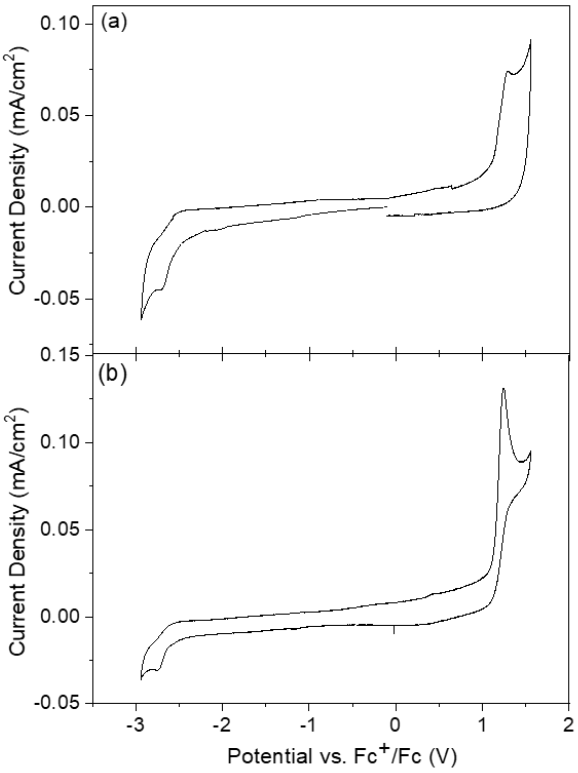

Figure 4.14 CVs in 0.5M [TBA][PF$_6$] acetonitrile solution under Ar of: (a) an IL-modified GCE by a covalent IL layer formed as previously described in the litterature[20] and (b) a bare GCE in solution containing 1mM 1-Ethylimidazole. Scan rate 0.01 V/s. WE= GCE.

We have already demonstrated in Figure 4.1 the formation by CV of an IL electrodeposited layer on different electrode materials, in particular GCE and AuE. The imidazolium reduction, as well as the reoxidation wave potentials were shifted to different values based on the electrode material used, as has already been reported in the literature[21,22]. In order to evaluate the IL surface coverage (Γ) achieved on the electrode surface by IL layer electrodeposition, we used the integration of the oxidation wave shown in the reverse CV scan after electrodeposition. This oxidation wave is centered at -0.7 V on GCE and -0.4 V *vs.* Fc^+/Fc on AuE. As we can observe in Figure 4.15 (a), applying more cathodic potential limits during IL electrodeposition provoked an increase in the maximum current displayed by the oxidation wave in the reverse scan and thus, higher IL surface coverage was achieved. However, by keeping the maximum current density of imidazolium reduction constant at almost 50 mA/cm^2, we established a proper comparison between those two electrode materials, which reached very similar surface coverage values for both electrodes, namely 1.3 10^{-7} mol/cm^2 and 1.4 10^{-7} mol/cm^2 for the AuE and GCE electrodes, respectively. This demonstrated that the electrodeposited layer was independent of the chemical nature of the electrode surface where it was deposited and did not follow an epitaxial growth. The electrodeposited IL layer used in most of the catalytic studies reported in this chapter was achieved by CV up to -3.95 V *vs.* Fc^+/Fc on either flat GCE or RVC foam electrodes. In particular, the IL surface

coverage determined for the flat GCE case was 2.3 10^{-7} mol/cm^2 (Figure 4.15 (b)), which is significantly larger than the usual surface coverage reached by heterogenized molecular catalysts in high surface area materials such as multi-walled carbon nanotubes (MWCNTs)[25], using a much smaller electroactive surface area in this case.

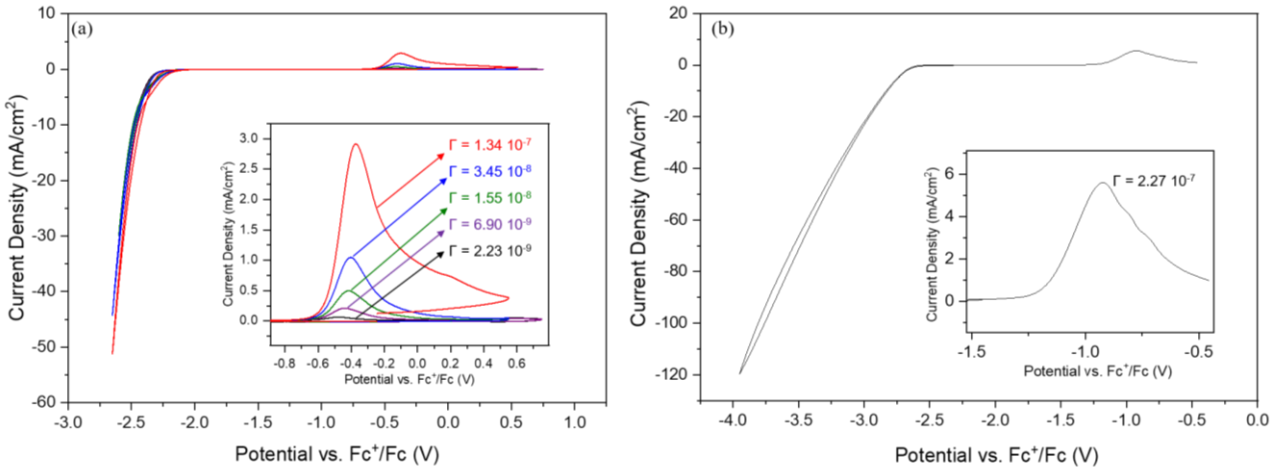

Figure 4.15 (a) Cyclic voltammograms of the electroreduction of 0.5 M [EMIM][PF_6] solution in acetonitrile on a 3 mm AuE in different potential windows under Ar. Inlet zoom on the resulting reoxidation peaks with their corresponding surface coverage values and (b) Cyclic voltammogram up to -3.95 V vs. Fc^+/Fc of the electroreduction of 0.5 M [EMIM][PF_6] solution in acetonitrile on a 3 mm GCE under Ar. Inlet zoom on the resulting reoxidation peak and its surface coverage value. Scan rate of 0.1 V/s.

The physicochemical characterization of the IL layer was done by X-ray photoelectron spectroscopy (XPS). In order to obtain clear spectral signature analysis of the IL layer, gold was selected as a more proper substrate electrode material than GCE. Given the similarities in CV redox features (Figure 4.1) and IL surface coverage, we considered gold to be a well-adapted model to perform XPS analysis on. For this purpose, three gold plates were prepared and sent for analysis, two with electrodeposited IL layers grown in an acetonitrile or aqueous environment and one with a covalent grafted IL layer. The survey XPS spectra shown in Figure 4.16 confirm the coexistence of C, O and N elements in all the samples. The XPS spectra of C(1s) (Figure 4.16 (a), (b) and (c)) present five main contributions at binding energies of 284.7, 285.6, 286.6, 287.4 and 288.5 eV. The second (285.6 eV) and third (286.6 eV) of these contributions correspond to amide and aromatic C-N bands, respectively, thus corroborating the presence of imidazolium moieties on the electrode surface. Moreover, the same bands are present for all three electrodes, though the intensities of the bands may vary. As far as the attribution of the XPS spectra of N(1s) (Figure 4.16 (d), (e) and (f)) is concerned, we observed three bands at 398.7, 400.1 and 401.7 eV. The first (398.7 eV), second (400.1 eV) and third (401.7 eV) are attributed to a pyridinic N, a

pyrrolic N and a quaternary N, respectively[26–28]. The electrodeposited IL layer grown in aqueous solution (Figures 4.17 (b) and (e)) exhibits a poorer signal to noise ratio than the one grown in acetonitrile (Figures 4.17 (a) and (d)). Overall, the XPS spectra corroborates the presence of a layer containing imidazole moieties immobilized on the electrode surface in all cases.

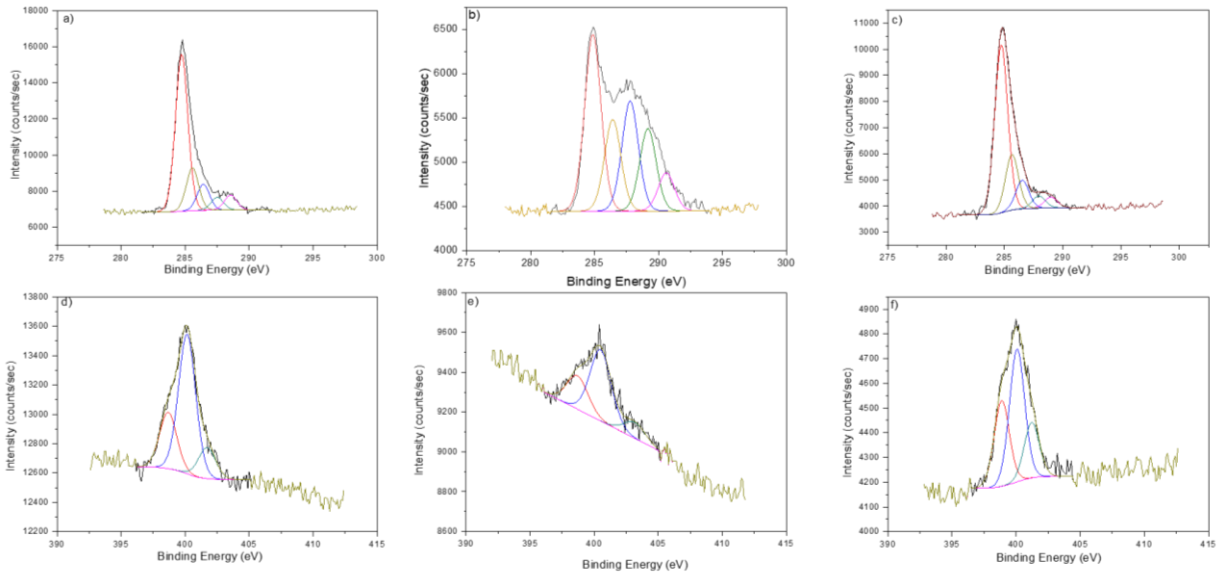

Figure 4.16 XPS high-resolution spectra for C (1s) on (a) IL-modified AuE (CPE of 10 s at -3.95 V vs. Fc^+/Fc in 0.5 M of [EMIM][PF_6] in acetonitrile), (b) IL-modified AuE (CPE of 10 s at -2.5 V vs. Ag/AgCl/KClsat in 0.5 M of [EMIM][BF_4] in water) and (c) covalent grafted IL layer. Bond attributions colored as follows: C-C, C-H (red plot), C-OH, C-O-C, C-N (yellow plot), C=N (blue plot), C=O (green plot) and O-C=O (pink plot). Also XPS high-resolution spectra for N (1s) on (d) IL-modified AuE (CPE of 10 s at -3.95 V vs. Fc^+/Fc in 0.5 M of [EMIM][PF_6] in acetonitrile), (e) IL-modified AuE (CPE of 10 s at -2.5 V vs. Ag/AgCl/KClsat in 0.5 M of [EMIM][BF_4] in water) and (f) covalent IL layer. Bond attributions colored as follows: pyridinic N (red plot), pyrrolic N (blue plot) and quaternary N (green plot).

Two redox probes were tested for reaching a deeper characterization of the electrodeposited IL layer. In particular, dopamine and ferrocene, an inner- and outer-sphere redox probe, respectively. Figure 4.17 (a) shows the electrochemical behaviour of dopamine studied by CV in acidic aqueous solution. Dopamine presents a reversible redox signal and follows an inner-sphere mechanism. As a consequence the presence of any immobilized species on the electrode surface provokes an increase in the redox peak-to-peak separation. This is indeed what we observed when comparing the bare GCE (peak-to-peak separation value of 0.08 V) and the electrodeposited IL-modified GCE (0.2 V). In addition to this, the covalent IL layer (blue plot) trumps the electrodeposited one (red plot) in terms of peak-to-peak separation by exhibiting a value of 0.32 V, that may be indicative of a more efficient immobilization. Figure 4.17 (b) compares the electrochemical behaviour of ferrocene on bare GCE and on the

electrodeposited IL-modified GCE in acetonitrile solution. Ferrocene follows an outer-sphere redox mechanism. As a consequence, regardless of the presence of immobilized species on the electrode surface, both its $E_{1/2}$ potential and the peak-to-peak separation remain unaltered, as is evidenced in Figure 4.17 (b).

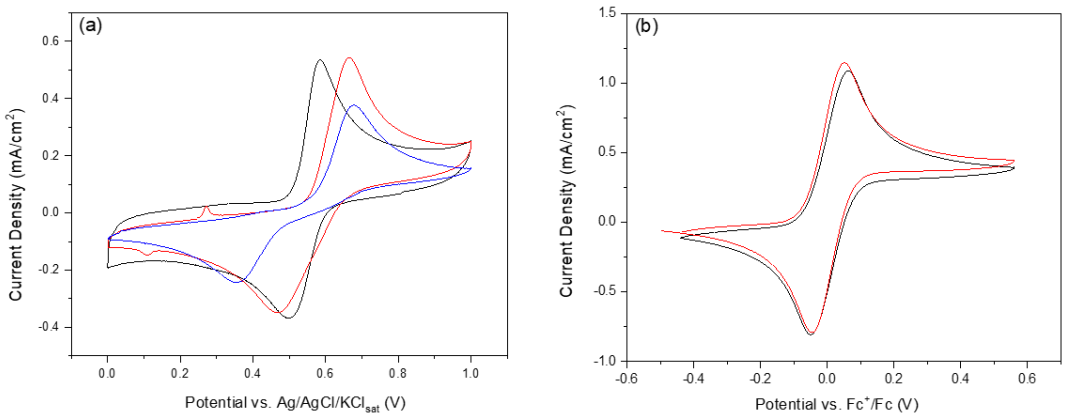

Figure 4.17 Cyclic voltammograms of : (a) 1 mM dopamine hydrochloride in a 0.1 M H_2SO_4 aqueous solution under Ar on a bare GCE (black plot), on an IL-modified GCE by an electrodeposited layer (CPE of 10 s at -3.95 V vs. Fc^+/Fc in 0.5 M [EMIM][PF_6] acetonitrile solution) (red plot) and on an IL-modified GCE by a covalent IL layer formed as previously described in the literatire[20] (blue plot) and (b) 5 mM ferrocene in a 0.1 M [TBA][PF_6] acetonitrile solution under Ar on a bare GCE (black plot) and on an IL-modified GCE by an electrodeposited layer (CPE of 10 s at -3.95 V vs. Fc^+/Fc in 0.5 M [EMIM][PF_6] acetonitrile solution) (red plot). Scan rate 0.1 V/s.

4.2.5 Electrodeposited IL layer impact on HER catalyzed by [Rh(bpy)(Cp*)Cl]Cl

Complex [2] exhibits the same catalytic features by CV in the presence of the electrodeposited imidazolium layer at the electrode surface than upon the presence of imidazolium-based ILs in solution, as has been shown in Figure 4.2. Thus, according to the experimental data and DFT calculations already presented in Chapter 3, we must not exclude that the electrodeposited IL layer remains positively charged, since it mimics the impact of imidazolium cations in the electrical double layer. Thus, our next goal was to understand the nature of the electrodeposited IL layer whether it was positively charged or resulted in a neutral molecular layer. To investigate that we used a positively charged inner-sphere redox probe whose electrochemical response would be able to distinguish between the presence (repulsion electrostatic effects) and absence (no repulsion electrostatic effects) of a positively charged layer on the electrode surface. For this purpose, HER was selected, since we could perform it with different added proton sources (trifluoroethanol (TFE), acetic acid (AcOH)) and it is also a reaction that complex [2] successfully catalyzes.

Figure 4.18 shows the electrodeposited IL layer, the covalent grafted IL layer and a control bare GCE tested under HER conditions in the absence of complex [2], more particularly in an acetonitrile solution under inert atmosphere containing a lower (0.01 M) and a higher (0.1 – 0.5 M) quantity of two different proton sources, TFE or AcOH. These two proton sources vary in acidity, TFE (pKa = 35.4) and AcOH (pKa = 23.5) in acetonitrile[29]. In Figure 4.18 (a) and (b) we see the effect of both proton sources. Even at the lowest concentration it is evident that the presence of an IL layer on the electrode surface suppresses HER activity compared to the control bare electrode by causing a more cathodic onset potential and a smaller maximum current density. However, this effect is much more marked at 0.5 M TFE (Figure 4.18 (b)), where both layers elicit a catalytic response at least five times lower than the bare electrode. In the presence of AcOH (Figures 4.19 (c) and (d)) as well, both layers were less efficient for HER than the bare electrode, but especially in the 0.1 M AcOH solution we observed that HER suppression was superior using the covalent grafted IL layer.

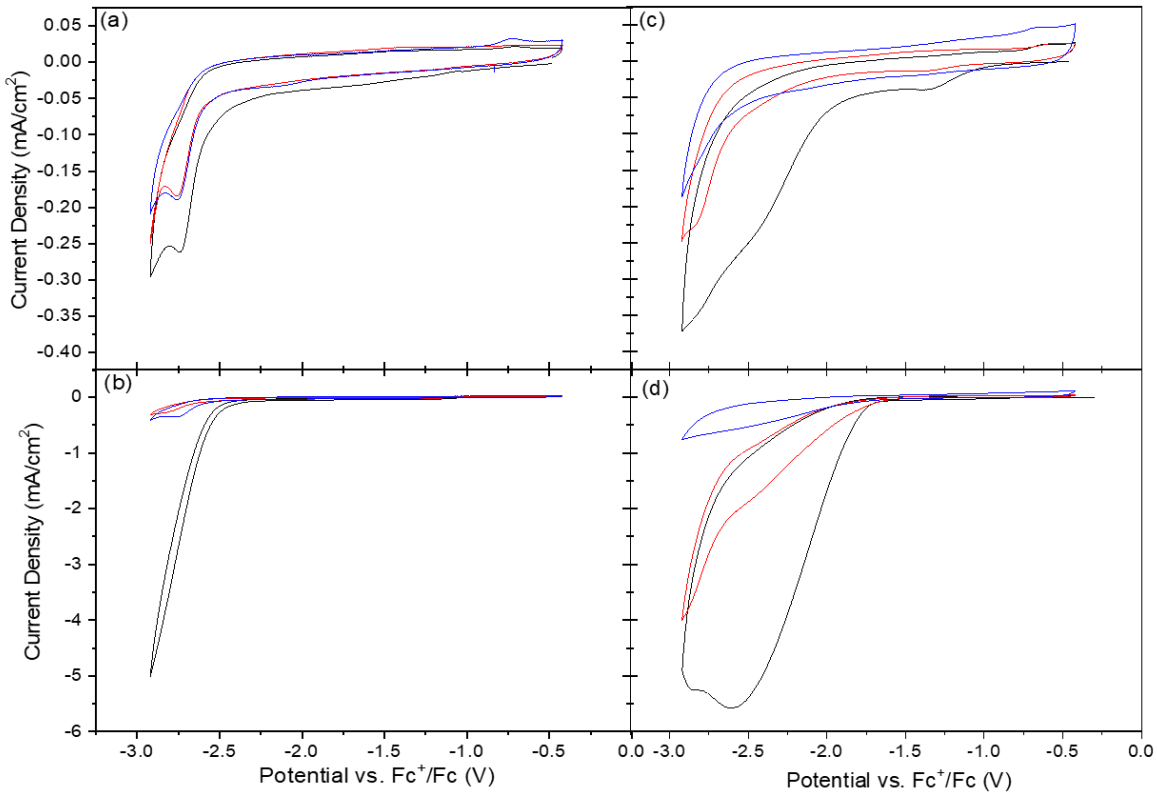

Figure 4.18 Cyclic voltammograms of an acetonitrile solution with 0.5 M of [TBA][PF$_6$] under Argon containing (a) 0.01 M TFE, (b) 0.5 M TFE, (c) 0.01 M AcOH or (d) 0.1 M AcOH for the following conditions: on a bare GCE (black plot), on an IL-modified GCE by an electrodeposited layer (CPE of 10 s at -3.95 V vs. Fc$^+$/Fc in 0.5 M [EMIM][PF$_6$] acetonitrile solution) (red plot) and on an IL-modified GCE by a covalent IL layer formed as previously described in the literature[20] (blue plot). Scan rate 0.1 V/s.

The next step was to test the electrodeposited IL layer alongside complex [2] for HER. For this purpose, 0.1 M of acetic acid was selected as the proton source. The catalytic behavior of complex [2] for HER was evaluated with and without the electrodeposited IL layer in Figure 4.19 (a) in 100 % acetonitrile solution and 50/50 % (vol.) acetonitrile/water solution, Figure 4.19 (b). In Figure 4.19 (a) we can see a clear suppression on HER activity by comparing the catalytic response of a bare GCE (black plot) and the one produced by a GCE with an electrodeposited IL layer (red plot). Furthermore, we can still observe the characteristic reduction waves associated with the formation of the active form of complex [2]. In contrast in Figure 4.19 (b) in the acetonitrile/water 50/50 % (vol.) mixture, we only observe a well-defined reduction wave for the first Rh-centered reduction process. Nevertheless, the catalytic HER response is visibly hindered in the presence of the electrodeposited IL layer (red plot).

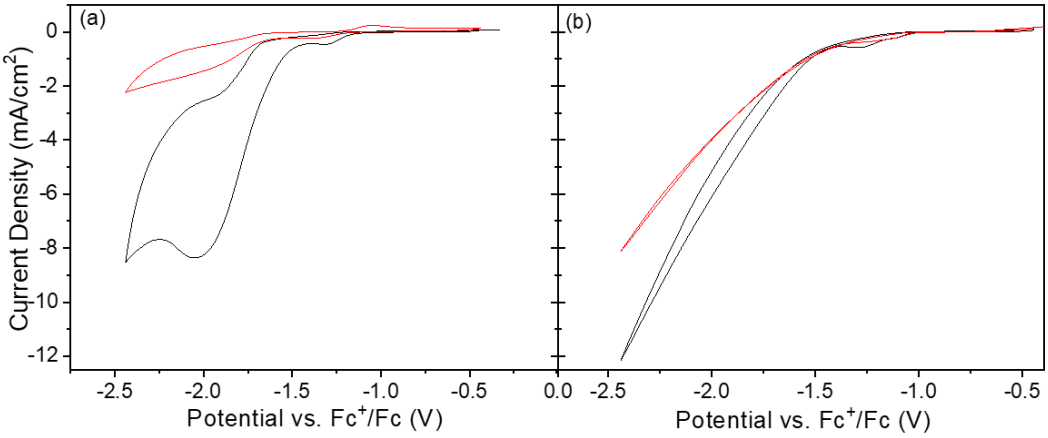

Figure 4.19 Cyclic voltammograms of a bare GCE (black plot) and an IL-modified GCE by an electrodeposited layer (CPE of 10 s at -3.95 V vs. Fc^+/Fc in 0.5 M [EMIM][PF_6] acetonitrile solution) (red plot) under an argon atmosphere in an electrolyte system containing 1 mM complex [2] and 0.1 M AcOH that is: (a) acetonitrile solution with 0.1 M of [TBA][PF_6] or (b) acetonitrile/water 50/50 % (vol.) solution with 0.1 M of [TBA][BF_4]. Scan rate 0.1 V/s.

4.2.6 Electrolysis for CO_2 reduction with immobilized ILs and catalyzed by [Rh(bpy)(Cp*)Cl]Cl. Impact in reaction selectivity

The effect of the electrodeposited IL layer on product distribution and energy efficiency for CO_2RR was studied by CCE electrolysis in an H-type cell at -3.33 mA/cm^2 of applied current density firstly in acetonitrile/H_2O 95/5 % (vol.) solutions. The results of these electrolysis were compared to those already reported in Chapter 3 on bare electrodes with and without ILs in solution. In all experiments, the only liquid product detected was formate and only H_2 was detected in the gas phase. Table 4.1 shows the

average cathode potential during electrolysis, overpotential, faradic efficiencies for both products and energy efficiency for CO_2 conversion to formate as a function of the presence or absence of different IL layers. In Figure 4.20 are represented the plots of electrolysis time *vs.* cathode potential (corresponding to Table 4.1, entries 1-4), as well as the thermodynamic potential for CO_2 reduction to formate, which for those conditions has been calculated at -1.32 V *vs.* Fc^+/Fc[30]. We observe that the presence of either an electrodeposited or a covalent grafted IL layer led to a reduction in overpotential very similar to the one displayed by a bare electrode with imidazolium-based IL in solution already reported in Chapter 3 (Table 3.8). This overpotential diminution is in the range of 800 mV. In addition to this, the formate production, already enhanced from 53 % (entry 1), to 69 % (entry 2) by the presence of $[EMIM]^+$ instead of $[TBA]^+$ in solution, is further enhanced by an additional (12-16) % in the presence of either electrodeposited (entry 3) or covalent (entry 4) IL layer and $[TBA]^+$ in solution. This increase in product selectivity for formate in the presence of the IL layers is also reflected on the energy efficiency values, which reached 59 % as a maximum value reported in this thesis in acetonitrile solution at -3.33 mA/cm^2 obtained either by electrolyte engineering or electrode surface engineering strategies. Finally, by increasing the % of H_2O present in solution to 50 % (entries 5 and 6 of Table 4.1), the beneficial effect of the electrodeposited IL layer was still evidenced and resulted in a product ratio (FE_{HCOO}-/FE_{H2}) enhancement of more than double from 1.5/1 on the bare electrode (entry 5) to 3.75/1 on the IL-modified GCE (entry 6).

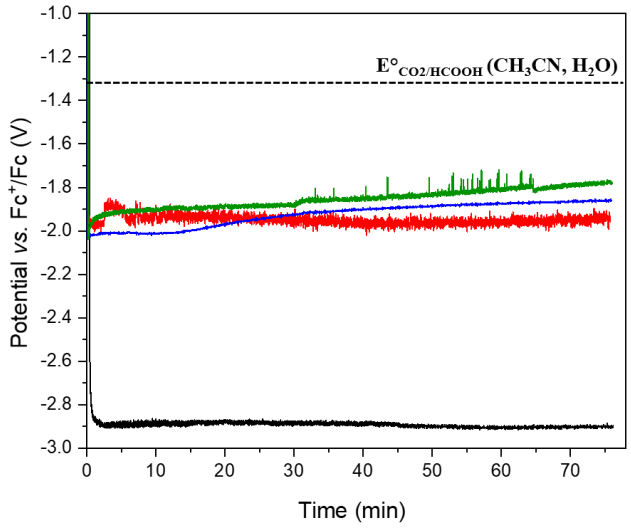

Figure 4.20 Constant current electrolysis (CCE) at -3.33 mA/cm^2 of 1 mM complex [2] in acetonitrile solution under CO_2 in presence of 5 % (vol.) H_2O on: a bare GCE in 0.5 M $[TBA][PF_6]$ (black plot), a bare GCE in 0.5 M $[EMIM][PF_6]$ (red plot), an IL-modified GCE by an electrodeposited layer (CPE of 10 s at -3.95 V vs. Fc^+/Fc in 0.5 M $[EMIM][PF_6]$ acetonitrile solution) in 0.5 M $[TBA][PF_6]$ (blue plot) and on an IL-modified GCE by a covalent grafted IL layer formed as previously described in the literature[20] *in 0.5 M $[TBA][PF_6]$ (green plot). Stirring rate: 400 rpm.*

Table 4.1 Constant current electrolysis for CO_2RR at an applied current density of 3.33 mA/cm^2 in acetonitrile using different % of H_2O as proton source in an electrochemical two compartments H-type cell. Total electrolysis duration to circulate 15 C. Electrodeposited layer on GCE electrode by CPE of 10 s at -3.95 V vs. Fc^+/Fc in 0.5 M [EMIM][PF_6] acetonitrile solution and covalent grafted IL layer on GCE according to the protocol as previously described in the literature[20].

Entry	IL layer	Solvent	Electrolyte	%H_2O (vol.)	Electrolysis applied current density (mA/cm^2)	Electrolysis E_{cat} average (V) vs. Fc^+/Fc	η (V)[a]	FE_{HCOO^-} (%)[b]	FE_{H2} (%)[b]	Energy efficiency (%)[c]
1	None	CH_3CN	[TBA][PF_6]	5	-3.33	-2.81	1.49	53	34	25
2	None	CH_3CN	[EMIM][PF_6]	5	-3.33	-1.95	0.63	69	22	47
3	Electrodeposited	CH_3CN	[TBA][PF_6]	5	-3.33	-1.90	0.58	85	15	59
4	Covalent	CH_3CN	[TBA][PF_6]	5	-3.33	-1.85	0.53	81	12	58
5	None	CH_3CN	[TBA][PF_6]	50	-3.33	-2.60	1.28	47	31	24
6	Electrodeposited	CH_3CN	[TBA][PF_6]	50	-3.33	-2.10	0.78	75	20	47

[a]Determined based on $E_{cat/2}$ using $E^0_{CO2/HCOOH}$ (CH_3CN, H_2O) = -1.32 V vs. Fc^+/Fc. [b]Faradaic efficiency for each product (FE_{HCOOH} and FE_{H2}). [c]Energy Efficiency = $E_T/E \cdot FE$, where E_T = $E^o_{CO2/HCOOH}$ (CH_3CN, H_2O) = -1.32 V vs. Fc^+/Fc.

We also performed CCE (applied current density -3.33 mA/cm^2) with complex [2] and either the electrodeposited or covalent IL layer on the electrode in purely aqueous CO_2-saturated solution. These electrolysis results are shown in Table 4.2 and were compared to some of those already reported in Chapter 3 (Table 3.9) on bare electrodes with and without ILs in solution. We tested three different electrolytes: i) 0.1 M [TBA][BF_4] together with 0.1 M AcOH as a proton source (pH = 2.5) (entries 1-3), ii) 0.5 M [EMIM][BF_4] without any additional proton source (entries 4-6) (pH = 3.1) and iii) 0.1 M [TBA][BF_4] together with 0.1 M acetate buffer solution (pH = 3.8) (entries 7-8). All those electrolysis were performed using 3D RVC foam electrodes in order to reach the desired current density of 3.33 mA/cm^2. In Figure 4.21 are depicted the plots of electrolysis time *vs.* cathode potential (corresponding to Table 4.2, entries 1-3 and 8), as well as the thermodynamic potential for CO_2 reduction to formate, which has been calculated at -0.55 V *vs.* Ag/AgCl/KClsat for pH=2.5, -0.58 V *vs.* Ag/AgCl/KClsat for pH=3.1 and -0.62 V *vs.* Ag/AgCl/KClsat for pH=3.8. The cathode potential evolution during electrolysis

displayed in Figure 4.21 was not very different in all 4 cases, which pointed out to that the cathode potential was not limited by the presence or absence of an IL layer on the electrode surface. In contrast, the change in product selectivity was drastic. The products ratio (FE_{HCOO^-}/FE_{H2}) did pass from 0.6/1 on the bare electrode (entry 1) to almost double than that at 1.2/1 (entry 2) and 1/1 (entry 3) on the modified RVC electrodes with electrodeposited and covalent IL layers, respectively. As a consequence, the formate EE increased up to 25 % with an electrodeposited layer (entry 2), 1.5 times higher than the EE on the bare electrode.

At this point, we decided to combine both strategies developed in this thesis for enhancing CO_2RR. On the one hand, electrolyte engineering by selecting 0.5 M [EMIM][BF_4] as unique electrolyte in solution (entry 4) and on the other hand, electrode surface engineering strategy by testing the different IL layers immobilized on the cathode (entries 5 and 6). A decrease of 100 and 200 mV in overpotential compared to the bare RVC cathode was observed for the electrodeposited and covalent layers, respectively (entries 5, 6). However, their overall overpotential was 400-500 mV higher than the one containing 0.1 M AcOH at the same pH value. In addition to this, a significant change in product selectivity was observed. The products ratio (FE_{HCOO^-}/FE_{H2}) did pass from 1.1/1 on the bare electrode (entry 4) to a maximum of 1.7/1 on the electrodeposited IL layer modified electrode (entry 5). Nevertheless, even though the combination of ILs in solution and immobilized at the electrode surface favored formate production over HER in acidic aqueous solution, the resulting EE values were generally lower than those obtained in the presence of a proton source, such as AcOH (entries 2-3). For this reason, we also tested the addition of AcOH in solution by using an acetate buffer solution at pH=3.8 (entries 7 and 8), which was already successfully tested in Chapter 3 upon evaluation of the electrolyte engineering strategy. Thus, entry 8 in Table 4.2 shows the combination of the electrodeposited IL layer with the acetate buffer solution, which reached the lowest cathode potential displayed in Figure 4.21 (red plot) and the highest EE value out of the entire series, at 33 %.

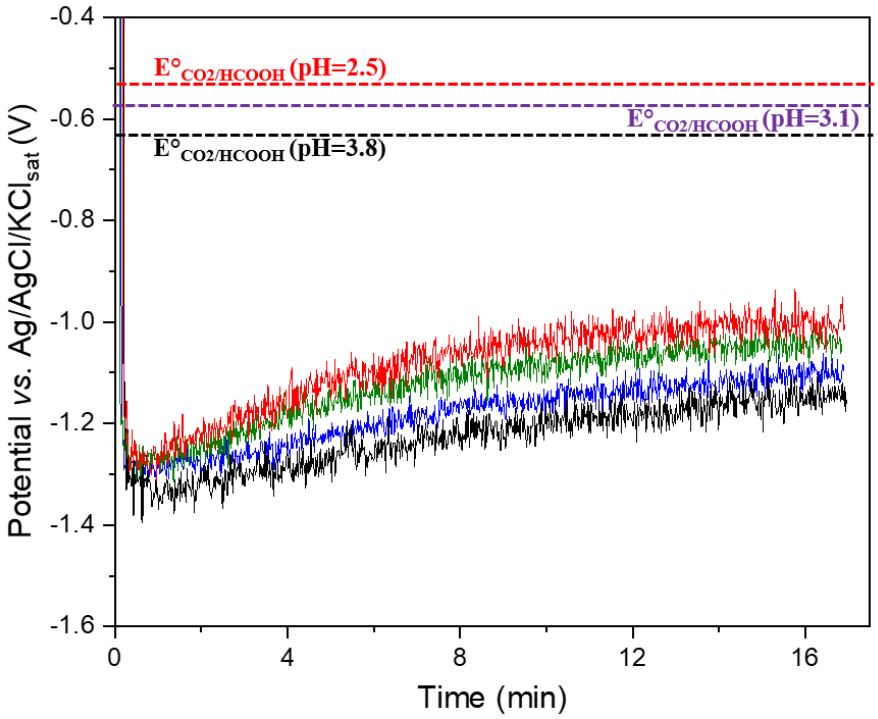

Figure 4.21 Constant current electrolysis (CCE) at -3.33 mA/cm^2 of 1 mM complex [2] in aqueous solution under CO_2 in presence of 0.1 M [TBA][BF_4] and 0.1 M AcOH (pH=3.1) on: a bare RVC (black plot), an IL-modified RVC by an electrodeposited layer (CPE of 10 s at -3.95 V vs. Fc^+/Fc in 0.5 M [EMIM][PF_6] acetonitrile solution) (blue plot), an IL-modified RVC by a covalent grafted IL layer formed as previously in the literature[20] (green plot) and an IL-modified RVC by an electrodeposited layer (CPE of 10 s at -3.95 V vs. Fc^+/Fc in 0.5 M [EMIM][PF_6] acetonitrile solution) in 0.1 M [TBA][BF_4] and 0.1 M acetate buffer (pH=3.8). Stirring rate: 400 rpm.

Table 4.2 Constant current electrolysis for CO_2RR at -3.33 mA/cm^2 in aqueous solution in an electrochemical two compartments H-type cell. Total electrolysis duration to circulate 10 C. Electrodeposited layer on RVC foam electrode by CPE of 10 s at -3.95 V vs. Fc^+/Fc in 0.5 M [EMIM][PF_6] acetonitrile solution and Covalent grafted IL layer on RVC foam electrode according to the protocol as previously described in the literature [20].

Entry	IL layer	Electrolyte	pH_0	pH_f	Electrolysis E_{cat} average (V) vs. Fc^+/Fc	η (V)	FE_{HCOO^-} (%)[a]	FE_{H2} (%)[a]	Energy efficiency (%)
1	None	0.1 M [TBA][BF_4][b] + 0.1 M AcOH	2.5	3.1	-1.20	0.65[c]	38	61	17
2	Electrodeposited	0.1 M [TBA][BF_4][b] + 0.1 M AcOH	2.5	3.1	-1.15	0.60[c]	53	44	25
3	Covalent	0.1 M [TBA][BF_4][b] + 0.1 M AcOH	2.5	3.1	-1.10	0.55[c]	49	46	25
4	None	0.5 M [EMIM][BF_4]	3.1	3.4	-1.60	1.02[d]	49	46	18
5	Electrodeposited	0.5 M [EMIM][BF_4]	3.1	3.4	-1.50	0.92[d]	58	35	22
6	Covalent	0.5 M [EMIM][BF_4]	3.1	3.4	-1.40	0.82[d]	56	39	23
7	None	0.1 M [TBA][BF_4][b] + 0.1 M CH_3COONa/CH_3COOH	3.8	3.8	-1.00	0.38[e]	40	55	25
8	Electrodeposited	0.1 M [TBA][BF_4][b] + 0.1 M CH_3COONa/CH_3COOH	3.8	3.8	-1.00	0.38[e]	53	42	33

[a]Faradaic efficiency for each product (FE_{HCOOH} and FE_{H2}). [b]0.1 M is the maximum solubility of [TBA][BF_4] in aqueous solution. [c]$E^o_{CO2/HCOOH}$ = -0.55 V vs. Ag/AgCl (pH=2.5). [d]$E^o_{CO2/HCOOH}$ = -0.58 V vs. Ag/AgCl (pH=3.1). [e]$E^o_{CO2/HCOOH}$ = -0.62 V vs. Ag/AgCl (pH=3.8).

4.2.7 Electrolysis for CO_2 reduction with immobilized ILs and catalyzed by [Rh(bpy)(Cp*)Cl]Cl. Performance stability evaluation.

The results displayed in Table 4.2 have demonstrated that electrodeposited IL layer on the electrode surface impacted complex [2]'s performance for CO_2RR and in particular, the product selectivity by enhancing formate production. However, all electrolysis described in Table 4.2 lasted for 10 C (~ 17 min). For this reason, some additional longer electrolysis in H-type cell were performed to evaluate the performance stability of the IL-modified cathode before scaling up the process in a flow electrolyzer, which will be described in the next chapter of this thesis (Chapter 5). To assess that, we performed three consecutive CCE electrolysis of different duration (10 C, 40 C and 10 C) keeping the same cathode

(either a bare RVC foam or an IL-modified RVC foam) and using a fresh solution before the first and the third electrolysis (0.1 M [TBA][BF_4] and 0.1 M acetate buffer (pH=3.8)). Moreover, to overcome the limited solubility of CO_2 in aqueous solution we decided to use an open configuration of the H-type cell for electrolysis, meaning that CO_2 was continuously bubbled through the solution during the experiment, even if it rendered H_2 measurements impossible. Figure 4.22 shows that the formate FE values were fairly repeatable when comparing the first and the third electrolysis in both electrodes, but decreased significantly during the second electrolysis. That decrease in performance was attributed to the accumulation of formate in solution after 50 C and for this reason, the solution was substituted by a fresh one before starting the third electrolysis. Then, the IL modified-cathode exhibited FE_{HCOO^-} of 52 % and 53 % in the first (10 C) and the third (10 C) electrolysis, respectively, while the bare electrode produced 41 % and 39 % of formate. Therefore, we consider that a single electrodeposited layer could withstand at least for three consecutive electrolysis and accumulate 60 C without losing any of the benefits it provides in terms of selectivity towards formate production.

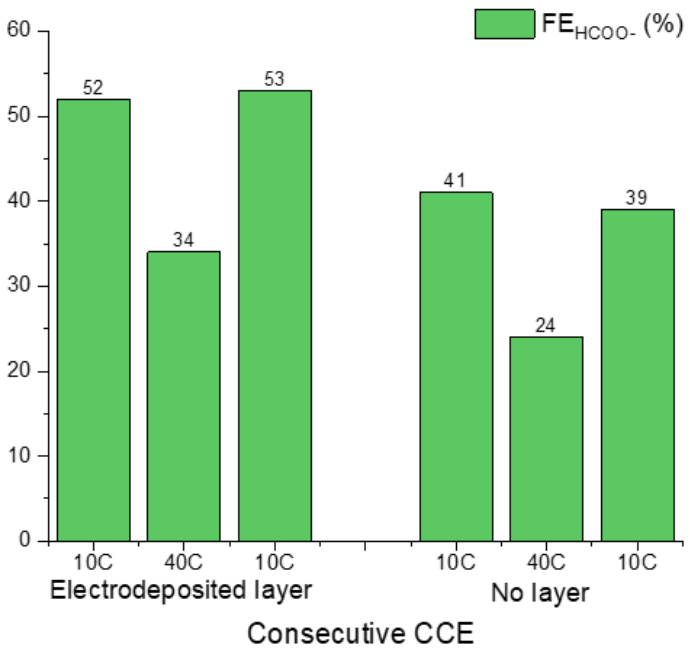

Figure 4.22 Faradaic efficiency for formate production results of three consecutive CCE (for 10, 40 and 10 C respectively) at -3.33 mA/cm^2 of 1 mM complex [2] in aqueous solution in presence of 0.1 M [TBA][BF_4] and 0.1 M acetate buffer solution (pH=3.8). CCE performed in an open H-type cell under constant CO_2 bubbling on an IL-modified RVC electrode by an electrodeposited layer (CPE of 10 s at -3.95 V vs. Fc^+/Fc in 0.5 M [EMIM][PF_6] acetonitrile solution) and on a bare RVC electrode.

4.3 Discussion

Other methods of electrode surface engineering have been previously reported in heterogeneous electrocatalysis using a range of usually small organic molecules with the goal of tuning product selectivity and decreasing energetic barriers for CO_2RR[1–12,31]. ILs themselves have in some cases exhibited the ability to decrease overpotentials and to drive certain systems towards CO_2RR[13–15] by suppressing HER[17], which makes them interesting candidates for surface modification. In particular, the work from T. Agapie group in Caltech (USA)[10–12] has demonstrated the relevant impact in products selectivity achieved by electrodeposition of an IL layer on copper and silver electrodes for CO_2RR. Actually, those authors use a strategy based on electro-dimerization of IL cations, which is very similar to the one presented in this thesis, but using arylpyridinium instead of imidazolium IL cations. However, the role of electrodeposited IL layers has never been addressed before in CO_2 conversion by molecular electrocatalysts. Thus, this fact highlights the originality of the work presented in this thesis.

In this chapter, we present a rapid, in-situ and efficient electrochemical deposition method of imidazolium-based IL cations. This is based on a protocol that relies in imidazolium-based ILs's intrinsic reduction and subsequent reoxidation features and can be performed in both organic and aqueous solutions. This electrodeposited IL layer was tested for CO_2 electroreduction in different electrolytes alongside model molecular catalyst [Rh(bpy)(Cp*)Cl]Cl (complex [2]) and managed to increase catalytic activities. We also demonstrated that this surface modification strategy could produce a positive effect on CO_2RR catalysis with other molecular catalysts such as complex [1]. More pertinent though was its effect in driving complex [2]'s selectivity towards formate versus H_2 evolution. Actually, the electrodeposited IL-modified electrode exhibited a superior electrochemical performance catalyzing CO_2RR by complex [2] than the bare electrode upon presence of the same IL in solution, which seems to indicate that the arrangement of the IL cations layer at the electrode interface is a little bit more efficient than the free cations arrangement at the electrical double layer. Thus, throughout this chapter we have compared the catalytic performance for CO_2RR of the imidazolium based electrodeposited layer with the effect played by the imidazolium-based ILs in solution reported in Chapter 3 and an additional covalently grafted IL layer synthesized from previous reports in the literature. The nature of the electrodeposited IL layer was evaluated by surface coverage evaluation, XPS analysis and CVs in the presence of 3 different redox probes (dopamine, ferrocene and protons).

Firstly, an extensive optimization study of the synthetic parameters to obtain the electrodeposited IL layer was carried out using complex [2] catalytic performance for CO_2RR in acetonitrile solution as evaluation tool. In particular, the production of formate was used as key parameter to select the optimal

synthetic conditions. Two synthetic protocols were established either based on scanning the applied potential by CV or applying a constant potential by CPE. Studies of the cathodic potential limit for the IL layer deposition by CV (Figure 4.3) show that the electrodeposited layer is more efficient the further we scan cathodically and as a consequence the more efficiently imidazolium was reduced. On the contrary, in terms of CPE length, longer times of applied constant potential led to electrodeposited layers with lower catalytic performance (Figure 4.4), pointing towards a certain optimal thickness to promote CO_2RR catalytic activity. The nature of the IL used for synthesizing the IL layer (Figure 4.6) is confirming, what was previously reported in Chapter 3 concerning imidazolium-based ILs in solution; that the role of the IL anion is minor on the catalytic performance of the IL layer, but that the $[EMIM]^+$ cation produces superior catalytic performance than the $[BMIM]^+$ cation, probably due to a more closely packed layer achieved using less sterically impeded $[EMIM]^+$ cations. Finally, the electrodeposition protocol necessitates an inert atmosphere, as it is not efficient under a CO_2 atmosphere (see Figure 4.7). This is probably due to the interaction of reduced imidazolium species with CO_2 molecules to form adducts that are liberated towards the solution and as a consequence cannot be immobilized on the electrode surface.

Subsequently, we studied the optimized electrodeposited IL layer in different electrolyte compositions alongside the covalent IL layer and a bare electrode with IL in its solution. The blatant similarity in terms of catalytic activity of the electrodeposited IL layer with a bare electrode when IL is in solution (see Figure 4.2) and with the covalent IL layer (see Figures 4.9 and 4.10) led us to consider that they may also have some structural similarities. It should be mentioned that in the case of the covalent grafted IL layer we know from the literature data that the attached molecule at the solution side is an imidazolium ring with a positive charge (quaternary N). XPS results further corroborated the hypothesis that both the electrodeposited and the covalent layers are similar in nature, because in both layers the same band attributions were present (Figure 4.16). This led us to infer that some sort of imidazole moiety was bound on the electrode surface. Moreover, the integration of the oxidation wave shown in the reverse CV scan after electrodeposition allowed us to evaluate the surface coverage. In particular, the IL surface coverage determined for the flat GCE case was $2.3\ 10^{-7}$ mol/cm^2. A further confirmation of an electrode surface modification came from the use of the inner-sphere redox probe dopamine, whose peak-to-peak separation was visibly larger for the electrodes with IL layers compared to the bare electrode. This effect was comparatively larger for the covalent grafted IL layer, possibly due to a higher surface coverage due to a higher packing of the less hindered amine grafting to the electrode. Unfortunately, the surface coverage evaluation done for the electrodeposited IL layer on both GCE and AuE (Figure 4.15), was not applicable to the electrodes with a covalent IL layer, since there was no reoxidation peak to measure in that case.

The other interesting point witnessed, was the electrodeposited layer's effect on HER catalyzed by complex [2]. Our working hypothesis in that study was that if the electrodeposited IL layer was positively charged, the approach of protons in close proximity to the cathode would be hampered due to electrical repulsion between two positive charges and this could be represented by either HER onset being shifted to more cathodic potentials, overall current drop or both. On the other hand, considering the electrodeposited IL layer as a neutral molecular layer, no particular difference would be visible in the CVs of HER catalyzed by complex [2] with and without an electrodeposited IL layer. Therefore, the observed HER suppression effect (see Figures 4.18 and 4.19) could be indicative of positive charges present on the coated electrodes' surface that repel protons from the cathode surface. However, this difference observed in aqueous acidic conditions cannot be witnessed in neutral or alkaline media, as the proton source will no longer be protons (H_3O^+), but instead water molecules or hydroxyl anions.

This HER suppression effect demonstrated by the electrodeposited IL layer translates also in terms of product selectivity, increasing formate production compared to control conditions (bare electrode) by +32 %, +28 % and +13 % in 95/5 % (vol.) acetonitrile/water, 50/50 % (vol.) acetonitrile/water and 100 % 0.1 M AcOH aqueous solutions, respectively. Theoretical studies described in section 3.2.8 of Chapter 3 of this thesis also corroborated the suggestion that enhanced selectivity for formate is due to decreased concentration of protons in the electrode's vicinity induced by repulsion from the positively charged layer. This also leads to the highest EE values for complex [2] at -3.33 mA/cm^2 (59 %) with comparison to the previous chapter as well (Chapter 3), demonstration that immobilizing an IL at the electrode surface enhances +12 % in EE for formate production in comparison with adding the same IL in solution (entries 2 and 3 in Table 4.1). The relevant increase in FE_{HCOO^-} between a bare electrode and one with an electrodeposited IL layer in acetonitrile/water 50/50 % (vol.) solution containing [TBA][PF_6] together with a significant decrease in overpotential of approximatively 500 mV, led to an increase in EE of +23 % (entries 5 and 6 of Table 4.1). Finally, in aqueous solution the presence of acetic acid in solution was shown to be vital in order to observe the beneficial effect of the IL layer in terms of formate selectivity, as well as overall overpotential minimization. As a consequence, using both buffered acetic conditions and an electrodeposited IL layer (entry 8 in Table 4.2) we managed to get the best yet EE of complex [2] in acidic aqueous solution, at 33 %. Furthermore, the catalytic performance of this electrodeposited layer was proven to be stable, as it could maintain its FE for formate and even increase its EE over consecutive CCE.

So far, we have not enough evidences to propose an unambiguous structure and composition for the chemical species synthesized by imidazolium-based IL electrodeposition. Nevertheless, supported by previous studies reported in the literature using arylpyridinium[10–12] and imidazolium IL cations[21,22], electrodimerized species are the most likely species formed during the IL cation electroreduction

process. However, we think it is not just a molecular layer, we think those dimeric species undergo spontaneous oxidation at open circuit potential an become positively charged, which is supported by the HER suppressing observed on the IL-modified electrodes only in acidic solution and the almost identical catalytic behavior for CO_2RR catalyzed by complex [2] displayed by imidazolium-ILs in solution and immobilized on the electrode surface.

.

4.4 Conclusion

In conclusion, in the present chapter we have presented a method to synthesize an IL layer based on electrodeposition, applicable to at least two different electrode material surfaces (GCE and AuE). It was also shown that this in-situ, simple and electrochemically induced layer deposition protocol can be performed in either acetonitrile or aqueous solutions. A schematic representation of this electrodeposited layer and its catalytic role are shown in Scheme 4.1. The formation of a layer at the electrode surface containing immobilized imidazolium moieties was confirmed and characterized by cyclic voltammetry and XPS analysis. It was furthermore compared and contrasted with a known covalent grafted IL layer to draw information of the layer's nature based on their similarities and differences, the latter proving minimal. The effect of this electrodeposited IL layer on CO_2RR was studied and optimized when in use alongside molecular catalyst [Rh(bpy)(Cp*)Cl]Cl and it produced a catalytic effect similar to the one of imidazolium ILs in solution. However, this electrodeposited layer was also tested with another molecular catalyst, [Re(CO)$_3$bpyCl], to prove that its interaction with different catalytic systems was not excluded. It was also demonstrated that this layer effectively suppressed HER in different electrolyte conditions based on its presumed cationic nature. Finally, through electrolysis we were able to assess its beneficial effect in driving product distribution towards formate rather than H_2 to varying extends in different electrolytes, exhibiting a more marked effect in acetonitrile than in aqueous solutions. Finally, a singular electrodeposited IL layer was proved to result in the same product selectivity for several consecutive electrolysis, leading to the conclusion that its catalytic performance was stable.

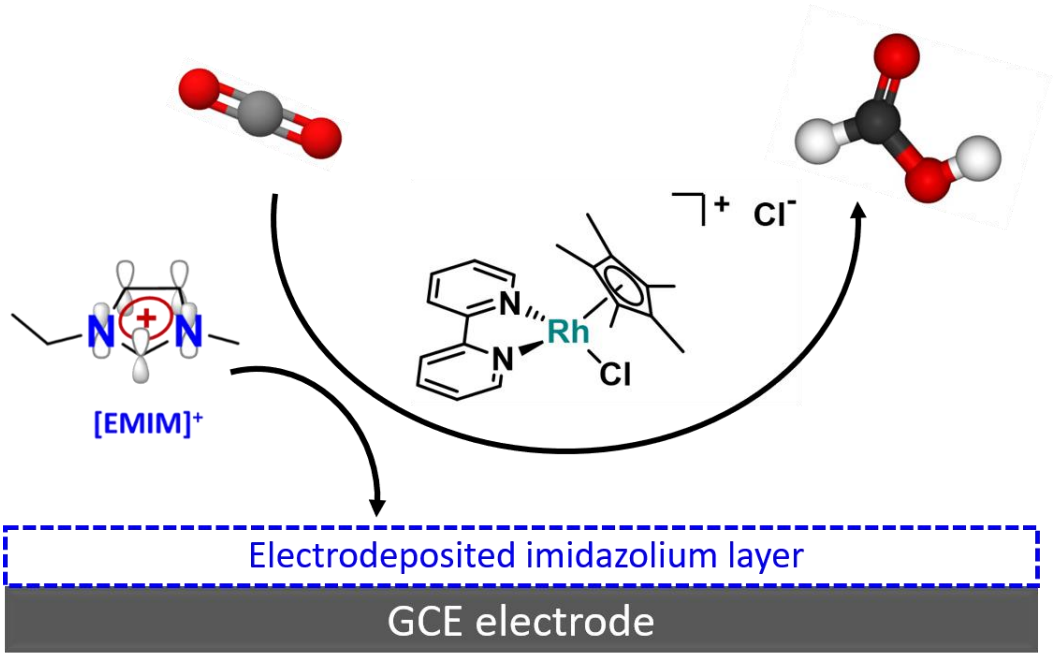

Scheme 4.1 Representation of the electrodeposited imidazolium layer and its interaction with [Rh(bpy)(Cp)Cl]Cl to enhance CO_2RR to formate.*

4.5 References

(1) Nam, D.-H.; De Luna, P.; Rosas-Hernández, A.; Thevenon, A.; Li, F.; Agapie, T.; Peters, J. C.; Shekhah, O.; Eddaoudi, M.; Sargent, E. H. Molecular Enhancement of Heterogeneous CO_2 Reduction. *Nat. Mater.* **2020**, *19* (3), 266–276. https://doi.org/10.1038/s41563-020-0610-2.

(2) Kim, C.; Eom, T.; Jee, M. S.; Jung, H.; Kim, H.; Min, B. K.; Hwang, Y. J. Insight into Electrochemical CO_2 Reduction on Surface-Molecule-Mediated Ag Nanoparticles. *ACS Catal.* **2017**, *7* (1), 779–785. https://doi.org/10.1021/acscatal.6b01862.

(3) Zhao, Y.; Wang, C.; Liu, Y.; MacFarlane, D. R.; Wallace, G. G. Engineering Surface Amine Modifiers of Ultrasmall Gold Nanoparticles Supported on Reduced Graphene Oxide for Improved Electrochemical CO_2 Reduction. *Adv. Energy Mater.* **2018**, *8* (25), 1801400. https://doi.org/10.1002/aenm.201801400.

(4) Kim, C.; Jeon, H. S.; Eom, T.; Jee, M. S.; Kim, H.; Friend, C. M.; Min, B. K.; Hwang, Y. J. Achieving Selective and Efficient Electrocatalytic Activity for CO_2 Reduction Using Immobilized Silver Nanoparticles. *J. Am. Chem. Soc.* **2015**, *137* (43), 13844–13850. https://doi.org/10.1021/jacs.5b06568.

(5) Wakerley, D.; Lamaison, S.; Ozanam, F.; Menguy, N.; Mercier, D.; Marcus, P.; Fontecave, M.; Mougel, V. Bio-Inspired Hydrophobicity Promotes CO_2 Reduction on a Cu Surface. *Nat. Mater.* **2019**, *18* (11), 1222–1227. https://doi.org/10.1038/s41563-019-0445-x.

(6) Xie, M. S.; Xia, B. Y.; Li, Y.; Yan, Y.; Yang, Y.; Sun, Q.; Chan, S. H.; Fisher, A.; Wang, X. Amino Acid Modified Copper Electrodes for the Enhanced Selective Electroreduction of Carbon Dioxide towards Hydrocarbons. *Energy Environ. Sci.* **2016**, *9* (5), 1687–1695. https://doi.org/10.1039/C5EE03694A.

(7) Mun, Y.; Kim, K.; Kim, S.; Lee, S.; Lee, S.; Kim, S.; Choi, W.; Kim, S.; Han, J. W.; Lee, J. A Novel Strategy to Develop Non-Noble Metal Catalyst for CO_2 Electroreduction: Hybridization of Metal-Organic Polymer. *Appl. Catal. B Environ.* **2018**, *236*, 154–161. https://doi.org/10.1016/j.apcatb.2018.05.025.

(8) Cao, Z.; Derrick, J. S.; Xu, J.; Gao, R.; Gong, M.; Nichols, E. M.; Smith, P. T.; Liu, X.; Wen, X.; Copéret, C.; Chang, C. J. Chelating N-Heterocyclic Carbene Ligands Enable Tuning of Electrocatalytic CO_2 Reduction to Formate and Carbon Monoxide: Surface Organometallic Chemistry. *Angew. Chem. Int. Ed.* **2018**, *57* (18), 4981–4985. https://doi.org/10.1002/anie.201800367.

(9) Thevenon, A.; Rosas-Hernández, A.; Peters, J. C.; Agapie, T. In-Situ Nanostructuring and Stabilization of Polycrystalline Copper by an Organic Salt Additive Promotes Electrocatalytic CO_2 Reduction to Ethylene. *Angew. Chem. Int. Ed.* **2019**, *58* (47), 16952–16958. https://doi.org/10.1002/anie.201907935.

(10) Han, Z.; Kortlever, R.; Chen, H.-Y.; Peters, J. C.; Agapie, T. CO_2 Reduction Selective for C≥2 Products on Polycrystalline Copper with N-Substituted Pyridinium Additives. *ACS Cent. Sci.* **2017**, *3* (8), 853–859. https://doi.org/10.1021/acscentsci.7b00180.

(11) Li, F.; Thevenon, A.; Rosas-Hernández, A.; Wang, Z.; Li, Y.; Gabardo, C. M.; Ozden, A.; Dinh, C. T.; Li, J.; Wang, Y.; Edwards, J. P.; Xu, Y.; McCallum, C.; Tao, L.; Liang, Z.-Q.; Luo, M.; Wang, X.; Li, H.; O'Brien, C. P.; Tan, C.-S.; Nam, D.-H.; Quintero-Bermudez, R.; Zhuang, T.-T.; Li, Y. C.; Han, Z.; Britt, R. D.; Sinton, D.; Agapie, T.; Peters, J. C.; Sargent, E. H. Molecular Tuning of CO_2-to-Ethylene Conversion. *Nature* **2020**, *577* (7791), 509–513. https://doi.org/10.1038/s41586-019-1782-2.

(12) Thevenon, A.; Rosas-Hernández, A.; Fontani Herreros, A. M.; Agapie, T.; Peters, J. C. Dramatic HER Suppression on Ag Electrodes via Molecular Films for Highly Selective CO_2 to CO Reduction. *ACS Catal.* **2021**, *11* (8), 4530–4537. https://doi.org/10.1021/acscatal.1c00338.

(13) Sanchez-Sanchez, C. M. Electrocatalytic Reduction of CO_2 in Imidazolium-Based Ionic Liquids. In *Reference Module in Chemistry, Molecular Sciences and Chemical Engineering.*

Encyclopedia of Interfacial Chemistry : Surface Science and Electrochemistry; Wandelt, K., Ed.; Elsevier, 2018; pp 539–551.

(14) Rosen, B. A.; Salehi-Khojin, A.; Thorson, M. R.; Zhu, W.; Whipple, D. T.; Kenis, P. J. A.; Masel, R. I. Ionic Liquid-Mediated Selective Conversion of CO_2 to CO at Low Overpotentials. *Science* **2011**, *334* (6056), 643–644.

(15) Hanc-Scherer, F. A.; Montiel, M. A.; Montiel, V.; Herrero, E.; Sánchez-Sánchez, C. M. Surface Structured Platinum Electrodes for the Electrochemical Reduction of Carbon Dioxide in Imidazolium Based Ionic Liquids. *Phys. Chem. Chem. Phys.* **2015**, *17* (37), 23909–23916. https://doi.org/10.1039/C5CP02361K.

(16) Zhao, S.-F.; Horne, M.; Bond, A. M.; Zhang, J. Is the Imidazolium Cation a Unique Promoter for Electrocatalytic Reduction of Carbon Dioxide? *J. Phys. Chem. C* **2016**, *120* (42), 23989–24001. https://doi.org/10.1021/acs.jpcc.6b08182.

(17) Feaster, J. T.; Jongerius, A. L.; Liu, X.; Urushihara, M.; Nitopi, S. A.; Hahn, C.; Chan, K.; Nørskov, J. K.; Jaramillo, T. F. Understanding the Influence of [EMIM]Cl on the Suppression of the Hydrogen Evolution Reaction on Transition Metal Electrodes. *Langmuir* **2017**, *33* (37), 9464–9471. https://doi.org/10.1021/acs.langmuir.7b01170.

(18) Fontaine, O.; Ghilane, J.; Martin, P.; Lacroix, J.-C.; Randriamahazaka, H. Ionic Liquid Viscosity Effects on the Functionalization of Electrode Material through the Electroreduction of Diazonium. *Langmuir* **2010**, *26* (23), 18542–18549. https://doi.org/10.1021/la103000u.

(19) Chi, Y. S.; Hwang, S.; Lee, B. S.; Kwak, J.; Choi, I. S.; Lee, S. Anion Exchange-Promoted Ru3+/2+ Redox Switch in Self-Assembled Monolayers of Imidazolium Ions on a Gold Electrode. *Langmuir* **2005**, *21* (10), 4268–4271. https://doi.org/10.1021/la046806k.

(20) Bouden, S.; Gómez-Mingot, M.; Randriamahazaka, H.; Ghilane, J. Surface Initiated Immobilization of Molecules Contained in an Ionic Liquid Framework. *Anal. Chem.* **2016**, *88* (1), 1017–1021. https://doi.org/10.1021/acs.analchem.5b03922.

(21) Michez, R.; Doneux, T.; Buess-Herman, C.; Luhmer, M. NMR Study of the Reductive Decomposition of [BMIm][NTf2] at Gold Electrodes and Indirect Electrochemical Conversion of CO_2. *ChemPhysChem* **2017**, *18* (16), 2208–2216. https://doi.org/10.1002/cphc.201700421.

(22) Michez, R.; Vander Steen, J.; Doneux, T.; Luhmer, M.; Buess-Herman, C. Electroreduction of 1-Butyl-3-Methylimidazolium Bis(Trifluoromethanesulfonyl)Imide Ionic Liquid: Oriented Product Selectivity through the Electrode Material. *Electrochimica Acta* **2018**, *270*, 434–439.

(23) Wang, Y.; Hayashi, T.; He, D.; Li, Y.; Jin, F.; Nakamura, R. A Reduced Imidazolium Cation Layer Serves as the Active Site for Electrochemical Carbon Dioxide Reduction. *Appl. Catal. B Environ.* **2020**, *264*, 118495. https://doi.org/10.1016/j.apcatb.2019.118495.

(24) Tomita, Y.; Teruya, S.; Koga, O.; Hori, Y. Electrochemical Reduction of Carbon Dioxide at a Platinum Electrode in Acetonitrile-Water Mixtures. *J. Electrochem. Soc.* **2000**, *147* (11), 4164.

(25) Pugliese, S.; Huan, N. T.; Forte, J.; Grammatico, D.; Zanna, S.; Su, B.-L.; Li, Y.; Fontecave, M. Functionalization of Carbon Nanotubes with Nickel Cyclam for the Electrochemical Reduction of CO_2. *ChemSusChem* **2020**, *13* (23), 6449–6456. https://doi.org/10.1002/cssc.202002092.

(26) Bermúdez, M.-D.; Jiménez, A.-E.; Sanes, J.; Carrión, F.-J. Ionic Liquids as Advanced Lubricant Fluids. *Molecules* **2009**, *14* (8), 2888–2908. https://doi.org/10.3390/molecules14082888.

(27) Efthimiadis, J.; Neil, W. C.; Bunter, A.; Howlett, P. C.; Hinton, B. R. W.; MacFarlane, D. R.; Forsyth, M. Potentiostatic Control of Ionic Liquid Surface Film Formation on ZE41 Magnesium Alloy. *ACS Appl. Mater. Interfaces* **2010**, *2* (5), 1317–1323. https://doi.org/10.1021/am900889n.

(28) Wu, J.-B.; Lin, Y.-F.; Wang, J.; Chang, P.-J.; Tasi, C.-P.; Lu, C.-C.; Chiu, H.-T.; Yang, Y.-W. Correlation between N 1s XPS Binding Energy and Bond Distance in Metal Amido, Imido, and Nitrido Complexes. *Inorg. Chem.* **2003**, *42* (15), 4516–4518. https://doi.org/10.1021/ic034261w.

(29) Clark, M. L.; Cheung, P. L.; Lessio, M.; Carter, E. A.; Kubiak, C. P. Kinetic and Mechanistic Effects of Bipyridine (Bpy) Substituent, Labile Ligand, and Brønsted Acid on Electrocatalytic CO_2 Reduction by Re(Bpy) Complexes. *ACS Catal.* **2018**, *8* (3), 2021–2029. https://doi.org/10.1021/acscatal.7b03971.

(30) Huan, T. N.; Simon, P.; Rousse, G.; Génois, I.; Artero, V.; Fontecave, M. Porous Dendritic Copper: An Electrocatalyst for Highly Selective CO_2 Reduction to Formate in Water/Ionic Liquid Electrolyte. *Chem. Sci.* **2016**, *8* (1), 742–747. https://doi.org/10.1039/C6SC03194C.

(31) Fang, Y.; Flake, J. C. Electrochemical Reduction of CO_2 at Functionalized Au Electrodes. *J. Am. Chem. Soc.* **2017**, *139* (9), 3399–3405. https://doi.org/10.1021/jacs.6b11023.

CHAPTER 4: IMMOBILIZATION OF IONIC LIQUIDS FOR TUNING CO2 ELECTROREDUCTION SELECTIVITY IN MODEL MOLECULAR ELECTROCATALYSIS

CHAPTER 5: SCALE-UP TEST OF A HOMOGENEOUS CATALYST IN A FLOW ELECTROLYZER FOR ELECTROCATALYTIC CO2 REDUCTION

CHAPTER 5: SCALE-UP TEST OF A HOMOGENEOUS CATALYST IN A FLOW ELECTROLYZER FOR ELECTROCATALYTIC CO2 REDUCTION

5.1 Introduction

In this chapter, we test the feasibility of using the homogeneous molecular catalyst [Rh(bpy)(Cp*)Cl]Cl (referred to as complex [2]), which has been already studied in Chapters 3 and 4 as a catalytic model for CO_2 conversion to formate in an H-type cell, but scaling the electrodes size up to 10 cm^2 in a flow electrolyzer. This approach combines the high selectivity of a molecular catalyst with the scalability of a flow electrolyzer, which should allow a significant increase in the catalytic current density achieved.

The development of efficient, selective and stable catalysts for CO_2 electroreduction has long been a subject of study[1,2]. For these catalysts to be able to be considered economically viable for CO_2 electroreduction at an industrial scale they need to simultaneously meet a few criteria. Those are exhibiting high activity, as illustrated by partial current density values exceeding 150 mA/cm^2, for CO_2RR products like CO, while maintaining overall cell overpotential (|ηcell|) below 1 V and overall good catalyst stability[3]. However challenging it may be fitting into these criteria[4], testing electrocatalysts in a flow electrolyzer, remains the way of assessing a catalyst's potential application at larger scale. Flow electrolyzers are also often called flow-cell or small-scale reactor. This is the case herein, because screening tests performed in H-type cells in the previous chapters, though very useful in pinpointing the optimal catalytic conditions, cannot substitute actual experiments at much higher partial current densities achieved within a flow electrolyzer[5]. In particular, the electrolyte engineering strategy developed within Chapter 3 and based on comparing the role as co-catalyst of different ILs in solution was not selected for scale up tests. In contrast, the electrode surface engineering strategy developed within Chapter 4 and based on the immobilization by electrodeposition of imidazolium-based ILs at the electrode surface was scaled up in acidic aqueous solution due to its potential industrial interest.

Initially, the benchmark conditions without the presence of ILs were explored in different flow electrolyzer configurations to reach optimal CO_2RR catalytic performance and demonstrate the system's stability and product efficiency at charge values up to hundred-fold higher than previously tested in H-type cell. Finally, the effect of an electrodeposited IL layer on the cathode within the optimized flow electrolyzer configuration was investigated and compared to the results obtained in benchmark conditions. However, in order to better organize this study and facilitate comparison of catalytic performance with other flow electrolyzers with molecular catalysts we needed a set of criteria. Here below are mentioned some parameters that are relevant to the flow electrolyzer tests presented throughout this chapter:

[1] Galvanostatic versus potensiostatic tests. Throughout this chapter we have opted for galvanostatic control by using an external power source connected between cathode and anode that maintains the cathodic current value stable for a set time period, while simultaneously tracking the cell potential with the aid of a voltmeter. The alternative would have been to apply a controlled cathode potential and follow the evolution of the observed current, which requires an additional reference electrode and a potentiostat. Thus, galvanostatic approach was considered closer to industrial scale.

[2] One compartment versus two compartments electrolyzer configuration. Either CO_2RR is performed in a one compartment cell sharing the same solution for both cathode and anode or a separator is used, such as an ion selective membrane or a polymeric porous separator, that creates two separate compartments for the cathode and anode respectively. In this latter case CO_2RR is performed in a two compartment configuration and the catholyte and anolyte compositions can be kept the same of be different.

[3] Recirculating flow versus single-pass flow electrolyzer configuration. During recirculating flow mode, the electrolyte solution is in a constant feedback loop through the electrolyzer for the duration of the experiment, which modifies the solution composition as a function of electrolysis time. On the contrary, in single-pass configuration, there are separate input and output electrolyte recipients ensuring all electrolyte passes through the electrolyzer only once and only initial solution composition is in contact with the electrodes.

[4] CO_2 solubilized in liquid-phase versus direct gas-phase feeding. In the first case the cathode is typically a planar electrode, CO_2 reaches it after first being solubilized in the electrolyte solution and the reduction reaction takes place on the cathode surface. This process is illustrated in Figure 5.1 (a) and it is limited by the CO_2 solubility in each particular solvent (33 mM at 25 ºC in aqueous solution). On the other hand, direct gas-phase feeding allows CO_2 to be fed directly through the electrode without necessarily being bubbled in the electrolyte solution. The cathode used in this case is referred to as Gas Diffusion Electrode (GDE)[6], it results in minimizing CO_2 mass transport limitations within the electrolyzer. Therefore, the cathode acts as a three-phase interface where the electrode itself encounters on each side the electrolyte and the CO_2 gas, the catalytic reaction taking place only within its confines, as is illustrated in Figure 5.1 (b). The CO_2RR products are then released according to their nature, gaseous products towards the gas phase and liquid products accumulating in the electrolyte[6]. Many electrolyzers that contain GDEs with heterogeneous precious metal catalysts are approaching industrially interesting catalytic activity[7]. Moreover, there are an increasing number of examples in recent years where heterogenized molecular catalysts are also supported on GDEs[8–11]. However, according to the available literature at this time, there are no examples of molecular catalysts in solution tested with

GDEs, nor any examples of IL electrodeposition on GDEs. Therefore, the present study aimed to explore these topics for the first time.

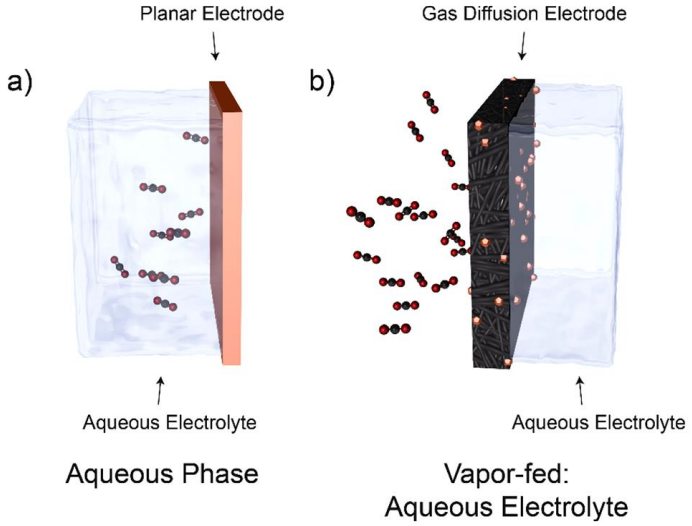

Figure 5.1 (a) Schematic illustration of (a) liquid-phase CO_2RR, where CO_2 reaches the planar electrode surface through the electrolyte and (b) gas-phase CO_2RR, where CO_2 is vapor-fed through a GDE[12].

The vast majority of molecular CO_2 electrocatalysts used in flow electrolyzers described in the literature are in fact heterogenized molecular catalysts[7,9–11,13–15]. Heterogenization of molecular catalysts especially on carbon supports and subsequent use of them in flow electrolyzers presents advantages. These include enhancing their catalytic efficiency in some cases[7,9–11,13–15] and permitting their use in aqueous solution instead of less green organic solvents. Both these considerations are often pertinent in an industrial setting. However, using grafted molecular catalysts in flow electrolyzers also has one inherent limitation when reviewed from an industrial point of view. That consists of the necessity to force a flow electrolyzer to regularly go off-line whenever the heterogenized catalyst system needs replacement due to degradation issues. This process results in increased cost, resources and energy expenditure that counterbalances the advantages of continuous reactions, which are not only economically preferable, but also integral to green chemistry[16].

To the best of our knowledge, the only not grafted molecular catalyst for CO_2RR that has been tested in a flow electrolyzer to date is $[Ni(cyclam)]^{2+}$ in organic solvents (ACN and N, N-DMF) containing 0.5 M of $[NH_4][PF_6]$ as both supporting electrolyte and sacrificial proton donor in the catholyte. Graphite felt electrodes were used as both cathode and anode. Meanwhile, in the anodic compartment the reaction taking place was the oxidation of 0.1 M ferrocene (Fc), which acted as a sacrificial electron donor. This system produced CO and their best FE for CO observed was 83 % at an |Ecell| value of 1.7 V, but only at the moderate current density value of 12.7 mA/cm^2. The maximum current density of 18.9 mA/cm^2 reported in this study was achieved at an |Ecell| of 1.8 V and resulted in 80 % of CO, with H_2 being the

only other detected product. It should also be mentioned that these results were observed in a two-compartment recirculating flow electrolyzer configuration using 10 mM of $[Ni(cyclam)]^{2+}$ in solution[17]. In order to assess the scalability of the catalytic conditions already reported using a H-type cell in Chapters 3 and 4 , those conditions were transposed in a commercially available flow electrolyzer, seen here assembled and disassembled in Figure 5.2. This flow electrolyzer that can accommodate electrodes of 10 cm^2 geometric area or others of similar size have been used in several previous studies[9,17,18] to illustrate the applicability of such systems in even bigger scale, that may be of industrial interest. In this chapter, we explored different electrolyzer configurations using the [Rh(bpy)(Cp*)Cl]Cl catalyst in acidic aqueous catholyte. This model catalyst was selected since it provided two main advantages. Namely, it was soluble in purely aqueous solutions allowing us to scale-up the aqueous conditions already detailed in the previous chapters and its selectivity towards formate and H_2 was highly tunable by its environment, which made it a model system with which to assess the impact of the IL electrodeposited layer at larger scale. The reaction conditions were initially optimized on bare carbon-based electrodes (graphite plate or GDE) and eventually, a cathode with an electrodeposited IL layer was also tested.

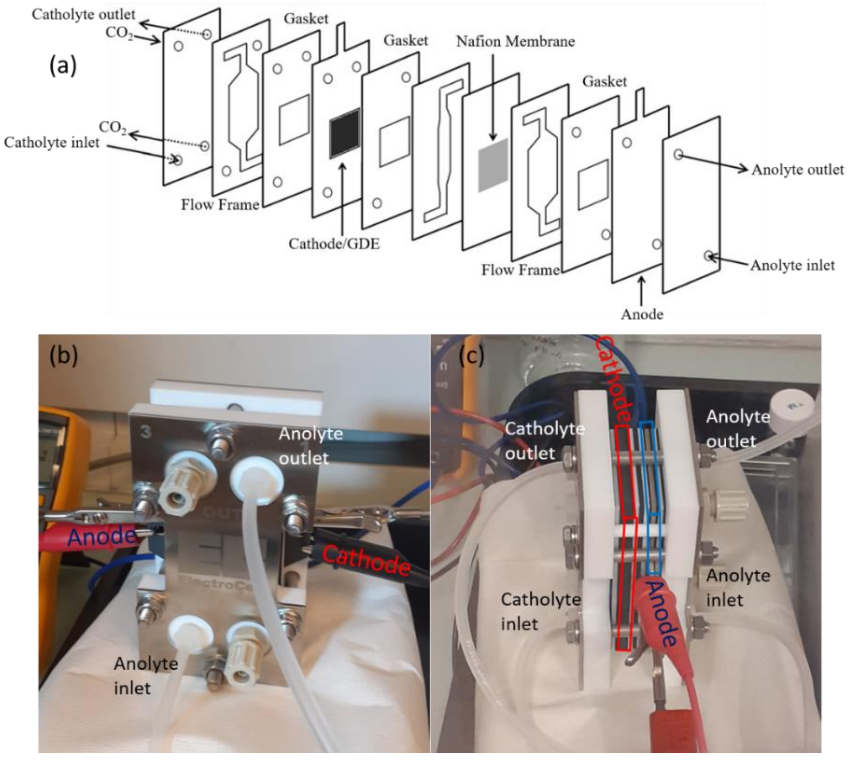

Figure 5.2 Illustration of the CO_2 flow electrolyzer. (a) Simplified cross-sectional view graphic scheme featuring the two-compartment configuration with a GDE cathode, (b)Frontal view of the reactor with illustrated all visible elements and (c) Side view of the reactor with illustrated the electrodes and the electrolyte inlets and outlets. *Adapted from Wang et. al.*[9]

5.2 Results

5.2.1 Single-compartment recirculating flow configuration for liquid-phase CO_2RR

The first setup of the flow electrolyzer tested was also the simplest, the single-compartment configuration. Under those conditions both the cathode and the anode are situated in a unique compartment without any membrane or other physical barrier between them and their distance was approximatively 4 mm. The cathode and anode used were a 2D graphite plate and a Dimensionally Stable Anode (DSA) electrode of 10 cm^2 active geometric area, respectively. The DSA consists of a IrO_2–Ta_2O_5 mixed oxide and is known to promote Oxygen Evolution Reaction (OER)[19] and thus decreasing the anodic contribution to the cell potential (|Ecell|). A reference electrode was not used and as a consequence, the potential was only screened as overall |Ecell| value with the aid of a voltmeter. The electrolyte of this single-compartment was an aqueous 0.1 M acetate buffer solution at pH=3.8 saturated with [TBA][BF_4] containing 1 mM [Rh(bpy)(Cp*)Cl]Cl. The recirculating flow configuration signifies that the solution composition continuously passing through the flow electrolyzer was evolving for the duration of the experiment. Final pH values, as well as the volume of the catholyte, were monitored after each test. All tests were performed under continuous flow of CO_2 being bubbled in the electrolyte solution. This CO_2 gas stream was previously saturated in water by passing through a bubbler filled with water before reaching the electrolyte. To feed the electrolyte solution through the flow electrolyzer a double head peristatic pump was used. It can accommodate a pumping speed range that based on the tubing diameter (1.6 mm of internal diameter) goes from approximatively 0.66 mL/min to 66.4 mL/min. Finally, an external power source with the capacity of applying up to 1 Ampere (over the span of 150 Volts) was used, though for this study we applied between 1 and 3.4 mA/cm^2. The gaseous products were not collected and only liquid phase products were quantified. The entire single compartment configuration is shown in Figure 5.3 (a).

In Figure 5.3 (b) we observe the results of tests using the single-compartment flow electrolyzer configuration, where at any time only one parameter was altered in order to assess its impact. At first (test 1), a current density of 3.4 mA/cm^2 was applied, as a 10 mL electrolyte solution was pumped at 22.1 mL/min, until 132 C were reached under continuous stream of CO_2. As observed, a mere 5.6 % of formate was produced, which led us to investigate the role of decreasing current density (test 2) and increasing the solution volume (test 3) for a constant charge of 100 C. The hypothesis was that in the former case we might be positioned closer to the onset potential of formate production, while in the latter case that by further diluting our product we would help it accumulate. Both conditions however only led to formate production diminishing. Equally inefficient towards formate promotion was diminishing the flow rate by one order of magnitude (test 4) and exchanging the anode material to graphite, instead of

the DSA (test 5). Overall, this configuration for all conditions tested led to formate faradaic efficiency (FE) values that ranged from 1.7 to 6.5 %. It was probably due to either the oxidation of electrogenerated formate or the rapid oxidation of the active form of complex [2] before performing CO_2RR, in both cases at the anode. Another note should be made on the |Ecell| values, which ranged from 2.2 to 3.5 V for all tests. Based on the assumption that only oxygen evolution reaction (OER) from water oxidation takes place in the anode ($2H_2O_{(l)} \leftrightarrow 4H^+ + O_{2(g)} + 4e^-$ E°=1.01 V)[20] and CO_2RR to formate in the cathode ($CO_{2(g)} + 2H^+ + 2e^- \leftrightarrow HCOOH_{(l)}$ E°= -0.42 V *vs.* NHE)[1] both at pH=3.8, the calculated absolute thermodynamic cell potential would be 1.43 V. Finally, the final value of the solution pH was not significantly modified during the electrolysis by comparing the average 3.6 versus the initial 3.8 value. It should also be stressed that no other CO_2 reduction products were detected in the liquid phase, while the experimental setup did not allow characterization of the gas phase. The assumption made in this case was that the only other undetected product is hydrogen, since the same setup had been tested in an H-type cell configuration and the only products were formate and hydrogen.

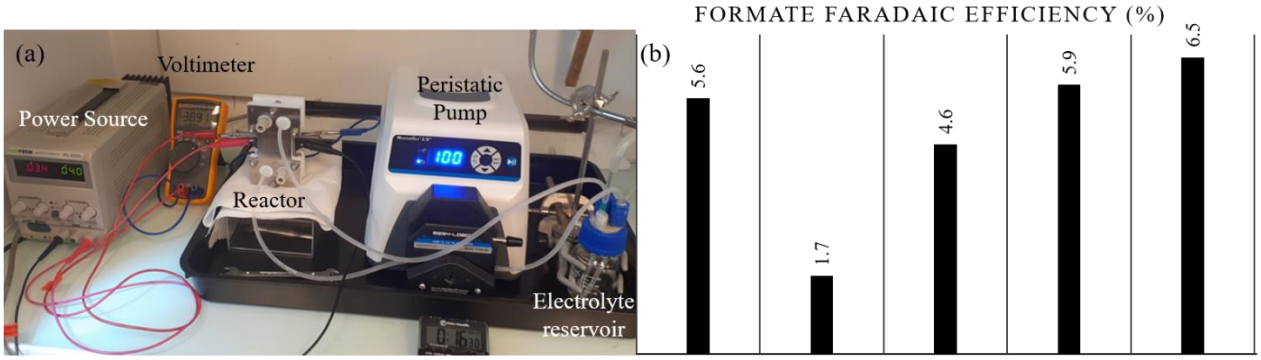

TEST	1	2	3	4	5
Current Density (mA/cm^2)	3.4	1	3.4	3.4	3.4
Catholyte (mL)	10	10	40	20	20
Flow rate (mL/min)	22.1	22.1	22.1	22.1	22.1
Counter electrode	DSA	DSA	DSA	DSA	Graphite
Average Cell Potential (V)	3.5	2.2	3.2	3.5	3.1
Final catholyte pH	3.6	3.5	3.6	3.6	3.6

Figure 5.3 (a) Picture of the single-compartment recirculating flow reactor configuration and (b) Results of formate Faradaic efficiency on a series of tests performed in a one-compartment recirculating flow reactor configuration on a bare 10 cm^2 graphite cathode at varying current density, catholyte volume, solution flow rate and anode material with the catholyte under continuous stream of "wet" CO_2.

5.2.2 Two-compartments recirculating flow electrolyzer configuration for liquid-phase CO_2RR

This flow electrolyzer configuration is similar to the one discussed in 5.2.1, with the exception that the addition of a cation selective Nafion membrane created two distinct compartments within the flow electrolyzer, the cathodic and the anodic compartment. As a consequence, there was a possibility to have different catholyte and anolyte solutions. We took the experimental conditions already studied for single-compartment configuration as starting point and we modified parameters one by one. Thus, the flow rate of 22.1 mL/min was kept constant in both compartments. The catholyte used throughout these tests was again a 0.1 M acetate buffer at pH=3.8 saturated with [TBA][BF_4] containing 1mM [Rh(bpy)(Cp*)Cl]Cl. The anolyte composition however varied in tests 6 and 7, presented in Figure 5.4, either having the same composition as the catholyte or consisting of a 0.5 M KOH solution. The cathode and anode remained a 2D graphite electrode and a DSA, respectively. In all experiments, a current density of 3.4 mA/cm^2 was applied for circulating 100 C and only the catholyte was under continuous CO_2 flow. Sampling for formate analysis was performed at 50 and 100 C charge values. The overall two-compartment configuration can be seen in Figure 5.4 (a).

In Figure 5.4 (b), we see the results of tests obtained in the two-compartment configuration. Initially (test 6), the anolyte composition is the same as the catholyte (acetate buffer solution at pH=3.8) and moving from one-compartment to two-compartments cell resulted in FE_{HCOO^-} of 28 % and 19 % for the 50 C and 100 C charge values, respectively. Meanwhile, whilst the optimization of |Ecell| was not the first priority, it must be noted that using the two-compartment configuration (test 6) resulted in an increased cell potential value of 7.3 V. In order to mitigate this effect, we switched the anolyte composition to a 0.5 M solution of KOH. In this case (test 7) the reaction taking place in the anode was OH^- oxidation, which is favored in basic conditions and occurs at 0.404 V *vs.* RHE. Therefore, the calculated absolute thermodynamic cell potential would be smaller (0.82 V), taking into consideration the CO_2RR to formic acid as cathodic reaction. The FE_{HCOO^-} observed in that case was 30 % and 23 % for 50 C and 100 C, respectively. These results were almost identical to those obtained using the previous anolyte composition, while the |Ecell| significantly decreased from test 6 to test 7, from 7.3 V to a value of 2.8 V, thus demonstrating that a pH gradient between the anolyte and catholyte was highly beneficial in terms of decreasing |Ecell|. For that reason, 0.5 M KOH aqueous solution as anolyte was used for all subsequent studies. It should also be mentioned that the change of anolyte incurred a slight increase in the final values of the catholyte pH, which after each experiment reached an average pH value of 4.5 versus the initial 3.8.

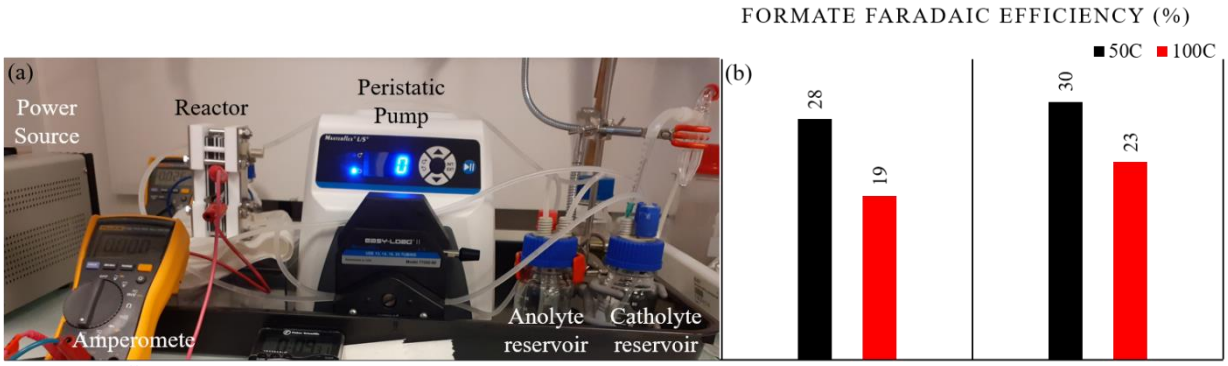

TEST	6	7
Anolyte solution	CH_3COONa/CH_3COOH buffer with $[TBA][BF_4]$	0.5M KOH
Average Cell Potential (V)	7.3	2.8
Final catholyte pH	3.8	4.5

Figure 5.4 (a) Picture of the two-compartment recirculating flow reactor configuration and (b) Results of formate Faradaic efficiency at 50 C (black bar) and 100 C (red bar) charge in a two-compartment recirculating flow reactor configuration on a bare 10 cm^2 graphite cathode with different anolyte compositions at 3.4 mA/cm^2 current density and 22.1 mL/min catholyte and anolyte flow rate.

5.2.3 Two-compartments recirculating flow configuration for gas-phase CO_2RR

Having adopted the two-compartment recirculating flow configuration, we subsequently turned our attention to performing gas phase CO_2RR, in order to be able to optimize the performance of the system and especially increase the applied current density. The catholyte and anolyte compositions remained 0.1 M acetate buffer at pH=3.8 saturated with $[TBA][BF_4]$ containing 1 mM [Rh(bpy)(Cp*)Cl]Cl and 0.5 M KOH respectively. The anode remained a 10 cm^2 DSA, while as cathode a commercially available carbon-based GDE (Sigracet 28BC, built by a hydrophobized gas diffusion layer (5 wt. % PTFE) and a microporous carbon layer) of the same geometrical area was employed. In this configuration, CO_2 flow was directly pumped in gas phase from the back side of the GDE through a different entry than the catholyte in order to ensure their combined presence only on the electrode interface. However, prior to starting a test, CO_2 was also directly bubbled in the catholyte for 5 minutes to remove oxygen. The direct CO_2 flow rate through the electrolyzer had not undergone any "wetting" process and was manually controlled to correspond to 190 mL/min. The entire configuration is depicted in Figure 5.5 (a).

Using this flow electrolyzer configuration, we were able to apply current densities of 10 and 20 mA/cm^2. Furthermore, in Figure 5.5 are shown the results of a series of gas-phase CO_2RR tests performed in this

electrolyzer configuration in order to determine relevant catalytic parameters. In test 8, a current density value of 3.4 mA/cm^2 using a GDE as cathode was tested and resulted in FE_{HCOO^-} of 23 % and 16 % at 50 C and 100 C, respectively. Meanwhile, increasing the applied current density to 10 mA/cm^2 in test 9 has a slight beneficial effect for the FE_{HCOO^-} at both analyzed points, while further increase at 20 mA/cm^2 in test 11 resulted in similar FE values of 28 % at 50 C and 24 % for 100 C. The evolution of FE_{HCOO^-} for test 9 is also presented in Figure 5.6, where 10 mA/cm^2 was applied to the system. It resulted in 30 % FE_{HCOO^-} at 50 C of charge passed. However, we clearly observed a decrease in formate production over electrolysis time, where further analyzed points that corresponded to 100 C and 367 C afforded only 19 % and 6 % of FE_{HCOO^-}, respectively. Finally, the increase of the catalyst concentration to 5 mM in test 10 did however not produce any significant effect on formate production. The |Ecell| values decrease along the electrolysis and an average value is reported in Figure 5.5 while the final catholyte pH measured was approximatively at a value of 4.5.

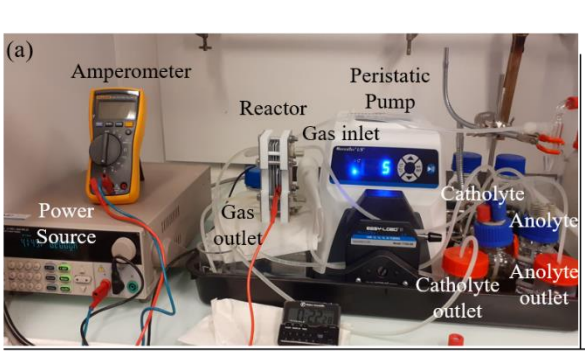

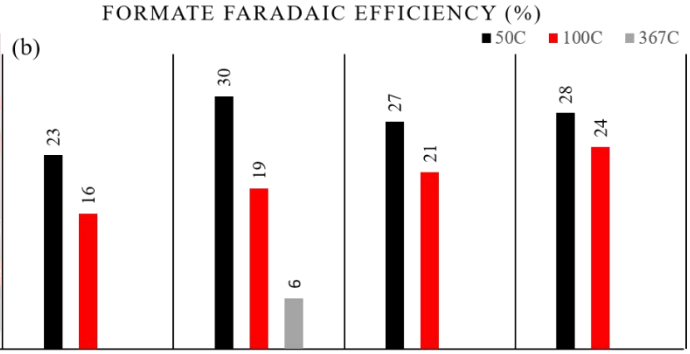

TEST	8	9	10	11
Current Density (mA/cm^2)	3.4	10	10	20
Catalyst concentration (mM)	1	1	5	1
Average Cell Potential (V)	2.3	3.6	4.6	6.7
Final catholyte pH	4.6	4.5	4.5	4.5

Figure 5.5 (a) Picture of the two-compartment in-flow reactor configuration and (b) Representation of formate Faradaic efficiency for 50 C (black bar), 100 C (red bar) and in one case 367 C (grey bar) on a series of tests performed in a two-compartment recirculating flow reactor configuration on a bare 10 cm^2 GDE cathode at varying current density and catalyst concentration. The solution flow rate was kept constant at 22.1 mL/min and the CO_2 flow rate of 190 mL/min.

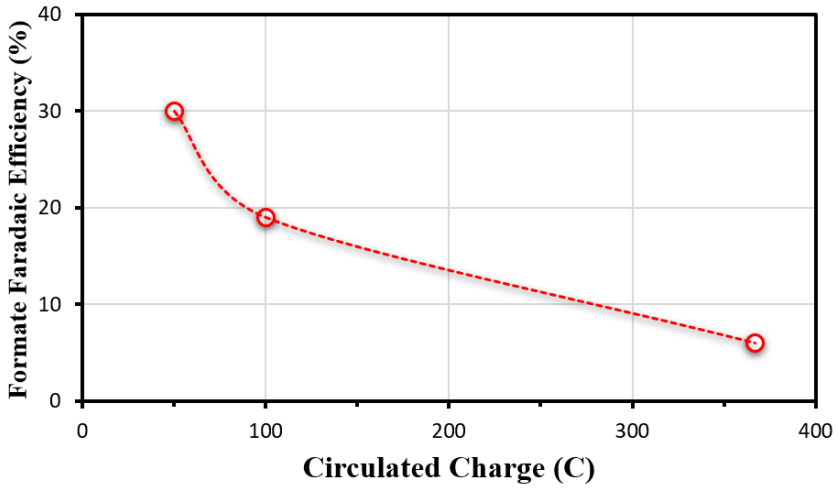

Figure 5.6 Formate Faradaic efficiency evolution during electrolysis at 10 mA/cm^2 on a bare 10 cm^2 GDE cathode (red plot) in a recirculating flow two-compartment reactor configuration under a 22.1 mL/min solution flow rate and a CO_2 flow rate of 190 mL/min (test 9).

5.2.4 Two-compartments single pass flow configuration for gas-phase CO_2RR

The recirculating flow conditions used up to this point provided a formate efficiency that decayed over time and were inconclusive as to the system's stability towards degradation over time. We needed to overcome the obstacles linked with recycling the solution during the electrolysis, which could distort the effect due to the use of a GDE in a flow electrolyzer. For this reason, we opted for a single-pass flow configuration with separate inlet and outlet reservoirs. Then, the catalyst would only be passing through the electrolyzer once. In order to avoid needless catalyst waste and to increase the catalyst residence time in contact with the cathode, the solution flow rate was reduced to 1.1 mL/min , which would allow reaching 1000 C without surpassing 100 mL of catholyte solution. The anode and cathode electrodes, as well as both catholyte and anolyte compositions, remained unaltered from the previous configuration. The current density applied for this test was 20 mA/cm^2 and sampling for formate quantification was performed every 250 C for a total charge value of 1000 C.

In Figure 5.7, we observe the formate faradaic efficiency over time in a single pass flow configuration. The apparent stability of FE_{HCOO^-} at approximatively 32 % throughout the test allowed us to test for a greater charge value than in any of the previous configuration, reaching 1000 C. Attempts to run at higher current densities were also undergone, more precisely at 30 mA/cm^2. However, after an initial smooth run of a few minutes the |Ecell| values skyrocketed, indicating a power short cut due to gas accumulating at the anode surface. The cause was identified to be the small solution flow rate also used in the anolyte flow (1.1 mL/min), which was not able to remove fast enough the O_2 bubbles generated at the anode

surface. Therefore, since the setup did not allow to increase solely the anolyte flow, but instead both catholyte and anolyte would be affected, we instead conducted tests at 20 mA/cm^2. Final catholyte pH values after the passage of 1000 C ranged from 5.5 to 6.5, a basification not entirely unexpected after the prolonged consumption of protons during formate production.

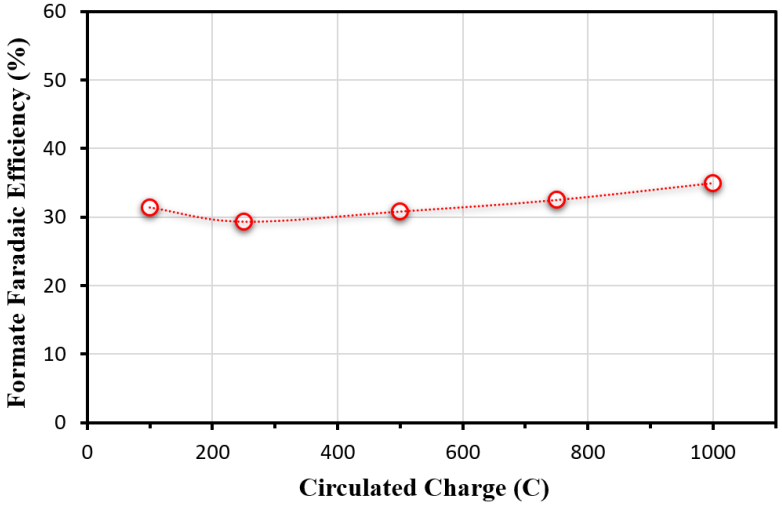

Figure 5.7 Formate Faradaic efficiency evolution on a bare GDE cathode in a single pass flow configuration (red curve) in a two-compartment reactor setup for a current density of 20 mA/cm^2, at a CO_2 flow rate of 190 mL/min.

5.2.5 Two-compartments single pass flow configuration for gas-phase CO_2RR on a GDE with an electrodeposited IL layer

Since adopting the single pass flow configuration allowed for an average formate production of 32 % for the whole span of points analyzed at a current density of 20 mA/cm^2, we proceeded to create an electrodeposited layer on another piece of the same GDE again measuring 10 cm^2. The electrodeposition was performed in a 0.5 M [EMIM][PF_6] aqueous solution under inert atmosphere by a 10 second CPE at -2.5 V *vs.* the Ag/AgCl/KCl_{sat} reference used. The catholyte and anolyte composition remained the acetate buffer solution at pH=3.8 saturated with [TBA][BF_4] and 0.5 M KOH, respectively and the CO_2 flow rate was also kept at 190 mL/min. Under those conditions, three experiments spanning 1000 C at 20 mA/cm^2 were performed, that are represented as an average with standard deviation error bars (≤ 3%) in the red curve of Figure 5.8. As we can observe, in all points the GDE with electrodeposited layer produced higher amounts of formate than the bare GDE, which resulted in an average FE of formate of 45 % in the presence of the electrodeposited layer. Energy Efficiency (EE) and Energy Consumption (EC) were also calculated for these two conditions. The simultaneous increase in FE_{HCOO^-} alongside the small decrease in cell potential in the presence of the electrodeposited layer led to a higher EE value than the bare electrode. The same

effect could also be described by reduced EC for the cathode modified by an electrodeposited layer. It should also be highlighted that due to the dead volume in the electrolyzer and the manner of sampling of the 1000 C final point, a small underestimation of the FE value is possible. Finally, the full-cell energy efficiency is calculated being almost double in the presence of an electrodeposited IL layer on the GDE (7%).

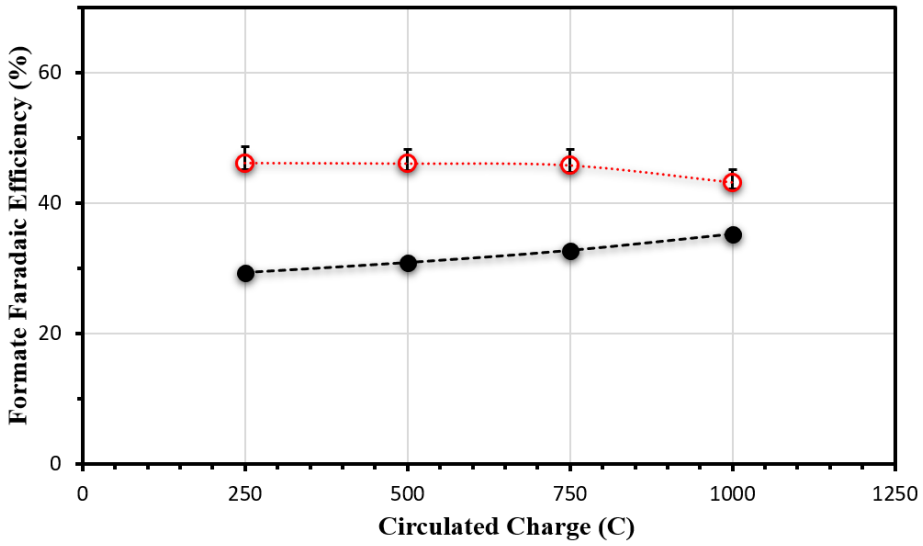

GCE	Non-modified	With electrodeposited layer[a]
FE_{HCOO^-} (%)[b]	32	45
Average Cell Potential (V)	6.4	5.1
Initial catholyte pH	3.8	3.8
Final catholyte pH	5.5	6.0
Energy Efficiency (%)	4.1	7.2
Energy Consumption (kWh/kmol)	953	598

Figure 5.8 Formate Faradaic efficiency over 1000 C charge passed for a bare GDE cathode (black curve) and an IL-modified by electrodeposited layer GCE cathode (red curve) in a two-compartment single pass flow reactor configuration for a current density of 20 mA/cm^2, at a solution flow rate of 1.1 mL/min and CO_2 flow rate of 190 mL/min. Also mentioned are the average values of cell potential, as well as initial and final pH value of the catholyte, while anolyte was stable at pH=13 throughout. Energy Efficiency (EE) = (E_{Tcell}/E_{cell}) · FE_{HCOO^-}, where E_{Tcell} is the theoretical cell potential for CO_2RR/OER in those conditions (E_{Tcell} = 0.82 V), E_{cell} is the average cell potential and FE_{HCOO^-} is the faradaic efficiency for formate production. Energy Consumption (EC): EC = (Q · |Ecell| / N) · 2.78 10^{-4} (kWh/kmol), where Q represents the total charge circulated measured in Coulombs, |Ecell| represents the absolute cell potential in volts and N is the number of moles of each product.[21]

[a]*Averages of three independent experiments.* [b]*Average of values taken during each experiment.*

5.3 Discussion

Testing a catalytic system in a flow electrolyzer configuration is a laboratory available strategy to investigate the system's efficiency and productivity at larger scale than an H-type cell setup and provides invaluable information about the feasibility of further scaling up at industrial level. In recent years, an increasing number of CO_2RR electrolyzers with heterogeneous metallic catalysts, usually Ag and Cu, report CO_2 reduction product generation at commercially relevant values of current density[6]. Heterogenized molecular catalysts grafted on carbon support materials and also often incorporated in GDEs have shown catalytic performances that rival those of noble-metal nanocatalysts[9]. However, testing the effects of a GDE with an electrodeposited IL layer on a molecular catalyst with tunable selectivity towards formate in a flow electrolyzer in acidic aqueous conditions remains, to the best of our knowledge, a completely novel approach. Furthermore, the only other example in literature where a molecular catalyst is used homogeneously presents many differences that complicate direct comparisons[17].

In this chapter we have elucidated how several parameters pertaining to the reactor configuration impact the system, which was monitored in terms of formate faradaic efficiency, as well as |Ecell|. Firstly, we saw that in a single-compartment recirculating flow configuration on a graphite cathode the formate production was far inferior than the expected values based on the previous studies of this system in an H-type cell with porous carbon cathode, even though tuning of several parameters was tested. More particularly, a CCE for 10 C using the benchmark electrolyte had previously been tested in a single-compartment of the H-type cell, that led to a FE_{HCOO^-} of 39 % and FE_{H2} of 40 %. Nevertheless, the greater proximity of cathode and anode in the flow electrolyzer resulted in very low FE_{HCOO^-} (< 7 %) and led to the adoption of a two-compartment configuration. As expected, this passage from a single to a two-compartment configuration led to a fourfold increase in formate production (< 30 %). This observation allowed us to infer that the main limitation of single-compartment reactor setup derived from having the electrolyte containing the catalyst and the accumulated product in contact with the anode, which could reoxidize both formate and the active form of the catalyst.

The two-compartment configuration also provided the opportunity to employ two different solution compositions as catholyte and anolyte, thus allowing to maintain the weakly acidic conditions in the cathodic compartment that lead to better performance of the electrodeposited IL layer, while using a KOH solution as anolyte resulting in lower |Ecell| values. Though acidic, neutral and basic conditions have all been used for OER, more basic pH values have been shown to promote OER at lower potentials because O_2 is produced from OH^- oxidation that in basic conditions occurs at 0.404 V *vs.* RHE instead of water oxidation which is energetically more costly (1.23 V *vs.* RHE)[20,23]. The other important point

in having a basic anolyte pH is that the presence of a pH gradient between a neutral cathode and basic anode compartment was proven beneficial in terms of energy efficiency in a flow electrolyzer for CO_2RR and water splitting[23]. Therefore ideally, we want to perform CO_2RR under acidic conditions in order to minimize the cell overpotential, which is also one of the reasons that led us to adopt the pH=4 buffered conditions. Another benefit of acidic catholyte was avoiding the inevitable loss of CO_2 as bicarbonate and carbonate when working in very basic conditions[24], which would have only regenerated CO_2 when they crossed over to the anode[25]. However, to date only few examples of efficient systems for CO_2RR have been reported in acidic media[25,26].

Subsequently, we compared the same two-compartment recirculation setup for gas-phase CO_2RR using a bare GDE instead of the liquid-phase CO_2RR performed with the 2D graphite plate as cathode. As expected, formate production remained stable, but at higher current density values, due to the fact that in GDEs we were not limited by the moderate CO_2 solubility in aqueous conditions, as we had been when using the graphite plate cathode.

However, gas-phase CO_2RR was limited by the recirculation solution, since beyond 100 C the system's product selectivity drastically deteriorated. A possible explanation for this deleterious effect is that when formate accumulates at high concentrations, [Rh(bpy)(Cp*)Cl]Cl can catalyze the conversion of HCOOH to CO_2 and H_2[27]. However, we were able to circumvent it by utilizing a single-pass flow configuration, that by definition ensures the catholyte containing the catalyst only goes through the reactor once. With this configuration we observed stable FE_{HCOO^-} over a span of 1000 C for a partial current density value of 20 mA/cm^2. Another advantage of employing a single-pass flow configuration was the extinction of all formate crossover from catholyte to anolyte. Despite knowing that theoretically formate should not be able to traverse a cation exchange Nafion membrane, this crossover was apparent in all recirculation configurations tested and necessitated analysis of both catholyte and anolyte in order to obtain complete product quantification. In contrast, with the in-flow configuration formate quantification was simplified to only testing the catholyte in the outlet reservoir.

Another point to be stressed is that this catalytic system was not inherently limited to only 20 mA/cm^2 because of the molecular catalyst, but merely because of technical limitations in the setup. More particularly, with the employed low solution flow rate of 1.1 mL/min, higher current densities like 30 mA/cm^2 resulted in an overproduction of O_2 bubbles on the anode surface that could not be removed fast enough and led to power shortcuts. We are confident this is truly due to the anode limitation, since increasing the flow rate from 1.1 to 4.4 mL/min led to a return to usual |Ecell| values. A promising perspective in order to test higher current densities would therefore be to separate the anolyte and

catholyte flow by using separate peristatic pumps, allowing for a slow and so economically sustainable catholyte flow rate and simultaneously a fast anolyte rate to remove O_2 from the anode surface.

Finally, when the flow electrolyzer using GDE was proven to be stable and reproducible, we prepared an electrodeposited IL layer on a GDE and compared its activity with the optimized bare GDE conditions in the two-compartment single pass flow configuration for gaseous CO_2RR. What emerged was that the selectivity tuning of the [Rh(bpy)(Cp*)Cl]Cl towards formate in presence of the electrodeposited IL layer previously witnessed in an H-type cell configuration, was also maintained in the single-pass electrolyzer configuration used. More outstanding still was the fact that though FE_{HCOO^-} in the reactor was at an average 7-8 % inferior to that in the H-type cell for both the bare electrode and the one with the electrodeposited layer, the increment between the electrodeposited layer-containing electrode and the bare one was almost identical in both H-type cell and flow electrolyzer (13 %). This effect is shown in Table 5.1 and renders credibility to the hypothesis that the electrodeposited layer had the same effect on enhancing formate production selectivity regardless of the scale of application.

Table 5.1 Comparison of formate Faradaic efficiency on a non-modified cathode and on a IL-modified by electrodeposited layer cathode in an H-type cell (cathode electrode is RVC) for a charge of 10 C at a current density of 3.4 mA/cm^2 and in a single pass flow electrolyzer in two-compartment in-flow configuration on a GDE cathode for a charge of 1000 C at a current density of 20 mA/cm^2 and a solution flow rate of 1.1 mL/min. Catholyte composition in both cases was 1 mM [Rh(bpy)(Cp)Cl]Cl in a 0.1 M acetate buffer solution at pH=3.8 saturated with [TBA][BF$_4$] and CO$_2$.*

H-type cell		**Flow Electrolyzer**	
Without layer	Electrodeposited layer	Without layer	Electrodeposited layer
40 %	53 %	32 %	45 %
Increment = 13 %		Increment = 13 %	

The majority of systems containing molecular catalysts described in literature have heterogenized catalysts and are therefore too dissimilar to be directly compared with our system[7,9–13,15]. The only other case where a molecular catalyst reduces CO_2 homogeneously is the case of [Ni(cyclam)$^{2+}$] in a non-aqueous flow electrolyzer[17], which despite our dissimilarities constitutes the most pertinent comparison for our conditions. In this study, [Ni(cyclam)$^{2+}$] is used to catalyze CO_2 reduction to CO in organic solvents (ACN or N, N'-DMF), using the supporting electrolyte $[NH_4][PF_6]$ simultaneously as sacrificial proton donor. Their overall cathodic reaction is therefore: $CO_2 + 2\ [NH_4]^+ + 2e^- \rightarrow CO + NH_3 + H_2O$. Meanwhile, in the anode they add ferrocene (Fc) as a sacrificial electron donor according to the half-

reaction: 2 Fc → 2 Fc^+ +2e^-. As a consequence, the |Ecell| reported are not easily comparable with our conditions of CO_2RR to formate coupled with OER. Though the aforementioned sacrificial donors do not themselves produce other CO_2RR products and some of their decomposition products can be isolated and recycled (it is not the case of Fe_3O_4 formed from oxidized ferrocene reacting with O_2), this process nevertheless is restrictive to the system's stability since they occasionally need replacement, especially in the recirculating flow configuration that they are implementing. In contrast, our system works in acidic aqueous conditions which are more environmentally-friendly, overcomes the CO_2 solubility limitation (0.033 M) by implementing gas-phase CO_2RR and does not need any further addition of sacrificial electron donor in the anolyte. As far as their best catalytic conditions are concerned, it is difficult to contrast, since their CO_2RR product is CO and they have selected a catalyst selective towards it, whereas we have deliberately opted for a catalyst that gives a mixture of products because our primary aim was always to study its selectivity in relation to the electrodeposited IL layer. Nevertheless, their highest CO selectivity of 83 % is observed at a moderate current density value of 12.7 mA/cm^2, whereas our highest formate production (average of 45 % with the electrodeposited layer) was obtained at 20 mA/cm^2. Another significant difference is the catalyst concentration used. Where our test at 5 mM of [Rh(bpy)(Cp*)Cl]Cl does not produce any more formate than the 1 mM originally used since the H-type cell tests presented in previous chapters, they report that increasing from 1 to 10 mM lead the optimal observed CO FE. Finally, contrary to our promising stability results over a span of 1000 C, they have observed poor stability of their catalyst in an environment that contains high amounts of CO. More particularly, $[Ni(cyclam)]^{2+}$ has been proven spectroscopically to decompose during the experiments and this effect is exacerbated by high overpotential values. This comparison is summarized in Table 5.2.

Table 5.2 Comparison of catalytic parameters for CO_2RR by homogeneous molecular catalysts in flow electrolyzers, according to cathode material, solvent, anodic half-reaction, configuration of flow electrolyzer, applied or measured current density, overall cell potential, CO_2 reduction product and FE for aforementioned product.

Molecular catalyst	Cathode material	Solvent/ Electrolyte	Anodic reaction	Electrolyzer type	Current density (mA/cm^2)	Cell potential (V)	Principal product	FE (%)	Reference
$[Ni(cyclam)^{2+}]$	Graphite felt	CH_3CN/ NH_4PF_6	Fc oxidation	2-compartment recirculation mode	12.7	1.7	CO	83	Jiang et. al.[17]
					18.9	1.8	CO	80	
[Rh(bpy)(Cp*)Cl]Cl	Bare GDE	H_2O/ 0.1 M acetate buffer 0.1M TBABF4	OER	2-compartment in-flow mode	20	6.4	$HCOO^-$	32	This study
	GDE with electrodeposited layer				20	5.1		45	

Though our system would not fare well in comparison to some heterogenized molecular catalysts in terms of activity and energy efficiency, it is in many ways superior to the other existing example of not

grafted CO_2RR catalyst in a flow electrolyzer setup. Most importantly, despite our catalyst's inherent low selectivity for formate, it is still highly promising that almost all of its catalytic features were clearly ameliorated through the implementation in the flow electrolyzer using an acidic aqueous catholyte composition.

5.4 Conclusions

In conclusion, for the first time, a study of an IL electrodeposited layer in molecular electrocatalysis of CO_2 was scaled-up from an H-type cell into a flow electrolyzer in aqueous acidic catholyte solution . The optimal catalytic conditions with a homogeneous molecular catalyst with modulable selectivity towards formate were obtained when the layer was grown on a GDE. Moreover, the most efficient setup for the flow electrolyzer itself was a two-compartment single-pass flow configuration. We have demonstrated the necessity of having a membrane separating the two compartments in order to achieve appreciable FE_{HCOO^-} and the importance of using highly basic anolyte to ensure the |Ecell| values remain at minimal values. Furthermore, we have provided evidence that a single-pass flow configuration is preferable when the [Rh(bpy)(Cp*)Cl]Cl used is in solution, since employing a recirculating flow configuration led to rapid formate production decrease over time, probably due to reoxidation of produced formate and/or the reduced active form of the catalyst. Besides, by implementing a bare GDE for gas-phase CO_2RR we were able to reach current densities up to 6 times higher than those in H-type cells, as well as maintain a stable FE_{HCOO^-} (32%) over the span of 1000 C, only 8 % inferior than the same value in an H-type cell with a porous carbon electrode at only 10 C. Finally, an electrodeposited IL layer was formed in aqueous solution on a GDE, as was evident by the system's increased selectivity towards formate that reached an average of 45% and was stable for 3 independent electrolysis of 1000 C, thus accumulation the same electrode a total of 3000 C without exhibiting any evident degradation in its performance. To sum up, the increment in FE_{HCOO^-} observed between the GDE with electrodeposited layer and the one without, which exhibits the same value as the one remarked in the H-type cell tests, is accompanied by an evident improvement in full-cell energy efficiency and significant decrease in energy consumption, proving that the effect of the electrodeposited IL layer is applicable in larger scale systems in weakly acidic aqueous solution.

5.5 References

(1) Qiao, J.; Liu, Y.; Hong, F.; Zhang, J. A Review of Catalysts for the Electroreduction of Carbon Dioxide to Produce Low-Carbon Fuels. *Chem Soc Rev* **2014**, *43* (2), 631–675.

(2) Benson, E. E.; Kubiak, C. P.; Sathrum, A. J.; Smieja, J. M. Electrocatalytic and Homogeneous Approaches to Conversion of CO_2 to Liquid Fuels. *Chem. Soc. Rev.* **2008**, *38* (1), 89–99.

(3) Verma, S.; Kim, B.; Jhong, H.-R. "Molly"; Ma, S.; Kenis, P. J. A. A Gross-Margin Model for Defining Technoeconomic Benchmarks in the Electroreduction of CO_2. *ChemSusChem* **2016**, *9* (15), 1972–1979. https://doi.org/10.1002/cssc.201600394.

(4) Verma, S.; Hamasaki, Y.; Kim, C.; Huang, W.; Lu, S.; Jhong, H.-R. M.; Gewirth, A. A.; Fujigaya, T.; Nakashima, N.; Kenis, P. J. A. Insights into the Low Overpotential Electroreduction of CO_2 to CO on a Supported Gold Catalyst in an Alkaline Flow Electrolyzer. *ACS Energy Lett.* **2018**, *3* (1), 193–198. https://doi.org/10.1021/acsenergylett.7b01096.

(5) Moeller, T.; Ju, W.; Bagger, A.; Wang, X.; Luo, F.; Thanh, T. N.; Varela, A. S.; Rossmeisl, J.; Strasser, P. Efficient CO_2 to CO Electrolysis on Solid Ni-N-C Catalysts at Industrial Current Densities. *Energy Environ. Sci.* **2019**, *12* (2), 640–647. https://doi.org/10.1039/c8ee02662a.

(6) Senocrate, A.; Battaglia, C. Electrochemical CO_2 Reduction at Room Temperature: Status and Perspectives. *J. Energy Storage* **2021**, *36*, 102373. https://doi.org/10.1016/j.est.2021.102373.

(7) Torbensen, K.; Boudy, B.; Joulié, D.; von Wolff, N.; Robert, M. Emergence of CO_2 Electrolyzers Including Supported Molecular Catalysts. *Curr. Opin. Electrochem.* **2020**, *24*, 49–55. https://doi.org/10.1016/j.coelec.2020.07.001.

(8) Verma, S.; Lu, X.; Ma, S.; Masel, R. I.; Kenis, P. J. A. The Effect of Electrolyte Composition on the Electroreduction of CO_2 to CO on Ag Based Gas Diffusion Electrodes. *Phys. Chem. Chem. Phys.* **2016**, *18* (10), 7075–7084. https://doi.org/10.1039/C5CP05665A.

(9) Wang, M.; Torbensen, K.; Salvatore, D.; Ren, S.; Joulié, D.; Dumoulin, F.; Mendoza, D.; Lassalle-Kaiser, B.; Işci, U.; Berlinguette, C. P.; Robert, M. CO_2 Electrochemical Catalytic Reduction with a Highly Active Cobalt Phthalocyanine. *Nat. Commun.* **2019**, *10* (1), 3602.

(10) Ren, S.; Joulié, D.; Salvatore, D.; Torbensen, K.; Wang, M.; Robert, M.; Berlinguette, C. P. Molecular Electrocatalysts Can Mediate Fast, Selective CO_2 Reduction in a Flow Cell. *Science* **2019**, *365* (6451), 367. https://doi.org/10.1126/science.aax4608.

(11) Lu, X.; Wu, Y.; Yuan, X.; Huang, L.; Wu, Z.; Xuan, J.; Wang, Y.; Wang, H. High-Performance Electrochemical CO_2 Reduction Cells Based on Non-Noble Metal Catalysts. *ACS Energy Lett.* **2018**, *3* (10), 2527–2532. https://doi.org/10.1021/acsenergylett.8b01681.

(12) Higgins, D.; Hahn, C.; Xiang, C.; Jaramillo, T. F.; Weber, A. Z. Gas-Diffusion Electrodes for Carbon Dioxide Reduction: A New Paradigm. *ACS Energy Lett.* **2019**, *4* (1), 317–324. https://doi.org/10.1021/acsenergylett.8b02035.

(13) Abdinejad, M.; Dao, C.; Zhang, X.-A.; Kraatz, H. B. Enhanced Electrocatalytic Activity of Iron Amino Porphyrins Using a Flow Cell for Reduction of CO_2 to CO. *J. Energy Chem.* **2021**, *58*, 162–169. https://doi.org/10.1016/j.jechem.2020.09.039.

(14) Jones, J.-P.; Prakash, G. K. S.; Olah, G. A. Electrochemical CO_2 Reduction: Recent Advances and Current Trends. *Isr. J. Chem.* **2014**, *54* (10), 1451–1466. https://doi.org/10.1002/ijch.201400081.

(15) Torbensen, K.; Han, C.; Boudy, B.; Wolff, N. von; Bertail, C.; Braun, W.; Robert, M. Iron Porphyrin Allows Fast and Selective Electrocatalytic Conversion of CO_2 to CO in a Flow Cell. *Chem. – Eur. J.* **2020**, *26* (14), 3034–3038. https://doi.org/10.1002/chem.202000160.

(16) Rogers, L.; Jensen, K. F. Continuous Manufacturing – the Green Chemistry Promise? *Green Chem.* **2019**, *21* (13), 3481–3498. https://doi.org/10.1039/C9GC00773C.

(17) Jiang, C.; Nichols, A. W.; Walzer, J. F.; Machan, C. W. Electrochemical CO_2 Reduction in a Continuous Non-Aqueous Flow Cell with [Ni(Cyclam)]2+. *Inorg. Chem.* **2020**, *59* (3), 1883–1892. https://doi.org/10.1021/acs.inorgchem.9b03171.

(18) Azcarate, I.; Costentin, C.; Robert, M.; Savéant, J.-M. Through-Space Charge Interaction Substituent Effects in Molecular Catalysis Leading to the Design of the Most Efficient Catalyst of CO_2-to-CO Electrochemical Conversion. *J. Am. Chem. Soc.* **2016**, *138* (51), 16639–16644.

(19) Hu, J.-M.; Zhang, J.-Q.; Cao, C.-N. Oxygen Evolution Reaction on IrO_2-Based DSA® Type Electrodes: Kinetics Analysis of Tafel Lines and EIS. *Int. J. Hydrog. Energy* **2004**, *29* (8), 791–797. https://doi.org/10.1016/j.ijhydene.2003.09.007.

(20) Paul, R.; Zemlyanov, D.; Roy, A. K.; Voevodin, A. A. Chapter 3 - Characterization Techniques and Analytical Methods of Carbon-Based Materials for Energy Applications. In *Carbon Based Nanomaterials for Advanced Thermal and Electrochemical Energy Storage and Conversion*; Paul, R., Etacheri, V., Wang, Y., Lin, C.-T., Eds.; Micro and Nano Technologies; Elsevier, 2019; pp 63–88. https://doi.org/10.1016/B978-0-12-814083-3.00003-2.

(21) Merino-Garcia, I.; Tinat, L.; Albo, J.; Alvarez-Guerra, M.; Irabien, A.; Durupthy, O.; Vivier, V.; Sánchez-Sánchez, C. M. Continuous Electroconversion of CO_2 into Formate Using 2 Nm Tin Oxide Nanoparticles. *Appl. Catal. B Environ.* **2021**, *297*, 120447.

(22) Whipple, D. T.; Kenis, P. J. A. Prospects of CO_2 Utilization via Direct Heterogeneous Electrochemical Reduction. *J. Phys. Chem. Lett.* **2010**, *1* (24), 3451–3458. https://doi.org/10.1021/jz1012627.

(23) Peugeot, A.; Creissen, C. E.; Schreiber, M. W.; Fontecave, M. Advancing the Anode Compartment for Energy Efficient CO_2 Reduction at Neutral PH. *ChemElectroChem* **2021**, *8* (14), 2726–2736. https://doi.org/10.1002/celc.202100742.

(24) König, M.; Vaes, J.; Klemm, E.; Pant, D. Solvents and Supporting Electrolytes in the Electrocatalytic Reduction of CO_2. *iScience* **2019**, *19*, 135–160. https://doi.org/10.1016/j.isci.2019.07.014.

(25) Huang, J. E.; Li, F.; Ozden, A.; Rasouli, A. S.; Arquer, F. P. G. de; Liu, S.; Zhang, S.; Luo, M.; Wang, X.; Lum, Y.; Xu, Y.; Bertens, K.; Miao, R. K.; Dinh, C.-T.; Sinton, D.; Sargent, E. H. CO2 Electrolysis to Multicarbon Products in Strong Acid. *Science* **2021**.

(26) Gu, J.; Liu, S.; Ni, W.; Ren, W.; Haussener, S.; Hu, X. Modulating Electric Field Distribution by Alkali Cations for CO_2 Electroreduction in Strongly Acidic Medium. **2021**. https://doi.org/10.33774/chemrxiv-2021-zgq9k.

(27) Chambers, M. B.; Wang, X.; Elgrishi, N.; Hendon, C. H.; Walsh, A.; Bonnefoy, J.; Canivet, J.; Quadrelli, E. A.; Farrusseng, D.; Mellot-Draznieks, C.; Fontecave, M. Photocatalytic Carbon Dioxide Reduction with Rhodium-Based Catalysts in Solution and Heterogenized within Metal-Organic Frameworks. *ChemSusChem* **2015**, *8* (4), 603–608.

CHAPTER 5: SCALE-UP TEST OF A HOMOGENEOUS CATALYST IN A FLOW ELECTROLYZER FOR ELECTROCATALYTIC CO2 REDUCTION

CHAPTER 6: GENERAL CONCLUSIONS AND OUTLOOK

Overall, in order to optimize a catalytic system, considerations about activity, selectivity and stability must be taken into account. Because of the recently reported cocatalytic activity between molecular catalysts and ionic liquids for CO_2RR, their combined study is considered appealing in this context. However, no in-depth study of the structure-activity relationship between different molecular catalysts and a variety of ILs had been reported at the beginning of this thesis, which is the reason we investigated them in depth experimentally, as well as with some theoretical calculations. We explored in this work the further improvement of catalytic performance by combining molecular catalysts with ILs in solution or immobilized on surfaces to favor CO_2RR activity and selectivity and scaled-up the most pertinent catalytic system by testing it within a flow electrolyzer.

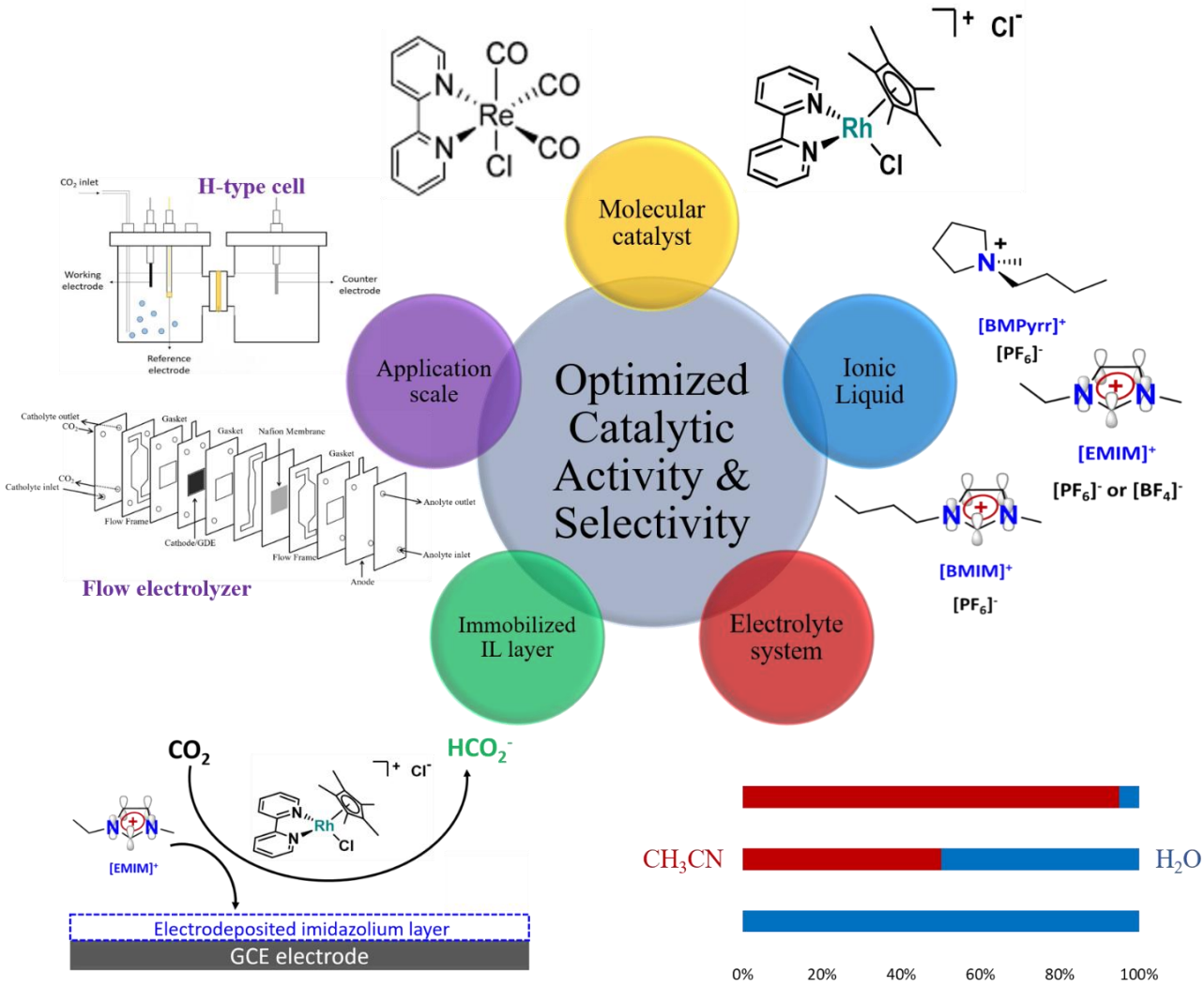

Figure 6.1 Outlook of this thesis

6.1 General Conclusions

The role of ionic liquids (ILs) as promoters for CO_2 electroreduction (CO_2RR) has been studied in this thesis following two different strategies:

1) Electrolyte engineering strategy:

- The interaction of a series of ILs used as supporting electrolytes with two model molecular catalysts with distinct CO_2RR mechanisms is shown and explained by experimental, as well as theoretical data.
- Selective CO_2-to-CO reduction catalyst [Re(bpy)$(CO)_3$Cl] displayed a cocatalytic interaction with both imidazolium-based and pyrrolidinium-based ILs in acetonitrile. This was demonstrated by significant decrease in its characteristic reduction potentials by as much as 370 mV under inert and CO_2 atmospheres. Imidazolium-based ILs produced a more prominent effect than pyrrolidinium-based ILs. The only protic IL tested did not interact with the catalyst and instead produced H_2 directly on the electrode surface.
- Under CO_2 and in the absence of an explicit proton source, ILs reduce the overpotential of [Re(bpy)$(CO)_3$Cl] by 200 – 330 mV compared to the benchmark supporting electrolyte. This is possibly due to an "electron-first" reported mechanistic pathway[1] that forms mono-anionic and di-anionic catalyst intermediates that can be successfully stabilized electrostatically by IL cations present in the electrical double layer. The superior effect produced by imidazolium over pyrrolidinium ILs can be attributed to their aromatic nature and they have been reported[2] to interact with the bipyridine ligand of catalyst [Re(bpy)$(CO)_3$Cl] through π^+-π interaction.
- However, in the presence of an explicit proton source (1.5 M TFE) the decrease in overpotential for CO_2RR by catalyst [Re(bpy)$(CO)_3$Cl] is down to 30 – 70 mV. In those conditions, a "proton-first" mechanistic pathway is favored[1], that involves formation of a neutral and a mono-anionic catalyst intermediate, which are less efficiently involved in electrostatic stabilization by IL cations in the electrical double layer.
- Overall, the beneficial effect of ILs on [Re(bpy)$(CO)_3$Cl] catalyst by overpotential diminution was offset by slight loss of selectivity for CO over H_2. This led to high energy efficiency values (47 % – 53 %) for the entire series of ILs in presence of an external proton source, but they were lower than the value obtained using the benchmark electrolyte (61 %).
- Catalyst [Rh(bpy)(Cp*)Cl]Cl, that produces a mixture of formate and H_2 under reductive conditions, was explored with the series of ILs and tested in both acetonitrile and aqueous conditions.

- Electrolysis experiments performed with catalyst [Rh(bpy)(Cp*)Cl]Cl and ILs in acetonitrile solution displayed an almost 800 mV decrease in overpotential compared to the benchmark electrolyte for the appreciable current density value of 3.33 mA/cm^2. Meanwhile, the selectivity was tuned in favor of formate evolution, resulting in faradaic efficiency values equal to or exceeding 90 %, leading to a maximum EE value of 66 %.
- [Rh(bpy)(Cp*)Cl]Cl was also tested alongside imidazolium IL [EMIM][BF_4] in acidic aqueous solution. The decrease of current density due to decreased CO_2 solubility (33 mM in 25 °C) was compensated by the addition of acetic acid as an additional proton source. This allowed not only to restore high current densities, but also to obtain a CO_2RR product distribution of 1/1 for FE_{HCOO^-}/FE_{H2}. Overall, this catalytic system operated at the exceptionally low overpotential of 280 mV and reached a maximum EE value of 32 %.
- DFT calculations corroborated the decrease in overpotential seen in experimental results, as they proved the formation of an adduct between the active form of catalyst [Rh(bpy)(Cp*)Cl]Cl and the [EMIM]$^+$. They also explain the HER suppression and CO_2RR promoting effect of ILs, because in the presence of ILs the free-energy of the HER pathway is disproportionately increased in comparison to the free-energy for formate production.

2) <u>Electrode surface engineering strategy:</u>

- A simple and convenient method for imidazolium-based IL electrodeposition on different electrode materials (GCE, AuE) is presented and its resulting catalytic effect for CO_2RR is assessed on the model catalyst [Rh(bpy)(Cp*)Cl]Cl system in both acetonitrile and aqueous conditions. Optimization studies of this electrodeposited IL layer are presented on this catalytic system, as well as catalytic comparisons with a IL layer covalently attached to the electrode described in the literature[3], but never applied before for a catalytic purpose.
- Elucidation of the nature of this electrodeposited IL layer is achieved through XPS and electrochemical characterization. More particularly, the presence of N atoms bound on the electrode surface and N from an imidazole ring in XPS spectra, proved the presence of this IL layer on the electrode surface.
- The ability of the electrodeposited IL layer to suppress HER is also demonstrated in various electrolyte compositions with and without catalyst [Rh(bpy)(Cp*)Cl]Cl. This could be attributed to electrostatic repulsion between the protons and the apparently cationic nature of this IL layer.
- In electrolysis experiments with [Rh(bpy)(Cp*)Cl]Cl catalyst, the electrodeposited IL layer led to even higher formate production over HER than using the same IL in solution. In acetonitrile conditions with the electrodeposited IL layer, we obtained a maximum FE_{HCOO^-} of 85 % at a current density value of 3.33 mA/cm^2 and EE of 59 % in comparison with FE_{HCOO^-} of 69 % and

EE of 47 % with IL in solution. All at an overpotential 800 mV lower than on a bare electrode with the benchmark electrolyte. Meanwhile, in acidic acetate buffer solutions, the electrodeposited IL layer led to FE_{HCOO^-} of 53 % at only 380 mV of overpotential, resulting in an EE value of 33 %.

- Overall, this IL layer proved to be stable and obtain appreciable formate yields in acidic aqueous conditions, that are crucial in avoiding CO_2 loss as bicarbonate or carbonate, as is the case at alkaline pH values.

In addition to the fundamental knowledge accumulated, a significant effort to scale up the CO_2 conversion to formate process have been also carried out in this thesis. Then, from 10 C electrolysis in an H-type cell at 3.33 mA/cm^2, we have been able to reach 1000 C electrolysis by scaling the electrodes size up to 10 cm^2 in a flow electrolyzer working at 20 mA/cm^2. This approach combining the high selectivity of a molecular catalyst with the scalability of a flow electrolyzer reaches a significant catalytic current density and keeps the product selectivity control.

In conclusion, extensive study and rationalization of the interactions between molecular catalysts and ILs were shown in this thesis. We have used different model catalysts, varied the nature and components of the ILs used, as well as immobilizing them and tested them in different electrolyte conditions. Those studies permitted us to determine the factors governing the catalytic activity, illustrated by increasing values of current density in aqueous solution, and the product selectivity at very low overpotential values by simultaneous HER suppression and enhanced efficiency for CO_2RR products. Finally, the stability of the catalytic system containing an electrodeposited IL layer was demonstrated over long-term electrolysis (over 3000 C) performed within the flow electrolyzer.

6.2 Outlook

From the aforementioned results, many new and exciting research pathways shine strongly and will be worthy to explore them. Listed here are a few outlooks related to the results mentioned above:

- Since the bipyridine ligand of both of the catalysts used in the thesis was reported to present π^+-π interaction with imidazolium-based ILs, the cocatalytic effect of ILs could be explored with other molecular catalysts containing one or more bpy ligands, such as the ones shown in Figure 6.2.

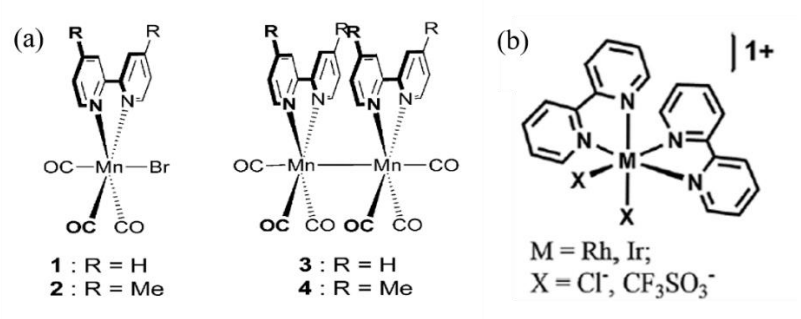

Figure 6.2 Structures of molecular catalysts with one or multiple bpy ligands: (a) Manganese monomer and dimer complexes with bpy and carbonyl ligands[4] *and (b) Polyriridyl Rhodium or Iridium complexes*[5].

- In order to broaden the scope of IL interactions with molecular catalysts would also be of interest to target other CO_2RR products different than CO and formate, such as methane[6].
- Another strategy that would permit studying IL interactions with molecular catalysts consists of incorporating an IL moiety and more specifically an imidazolium ring, into the structure of the molecular catalyst itself leading to the synthesis of a novel catalyst. A couple of examples in the literature have already demonstrated that such inclusions led to enhanced catalytic performance[7,8].
- Considering the outstanding catalytic performance of the presented electrodeposited IL layer with molecular catalysts, studies could also be envisioned about its potential cocatalytic effect with heterogeneous catalysts. Some studies have already shown the possibility of growing an IL-based layer on Cu electrodes for enhanced CO_2RR[9]. Building on our own results, alongside other studies performed on layers from pyridinium cations[10], it could open many original possibilities in the field of heterogeneous surface modification.
- Meanwhile, the effect of this electrodeposited IL layer could also be tested in other electrochemical reduction reactions besides CO_2RR, such as N_2O reduction[11].
- Finally, the selected catalytic system already tested in laboratory scale within a flow electrolyzer could be further optimized and scaled up to industrial scale. This would lead to additional tests from an engineering perspective, such as more extensive design of the flow electrolyzer.

6.3 References

(1) Clark, M. L.; Cheung, P. L.; Lessio, M.; Carter, E. A.; Kubiak, C. P. Kinetic and Mechanistic Effects of Bipyridine (Bpy) Substituent, Labile Ligand, and Brønsted Acid on Electrocatalytic CO_2 Reduction by Re(Bpy) Complexes. *ACS Catal.* **2018**, *8* (3), 2021–2029. https://doi.org/10.1021/acscatal.7b03971.

(2) Matsubara, Y.; Grills, D. C.; Kuwahara, Y. Thermodynamic Aspects of Electrocatalytic CO_2 Reduction in Acetonitrile and with an Ionic Liquid as Solvent or Electrolyte. *ACS Catal.* **2015**, *5* (11), 6440–6452. https://doi.org/10.1021/acscatal.5b00656.

(3) Bouden, S.; Gómez-Mingot, M.; Randriamahazaka, H.; Ghilane, J. Surface Initiated Immobilization of Molecules Contained in an Ionic Liquid Framework. *Anal. Chem.* **2016**, *88* (1), 1017–1021. https://doi.org/10.1021/acs.analchem.5b03922.

(4) Bourrez, M.; Molton, F.; Chardon-Noblat, S.; Deronzier, A. [Mn(Bipyridyl)$(CO)_3$Br]: An Abundant Metal Carbonyl Complex as Efficient Electrocatalyst for CO_2 Reduction. *Angew. Chem. Int. Ed.* **2011**, *50* (42), 9903–9906. https://doi.org/10.1002/anie.201103616.

(5) Bolinger, C. M.; Sullivan, B. P.; Conrad, D.; Gilbert, J. A.; Story, N.; Meyer, T. J. Electrocatalytic Reduction of CO_2 Based on Polypyridyl Complexes of Rhodium and Ruthenium. *J. Chem. Soc. Chem. Commun.* **1985**, No. 12, 796–797. https://doi.org/10.1039/C39850000796.

(6) Nganga, J. K.; Wolf, L. M.; Mullick, K.; Reinheimer, E.; Saucedo, C.; Wilson, M. E.; Grice, K. A.; Ertem, M. Z.; Angeles-Boza, A. M. Methane Generation from CO_2 with a Molecular Rhenium Catalyst. *Inorg. Chem.* **2021**, *60* (6), 3572–3584. https://doi.org/10.1021/acs.inorgchem.0c02579.

(7) Sung, S.; Kumar, D.; Gil-Sepulcre, M.; Nippe, M. Electrocatalytic CO_2 Reduction by Imidazolium-Functionalized Molecular Catalysts. *J. Am. Chem. Soc.* **2017**, *139* (40), 13993–13996. https://doi.org/10.1021/jacs.7b07709.

(8) Khadhraoui, A.; Gotico, P.; Boitrel, B.; Leibl, W.; Halime, Z.; Aukauloo, A. Local Ionic Liquid Environment at a Modified Iron Porphyrin Catalyst Enhances the Electrocatalytic Performance of CO_2 to CO Reduction in Water. *Chem. Commun.* **2018**, *54* (82), 11630–11633. https://doi.org/10.1039/C8CC06475J.

(9) Wang, Y.; Hayashi, T.; He, D.; Li, Y.; Jin, F.; Nakamura, R. A Reduced Imidazolium Cation Layer Serves as the Active Site for Electrochemical Carbon Dioxide Reduction. *Appl. Catal. B Environ.* **2020**, *264*, 118495. https://doi.org/10.1016/j.apcatb.2019.118495.

(10) Han, Z.; Kortlever, R.; Chen, H.-Y.; Peters, J. C.; Agapie, T. CO_2 Reduction Selective for C≥2 Products on Polycrystalline Copper with N-Substituted Pyridinium Additives. *ACS Cent. Sci.* **2017**, *3* (8), 853–859. https://doi.org/10.1021/acscentsci.7b00180.

(11) Deeba, R.; Molton, F.; Chardon-Noblat, S.; Costentin, C. Effective Homogeneous Catalysis of Electrochemical Reduction of Nitrous Oxide to Dinitrogen at Rhenium Carbonyl Catalysts. *ACS Catal.* **2021**, *11* (10), 6099–6103. https://doi.org/10.1021/acscatal.1c01197.

Résumé de la Thèse en Français

La réduction électrochimique du CO_2 (CO_2RR) est une approche écologique qui permet de créer des produits à valeur ajoutée à partir d'un polluant et de potentiellement stocker l'énergie intermittente générée par des sources d'énergie renouvelable. Parmi ces produits potentiels on peut citer ceux qui nécessitent deux électrons, tels que le monoxyde de carbone (CO) et l'acide formique (HCOOH) et d'autres qui en nécessitent plus comme le méthanol (CH_3OH), l'éthanol (CH_3CH_2OH), l'éthylène (C_2H_4), l'acétone ($(CH_3)_2CO$), etc. Cependant, la réduction du CO_2 est thermodynamiquement et cinétiquement défavorable. Afin de dépasser les contraintes cinétiques, l'usage des catalyseurs est nécessaire[1–3]. Le catalyseur doit être économiquement intéressant et suffisamment stable, doté d'une haute sélectivité des produits de réduction de CO_2 et d'une excellente performance catalytique[4]. Hormis le choix du catalyseur, plusieurs paramètres doivent être également pris en compte et optimisés pour permettre la conversion du CO_2, tels que le choix d'électrolyte et de sel de fond, la solubilité du CO_2, le pH local, la conception de la cellule électrochimique, la température et la pression[5–7].

En ce qui concerne le catalyseur, on peut utiliser soit des catalyseurs hétérogènes (d'habitude les électrodes métalliques), soit des catalyseurs homogènes, qui sont des complexes organométalliques capables de réduire le CO_2. Cette thèse concerne exclusivement l'usage des catalyseurs moléculaires. Ils permettent notamment d'améliorer l'activité de la catalyse, sa sélectivité et son efficacité[8–10]. Les catalyseurs moléculaires ont été largement étudiés puisqu'ils possèdent des caractéristiques électroniques réglables en fonction de leurs centres métalliques et de leurs ligands[11]. Un autre avantage des catalyseurs moléculaires est le fait que leurs mécanismes catalytiques de réduction de CO_2 sont souvent bien compris et peuvent alors servir en tant que systèmes modèles. Les deux catalyseurs utilisés pendant cette thèse appartiennent à la catégorie des catalyseurs moléculaires. Le premier catalyseur est le complexe $[Re(bpy)(CO)_3Cl]$, connu également comme catalyseur de Lehn. Ce catalyseur est capable de réduire le CO_2 en CO de manière sélective par voie électrochimique et photochimique[12,13]. Plusieurs études ont cherché à améliorer son efficacité énergétique, c'est-à-dire de maintenir une haute sélectivité pour la production de CO tout en diminuant le surpotentiel et en ayant une haute densité de courant[13]. Le deuxième catalyseur moléculaire modèle utilisé est le complexe $[Rh(bpy)(Cp^*)Cl]Cl$, qui produit un mélange d'acide formique et d'hydrogène, parce qu'il catalyse à la fois la réduction de CO_2 et la réduction des protons en H_2[14,15]. Son mécanisme catalytique de la réduction de CO_2 est également compris et peut varier en fonction des plusieurs paramètres, comme par exemple le potentiel appliqué ou l'environnement catalytique. De plus, ce catalyseur est soluble dans des solvants organiques, ainsi que dans l'eau, ce qui en fait un système très intéressant pour étudier l'effet produit sur sa sélectivité par

divers solvants et électrolytes. Les mécanismes catalytiques de la réduction de CO_2 de ces deux catalyseurs moléculaires sont montrés sur la Figure 1.

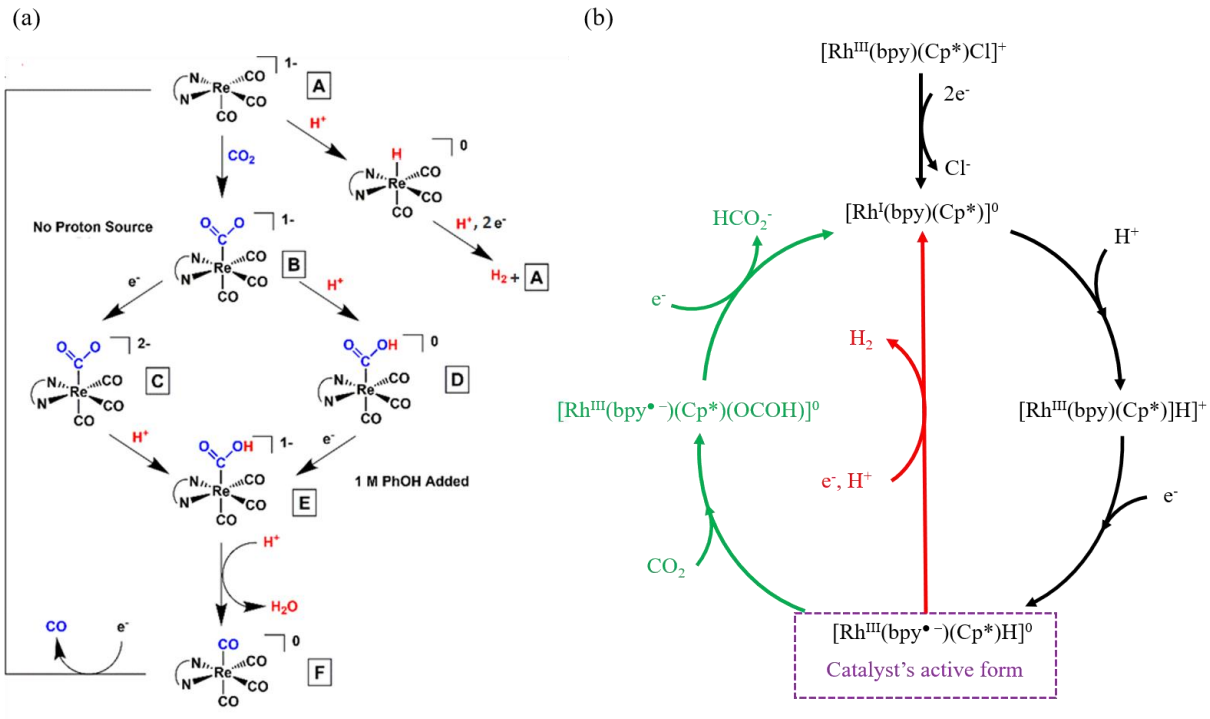

Figure 1. Mécanisme catalytique de la réduction de CO_2 par : (a) le catalyseur de Lehn [Re(bpy)(CO)$_3$Cl] en présence et en absence d'une source des protons externe[13] *et (b) le catalyseur [Rh(bpy)(Cp*)Cl]Cl. Le chemin (b) est adapté de Caix et. al.*[15] *et des études théoriques présentées dans la thèse.*

Une stratégie complémentaire visant à améliorer l'efficacité catalytique des catalyseurs moléculaires est l'ingénierie du système électrolytique et, plus particulièrement, le choix judicieux du solvant et du sel de fond. L'eau est souvent privilégiée en tant que solvant pour des raisons économiques et écologiques. Cependant, parmi ses désavantages on peut citer une solubilité de CO_2 inférieure à celle constatée dans des solvants organiques, le fait que la production du H_2 est souvent favorisée et, finalement, le fait que certains catalyseurs moléculaires ne sont solubles que dans des milieux organiques. Les liquides ioniques (ILs) sont considérés en tant que solvants alternatifs. Ils sont entièrement composés de cations organiques et d'anions organiques ou inorganiques, ce qui leur permet d'assurer la conductivité de la solution sans ajout d'un autre sel de fond. De plus, ils sont stables sur une large fenêtre électrochimique et améliorent la solubilité de CO_2 par rapport à l'eau[16–18]. Leur désavantage principal est leur grande viscosité, inversement proportionnelle à la conductivité du solvant. La faible conductivité se traduit en une limitation de transfert de masse et, par conséquent, mène à la baisse la densité maximale du courant observé[6]. Une possibilité alternative sera alors d'utiliser les ILs en tant que le sel de fond dans des mélanges binaires avec d'autres solvants.

RÉSUMÉ EN FRANÇAIS

Depuis le travail fondamental de Rosen et. al.[19] paru en 2011, l'effet synergique d'un IL a été montré sur des électrodes d'argent. Dans cette étude, la présence de 18 mol % de 1-Ethyl-3-methylimidazolium tetrafluoroborate ([EMIM][BF_4]) dans l'eau a baissé de manière significative la barrière énergétique de réduction de CO_2 en formant des adduits entre la forme réduite du cation imidazolium et le CO_2. Depuis, de nombreuses études ont été consacrées au rôle cocatalytique des cations imidazolium pour la CO_2RR. Plus récemment, il a été montré que les cations imidazolium peuvent être réduits sur la surface des divers électrodes (ex. Ag, Pt) pour ensuite former des complexes avec le CO_2. Cela conduit à la diminution du surpotentiel nécessaire pour la réduction défavorable de CO_2 à un électron vers $CO_2^{\bullet -}$[18,20]. Ainsi, dans une autre étude, en utilisant aussi l'électrode d'argent, les auteurs ont montré le rôle majeur que jouent les protons sur les positions C4 et C5 de l'imidazolium grâce à leur capacité de former des liaisons hydrogène avec le CO_2 adsorbé à la surface de l'électrode[21]. Hormis des ILs de type imidazolium, d'autres ILs avec des cations non réductibles, tels que les pyrrolidinium, ont prouvé leur capacité de favoriser la CO_2RR en modifiant la double couche electrochimique[20].

Néanmoins, la plupart des études qui utilisent des ILs sont réalisées avec des catalyseurs hétérogènes. En revanche, il n'existe que peu d'exemples dans la littérature traitant le rôle cocatalytique des ILs dans la CO_2RR électrochimique utilisant des catalyseurs moléculaires dans des milieux organiques. Matsubara et. al.[22] ont étudié par la voltamètrie linéaire et par des calculs théoriques le rôle du IL de type imidazolium, le $[EMIM]^+$, dans l'acétonitrile pour la réduction du CO_2 catalysée par le catalyseur de Lehn. De plus, Choi et. al.[23] ont étudié le rôle cocatalytique d'un autre IL, le 1-Butyl-3-methylimidazolium tetrafluoroborate ([BMIM][BF4]), dans un autre solvant organique pour la conversion du CO_2 en CO catalysée par une tetraphenylporphyrine de fer (Fe-TPP). Dans ces deux cas, une diminution du surpotentiel nécessaire pour la réduction a été constatée en présence des ILs. On peut également citer des exemples de catalyseurs moléculaires synthétiquement modifiés pour inclure des bras imidazolium sur leurs ligands. C'est le cas d'un catalyseur du type de celui de Lehn[24] et d'une tetraphenylporphyrine de fer[25]. Dans les deux cas, l'introduction des unités imidazolium a été montrée bénéfique pour l'efficacité de la catalyse de CO_2RR.

Les objectifs principaux de cette thèse sont :

1. D'étudier l'effet des ILs sur les catalyseurs moléculaires modèles pour la CO_2RR
2. D'explorer des concepts d'ingénierie de l'électrolyte et d'immobilisation des ILs pour la CO_2RR
3. De montrer l'applicabilité de ce système à grande échelle par des expériences réalisées au sein d'un électrolyseur en flux continu.

RÉSUMÉ EN FRANÇAIS

Chapitre 1

Dans le chapitre 1, l'état de l'art servant la base théorique de cette thèse est présenté en détail.
Il comprend une brève description des enjeux autour de la réduction catalytique du CO_2, ainsi que des exemples de catalyseurs moléculaires. Ensuite, les caractéristiques des liquides ioniques, des solvants alternatifs et cocatalyseurs de CO_2RR, sont détaillées. Finalement, la possibilité de la combinaison des catalyseurs moléculaires et des liquides ioniques en solution est discutée.

Chapitre 2

Le chapitre 2, nommé « matériaux et méthodes » comprend la liste des réactifs chimiques utilisés pendant la thèse, des matériaux des électrodes, des composants au sein de l'électrolyseur en flux et des équipements utilisés. Le chapitre inclut également les brèves descriptions des techniques électrochimiques utilisées pendant ces travaux, ainsi que des techniques physicochimiques de caractérisation de surface, tels que la spectrométrie de photoélectrons induits par rayons X. En outre, la description des techniques d'analyses des produits de réduction de CO_2 après des expériences d'électrolyse est présentée. Ce chapitre comprend également les détails des calculs théoriques autour de l'interaction entre le catalyseur [Rh(bpy)(Cp*)Cl]Cl et les cations imidazolium, qui ont été réalisés par nos collaborateurs.

Chapitre 3

Le chapitre 3 est consacré à l'étude de l'activité catalytique des catalyseurs moléculaires en présence d'une série de liquides ioniques utilisés en tant que sels de fond afin de rationaliser leur rôle cocatalytique. La Figure 2 montre les structures des deux catalyseurs [Re(bpy)$(CO)_3$Cl] [1] et [Rh(bpy)(Cp*)Cl]Cl [2], où bpy est 2,2'-bipyridine et Cp* est 1,2,3,4,5-pentacyclopentadienyl, ainsi que tous les liquides ioniques utilisés pendant cette étude. Les mécanismes catalytiques de deux catalyseurs modèles choisis sont bien compris[12–15]. Parmi cette série des liquides ioniques on a testé quatre cations et trois anions distincts. La plupart des cations appartiennent à la famille des imidazolium (Fig. 2a, b, c, e), l'un appartient à la famille des pyrrolidinium (Fig. 2d). La Figure 2f montre la structure du sel de fond conventionnel utilisé.

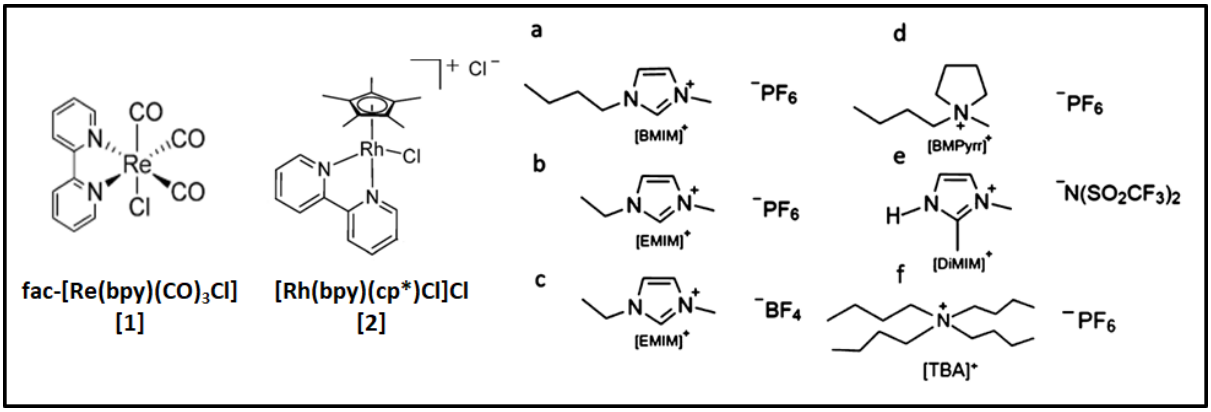

Figure 2. Structures des complexes [Re(bpy)(CO)$_3$Cl] [1] et [Rh(bpy)(Cp)Cl]Cl [2], dont bpy = 2,2'-bipyridine et Cp* = 1,2,3,4,5-pentacyclopentadienyl, et la série des sels de fond: a) 1-Butyle-3-methylimidazolium hexafluorophosphate ([BMIM][PF$_6$]), b) 1-Ethyle-3-methylimidazolium hexafluorophosphate ([EMIM][PF$_6$]), c) 1-Ethyle-3-methylimidazolium tetrafluoroborate ([EMIM][BF$_4$]), d) 1-Butyle-1-methylpyrrolidinium hexafluorophosphate ([BMPyrr][PF$_6$]), e) 1,2-Dimethylimidazolium bis(trifluoromethylsulfonyl)imide ([DiMIM][N(SO$_2$CF$_3$)$_2$]) et f) Tetrabutyle ammonium hexafluorophosphate ([TBA][PF$_6$]).*

La Figure 3a montre les voltammogrammes cycliques sous atmosphère inerte des solutions d'acétonitrile contenant du catalyseur [1] à 1 mM en présence de 0,5 M de trois sels de fond différents, le conventionnel [TBA][PF$_6$] et les deux liquides ioniques, l'imidazolium ([BMIM][PF$_6$]) et le pyrrolidinium ([BMPyrr][PF$_6$]). L'anion est le même dans ces trois cas, ce qui permet d'évaluer exclusivement l'importance du cation. Le premier pic de la réduction quasi-réversible est attribué à la réduction à un électron situé sur le ligand bipyridine, tandis que le deuxième pic est attribué à la réduction du centre métallique de Re^I à Re^0. Notons que : (i) les deux processus redox sont déplacés vers des valeurs de potentiel plus anodiques quand des liquides ioniques sont présents par rapport au [TBA][PF$_6$] ; (ii) le déplacement de la deuxième réduction est bien plus marqué par rapport à celui de la première ; (iii) ces déplacements sont dépendants de la nature du liquide ionique utilisé, avec l'imidazolium produisant un effet supérieur par rapport au pyrrolidinium. La même tendance se dessine quand la comparaison est faite sous une atmosphère de CO_2 (Fig. 3b). On constate que le deuxième pic de la réduction est plus haut en termes de densité de courant. Cela reflète la présence d'une vague catalytique de réduction de CO_2 quand le catalyseur est réduit à deux électrons. En fonction du liquide ionique utilisé la réduction de surpotentiel de CO_2RR est plus ou moins importante, ses valeurs allant de 200 mV à 330 mV. En revanche, une fois qu'une source des protons, 1,5 M de trifluoroéthanol, est ajoutée au système, la diminution du surpotentiel est moins marquée, comme le montre la Figure 3c. Néanmoins, la vague catalytique est plus intense dans les trois cas, parce que l'abondance des protons accessibles facilite les réactions de transfert d'électrons qui abaissent les barrières énergétiques pour la CO_2RR. Le fait que les liquides ioniques diminuent plus drastiquement le surpotentiel en absence de source des protons peut

être expliqué par le mécanisme d'action du catalyseur. Selon le mécanisme représenté sur la Figure 1a, en absence de source des protons l'ajout d'un électron précède celui d'un proton et, par conséquent, les intermédiaires du catalyseur sont chargés négativement à un ou deux électrons. Ces formes peuvent être électrostatiquement stabilisées par les cations des liquides ioniques et si ceux-là sont aromatiques, tels que les imidazolium, ils peuvent avoir des interactions de type π-π *stacking*. Par contre, si une source de protons est présente dans le milieu catalytique, l'ajout d'un proton est prioritaire. Cela produit un intermédiaire neutre et un autre chargé -1, qui ne peut pas être si efficacement stabilisé par les cations imidazolium. Sur la Figure 3d l'efficacité faradique en CO et H_2 d'une série des électrolyses à potentiel -2,05 V *vs.* Fc^+/Fc est montrée. Dans toutes les conditions le produit majoritaire est le CO et le seul autre produit minoritaire détecté est du H_2[26].

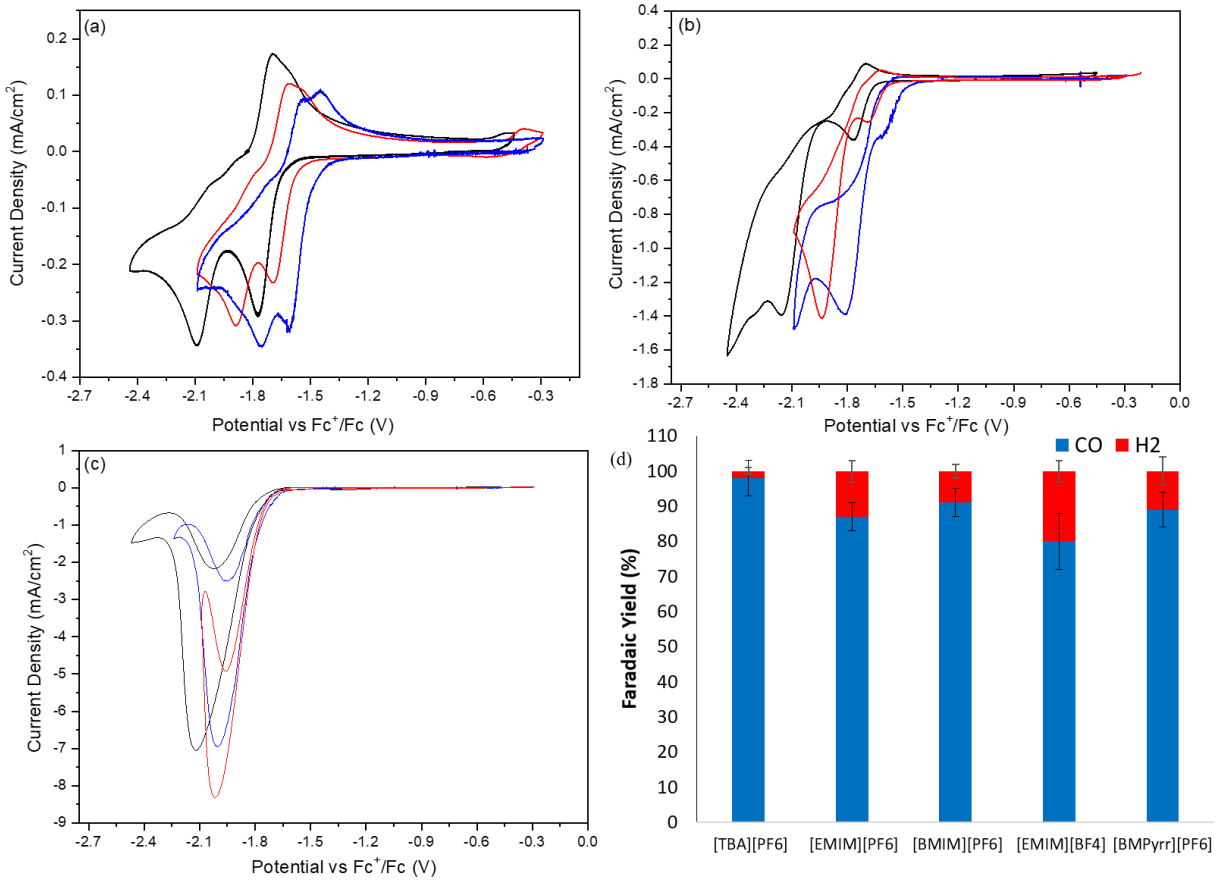

Figure 3. Voltammogrammes cycliques de 1 mM catalyseur [1] et 0,5 M de sels de fond différents dans l'acetonitrile, [TBA][PF_6] est en noir, [BMPyrr][PF_6] est en vert et [BMIM][PF_6] est en bleue : (a) sous atmosphère inerte, (b) sous CO_2 et (c) sous CO_2 avec 1,5 M de trifluoroéthanol ajouté. Vitesse de balayage est 0,1 V/s. (d) Efficacité faradique des électrolyses dans l'acetonitrile avec 0,5 M de chaque sel de fond et 1,5 M de trifluoroéthanol sous CO_2 à potentiel appliqué de -2,05 V vs. Fc^+/Fc pour une charge passée de 15 C.

En utilisant le catalyseur [2] des analyses sont réalisées à la fois dans des solutions d'acétonitrile (Figure 4a et b) et dans des solutions aqueuses (Figure 5a et b) sous conditions catalytiques. Dans l'acétonitrile, ce catalyseur possède deux pics caractéristiques de la réduction, l'un centré à -1,21 V *vs.* Fc^+/Fc correspondant à la réduction réversible à deux électrons du centre métallique, suivi par un deuxième pic à -2,60 V attribué à la réduction à un électron du ligand bipyridine sous atmosphère inerte ou sous CO_2 sans ajout de source de protons. Néanmoins, la réduction des cations imidazolium aux potentiels inferieures à -2,3 V empêche d'évaluer l'interaction entre le catalyseur et les liquides ioniques sous ces conditions. Pourtant, quand une source de protons est présente le pic de réduction de bipyridine est déplacé anodiquement vers -2,14 V et suivi par une hausse de densité de courant avec le sel de fond conventionnel. Sur la Figure 4a et 4b on observe la réponse catalytique en présence de catalyseur [2] à 1 mM, 5 % (vol.) de l'eau, ainsi que de 0,5 M de sels de fond différents dans l'acétonitrile sous CO_2. La présence des liquides ioniques conduit à une légère diminution du surpotentiel de la CO_2RR de 30 à 70 mV et à une augmentation de la densité de courant catalytique dans tous les cas représentés. De plus, le changement de l'anion du liquide ionique entre $[PF_6]^-$ et $[BF_4]^-$ n'a que peu d'effet : ni le potentiel ni la densité de courant ne sont pas impactés de manière significative (Fig. 4a). En revanche, le changement de la longueur de la chaine alkyle sur le cation imidazolium d'éthyle en butyle diminue à la fois le potentiel et la densité de courant observés (Fig. 4b). Par conséquent, dans la suite de l'étude le liquide ionique [EMIM][PF_6] est utilisé.

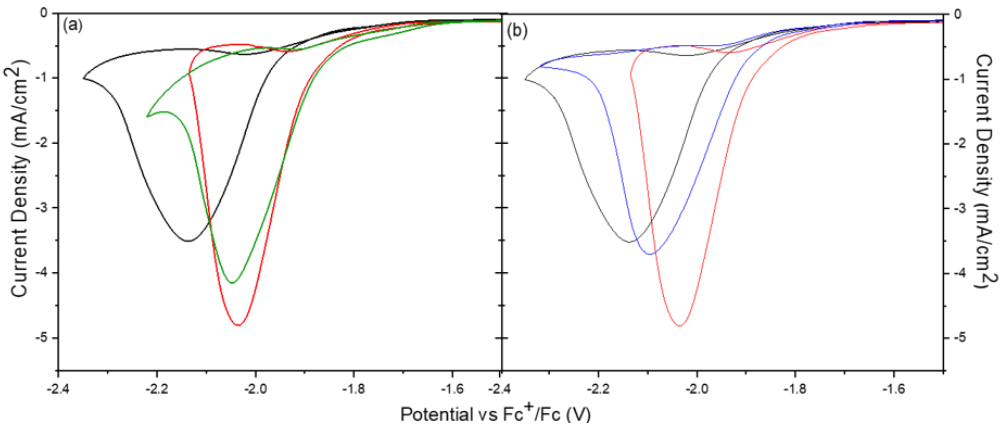

Figure 4. (a) et (b) Voltammogrammes cycliques de 1 mM catalyseur [2] et 0,5 M de sels de fond différents dans la solution d'acétonitrile qui contient 5 % (vol.) de l'eau sous atmosphère de CO2 : [TBA][PF_6] (en noir), [EMIM][PF_6] (en rouge), [EMIM][BF_4] (en vert) et [BMIM][PF_6] (en bleu). Potentiels rapportés versus le standard interne Fc^+/Fc (V).

En outre, la Figure 5 montre l'effet catalytique du catalyseur [2] à 1 mM dans une solution aqueuse contenant soit le sel de fond [TBA][BF_4] (5a), soit du liquide ionique [EMIM][BF_4] (5b). On constate

une diminution de surpotentiel de 80 mV similaire aux conditions organiques, mais également une baisse importante de la densité de courant liée à la diminution de solubilité de CO_2 (en bleu) d'une valeur de 240 mM dans l'acétonitrile contenant 5 % (vol.) H_2O[27] à une valeur de 33 mM[6] dans une solution aqueuse. Une valeur de densité de courant plus élevée peut être atteinte avec l'ajout du tampon acétate à pH=4 (en bleu pointillé), qui maintien le pH de la solution stable et assure la disponibilité des protons pour la réduction de CO_2.

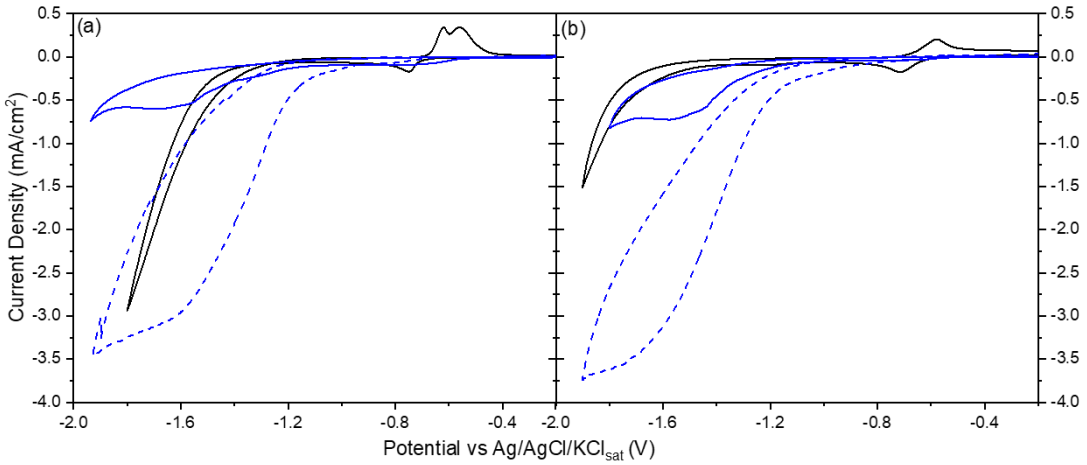

Figure 5. (a) et (b) Voltammogrammes cycliques de 1 mM catalyseur [2] dans une solution aqueuse contenant : (a) 0,1 M de [TBA][BF_4] sous Ar (en noir), 0,1 M de [TBA][BF_4] sous CO_2 (en bleu solide) et 0,1 M de tampon acétate à pH=4 saturé en [TBA][BF_4] sous CO_2 (en bleu pointillé) et (b) 0,5 M de [EMIM][BF_4] sous Ar (en noir), 0,5 M de [EMIM][BF_4] (en bleu solide) et 0,1 M de tampon acétate à pH=4 avec 0,1 M de [EMIM][BF_4] (en bleu pointillé). Potentiels rapportés versus l'électrode de référence Ag/AgCl/KCl$_{saturé}$. Vitesse de balayage 0,01 V/s.

La sélectivité du catalyseur [2] est aussi affectée par la présence des liquides ioniques en solution, comme le détaille le Tableau 1. Ce tableau présente des électrolyses à la même densité de courant (3,33 mA/cm^2) dans différents solvants et différents sels de fond. Les expériences 1 et 2 montrent que dans une solution d'acétonitrile contenant 5 % d'eau, le remplacement du sel de fond conventionnel [TBA][PF_6] par la même concentration de [EMIM][PF_6] augmente l'efficacité faradique de l'évolution de l'acide formique d'approximativement 16 %. En parallèle, le potentiel de l'electrode de travail pendant l'électrolyse est de 800 mV moins négatif en présence d'un IL en solution. Par conséquence, l'efficacité énergétique, qui est impactée par l'efficacité faradique ainsi que la surtension, est également presque doublée en présence de l'IL. Dans les expériences 3 et 4 on compare l'effet de présence ou d'absence de liquide ionique dans un milieu aqueux. On constate que la présence de [EMIM][BF_4] dans un milieu réactionnel est capable d'augmenter le taux de production de l'acide formique de 8 %, due au changement de l'interface entre

l'électrode et la solution en présence du liquide ionique. De plus, une alcalinisation du catholyte a été constatée après l'électrolyse avec [TBA][BF_4], ce qui nous a conduit à ajouter un tampon acétate à pH=4, capable de maintenir le pH du catholyte stable après les électrolyses à 10 C de charge (expériences 5 et 6.) L'addition de l'acide acétique favorise l'électrolyse avec une surtension très faible (0,28 V) et conduit à une valeur de EE de 32 %.

Tableau 1. Electrolyses à courant constant de 1 mM catalyseur [2] dans l'acétonitrile ou dans l'eau réalisés dans une cellule électrochimique de type H sous atmosphère CO_2. Charge totale circulée : 10-15 C.

Expérience	Solvant	Electrolyte	% H_2O (vol.)	Densité de courante appliquée (mA/cm_2)	FY $HCOO^-$ (%)	FY H_2 (%)	Efficacité Energétique (%)
1	CH_3CN	0.5 M [TBA][PF_6]	5	3.3	53	34	25[a]
2	CH_3CN	0.5 M [EMIM][PF_6]	5	3.3	69	22	47[a]
3	H_2O	0.1M [TBA][BF_4]	100	3.3	41	42	12[b]
4	H_2O	0.5M [EMIM][BF_4]	100	3.3	49	46	18[c]
5	H_2O	0.1M CH_3COO^-/CH_3COOH + 0.1M [TBA][BF_4]	100	3.3	40	55	25[b]
6	H_2O	0.1M CH_3COO^-/CH_3COOH + 0.1M [EMIM][BF_4]	100	3.3	46	40	32[b]

Efficacité Energétique (EE) % = $E_T/E \cdot FE_{HCOO^-}$, où $E_T = E^o_{CO2/HCOOH}$. [a]$E^o_{CO2/HCOOH}$ (CH_3CN, H_2O) = -1.32 V vs. Fc^+/Fc[28]. [b]$E^o_{CO2/HCOOH}$ = -0.62 V vs. Ag/AgCl (pH=3.8). [c]$E^o_{CO2/HCOOH}$ = -0.58 V vs. Ag/AgCl (pH=3.1).

Ces résultats expérimentaux sont complétés par des calculs théoriques sur le mécanisme d'action du catalyseur [2] pour la CO_2RR, ainsi que l'évolution de H_2. La Figure 6 montre que la forme active du catalyseur [2], ici nommé **1**, peut soit réduire le CO_2 à travers l'état de transition (TS) TS1 en surpassant la barrière énergétique de 14,3 kcal/mol, soit produire du H_2 à travers l'intermédiaire TS2 avec une barrière de 0,5 kcal/mol. Pourtant, dans l'acétonitrile le produit principal de réduction est l'acide formique, même si la barrière énergétique pour la réduction de CO_2 est significativement plus grande que celle de l'évolution de H_2. Ceci est raisonnable vu que dans la solution 95/5 (vol.) acétonitrile/H_2O, la concentration des protons est inférieure à celle de CO_2 de plusieurs ordres de grandeur, favorisant la voie du CO_2RR. Ensuite, l'incorporation du cation $[EMIM]^+$ sur l'interface de l'électrode conduit, selon les calculs théoriques, à l'augmentation de l'énergie libre pour les deux voies de réduction. Ceci est le résultat de la réduction du caractère nucléophile de l'hydrure de Rh par la polarisation du catalyseur vers le cation organique. Cet effet affecte pourtant beaucoup plus l'évolution de H_2. Par conséquent, la différence énergétique entre TS1 et TS2 diminue de 13,8 à 10,3 kcal/mol dans l'acétonitrile et 9,8

kcal/mol dans l'eau, ce qui est en accord avec l'augmentation de sélectivité vers l'acide formique expérimentalement constatée en présence de $[EMIM]^+$ en solution.

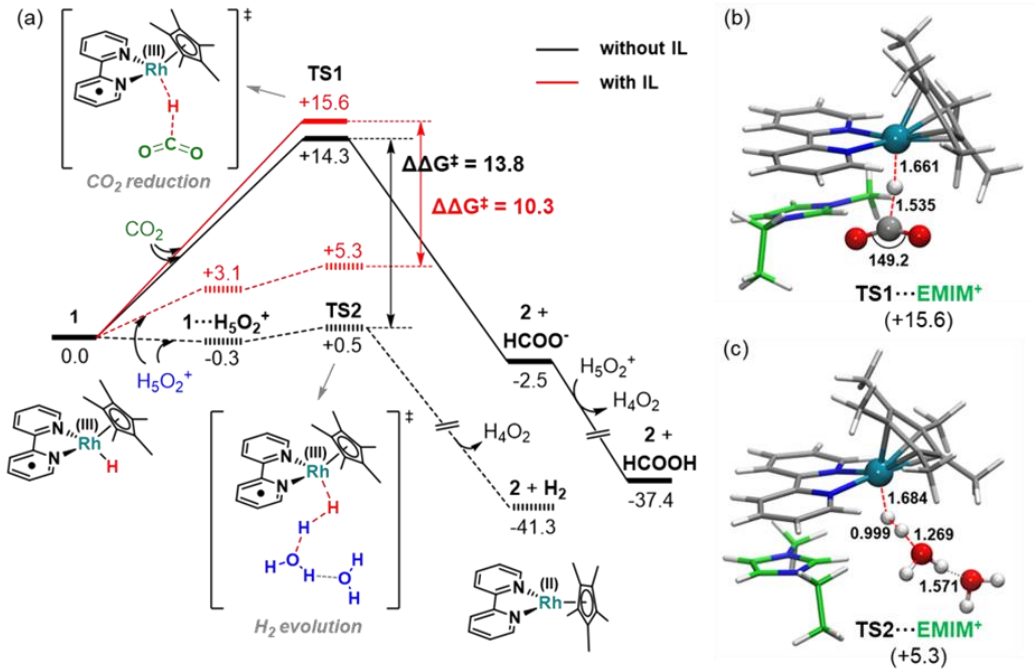

Figure 6. (a) Energies de Gibbs libres (kcal/mol) calculées pour la réduction de CO_2 et l'évolution de H_2 (lignes solides et pointillées respectivement) par l'espèce 1 en absence (lignes noires) et en présence (lignes rouges) d'un cation $[EMIM]^+$. (b) et (c) Géométries optimisées selon la théorie de la fonctionnelle de la densité (DFT) pour les états de transition TS1 et TS2 en présence de $[EMIM]^+$.

Chapitre 4

Dans le chapitre 4, nous introduisons la possibilité d'électrodéposer une couche de liquides ioniques sur l'électrode. La couche est formée grâce à la capacité intrinsèque des liquides ioniques à base de imidazolium d'être réduits à bas potentiel, comme on peut l'observer sur la Figure 7a. Dans la solution d'acétonitrile contenant 0,5 M de $[EMIM][PF_6]$ sous atmosphère inerte la réduction des cations imidazolium est induite sous des potentiels inferieurs à -2,5 V *vs.* Fc^+/Fc sur une électrode de carbone vitreux (la courbe noire, Fig. 7a). Cette réduction est également couplée à un pic de réoxydation positionné approximativement à -0,7 V[29]. Les potentiels de ces processus redox dépendent du matériel de l'électrode. Sur l'électrode d'or de la même géométrie (la courbe rouge, Fig. 7a) ces pics sont déplacés à des potentiels moins négatifs. Le taux de recouvrement de l'électrode par des espèces réduites dans ces deux cas peut être quantifié selon l'équation suivante :

$$\Gamma = \frac{Q\ (C)}{n\ F\ (C/mol)\ A\ (cm^2)}$$

où Q est la charge (mesurée en C), n est le nombre d'électrons impliqués dans le processus (selon la littérature[30] n=1), F est la constante de Faraday (egale à 96500 C/mol) et A est la surface géometrique de l'électrode de travail (mesurée en cm^2)[31,32]. Les valeurs de recouvrement pour les électrodes d'or et de carbone vitreux sont calculées à 1,34 10^{-7} mol/cm^2 et à 1,39 10^{-7} mol/cm^2 respectivement. La formation de la couche est ensuite longuement optimisée, toujours en prenant le système de catalyseur [2] comme référence, en fonction de la méthode de formation de la couche (voltammetrie cyclique *vs.* Chronoampérométrie) et en variant la composition du solvant et de l'atmosphère. Les conditions optimales identifiées correspondent à un CV ou alternativement 10 secondes de chronoampérométrie à -3,95 V *vs.* Fc^+/Fc dans une solution d'acétonitrile avec 0,5 M de [EMIM][PF_6] sous atmosphère inerte. Une fois que la couche des liquides ioniques électrodéposée a été optimisée, la caractérisation de l'électrode par la spectrométrie de photoélectrons X (XPS) a été réalisée sur les électrodes d'or. L'analyse des pics indique la présence des atomes d'azote liés à la surface, ainsi que la présence des unités d'imidazole. Ces informations prouvent l'existence d'une couche électrodéposée sur la surface. Ensuite, ces électrodes sont sorties de la solution contenant du [EMIM][PF_6], rincés avec de l'acétonitrile et mises dans une nouvelle solution pour évaluer leur comportement catalytique. Pour ce but le catalyseur [2] a été choisi. La Figure 7b montre la vague catalytique de catalyseur [2] à 1 mM dans l'acétonitrile/H_2O 95/5 (vol.) sous CO_2 produite sur l'électrode de carbone vitreux nue avec 0,5 M [TBA][PF_6] pour assurer la conductivité (courbe noire), sur l'électrode de carbone vitreux nue avec 0,5 M [EMIM][PF_6] en solution (courbe verte) et sur l'électrode avec la couche électrodéposée avec 0,5 M [TBA][PF_6] en solution (courbe rouge). Le potentiel catalytique de l'électrode avec la couche électrodéposée est similaire à celui obtenu avec l'électrode de carbone contrôle travaillant dans l'électrolyte qui contient du [EMIM][PF_6] et sa densité de courant est légèrement améliorée. Ensuite, cette couche électrodéposée est comparée avec une couche de liquides ioniques fixée de façon covalente sur l'électrode selon des protocoles décrits dans la littérature[33]. De plus, la couche électrodéposée est testée en présence du catalyseur [2] pour la réduction de CO_2 dans un milieu aqueux. On constate un effet bénéfique modéré pour la catalyse par déplacement anodique du potentiel catalytique. Les voltammogrammes indiquent qu'en présence de cette couche une forte suppression de la production d'hydrogène a lieu par rapport à l'électrode nue.

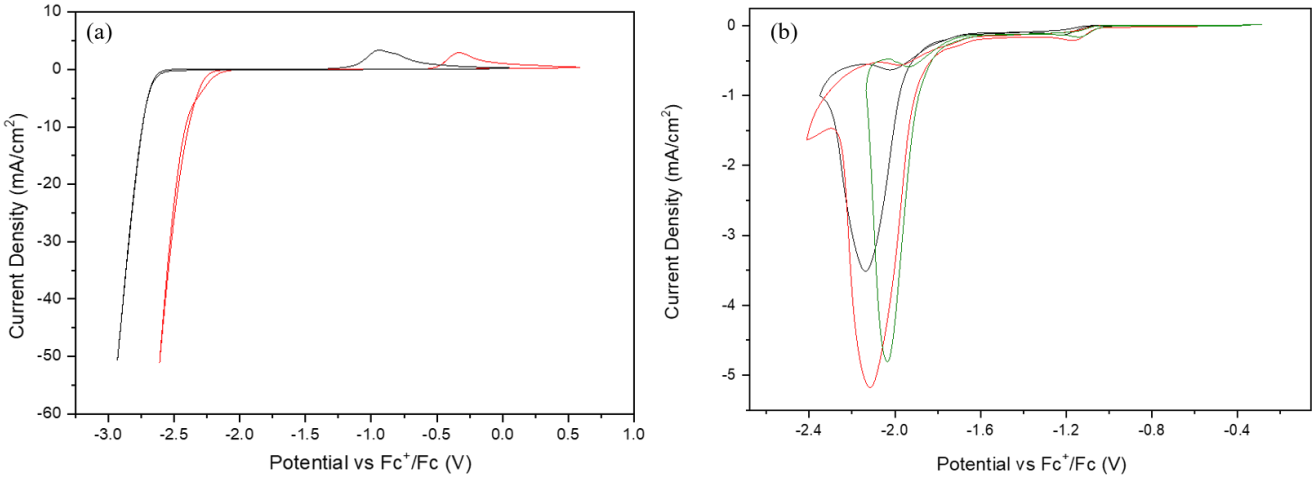

Figure 7. (a) Voltammogrammes cycliques de 0,5 M [EMIM][PF_6] dans l'acétonitrile sous atmosphère inerte sur électrode de carbon vitreux (en noir) et sur électrode d'or (en rouge) de 3 mm diamètre et (b) Voltammogrammes cycliques de catalyseur [2] à 1 mM dans une solution d'acétonitrile sous CO_2 contenant : 0,5 M de [TBA][PF_6] (en noir), 0,5 M de [EMIM][PF_6] (en vert) et une couche électrodéposée de [EMIM][PF_6] testée dans du 0,5 M [TBA][PF_6]. Couche électrodéposée par 10 sec de chronoampérométrie à -3,95 V vs. Fc^+/Fc dans une solution d'acétonitrile contenant 0,5 M de [EMIM][PF_6]. Vitesse de balayage 0,01 V/s.

Finalement, la sélectivité de la couche électrodéposée est évaluée par électrolyse à courant constant (3,33 mA/cm^2) dans l'acétonitrile et dans l'eau. Les résultats sont représentés dans le Tableau 2. Le potentiel de l'electrode de travail contenant la couche électrodéposée dans des solutions d'acétonitrile (expériences 1-4 du tableau 2) est semblable à celui d'une electrode nue avec IL en solution (expérience 2). Au contraire, en comparant les expériences 1-3 on voit que la présence de la couche électrodéposée est à l'origine d'une augmentation de taux de formiate produit. Ceci est également à l'origine d'une augmentation de la valeur d'efficacité énergétique jusqu'à 59 %. Notons que la production de formiate est plus efficace que quand le même liquide ionique se trouve en solution. L'efficacité faradique maximale pour le formiate de 85 % (expérience 3) est comparable à celle engendrée par la couche covalente (expérience 4). En outre, dans un milieux aqueux acide, la présence de la couche électrodéposée est capable de doubler le ratio FE_{HCOO^-}/FE_{H2} par rapport à une électrode nue passant de 0,6/1 à presque 1,2/1. Finalement, l'électrolyse réalisée avec une couche électrodéposée en présence d'une solution de tampon acétate à pH=3,8 (expérience 8) permet d'obtenir la plus haute efficacité faradique de formiate en milieu aqueux à la surtension la plus faible. Par conséquent, cette expérience a le EE le plus élevé parmi toutes les electrolyses dans l'eau.

Tableau 2. Electrolyses à courant constant avec du catalyseur [2] à 1 mM dans l'acétonitrile ou dans l'eau réalisées dans une cellule électrochimique de type H sous atmosphère CO_2. Durée totale d'électrolyse correspond à la circulation de 10 C de charge. Couches électrodéposées par 10 sec de chronoampérométrie à -3,95 V vs. Fc^+/Fc dans une solution d'acétonitrile contenant 0,5 M de [EMIM][PF_6]. Couches covalentes formées selon les protocoles décrits par Bouden et. al.[33]

Expérience	Solvant	Electrolyte	Couche IL	%H_2O (vol.)	Densité de courant (mA/cm^2)	FE $HCOO^-$ (%)	FE H_2 (%)	Efficacité Energétique (%)
1	CH_3CN	0.5 M [TBA][PF_6]	Aucune	5	3.33	53	34	25[a]
2	CH_3CN	0.5 M [EMIM][PF_6]	Aucune	5	3.33	69	22	47[a]
3	CH_3CN	0.5 M [TBA][PF_6]	Electrodéposée	5	3.33	85	15	59[a]
4	CH_3CN	0.5 M [TBA][PF_6]	Covalente	5	3.33	81	12	58[a]
5	H_2O	0.1 M [TBA][BF_4] + 0.1 M CH_3COOH	Aucune	100	3.33	38	61	18[b]
6	H_2O	0.1 M [TBA][BF_4] + 0.1 M CH_3COOH	Electrodéposée	100	3.33	53	44	27[b]
7	H_2O	0.1 M [TBA][BF_4] + 0.1 M CH_3COOH	Covalente	100	3.33	49	46	26[c]
8	H_2O	0.1 M [TBA][BF_4] + 0.1 M tampon pH=3,8 CH_3COOH/CH_3COONa	Electrodéposée	100	3.33	53	42	33[c]

Efficacité Energétique (EE) % = $E_T/E \cdot FE_{HCOO^-}$, où $E_T = E^o_{CO2/HCOOH}$. [a]$E^o_{CO2/HCOOH}$ (CH_3CN, H_2O) = -1.32 V vs. Fc^+/Fc[28]. [b]$E^o_{CO2/HCOOH}$ = -0.58 V vs. Ag/AgCl (pH=3.1). [c]$E^o_{CO2/HCOOH}$ = -0.62 V vs. Ag/AgCl (pH=3.8).

Chapitre 5

Dans ce chapitre, on présente l'exploitation des travaux déjà décrits dans les chapitres 3 et 4 sur une échelle plus grande, en utilisant un électrolyseur en flux. Cet électrolyseur commercial permet l'installation d'électrodes à diffusion de gaz (GDE) de 10 cm^2 et permet donc de compenser la limitation de densité de courant dans l'eau due à la basse solubilité de CO_2. L'illustration schématique de cet électrolyseur est présentée sur la Figure 8a. En utilisant une GDE, le CO_2 n'est en contact avec la solution qu'au sein de la triple interface gaz-électrode-électrolyte. Cet électrolyseur est utilisé pour tester la réduction de CO_2 par le catalyseur [2] dans un milieux aqueux acide avec 0,1 M de tampon acétate à

pH=4 avec 0,1 M [TBA][BF_4] en tant que catholyte et le formiate a été quantifié par chromatographie ionique. Plusieurs configurations ont été testées afin d'augmenter l'efficacité faradique en formiate produit tout en contrôlant le potentiel global de la cellule (|Ecell|), ce qui a permis des définir des conditions optimales. Ces conditions correspondent à une configuration à deux compartiments séparés (anode et cathode) en flux unique (la solution de catholyte ne traverse l'électrolyseur qu'une fois) et en utilisant un GDE en tant que cathode (réduction du CO_2 en phase gazeuse au lieu de phase liquide) et 0,5 M de KOH en tant qu'anolyte (afin de minimiser le surpotentiel de la réaction de production d'oxygène qui peut avoir lieu sur l'anode).

Une fois que l'efficacité de production de formiate atteint la valeur de 31 % en moyenne et qu'elle reste stable pour une charge passée de 1000 C, le dépôt de la couche électrodéposée sur le GDE est réalisé. Sur la Figure 8b, la comparaison de l'effet catalytique du catalyseur [2] dans la configuration mentionnée ci-dessus sur un GDE sans couche (en noir) ou avec la couche électrodéposée (en rouge) est présentée. Dans cette configuration les densités de courant ont pu atteindre 20 mA/cm^2, presque 6 fois plus que dans les cellules H utilisées auparavant pour effectuer des electrolyses. De plus, la présence de la couche électrodéposée a augmenté l'efficacité moyenne de production de formiate jusqu'à 45 %. De manière intéressante, l'écart d'efficacité faradique pour le formiate entre l'absence et la présence de la couche dans une cellule type H pour une charge de 10 C dans des conditions catalytiques aqueuses acides était presque égal à celui qu'on a constaté au sein de l'électrolyseur pour ces mêmes conditions catalytiques, mais pour une charge 100 fois supérieure. Par conséquent, l'effet de la couche électrodéposée a été validé dans la configuration à grande échelle.

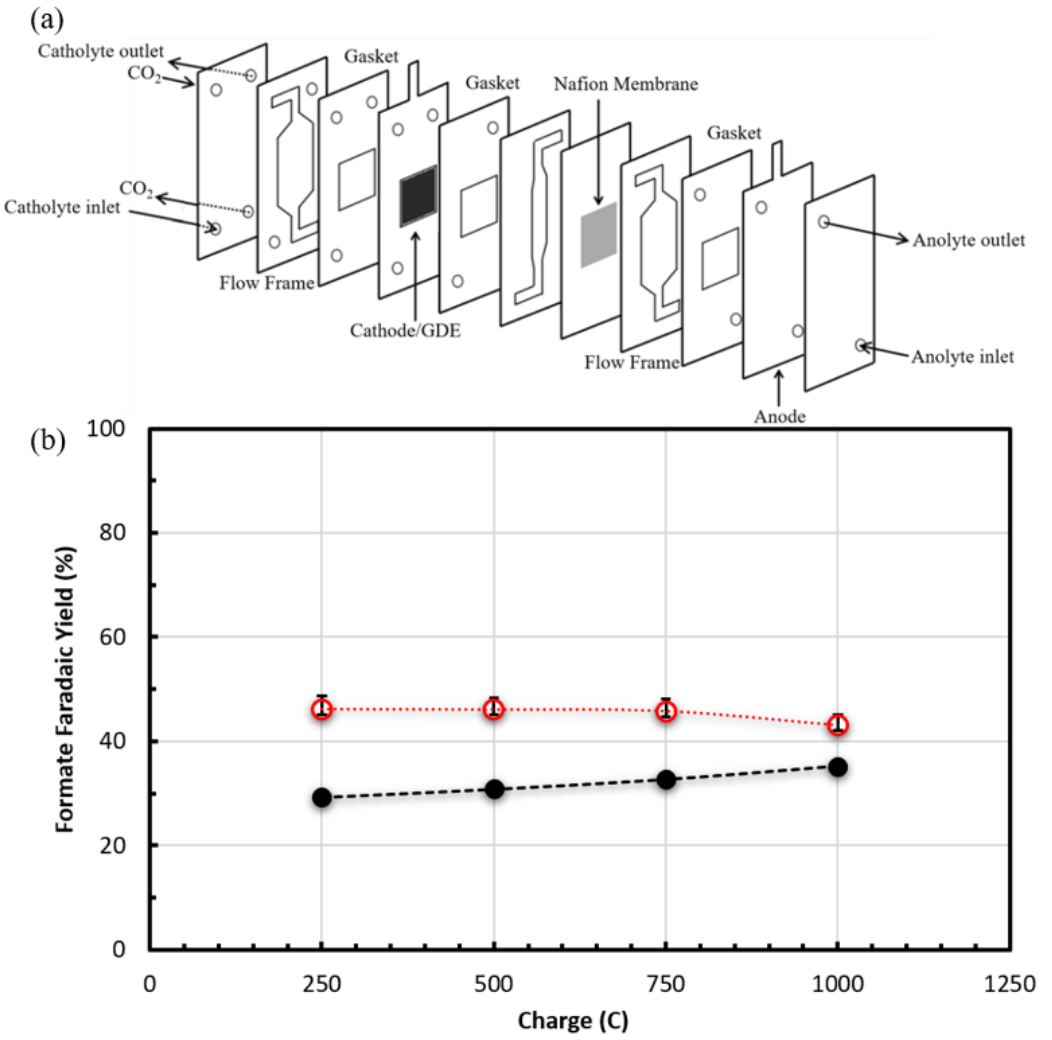

Figure 8. (a) Représentation schématique de l'électrolyseur en flux en configuration de deux compartiments et (b) Efficacité faradique en formiate produite par le catalyseur [2] sur un GDE sans couche (en noir) et avec couche électrodéposée (en rouge).

Chapitre 6

Dans le chapitre 6, les conclusions générales des travaux présentés dans cette thèse sont résumées et les perspectives sont présentées. Bien que le catalyseur [1] ait montré un effet cocatalytique marqué avec des liquides ioniques, sa sélectivité déjà exceptionnelle et son insolubilité dans l'eau ont empêché son utilisation pour la totalité de l'étude. En revanche, le catalyseur [2] a pu être utilisé comme modèle pour effectuer une étude d'ingénierie de l'electrolyte en variant à la fois le solvant et le liquide ionique. De plus, en immobilisant de manière simple des liquides ioniques sur la surface des électrodes, leur effet bénéfique vers la production de formiate a été encore plus évidente, tant dans l'acétonitrile que dans l'eau. Finalement, cette technique a été testée à grande échelle au sein d'un électrolyseur en flux. Il est donc impératif d'exploiter les résultats obtenus de l'interaction cocatalytique entre catalyseurs moléculaires et liquides ioniques en solution ou immobilisés afin de développer des systèmes catalytiques plus efficaces, en catalyse homogène et hétérogène de réduction de CO_2.

Bibliographie

(1) Lee, M.-Y.; Park, K. T.; Lee, W.; Lim, H.; Kwon, Y.; Kang, S. Current Achievements and the Future Direction of Electrochemical CO_2 Reduction: A Short Review. *Crit. Rev. Environ. Sci. Technol.* **2020**, *50* (8), 769–815. https://doi.org/10.1080/10643389.2019.1631991.

(2) Senocrate, A.; Battaglia, C. Electrochemical CO_2 Reduction at Room Temperature: Status and Perspectives. *J. Energy Storage* **2021**, *36*, 102373. https://doi.org/10.1016/j.est.2021.102373.

(3) Todorova, T. K.; Schreiber, M. W.; Fontecave, M. Mechanistic Understanding of CO_2 Reduction Reaction (CO_2RR) Toward Multicarbon Products by Heterogeneous Copper-Based Catalysts. *ACS Catal.* **2020**, *10* (3), 1754–1768. https://doi.org/10.1021/acscatal.9b04746.

(4) Lu, Q.; Jiao, F. Electrochemical CO_2 Reduction: Electrocatalyst, Reaction Mechanism, and Process Engineering. *Nano Energy* **2016**, *29*, 439–456. https://doi.org/10.1016/j.nanoen.2016.04.009.

(5) König, M.; Vaes, J.; Klemm, E.; Pant, D. Solvents and Supporting Electrolytes in the Electrocatalytic Reduction of CO_2. *iScience* **2019**, *19*, 135–160. https://doi.org/10.1016/j.isci.2019.07.014.

(6) Sanchez-Sanchez, C. M. Electrocatalytic Reduction of CO_2 in Imidazolium-Based Ionic Liquids. In *Reference Module in Chemistry, Molecular Sciences and Chemical Engineering. Encyclopedia of Interfacial Chemistry : Surface Science and Electrochemistry*; Wandelt, K., Ed.; Elsevier, 2018; pp 539–551.

(7) Supasitmongkol, S.; Styring, P. High CO_2 Solubility in Ionic Liquids and a Tetraalkylammonium-Based Poly(Ionic Liquid). *Energy Environ. Sci.* **2010**, *3* (12), 1961–1972. https://doi.org/10.1039/C0EE00293C.

(8) Qiao, J.; Liu, Y.; Hong, F.; Zhang, J. A Review of Catalysts for the Electroreduction of Carbon Dioxide to Produce Low-Carbon Fuels. *Chem. Soc. Rev.* **2013**, *43* (2), 631–675. https://doi.org/10.1039/C3CS60323G.

(9) Francke, R.; Schille, B.; Roemelt, M. Homogeneously Catalyzed Electroreduction of Carbon Dioxide—Methods, Mechanisms, and Catalysts. *Chem. Rev.* **2018**, *118* (9), 4631–4701. https://doi.org/10.1021/acs.chemrev.7b00459.

(10) Benson, E. E.; Kubiak, C. P.; Sathrum, A. J.; Smieja, J. M. Electrocatalytic and Homogeneous Approaches to Conversion of CO_2 to Liquid Fuels. *Chem. Soc. Rev.* **2008**, *38* (1), 89–99. https://doi.org/10.1039/B804323J.

(11) Costentin, C.; Drouet, S.; Robert, M.; Savéant, J.-M. A Local Proton Source Enhances CO_2 Electroreduction to CO by a Molecular Fe Catalyst. *Science* **2012**, *338* (6103), 90–94. https://doi.org/10.1126/science.1224581.

(12) Hawecker, J.; Lehn, J.-M.; Ziessel, R. Photochemical and Electrochemical Reduction of Carbon Dioxide to Carbon Monoxide Mediated by (2,2′-Bipyridine)Tricarbonylchlororhenium(I) and Related Complexes as Homogeneous Catalysts. *Helv. Chim. Acta* **1986**, *69* (8), 1990–2012. https://doi.org/10.1002/hlca.19860690824.

(13) Clark, M. L.; Cheung, P. L.; Lessio, M.; Carter, E. A.; Kubiak, C. P. Kinetic and Mechanistic Effects of Bipyridine (Bpy) Substituent, Labile Ligand, and Brønsted Acid on Electrocatalytic CO_2 Reduction by Re(Bpy) Complexes. *ACS Catal.* **2018**, *8* (3), 2021–2029. https://doi.org/10.1021/acscatal.7b03971.

(14) Caix, C.; Chardon-Noblat, S.; Deronzier, A.; Moutet, J.-C.; Tingry, S. (Pentamethylcyclopentadienyl)(Polypyridyl) Rhodium and Iridium Complexes as Electrocatalysts for the Reduction of Protons to Dihydrogen and the Hydrogenation of Organics. *J. Organomet. Chem.* **1997**, *540* (1), 105–111. https://doi.org/10.1016/S0022-328X(97)00096-X.

(15) Caix, C.; Chardon-Noblat, S.; Deronzier, A. Electrocatalytic Reduction of CO_2 into Formate with $[(\eta^5\text{-}Me_5C_5)M(L)Cl]^+$ Complexes (L = 2,2′-Bipyridine Ligands; M = Rh(III) and Ir(III)). *J. Electroanal. Chem.* **1997**, *434* (1), 163–170. https://doi.org/10.1016/S0022-0728(97)00058-2.

(16) Alvarez-Guerra, M.; Albo, J.; Alvarez-Guerra, E.; Irabien, A. Ionic Liquids in the Electrochemical Valorisation of CO_2. *Energy Environ. Sci.* **2015**, *8* (9), 2574–2599. https://doi.org/10.1039/C5EE01486G.
(17) Hapiot, P.; Lagrost, C. Electrochemical Reactivity in Room-Temperature Ionic Liquids. *Chem. Rev.* **2008**, *108* (7), 2238–2264. https://doi.org/10.1021/cr0680686.
(18) Hanc-Scherer, F. A.; Montiel, M. A.; Montiel, V.; Herrero, E.; Sánchez-Sánchez, C. M. Surface Structured Platinum Electrodes for the Electrochemical Reduction of Carbon Dioxide in Imidazolium Based Ionic Liquids. *Phys. Chem. Chem. Phys.* **2015**, *17* (37), 23909–23916. https://doi.org/10.1039/C5CP02361K.
(19) Rosen, B. A.; Salehi-Khojin, A.; Thorson, M. R.; Zhu, W.; Whipple, D. T.; Kenis, P. J. A.; Masel, R. I. Ionic Liquid-Mediated Selective Conversion of CO_2 to CO at Low Overpotentials. *Science* **2011**, *334* (6056), 643–644.
(20) Zhao, S.-F.; Horne, M.; Bond, A. M.; Zhang, J. Is the Imidazolium Cation a Unique Promoter for Electrocatalytic Reduction of Carbon Dioxide? *J. Phys. Chem. C* **2016**, *120* (42), 23989–24001. https://doi.org/10.1021/acs.jpcc.6b08182.
(21) Lau, G. P. S.; Schreier, M.; Vasilyev, D.; Scopelliti, R.; Gratzel, M.; Dyson, P. J. New Insights Into the Role of Imidazolium-Based Promoters for the Electroreduction of CO_2 on a Silver Electrode http://infoscience.epfl.ch/record/221801 (accessed 2021 -01 -22). https://doi.org/10.1021/jacs.6b03366.
(22) Matsubara, Y.; Grills, D. C.; Kuwahara, Y. Thermodynamic Aspects of Electrocatalytic CO_2 Reduction in Acetonitrile and with an Ionic Liquid as Solvent or Electrolyte. *ACS Catal.* **2015**, *5* (11), 6440–6452. https://doi.org/10.1021/acscatal.5b00656.
(23) Choi, J.; Benedetti, T. M.; Jalili, R.; Walker, A.; Wallace, G. G.; Officer, D. L. High Performance Fe Porphyrin/Ionic Liquid Co-Catalyst for Electrochemical CO $_2$ Reduction. *Chem. - Eur. J.* **2016**, *22* (40), 14158–14161.
(24) Sung, S.; Kumar, D.; Gil-Sepulcre, M.; Nippe, M. Electrocatalytic CO_2 Reduction by Imidazolium-Functionalized Molecular Catalysts. *J. Am. Chem. Soc.* **2017**, *139* (40), 13993–13996. https://doi.org/10.1021/jacs.7b07709.
(25) Khadhraoui, A.; Gotico, P.; Boitrel, B.; Leibl, W.; Halime, Z.; Aukauloo, A. Local Ionic Liquid Environment at a Modified Iron Porphyrin Catalyst Enhances the Electrocatalytic Performance of CO_2 to CO Reduction in Water. *Chem. Commun.* **2018**, *54* (82), 11630–11633. https://doi.org/10.1039/C8CC06475J.
(26) Vichou, E.; Li, Y.; Gomez-Mingot, M.; Fontecave, M.; Sánchez-Sánchez, C. M. Imidazolium- and Pyrrolidinium-Based Ionic Liquids as Cocatalysts for CO_2 Electroreduction in Model Molecular Electrocatalysis. *J. Phys. Chem. C* **2020**, *124* (43), 23764–23772.
(27) Tomita, Y.; Teruya, S.; Koga, O.; Hori, Y. Electrochemical Reduction of Carbon Dioxide at a Platinum Electrode in Acetonitrile-Water Mixtures. *J. Electrochem. Soc.* **2000**, *147* (11), 4164.
(28) Huan, T. N.; Simon, P.; Rousse, G.; Génois, I.; Artero, V.; Fontecave, M. Porous Dendritic Copper: An Electrocatalyst for Highly Selective CO_2 Reduction to Formate in Water/Ionic Liquid Electrolyte. *Chem. Sci.* **2016**, *8* (1), 742–747. https://doi.org/10.1039/C6SC03194C.
(29) Michez, R.; Vander Steen, J.; Doneux, T.; Luhmer, M.; Buess-Herman, C. Electroreduction of 1-Butyl-3-Methylimidazolium Bis(Trifluoromethanesulfonyl)Imide Ionic Liquid: Oriented Product Selectivity through the Electrode Material. *Electrochimica Acta* **2018**, *270*, 434–439. https://doi.org/10.1016/j.electacta.2018.03.057.
(30) Michez, R.; Doneux, T.; Buess-Herman, C.; Luhmer, M. NMR Study of the Reductive Decomposition of [BMIm][NTf_2] at Gold Electrodes and Indirect Electrochemical Conversion of CO_2. *ChemPhysChem* **2017**, *18* (16), 2208–2216. https://doi.org/10.1002/cphc.201700421.
(31) Prodromidis, M. I.; Florou, A. B.; Tzouwara-Karayanni, S. M.; Karayannis, M. I. The Importance of Surface Coverage in the Electrochemical Study of Chemically Modi®ed Electrodes. **2000**, No. 18, 4.
(32) Pugliese, S.; Huan, N. T.; Forte, J.; Grammatico, D.; Zanna, S.; Su, B.-L.; Li, Y.; Fontecave, M. Functionalization of Carbon Nanotubes with Nickel Cyclam for the Electrochemical Reduction of CO_2. *ChemSusChem* **2020**, *13* (23), 6449–6456. https://doi.org/10.1002/cssc.202002092.

(33) Bouden, S.; Gómez-Mingot, M.; Randriamahazaka, H.; Ghilane, J. Surface Initiated Immobilization of Molecules Contained in an Ionic Liquid Framework. *Anal. Chem.* **2016**, *88* (1), 1017–1021. https://doi.org/10.1021/acs.analchem.5b03922.

RÉSUMÉ EN FRANÇAIS

LIST OF PUBLICATIONS AND CONFERENCES

Publications

[1] *Imidazolium- and Pyrrolidinium-Based Ionic Liquids as Cocatalysts for CO_2 Electroreduction in Model Molecular Electrocatalysis*, E. Vichou, Y. Li, M. Gomez-Mingot, M. Fontecave, and C. M. Sanchez-Sanchez, *J. Phys. Chem. C*, 2020, 124, 23764-23772.

[2] *Electrocatalytic Conversion of CO_2 to Formate at Low Overpotential by Electrolyte Engineering in Model Molecular Catalysis*, E. Vichou, A. Solé-Daura, C. Mellot-Draznieks, Y. Li, M. Gomez-Mingot, M. Fontecave and C. M. Sánchez-Sánchez, submitted manuscript.

Conferences

[i]	1st French-Spanish Atelier/Workshop on Electrochemistry, flash presentation	Paris 07.21
[ii]	Elcorel International Conference, oral presentation (Online)	Leiden 03.21
[ii]	ElecNano Conference, flash presentation (Online)	Paris 11.20

ACKNOWLEDGEMENTS

Undertaking a PhD in chemistry had been one of my goals ever since my undergraduate studies. While it was at times challenging, it was an incredibly edifying learning experience, that was made possible with the help and support of several people, to whom I owe my sincere gratitude.

Firstly, I would like to thank my PhD directors, Dr. Carlos Sanchez-Sanchez and Prof. Marc Fontecave for selecting and entrusting me with a project in a domain I previously had little experience. Thanks to their invaluable guidance and constant support throughout my thesis, I was able to gain useful insight into not only my topic of research, but also into different scientific mentalities. Their patient feedback and constructive criticism coupled with encouragement helped me and kept me motivated in my work. My collaboration with two such highly regarded scientists has been a determining experience in my life that I will look back on for the rest of my career. I feel very fortunate to have been able to learn by their example about life and science. I am equally grateful to my co-supervisor Dr. Maria Gomez-Mingot, who shared with me not only an office, but also her knowledge and expertise. During these three years she was always by my side with suggestions, advice and her generous nature, making every day in the lab better.

I would also like to express my gratitude to the rest of the members of my thesis committee: Dr. Sylvie Chardon-Noblat, Dr. Sophie Griveau, Prof. Claude Jolivalt and Prof. Thomas Doneux for kindly accepting to devote time and effort into revising my thesis.

This work would not have been possible without the financial support from the doctoral program “Génie des Procédés” and the contribution of the Onassis Foundation.

My heartfelt thanks to Dr. Yun Li, for her advice on molecular catalysis and organic chemistry throughout my thesis. Special thanks also to our collaborators Dr. Albert Solé-Daura and Dr. Caroline Mellot-Draznieks for performing the theoretical calculations and all the edifying conversations that helped me better comprehend our catalytic system. I am also grateful to Dr. Huan Tran, for the help in the laboratory and in discussions, I will always consider him a valuable friend. I would also like to thank Dr. Charles Creissen for our recent collaboration and for always being very helpful in the lab. I would equally like to thank Dr. Antoine Miche for performing the XPS characterization tests.

A big thanks goes to all members of LCPB and LISE who made my time there very enjoyable. I would particularly like to mention Phong, Adèle, Youven, Alessandro, Sophia, Gabriel, Alice and to my former colleagues Sophie, Lin, Mathis, Alex, Dilan, Cécilia, Dave, Dona, Tanya, Cameron, Subal and Hemlata.

I would also like to extend my thanks to the administrative personnel of both laboratories, especially Jessica Duvoisin, Johnny Tondeleir, Isabelle Lefebvre and Martine Chaduc for their help. Finally, thanks to Iulia and Renaud, two amazing interns I had the pleasure to work with.

I am particularly grateful to my partner Gleb for the help and support during our PhDs these past few years. Thank you for always encouraging me to pursue my passion and also occasionally feeding me. I am extending my thanks to my dearest friends Lily, Katerina and Sam, who have known me for eons and have somehow managed to still bear me. You are some of the most wise, hilarious and compassionate individuals I have had the misfortune to spend 12 years in Moraitis with. Niko, thank you for being there through the good, but especially hard parts of our 4th year, M2 and PhDs. Your courage and passion for research are always an inspiration for me. Finally, I would not have been able to pursue a PhD without the love and support of both my parents, my mother Afroditi who especially taught me to value education and my father Nikos who always encouraged my creativity.